

01 May 1976

Performance of unstiffened compression elements

Venkatakrishnan Kalyanaraman

Follow this and additional works at: <https://scholarsmine.mst.edu/ccfss-library>



Part of the [Structural Engineering Commons](#)

Recommended Citation

Kalyanaraman, Venkatakrishnan, "Performance of unstiffened compression elements" (1976). *Center for Cold-Formed Steel Structures Library*. 184.

<https://scholarsmine.mst.edu/ccfss-library/184>

This Technical Report is brought to you for free and open access by Scholars' Mine. It has been accepted for inclusion in Center for Cold-Formed Steel Structures Library by an authorized administrator of Scholars' Mine. This work is protected by U. S. Copyright Law. Unauthorized use including reproduction for redistribution requires the permission of the copyright holder. For more information, please contact scholarsmine@mst.edu.

CCFSS LIBRARY Kalyanaraman, V. Pekoz, T.
22 1 * 281 Winter, G. PERFORMANCE OF
1976 UNSTIFFENED COMPRESSION ELEMENTS

CCFSS LIBRARY Kalyanaraman, V. Pekoz, T.
22 1 * 281 Winter, G. PERFORMANCE OF
1976 UNSTIFFENED COMPRESSION ELEMENTS

DATE	ISSUED TO

Technical Library
Center for Cold-Formed Steel Structures
University of Missouri-Rolla
Rolla, MO 65401

DEPARTMENT OF STRUCTURAL ENGINEERING
SCHOOL OF CIVIL AND ENVIRONMENTAL ENGINEERING
CORNELL UNIVERSITY

Report No. 362

-DRAFT-

PERFORMANCE OF UNSTIFFENED
COMPRESSION ELEMENTS

by

Venkatakrishnan Kalyanaraman

Teoman Peköz and George Winter

Project Directors

A Research Project sponsored by the
American Iron and Steel Institute

Ithaca, New York

May 1976

PREFACE

This report is based on a thesis presented to the Faculty of the Graduate School of Cornell University for the degree of Doctor of Philosophy.

The author wishes to thank Professors George Winter and Teoman Peköz for their help and guidance during this research undertaking.

The sponsorship of the American Iron and Steel Institute and the cooperation of the American Iron and Steel Institute Engineering Subcommittees of the Sheet Committees are gratefully acknowledged.

TABLE OF CONTENTS

	Page
LIST OF TABLES	ix
LIST OF FIGURES	xi
NOMENCLATURE	xv
ABSTRACT	xvii
CHAPTER 1. INTRODUCTION	1
1.1 General	1
1.1.1 Cold-Formed Structural Steel Members	2
1.2 Behavior of Unstiffened Element Under Compression	4
1.2.1 Local Buckling of Unstiffened Element	4
1.2.2 Postbuckling Behavior	7
1.2.3 Local Buckling in the Inelastic Range	12
1.2.4 Effect of Local Buckling on Structural Members	14
1.3 Purpose of the Investigation	17
1.4 Scope of the Investigation	20
1.4.1 Desired Information	20
1.4.2 Analytical and Experimental Investigation	21
1.5 Summary	23
CHAPTER 2. ANALYTICAL INVESTIGATION	24
2.1 Review of Analytical Methods	24
2.2 Local Buckling	25

3.4.4	Winter's Unstiffened Element Effective Width Equation	75
3.4.5	Out of Plane Deformation	79
3.5	Summary and Conclusions	80
CHAPTER 4.	INTERACTION OF THE LOCAL AND THE OVERALL BUCKLING IN COMPRESSION MEMBERS	83
4.1	General	83
4.1.1	The Flexural Instability of Columns	84
4.1.2	The Flexural Buckling Strength of Compression Members With Locally Buckling Elements	88
4.2	Experimental Investigation of Compression Members	92
4.2.1	Material Properties	92
4.2.2	Design of the Specimens	93
4.2.3	Fabrication and Instrumentation	93
4.2.4	Experimental Set-Up and Procedure	94
4.3	Background for Evaluation of Experimental Data	97
4.3.1	Determination of the Elastic Flexural Buckling Load from Experiments	97
4.4	Evaluation of the Experimental Results	100
4.4.1	Experimental Results	100
4.4.2	Comparison of Test Results to AISI Specification Procedure	101

DEPARTMENT OF STRUCTURAL ENGINEERING
SCHOOL OF CIVIL AND ENVIRONMENTAL ENGINEERING
CORNELL UNIVERSITY

Report No. 362

-DRAFT-

PERFORMANCE OF UNSTIFFENED
COMPRESSION ELEMENTS

by

Venkatakrishnan Kalyanaraman

Teoman Peköz and George Winter

Project Directors

A Research Project sponsored by the
American Iron and Steel Institute

Ithaca, New York

May 1976

2.2.1	Elastic Local Buckling Stress	25
2.2.2	Inelastic Local Buckling	30
2.3	Elastic Postbuckling Behavior	35
2.3.1	Postbuckling Behavior of Perfectly Flat Unstiffened Elements - Parameter Study	49
2.3.2	Postbuckling Behavior of Unstiffened Elements With Initial Imperfections - Parameter Study	53
2.4	Summary and Conclusions	54
CHAPTER 3. EXPERIMENTAL INVESTIGATION OF UNSTIFFENED ELEMENT BEHAVIOR		56
3.1	General	56
3.2	Stub-Column Test	57
3.2.1	Material	57
3.2.2	Design of Test Specimens	58
3.2.3	Fabrication and Instrumentation	60
3.2.4	Experimental Set-Up and Procedure	61
3.3	Background for Evaluation of Experimental Data	64
3.3.1	Local Buckling	64
3.3.2	Postbuckling Behavior	66
3.4	Evaluation and Experimental Results	67
3.4.1	Experimental Results	67
3.4.2	Experimental Results of DeWolf ³²	69
3.4.3	Comparison With Analytical Solution	70

3.4.4	Winter's Unstiffened Element Effective Width Equation	75
3.4.5	Out of Plane Deformation	79
3.5	Summary and Conclusions	80
CHAPTER 4.	INTERACTION OF THE LOCAL AND THE OVERALL BUCKLING IN COMPRESSION MEMBERS	83
4.1	General	83
4.1.1	The Flexural Instability of Columns	84
4.1.2	The Flexural Buckling Strength of Compression Members With Locally Buckling Elements	88
4.2	Experimental Investigation of Compression Members	92
4.2.1	Material Properties	92
4.2.2	Design of the Specimens	93
4.2.3	Fabrication and Instrumentation	93
4.2.4	Experimental Set-Up and Procedure	94
4.3	Background for Evaluation of Experimental Data	97
4.3.1	Determination of the Elastic Flexural Buckling Load from Experiments	97
4.4	Evaluation of the Experimental Results	100
4.4.1	Experimental Results	100
4.4.2	Comparison of Test Results to AISI Specification Procedure	101

4.4.3	Comparison of Test Results to Theoretical Solutions	105
4.4.3.1	Flexural Buckling Strength from Analytical Solution	106
4.4.3.2	Flexural Buckling Strength from Effective Width Equations	110
4.4.3.3	Comparison of Test Results	114
4.5	Summary and Conclusions	118
CHAPTER 5.	EFFECT OF LOCAL BUCKLING ON FLEXURAL MEMBERS	120
5.1	General	120
5.2	Flexural Member Tests	122
5.2.1	Material Properties	122
5.2.2	Design of Experimental Specimens	123
5.2.3	Fabrication and Instrumentation	124
5.2.4	Experimental Set-Up and Procedure	126
5.3	Background for Evaluation of Experimental Data	128
5.4	Evaluation of the Experimental Results	131
5.4.1	Experimental Results	131
5.4.2	Elastic Local Buckling and Postbuckling Behavior of Unstiffened Compression Flanges	135
5.4.3	Limiting Flat Width to Thickness Ratio	141
5.4.4	Inelastic Strain Capacity of Unstiffened Compression Elements	143

5.5	Summary and Conclusions	147
CHAPTER 6.	POSSIBLE DESIGN METHOD	149
6.1	General	149
6.2	Local Buckling of Unstiffened Element	150
6.2.1	General	150
6.2.2	Rotational Edge Restraint Factor	151
6.2.2.1	Channel and I Sections Subjected to Uniform Compression	153
6.2.2.2	Channel and I Sections Subjected to Uniform Bending	157
6.2.2.3	Rotational Edge Restraint Factor of Miscellaneous Sections	161
6.2.3	Elastic and Inelastic Buckling	162
6.3	Elastic Postbuckling Behavior of Unstiffened Elements	171
6.4	Analysis of Compression Members	175
6.5	Summary and Conclusions	179
CHAPTER 7.	SUMMARY AND CONCLUSIONS	181
7.1	Summary and Conclusions	181
7.2	Scope for Future Investigation	184
APPENDIX A.	EFFECTIVE WIDTH EQUATIONS FOR STIFFENED ELEMENTS	186
APPENDIX B.	COMPARISON OF EFFECTIVE WIDTH EQUATIONS AND POSSIBLE DESIGN PROCEDURES	188

B.1	General	188
B.2	Comparison of Effective Width Equations and Test Results of Stub-Columns and Beams	189
B.3	Flexural Buckling Strength of Columns	191
B.3.1	Tangent Modulus Method	192
B.3.2	Modified Column Research Council Method	192
B.3.3	Columns With Locally Buckling Stiffened Elements	196
B.3.4	Computation of Flexural Buckling Strength of Columns	199
B.4	Summary and Conclusions	207
	LIST OF REFERENCES	209
	TABLES	215
	FIGURES	247

LIST OF TABLES

- 2.2.1 Local Buckling and Postbuckling Parameters of Unstiffened Elements
- 3.2.1 Mechanical Properties of Hot Rolled Steel Sheets for Column Specimens
- 3.2.2 Stub-Column Specimen Dimensions
- 3.4.1 Local Buckling Coefficient from Stub-Column Tests
- 3.4.2 Experimental Effective Width at Ultimate Load
- 3.4.3 Stub-Column Specimen Dimensions
- 3.4.4 Initial Imperfection Parameter in Effective Width Equation
- 3.4.5 Comparison of Effective Width of Stub-Column Unstiffened Flanges
- 4.2.1 Dimensions and Section Properties of Compression Specimens
- 4.4.1 Test Results of Compression Specimens
- 4.4.2 Section Properties and Test Results of DeWolf's Compression Specimens
- 4.4.3 Dimensions and Section Properties of Bijlaard's Aluminum Compression Specimens
- 4.4.4 Section Properties and Test Results of Bijlaard's Aluminum Compression Specimens
- 4.4.5 Section Properties and Test Results of Stub-Column Specimens
- 4.4.6 Section Properties and Test Results of Slender Compression Specimens

- 5.2.1 Material Properties of Hot Rolled Steel Sheets for Beam Specimens
- 5.2.2 Dimensions of Beam Specimens
- 5.4.1 Theoretical and Experimental Moments of Beam Specimens
- 5.4.2 Elastic Local Buckling and Postbuckling Test Results of Beam Specimens
- 5.4.3 Ultimate Compressive Strain of Beam Specimens
- 6.2.1 Local Buckling Coefficient of Unstiffened Elements in Short Compression Members
- 6.2.2 Local Buckling Coefficient of Unstiffened Elements in Flexural Members
- 6.2.3 Compression Strain Capacity of Unstiffened Elements in Flexural Specimens
- 6.3.1 Effective Widths of Unstiffened Elements in Short Compression Members
- 6.3.2 Effective Widths of Unstiffened Elements in Flexural Members
- 6.3.3 Effective Widths of Unstiffened Elements in Short Compression Members
- 6.3.4 Effective Widths of Unstiffened Elements in Flexural Members

- B.2.1 Comparison of Effective Widths - Stub-Columns
- B.2.2 Comparison of Effective Widths - Beams
- B.3.1 Dimensions and Section Properties of Columns With Stiffened Elements
- B.3.2 Test Results of Columns With Stiffened Elements

LIST OF FIGURES

- 1.1 Common Cold-Formed Structural Shapes
- 1.2 Unstiffened Element Idealization
- 1.3 Out of Plane Deflection Diagram of Unstiffened
Compression Element
- 1.4 Stress Distribution in Unstiffened Element in the
Postbuckling Range
- 1.5 AISI Design Curves - Unstiffened Elements
- 2.2.1 Unstiffened Element Idealization
- 2.2.2 Elastic and Inelastic Local Buckling Coefficients
- 2.2.3 Plastic Buckling Strain versus w/t Ratio of
Unstiffened Elements
- 2.2.4 Average Stress versus Maximum Supported Edge Stress -
Perfectly Flat Unstiffened Elements
- 2.2.5 Postbuckling Parameters versus Buckling Coefficient -
Unstiffened Elements
- 2.2.6 Effective Width of Perfectly Flat Unstiffened Elements
- 2.2.7 Postbuckling Out of Plane Deflection of Perfectly
Flat Unstiffened Elements
- 2.2.8 Postbuckling Out of Plane Deflection of Perfectly
Flat Unstiffened Elements
- 2.2.9 Effective Width of Unstiffened Elements With Initial
Imperfection
- 2.2.10 Postbuckling Out of Plane Deflection of Unstiffened
Elements With Initial Imperfections

- 3.2.1 Typical Stress Strain Curve of Steel Sheets
- 3.2.2 Stub-Column Test Specimen
- 3.2.3 Stub-Column Test Set-Up and Specimen Section With Strain Gages
- 3.2.4 Wave Amplitude Measuring Instrument
- 3.2.5 Stub-Column Specimen - Before Test
- 3.2.6 Stub-Column Specimens - After Test
- 3.3.1 Determination of Local Buckling Stress - Experimental Method
- 3.4.1 Axial Load versus Shortening of Stub-Column
- 3.4.2 Comparison of Effective Width Equations and Stub-Column Test Results
- 3.4.3 Effective Width Equation (eqn. 3.4.1) Initial Imperfection Parameter
- 3.4.4 Average and Maximum Stresses at Ultimate Load of Unstiffened Elements
- 3.4.5 Comparison of Effective Width Equations
- 3.4.6 Comparison of Sub-Ultimate and Ultimate Test Results and the Effective Width Equations
- 3.4.7 Maximum Amplitude of Postbuckling Deflection of Unstiffened Elements
- 4.2.1 End Fixture for Column Tests
- 4.2.2 Location of Dial Gages in Column Tests
- 4.2.3 Compression Members Test Set-Up
- 4.2.4 Compression Members After Failure
- 4.3.1 A typical Southwell Plot

- 4.4.1 Bijlaard and Fischer's Specimen Cross-Section
- 4.4.2 Comparison of Test Results and the AISI Specification
to
- 4.4.6 Column Curve
- 4.4.7 Typical Compressive Stress Redistribution in
Locally Buckling Unstiffened Elements
- 4.4.8 Idealization of Effective Area of Unstiffened
Elements in the Postbuckling Range
- 4.4.9 Effective Sections and Stress Distribution for
Column Specimens
- 4.4.10 Comparison of Test Results, the Analytical Solution
to and Effective Width Equation (eqn. 3.4.1) Column
- 4.4.21 Curves
- 4.4.22 Comparison of Test Results and the Effective Width
to
- 4.4.33 Equation (eqn. 3.4.5) Column Curves.
- 5.2.1 Flexural Specimens - Section and Strain Gage Locations
- 5.2.2 Beam Test Set-Up and Instrumentation
- 5.2.3 Beam Specimens Load Set-Up
- 5.4.1 Typical Moment Curvature Diagram of Specimens
- 5.4.2 Typical Moment Curvature Diagram of Specimens
- 5.4.3 Typical Load versus Central Deflection Diagram
- 5.4.4 Comparison of Sub-Ultimate and Ultimate Beam Test
Results and Modified Form of Effective Width Equations
- 5.4.5 Comparison of Effective Width Equations and Beam Test
Results
- 5.4.6 Limiting w/t ratio of Unstiffened Elements
- 5.4.7 Plastic Compressive Strain Capacity of Unstiffened
Elements

- 6.2.1 Distorted Shape and Edge Moments Due to Local
&
- 6.2.2 Local Buckling of Unstiffened Elements
- 6.2.3 Variation of Buckling Coefficient With the K_y/K_e
Ratio
- 6.4.1 Column Flexural Buckling Strength Curves and Test
to
- 6.4.9 Results

- A.1 Comparison of Effective Width Equations for Stiffened
Elements

- B.2.1 Comparison of Effective Width Equations and Test
Results

- B.3.1 Tangent Modulus Column Curves and Test
to
- B.3.9 Results

- B.3.10 Modified CRC Curves and Test
to
- B.3.18 Results

- B.3.19 DeWolf's Column Specimen With S tiffened Elements

- B.3.20 Modified CRC Curves and Test
to
- B.3.23 Results

NOMENCLATURE

A	Total area of a cross section
A_0, A_1	Parameters of wave amplitude
B, b	Total width of a flange
BC	Width of a Compression Flange
BT	Width of a tension flange
B_1 through B_5	Constants
C	Coefficient of proportionality between moment and angle rotation at an edge
D	Depth of a specimen, Flexural rigidity
D'	Flexural rigidity
E	Young's modulus
e	Strain
F	Stress function
I	Moment of inertia
K	Local buckling coefficient
L, L_w	Length of a local buckling wave
L	Effective length of a column
M	Moment
P	Load
P_e	Euler buckling load
Q	Form factor
T_f	Thickness of a flange element
T_w	Thickness of a web element

t	Thickness of a plate element
w	Flat width of an element
Z, Z_0	Amplitude of a local buckling wave
ϵ	Rotational edge restraint factor
Δ	Non-dimensional parameter of local buckling wave amplitude
ϕ	Curvature
η, η'	Plasticity index
μ	Poisson's ratio
σ	Stress

Subscripts:

av	Average value
c	Compression
cr	Critical value
e	Elastic value
expt.	Experimental value
lim.	Limiting value
p	Plastic value
E_r	Reduced modulus value
E_s	Secant modulus value
E_t	Tangent modulus value
theory	Theoretical value
total	Total value
u	Ultimate value
x,y	Coordinate directions
y	Yield value

ABSTRACT

The elastic and inelastic local buckling and elastic postbuckling behavior of unstiffened elements in cold-formed steel members and their effects on bending of beams and overall flexural buckling of columns have been investigated.

An analytical investigation of the elastic and inelastic local buckling and the elastic postbuckling behavior of unstiffened elements with an elastic rotational edge restraint has been carried out. Results of experiments on short columns, long columns and beams are presented and compared with the analytical solution.

An effective width equation for the elastic postbuckling range of the unstiffened element behavior has been derived by modifying the analytical solution to include the effects of initial imperfections, as indicated by test results. An empirical effective width equation, having a format similar to the AISI effective width equation for stiffened elements, has also been presented. An equation for the inelastic compressive strain capacity of unstiffened element has been derived.

On the basis of the equations derived, methods for calculating the strength of cold-formed beams and columns with unstiffened compression elements subject to local buckling, are presented.

Chapter I
INTRODUCTION

1.1 General

Intensive theoretical and experimental investigations have led to recognition of modes of failure of structures and better understanding of factors governing such failures. On the other hand, recent advances in the area of reliability and probability have led to more accurate definition of loads, load factors and under strength factors. Developments in these two areas have brought about a change in design philosophy in the last few decades which has led to the replacement of time honored allowable stress design method by design based on ultimate strength of structures. Although other factors such as deflection and distortion of sections in the range of operating load may sometimes govern the design, the ultimate strength is the most commonly encountered design criterion.

Common modes of failure associated with steel structures are: (1) instability; (2) ductile fracture; (3) brittle fracture and (4) fatigue. Among these, instability is often the cause of failure of steel structures. The collapse may be either due to overall buckling of a member in a structure or a consequence of local buckling of some element in a member.

Local buckling of elements in a member takes place when the elements are very thin, as in cold-formed members, and are subject to compressive, bending or shear stresses.

1.1.1 Cold-Formed Structural Steel Members

Cold-formed structural steel members are fabricated either by cold rolling or press braking steel sheets to the desired shape. The forming process introduces strain hardening at the points of bending and the extent of the strain hardening depends upon the radius of the bend and the thickness of the material. The region of cold work is more localized in the process of press braking than in the cold rolling. In contrast, hot rolled members are subject to residual stress as a result of differential cooling and cold straightening.

Hot rolled steel members are commonly proportioned so that they do not buckle locally before the yield stress is reached. In fact, in most cases, elements are stocky enough even to undergo sufficient plastic strain leading to the overall failure of the structure by the formation of the collapse mechanism, or overall buckling of the compression member. The Manual of Steel Construction^{(1)*} serves as a guide for the design of such hot rolled steel

*Superscripts designate the entries in the list of references.

members.

Economic considerations often dictate the use of light gage steel members in structures covering a large area and subject to light loads. In contrast to hot rolled members, the cold forming process allows practically unlimited width to thickness ratio. Consequently, thin elements of cold-formed members may undergo local buckling before the ultimate load, thus decreasing the strength appreciably. This represents the primary difference between cold-formed and hot rolled steel members. The Specification for the Design of Cold-Formed Steel Structural Members² provides guidelines for the design of light gage steel members.

Generally the cold-formed sections used in practice are open in form, though closed tubular sections can be roll-formed or made up by joining two open sections. Fig. 1.1 shows some of the commonly encountered cold-formed structural shapes. It can be seen that the sections are composed of two typical types of elements:

- (1) Stiffened elements having two edges parallel to the longitudinal axis of the member supported against translation normal to the plane and elastically restrained against rotation by the adjoining elements.
- (2) Unstiffened elements having one edge parallel to the longitudinal axis of the member supported against trans-

lation normal to the plane and elastically restrained against rotation by the adjoining element and the other parallel edge is completely free to translate and rotate.

In the next few sections the elastic and inelastic buckling and postbuckling behavior of unstiffened elements and their effect on member behavior will be studied qualitatively. In the process, a brief review of other investigators work in this area will be presented.

1.2 Behavior of Unstiffened Element Under Compression

1.2.1 Local Buckling of Unstiffened Element

The history of the stability of plates under compression goes back to 1891, when Bryan³ presented an analysis for the buckling load of a rectangular plate simply supported on all four sides and subject to uniform compressive stress in one direction, using the energy method. Subsequently, though many investigators studied the problem of plate buckling, credit for the most extensive treatment of the buckling of plates with various boundary conditions belongs to Timoshenko⁴ who used the energy method to study the local instability of plates.

The unstiffened compression element of a member can be idealized as shown in Fig. 1.2 with one unloaded edge simply supported and elastically restrained against ro-

tation and the other edge fully free. If the plate is perfectly flat to begin with, it remains flat until the compressive stress equals critical buckling stress, beyond which it deflects normal to the plane and buckles into waves. Using the small deflection equation of the equilibrium of plates, buckling stress σ_{cr} is given by the equation;

$$\sigma_{cr} = \frac{K \pi^2 E}{12(1-\mu^2)(w/t)^2} \quad (1.2.1a)$$

where E is the Young's modulus, μ the poisson's ratio, w flat width of the element and t the thickness. The buckling coefficient K depends upon the edge rotational restraint, the type of loading and aspect ratio of the plate (ratio of length of the plate L to width of the plate w). Lundquist⁵ has computed the variation of buckling coefficient K of unstiffened elements subject to uniform compression for various values of the rotational edge restraint and aspect ratio. The buckling coefficient K of long plates (high aspect ratio) is independent of the aspect ratio and depends only on the rotational edge restraint, varying from 0.425 for the hinged edge condition to 1.277 for the fixed edge condition.

Contrary to the column and shell postbuckling behavior, the local buckling of plates does not mean the end of the useful strength of the plates. The buckled configuration of a plate is stable due to the stabilizing in-

plane tensile and shear stresses induced. The postbuckling behavior can be investigated analytically by using the large deflection equations of Von Karman. Curve OA (fig. 1.3) shows the stable postbuckling range where the increase in the amplitude of buckling waves is accompanied by an increase in the applied compressive stress. The compressive stress can be increased in the postbuckling range until yielding occurs in some region of the buckled plate which initiates load shedding, and the ultimate strength of the plate depends on the yield stress of the material. Since the local buckling stress increases as the flat width to thickness ratio (w/t) decreases, for smaller values of the w/t ratio yielding may take place before the element buckles locally. Local buckling of the unstiffened element in the inelastic range will be treated in section 1.2.4.

The bifurcation type of buckling, which is a term used to describe the sudden out of plane deformation experienced at critical stress, is encountered only in the case of an ideally flat plate. Actual plates have initial imperfections and the out of plane deformation starts to increase gradually even before the buckling stress is reached and near the critical state, the out of plane deformation increases at a faster rate. This type of behavior can be analyzed by using the large deflection equations. The curve O'A' in fig. 1.3 shows the typical load deflec-

tion behavior of a real plate. It can be seen that the difference in behavior between the real and ideal plate is most pronounced near the critical range.

So far, the local buckling of the unstiffened element has been studied without any reference to supporting elements. In an actual structure, the unstiffened element appears as a part of a member. Hence, the rotational edge restraint of the unstiffened element depends on the length of the buckling waves, the compressive stress on the supporting element and the stiffness of the supporting element. Many investigators ^{6,7,8,9} have presented analytical procedures, charts and tables for calculating the local buckling coefficient of unstiffened elements in different members. Some of these are more difficult to use than others in routine design applications.

1.2.2 Postbuckling Behavior

It was observed that even after the local buckling plate elements can sustain additional load, with increasing out of plane deformation, before failure. Consequently, all the design procedures based on strength take into consideration this postbuckling behavior.

In an ideally flat unstiffened element, compressive stress is uniformly distributed until the local buckling takes place. After this, there is a redistribution of

stress over the width of the plate with the stress near the supported edge being higher than that at the free edge. The wave length of buckles tend to become shorter, and more and more stress is redistributed towards the supported edge as the compressive stress is increased. The stress distribution in a typical unstiffened element after local buckling is shown in fig. 1.4. It has been observed that the failure of the element takes place when the compressive stress at the supported edge of the element (which is the maximum membrane compressive stress over the width) reaches the yield stress of the material. In a real plate, because of initial imperfections, the redistribution of stress takes place as the loading progresses even before the critical stress is reached. However, the difference between an ideally flat element and a real element with initial imperfections is very little in the advanced stages of the postbuckling range.

For design purposes, the non-uniform stress distribution over the width of the plate in the postbuckling range is idealized in two ways (fig. 1.4):

- 1) Effective width method: In this design idealization, the stress at the supported edge is assumed to be uniformly distributed over an effective width (b_e), so that the total load carried by the plate is equal to the actual load on the buckled plate.

2) Average or effective stress method: In this design idealization, an equivalent average stress is distributed over the entire width (w) of the plate, so that the total load carried by the plate is equal to the actual load on the buckled plate.

The effective width method is more popular of the two idealizations and is used extensively due to certain inherent advantages. Hence, only effective width formulation will be presented in this investigation.

The first use of effective width representing the postbuckling behavior of the stiffened element was presented by Von Karman.¹⁰ The approximate equation presented by him can be written in the form:

$$b_e/w = \sqrt{\sigma_{cr}/\sigma_{e \max}} \quad (1.2.1)$$

where b_e is the effective width, w is the total width, σ_{cr} is the local buckling stress and $\sigma_{e \max}$ is the maximum stress at the supported edges. Many other formulae for the effective width of a variety of plate elements have been proposed by others and tabulated by Gerard.¹¹ All these equations are for ideally flat plates and are applicable directly to real plates with initial imperfections only in the advanced stages of postbuckling. However, as already mentioned, in real plates the effective

width begins to decrease even before the buckling stress is reached, because of initial imperfections. Winter,^{12,13} on the basis of experimental investigation, modified Karman's equation to take into account effects of initial imperfections. Winter's equations can be written as¹⁴:

$$b_e/w = \sqrt{\sigma_{cr}/\sigma_{e \max}} (1 - .22\sqrt{\sigma_{cr}/\sigma_{e \max}}) \quad (1.2.2)$$

$$b_e/w = 1.19\sqrt{\sigma_{cr}/\sigma_{e \max}} (1 - 0.3\sqrt{\sigma_{cr}/\sigma_{e \max}}) \quad (1.2.3)$$

Eqn. 1.2.2 is the effective width equation for the stiffened elements and eqn. 1.2.3 is for the unstiffened elements. Even though the effective width equation for unstiffened elements has been available for some time now, its use has been limited because of the lack of extensive experimental investigation to support the validity of the equation and the fear of excessive cross section distortion in the postbuckling range.

There have been many analytical investigations^{15,16,17,18,19} of the postbuckling behavior of stiffened elements. All the investigators assume a deflected wave form and determine the amplitude by some approximation procedure. The author is not aware of any analytical investigation of the postbuckling behavior of unstiffened elements. A more detailed survey of the analytical investigations will be presented in Chapter 2.

The crippling strength of plates in edge compression can be obtained by substituting the yield stress (σ_y) for the maximum stress at the supported edge ($\sigma_{e \max}$). This condition is sufficiently accurate for thin plates with $(\sigma_y/\sigma_{cr}) \geq 1.5$ ⁽³¹⁾. For plates buckling near the yield stress, strain at the supported edge at the ultimate load is usually larger than the yield strain, though this does not increase the strength appreciably in the case of elastic plastic materials.

Objection has been raised by many^{17,19} to using the same effective width equation for both the ultimate and subultimate ranges of the postbuckling behavior. The argument has been:¹⁹ "Stiffness of a plate in compression at subultimate load is a function of end shortening of the plate, which is an integrated effect along the length of the plate. Collapse, however, at $\sigma_{e \max} = \sigma_y$, is a local phenomenon." Given the fact that (1) there is usually scatter in the postbuckling range due to the statistical nature of initial imperfections, and (2) subultimate stiffness is usually used in the computation of quantities involving many inherent approximations (deflection and stiffness of flexural members, and stiffness of axially loaded columns); it seems reasonable to use the effective width equation corresponding to the ultimate load for the computation of subultimate stiffness also, thus obtaining a conservative estimate of the subultimate

stiffness.

1.2.3 Local Buckling in the Inelastic Range

So far, the discussion has centered around slender plates which experience elastic postbuckling. As the width to the thickness ratio (w/t) of an element decreases, the theoretical elastic buckling stress increases as given by the eqn. 1.2.1. Below a limiting value of the flat width to thickness ratio $(w/t)_{lim}$ the theoretical buckling stress of a flat plate is larger than the yield stress. This limiting value can be found by substituting the yield stress (σ_y) for the local buckling stress (σ_{cr}) and solving for (w/t) ratio.

$$(w/t)_{lim} = \sqrt{\frac{12(1-\mu^2)}{\pi^2 E}} \sqrt{\sigma_y / K} \quad (1.2.4)$$

A perfectly flat plate having a width to thickness ratio less than or equal to the limiting ratio given by eqn. 1.2.4 will not buckle locally and remains fully effective to resist uniform compression until the yield stress is reached. However, for a real plate the limiting ratio will be smaller than that given by eqn. 1.2.4, because initial imperfections and non-linearity of the stress strain relationship near the yield stress tend to reduce the effective width even before the local buckling stress is reached.

Ros and Eichinger,²⁰ Bijlaard,²¹ and Ilyushin²² have formulated rational theory of the stability of plates beyond the elastic limit, based on modern failure theories. Bijlaard's theory seems to show good agreement with the test results. Stowell²³ using Ilyushin's general modification of Bijlaard's theory succeeded in developing a Unified Theory of Plastic Buckling of Columns and Plates. He has derived expressions for the plasticity index η which when multiplied by the elastic local buckling stress $(\sigma_{cr})_e$ yields the inelastic buckling stress for elements with different boundary conditions.

$$(\sigma_{cr})_p = \eta (\sigma_{cr})_e \quad (1.2.5)$$

In this equation, $(\sigma_{cr})_p$ and $(\sigma_{cr})_e$ correspond to plastic and elastic buckling stress respectively. Stowell²⁴ also has presented a procedure for computing the plastic local buckling stress of assembly of plates.

Bleich²⁵ has derived a semiempirical theory for the plastic buckling, which takes into account the directional dependence of the elastic plastic characteristics of a plate compressed into the plastic range. An analysis of plates buckling in the strain hardening range is presented by Haaiker^{26,27} using general expression for the buckling strength and assuming the material to have become orthogonally isotropic.

It has been suggested^{28,29,30} that the postbuckling behavior in the inelastic range can be approximately dealt with by using strains instead of stresses in the effective width equations. Assuming the rigid-plastic material behavior and a geometry of plastic mechanism, Walker and Murray³¹ have arrived at the postbuckling stiffness in the plastic range of a plate assembly using numerical minimization.

1.2.4 Effect of Local Buckling on Structural Members

In preceding sections, buckling and postbuckling behavior of the unstiffened compression elements was briefly discussed without any reference to the implications of local buckling of elements on the behavior of members. In practice, structural members are made up of an assembly of plates. Behavior of such members subject to compression and/or bending is influenced by the local buckling of the component plates. In this section, a review of the effect of local buckling of component plate elements on the member behavior and a survey of work done by other investigators in this area is presented.

Cold-formed steel columns often consist of stiffened and unstiffened elements which undergo local buckling. If the slenderness ratio of such a column is high, then the column may buckle before the local buckling of com-

ponent plates. However, in the case of columns not having a high slenderness ratio, the component plates may buckle locally before the overall buckling of the column. Since local buckling of elements does not mean the end of their load carrying capacity, columns can be subject to additional compression even after local buckling of component plates. The failure of short columns is initiated by the crippling of the component plates buckling locally, and intermediate columns fail by overall buckling after the local buckling of the component plates. The reduction in the stiffness of the component plates due to local buckling decreases the stiffness of the column, and hence reduces the buckling load. The effect of initial imperfections tend to reduce the effective stiffness of the component plates even before local buckling, complicating the problem further.

Bijlaard²⁶ was one of the earliest investigators to study the buckling strength of columns in the postbuckling range of the component plates. Other investigators^{14,27,28,29,31,32} have presented analytical, empirical and approximate solutions for the interaction of the overall buckling of columns of various shapes and local buckling of component plates. In most of these works,^{14,29,30,32} either the change in the slenderness ratio or the effec-

tive modulus obtained from effective width equations is considered in the column buckling equation. These methods involve tedious numerical procedures, unless simplifying assumptions are made.

In flexural members, if the compression flanges are thin plates, they may buckle locally before the member fails. The member behaves linearly until the compression flange effective width begins to reduce. An increase in the applied load beyond this is accompanied by a decrease in the effective width and a shifting of the neutral axis toward the tension flange. In the postbuckling range, the behavior becomes nonlinear, because the effective width depends upon the stress at the supported edge and this stress depends upon the section modulus and hence on the effective width. A decrease in the effective width due to local buckling also reduces the lateral buckling resistance of the compression flange. In the moment gradient region of a beam with a compression flange in the postbuckling range, the effective width of the compression flange and hence the moment of inertia of the member varies from section to section. This introduces additional complexity to the analysis of indeterminate structures with locally buckling elements. The local buckling of the compression elements in the inelastic range introduces limitations on the inelastic rotation capacity of members,

thus hindering the complete redistribution of moments as assumed in plastic design.

Many investigators have analyzed inelastic buckling of compression elements in flexural members. Lay and Galambos^{33,34} have studied the inelastic behavior of wide flange beams under uniform moment and moment gradient. Many experimental investigations have been carried out to study the inelastic behavior of beams^{35,36,37}. The effect of the elastic local buckling of both stiffened and unstiffened compression elements on the flexural strength of beams has also been studied extensively^{10,12,38,39,40}, where some form of the effective width equation is used to compute the section properties in the postbuckling range. The ultimate load is computed using the effective width, assuming that failure takes place when the stress at the supported edge reaches the yield stress.

1.3 Purpose of the Investigation

The purpose of this investigation is to study the elastic and inelastic local buckling and postbuckling behavior of unstiffened elements and the effect of this local buckling on the overall buckling of columns and bending of beams.

At this stage, it is appropriate to look at the American Iron and Steel Institute guidelines for the design of unstiffened element as outlined in the Specifica-

tion for the Design of Cold-Formed Steel Structural Members.² Allowable stresses for various values of the flat width to thickness ratio (w/t) of unstiffened elements are arrived at by using a sufficient factor of safety to limiting stresses. The limiting and allowable stresses are shown in Fig. 1.5. Curve C is the buckling stress of the unstiffened elements obtained by conservatively assuming the value of the buckling coefficient K to be 0.5. If compression elements are perfectly flat and if the material has a sharp yield point, the horizontal line A drawn at the yield stress will be the upper limit of the local buckling stress of the element. However, real unstiffened compression elements are rarely ideally flat and the material may not have a sharp yield point either as a result of the sheet forming process or the cold-forming process of the section. These tend to lower the local buckling stress for elements having the theoretical buckling stress around yield stress. Line B corresponds to the limiting value of the buckling stress in this range of w/t ratio. The upper and lower limits the line B are set at $144/\sqrt{\sigma_y}$ and $63.3/\sqrt{\sigma_y}$ respectively, based on test results. Curve D represents the postbuckling strength of the material when the local buckling takes place elastically. The postbuckling reserve, indicated by the difference between curve C and D, becomes larger with the increase in w/t ratio. Allowable stress for de-

sign is obtained from the limiting value, using a factor of safety of 1.67 with the exception of the region where elastic buckling takes place. In the case of angle sections under compression, which have the lowest buckling coefficient and deform considerably in the postbuckling range, the design value is obtained using a factor of safety of 1.67 to curve C. For other unstiffened elements in other sections allowable stress is given by line d with the postbuckling strength providing a factor of safety from 1.67 to as high as 4.0.

This type of allowable stress approach has been followed for unstiffened elements because of the lack of sufficient experimental evidence supporting an effective width equation for the postbuckling range and a concern about excessive distortion in the working range due to local buckling. It should, however, be mentioned that the idea of an effective width equation for unstiffened elements is not something new. As already pointed out in section 1.2.2, some investigators have already proposed effective width equations for unstiffened elements, and some of these equations are for stainless steel elements. One of the main objectives of this investigation has been to study unstiffened compression elements systematically in order to develop an effective width equation and get an idea about the out of plane deformation in the post-

buckling range.

For low values of w/t ratio of unstiffened elements, the buckling stress is nearly equal to the yield stress. However, the compressive strain at the local buckling is usually larger than the yield strain and the value of the compressive strain at local buckling increases with a decrease in the w/t ratio. This inelastic strain capacity of compression elements having a low w/t ratio could be used to take advantage of the section plastification and the moment redistribution in indeterminate structures. The determination of this inelastic strain capacity of unstiffened elements has been another objective of this investigation.

1.4 Scope of the Investigation

1.4.1 Desired Information

Based on the objectives specified in the last section, the following information is desired for the unstiffened compression elements.

- 1) Method of determining the local buckling stress.
- 2) Effective width equation for the postbuckling range.
- 3) Out of plane deformation in the postbuckling range.
- 4) Limiting value of the flat width to thickness ratio (w/t) below which the unstiffened com-

pression element remains fully effective until the yield stress is reached.

- 5) Inelastic strain capacity of compression elements having a w/t ratio less than the limiting value of the w/t ratio.
- 6) Effect of local buckling of unstiffened elements on the overall buckling of columns.
- 7) Effect of local buckling of unstiffened compression flanges on the bending of beams.

1.4. Analytical and Experimental Investigations

In contrast to the hot rolled sections where pre-designed shapes are selected, the light gage steel design presents a wide range of shapes and dimensions to choose from. This versatility in design, however, requires that one understand the behavior of elements forming a member, in order to be able to design members for any type of loading condition. A good understanding of the behavior of an element can be best obtained by completely isolating the element and studying it exactly under the same boundary conditions as one expects to use it. However, it is often difficult to simulate such boundary conditions exactly in an isolated environment. Sometimes it is even difficult to know the nature of the boundary condition that is imposed on an element in a member. Hence, the best method of studying the behavior of unstiffened elements under

these constraints is to test a member, the behavior of which is affected only by the local buckling of component unstiffened elements under axial compression. This reasoning led to the experimental investigation using stub columns with the unstiffened elements in compression. Having obtained the information about the element behavior from such tests, it is then logical to study members, such as beams and columns, which are encountered in practical structures. This will result in an understanding of the effect of the local buckling of component elements on the behavior of members in a structure, and thus the behavior of the structure itself.

This investigation has been planned with this basic philosophy in mind. An analytical investigation of the buckling and postbuckling behavior of the unstiffened elements was carried out to understand the influence of various parameters. The following specimens were tested in order to obtain the experimental information about the element and member behavior.

- 1) Ten stub columns with five different values of w/t ratio of unstiffened elements in compression in order to understand the element behavior.
- 2) Three long columns of different lengths corresponding to each of the five stub column sections to study the effect of local buckling on the flexural buckling of columns.

- 3) Eighteen beams with unstiffened elements in compression, to study the elastic and inelastic local buckling behavior of compression elements and their effect on flexural members.

1.5 Summary

A brief description of unstiffened compression elements as encountered in cold-formed structural applications was presented. Following this, the behavior of unstiffened compression elements and members with unstiffened compression elements was discussed qualitatively. Existing literatures in the area were also briefly reviewed. Subsequently, the objective and scope of the investigation were enumerated.

Chapter 2

ANALYTICAL INVESTIGATION

2.1 Review of Analytical Methods

Analytical investigation of the stability of plates and shells are difficult, especially as encountered in practice with complex boundary conditions. The stability of unstiffened compression elements, governed by the small deflection equation of plates subject to compression, has been solved by Timoshenko⁴ using the energy method. Closed form solutions for the two simple boundary conditions of hinged and fixed supported edge are available. However, when an exact solution to the stability of unstiffened elements with elastic rotational restraint at the supported edge is attempted, a transcendental equation not lending itself to a closed form solution is encountered. An approximate solution to this problem has been proposed in "closed" form.⁵ Local buckling in the inelastic range is affected by the non-isotropy of the material after yielding. This problem has been investigated by many researchers^{21,22,23,25}.

An analytical solution of the postbuckling behavior becomes even more involved. The postbuckling behavior of a plate, subject to compression, is governed by two

partial differential equations of the fourth order, which were originally proposed by Von Karman. Analytical solutions for the postbuckling behavior of stiffened elements, by assuming an approximate deflected shape, have been proposed^{16,17,18,19,46}. Although a similar procedure can be used to analyze the postbuckling behavior of unstiffened elements, there is no such solution to the author's knowledge. Investigations of the postbuckling behavior of plates also have been attempted through numerical methods, such as finite element and finite difference, using plate bending elements or equations. These solutions are too tedious to use in a design office situation and do not yield a closed form solution. Most of the equations used in the design of thin elements having postbuckling strength are semi-empirical in nature, and are based on experimental results. In the following sections, an analytical investigation of elastic buckling, inelastic buckling, and postbuckling behavior of unstiffened elements will be presented.

2.2.1 Elastic Local Buckling Stress

The local buckling stress of unstiffened elements with elastic moment restraint at support (fig. 2.2.1) will be solved in a "closed" form using an approximate de-

flected shape. The small deflection equation of plate bending subject to membrane stresses can be written as

$$D\left(\frac{\partial^4 Z}{\partial x^4} + 2\frac{\partial^4 Z}{\partial x^2 \partial y^2} + \frac{\partial^4 Z}{\partial y^4}\right) + t\left(\sigma_{xx}\frac{\partial^2 Z}{\partial x^2} + \sigma_{yy}\frac{\partial^2 Z}{\partial y^2} + 2\sigma_{xy}\frac{\partial^2 Z}{\partial x \partial y}\right) = 0 \quad (2.2.1)$$

where Z is the out of plane deflection, t the thickness, D the flexural rigidity and σ the membrane stress in the plate. This equation is attributed to St. Venant. The normal stress in x direction and shear stress in a perfectly flat plate, subject to compression only in the y direction, are zero before local buckling. Hence, eqn. 2.2.1 reduces to

$$D\left(\frac{\partial^4 Z}{\partial x^4} + 2\frac{\partial^4 Z}{\partial x^2 \partial y^2} + \frac{\partial^4 Z}{\partial y^4}\right) + t\sigma_{yy}\frac{\partial^2 Z}{\partial y^2} = 0$$

or

$$D(\nabla^4 Z) + t\sigma_{yy}\frac{\partial^2 Z}{\partial y^2} = 0 \quad (2.2.2)$$

The boundary conditions of the unstiffened element are: (1) deflection and moment are zero at loaded edges; (2) deflection is zero and moment is proportional to rotation at the unloaded supported edge; and (3) shear and moment are zero at the unloaded free edge. These boundary conditions can be written as

$$Z = \frac{\partial^2 Z}{\partial y^2} = 0 \quad \text{at } y = 0, L$$

$$Z = 0$$

$$D \frac{\partial^2 Z}{\partial x^2} = C \frac{\partial Z}{\partial x} \quad \text{at } x = 0$$

$$\left(\frac{\partial^2 Z}{\partial x^2} + \mu \frac{\partial^2 Z}{\partial y^2} \right) = 0$$

$$\text{at } x = W$$

$$\left(\frac{\partial^3 Z}{\partial x^3} + (2-\mu) \frac{\partial^3 Z}{\partial x \partial y^2} \right) = 0 \quad (2.2.3)$$

where C is the rotational edge restraint stiffness ($C = M/\theta$). It is assumed that the deflected shape of the unstiffened element after local buckling is given by

$$Z = A_1 f(x) \sin \frac{\pi y}{L}$$

$$= A_1 \sum_{n=1}^4 C_n \left(\frac{x}{w} \right)^n \sin \frac{\pi y}{L} \quad (2.2.4)$$

This deflected shape satisfies boundary conditions (1) along the loaded edges automatically. Substituting eqn. 2.2.4 in the boundary condition eqn. 2.2.3, a set of four simultaneous equations given below are obtained.

$$\begin{bmatrix} 1 & 0 & 0 & 0 \\ -\epsilon/2 & 1 & 0 & 0 \\ -\mu \frac{\pi^2 w^2}{L^2} & (2-\mu) \frac{\pi^2 w^2}{L^2} & (6-\mu) \frac{\pi^2 w^2}{L^2} & (12-\mu) \frac{\pi^2 w^2}{L^2} \end{bmatrix} \begin{bmatrix} C_1 \\ C_2 \\ C_3 \end{bmatrix} = \begin{bmatrix} 1 \\ 0 \\ 0 \end{bmatrix}$$

$$\begin{bmatrix} -(2-\mu) & -2(2-\mu) & (6-(6-3\mu)\frac{\pi^2 w^2}{L^2}) & (24-(8-4\mu)\frac{\pi^2 w^2}{L^2}) \\ \chi \frac{\pi^2 w^2}{L^2} & \chi \frac{\pi^2 w^2}{L^2} & & \end{bmatrix} \begin{bmatrix} C_1 \\ C_2 \\ C_3 \\ C_4 \end{bmatrix} = \begin{bmatrix} 0 \\ 0 \\ 0 \\ 0 \end{bmatrix} \quad (2.2.5)$$

where ϵ is the rotational edge restraint factor

($\epsilon = wC/D$). Constants C_1 through C_4 can be obtained by solving eqn. 2.2.5.

The small deflection eqn. 2.2.2 can be solved for buckling stress ($\sigma_{cr} = \sigma_{yy}$), by substituting Z given by eqn. 2.2.4 and using Galerkin's approximation as follows.

$$\begin{aligned} A_1 \int_0^L \int_0^W \nabla^4 Z f \sin \frac{\pi y}{L} dx dy \\ = -A_1 \frac{\sigma_{cr} t}{D} \int_0^L \int_0^W \frac{\partial^2 Z}{\partial y^2} f \sin \frac{\pi y}{L} dx dy \end{aligned} \quad (2.2.6)$$

Performing the integration and solving for buckling stress σ_{cr} ,

$$\sigma_{cr} = - \frac{D}{\pi^2 w^2 t} \frac{\sum_{n=0}^4 \sum_{m=1}^4 \frac{C_{4n} C_m}{(n+m+1)}}{\sum_{n=1}^4 \sum_{m=1}^4 \frac{C_n C_m}{(n+m+1)}} \quad (2.2.7a)$$

where

$$C_{4n} = \left[\frac{\pi^4 w^2}{L^2} C_n - \frac{2\pi^2 (n+2)!}{n!} C_{(n+2)} + \frac{L^2}{w^2} \frac{(n+4)!}{n!} C_{(n+4)} \right] \quad (2.2.7b)$$

with $C_n = 0$ when $n = 0$ and $n > 4$.

Since

$$\sigma_{cr} = - \frac{K\pi^2 D}{W^2 t} \quad (2.2.8a)$$

the buckling coefficient K is given by

$$K = \frac{1}{\pi^4} \frac{\sum_{n=0}^4 \sum_{m=1}^4 \left(\frac{C_{4n} C_m}{(n+m+1)} \right)}{\sum_{n=1}^4 \sum_{m=1}^4 \left(\frac{C_n C_m}{(n+m+1)} \right)} \quad (2.2.8b)$$

From equation 2.2.8b, it is seen that the buckling coefficient (K) depends upon the length of the wave and it is well known that for a given width (W) and the rotational edge restraint factor (ϵ), the buckling coefficient (K) is minimum at some discrete values of the length L . For high values of the aspect ratio (L/w), the buckling coefficient is nearly independent of length and is equal to the smallest value of the buckling coefficient. Since in a structure the aspect ratio of the component elements can be varied by varying the length of the member, only the smallest value of the buckling coefficient K is of interest. Fig. 2.2.2 and table 2.2.1 indicate the variation of the buckling coefficient K with the variation in the rotational edge restraint ϵ .

It has already been observed that the bifurcation

buckling is obtained only if the plate under compression is perfectly flat. In practice, no plate is perfectly flat and waving starts from almost the onset of loading. Consequently, one might be tempted to rule out the computation of the local buckling stress as an unnecessary academic exercise. However, it is important to have a knowledge of the local buckling stress, because this indicates the region where the effects of initial imperfections are most pronounced. The buckling stress is also a parameter, useful in the non-dimensional representation of postbuckling behavior, which will be demonstrated later in this chapter.

2.2.2 Inelastic Local Buckling

An analytical investigation of the local buckling in the inelastic range is complicated by the non-isotropic nature of the material beyond yielding. In this section, a brief treatment of the plastic buckling of plates, as proposed by Bijlaard and later modified by Ilyushin and Stowell, is presented.

Bijlaard²¹ studied the plastic buckling of plates by assuming that the distortion energy theory governs the plastic deformation and that the plastic part of the deformation is "quasi-isotropic"; that is, similar to the elastic deformation with the exception of the variable

modulus and Poisson's ratio of 0.5. He concluded that the buckling stress obtained using the flow theory was too high when compared with test results, whereas the buckling stress based on the deformation theory exhibited good agreement.

Ilyushin²² developed his theory by assuming a constant volume and adopting the principle as visualized in the double-modulus theory of column stability. Stowell²³ improved and simplified this by basing his analysis on Shanley's⁴¹ concept of non-reversal of stress during the inelastic buckling. Even though Stowell also assumed Poisson's ratio to be 0.5, any error in such an assumption was reduced by the introduction of plasticity index η , which when multiplied by the elastic buckling stress, yields plastic buckling stress. Since he used Poisson's ratio μ of 0.5 for calculating both the plastic and the elastic buckling stresses, η may be only marginally affected by the value of Poisson's ratio μ .

The differential equation of plastic buckling, used by Stowell can be written as

$$D' \left[\left(1 - \frac{3}{4}\kappa\right) \frac{\partial^4 Z}{\partial y^4} + 2 \frac{\partial^4 Z}{\partial x^2 \partial y^2} + \frac{\partial^4 Z}{\partial x^4} \right] + t \sigma_{yy} \frac{\partial^2 Z}{\partial y^2} = 0 \quad (2.2.8)$$

where

$$D' = E_s t^3 / 9, \quad \kappa = (1 - E_t / E_s)$$

E_s and E_t are the tangent and the secant modulus respectively. He expressed the plastic buckling stress $(\sigma_{cr})_p$, given by the solution of eqn. (2.2.8), in terms of the elastic buckling stress $(\sigma_{cr})_e$ and the plasticity index η as given below.

$$(\sigma_{cr})_p = \eta (\sigma_{cr})_e \quad (2.2.9)$$

For an unstiffened element with a given rotational edge restraint coefficient ϵ ($\epsilon = wC/D$), the plasticity index η is

$$\eta = \frac{E_s}{E} \frac{\frac{1}{2} + .1742\epsilon + .0192\epsilon^2}{\frac{1}{2} + .1742\epsilon + .0192\epsilon^2} + \frac{2\sqrt{\frac{1}{4} + \frac{3E_t}{4E_s}} \sqrt{.0834\epsilon + .0414\epsilon^2 + .00688\epsilon^3 + .00038\epsilon^4}}{2\sqrt{.0834\epsilon + .0414\epsilon^2 + .00688\epsilon^3 + .00038\epsilon^4}} \quad (2.2.10)$$

The rotational edge restraint factors for the two cases of hinged and fixed condition, reduce eqn. 2.2.10 to eqs. 2.2.11 and 2.2.12 respectively.

$$\eta = E_s/E \quad (2.2.11)$$

$$\eta = E_s/D \left(.33 + .67 \sqrt{\frac{1}{4} + \frac{3}{4} \frac{E_t}{E_s}} \right) \quad (2.2.12)$$

The elastic and plastic local buckling strains can be written in terms of the corresponding stresses and the moduli E_s and E as

$$(e_{cr})_p = (\sigma_{cr})_p / E_s$$

and

$$(e_{cr})_e = (\sigma_{cr})_e / E \quad (2.2.13)$$

Substituting values from eqn. 2.2.13 in eqn. 2.2.9

$$\begin{aligned} (e_{cr})_p &= \eta \frac{E}{E_s} (e_{cr})_e \\ &= \eta' (e_{cr})_e \end{aligned} \quad (2.2.14)$$

where

$$\eta' = \eta E / E_s \quad (2.2.15)$$

Steel members of material having an elastic perfectly plastic stress strain curve exhibit a yield plateau where

$$E_t = 0 \quad (2.2.16)$$

Substituting eqs. 2.2.10 and 2.2.16 in eqn. 2.2.15

$$\eta' = \frac{\frac{1}{2} + .1742\epsilon + .0192\epsilon^2}{\frac{1}{2} + .1742\epsilon + .0192\epsilon^2}$$

$$\frac{+\sqrt{.0834\epsilon+.0414\epsilon^2+.00688\epsilon^3+.00038\epsilon^4}}{+2\sqrt{.0834\epsilon+.0414\epsilon^2+.00688\epsilon^3+.00038\epsilon^4}} \quad (2.2.17)$$

The relationship between η' and ϵ expressed by eqn. 2.2.17 is shown in fig. 2.2.2 and table 2.2.1.

The elastic local buckling strain $(e_{cr})_e$ is equal to

$$(e_{cr})_e = K_e \frac{\pi^2}{12(1-\mu^2)(w/t)^2} \quad (2.2.18)$$

where K_e is the elastic local buckling coefficient. Substituting eqn. 2.2.18 in eqn. 2.2.14

$$\begin{aligned} (e_{cr})_p &= \eta' K_e \frac{\pi^2}{12(1-\mu^2)(w/t)^2} \\ &= K_p \frac{\pi^2}{12(1-\mu^2)(w/t)^2} \end{aligned} \quad (2.2.19a)$$

and

$$(\sigma_{cr})_p = K_p \frac{\pi^2 E_s}{12(1-\mu^2)(w/t)^2} \quad (2.2.19b)$$

The plastic buckling coefficient K_p is a function of only the edge rotation restraint coefficient ϵ for a large aspect ratio and is given by

$$K_p = \eta' K_e \quad (2.2.20)$$

Fig. (2.2.2) and table (2.2.1) show the relationship between K_p and ϵ . Eqn. 2.2.19a is plotted in fig. 2.2.3 showing the relationship between $(e_{cr})_p/K_p$ and (w/t) , for the two extreme values of Poisson's ratio ($\mu=0.3$ and 0.5). It is important to realize that equation 2.2.19a and fig. 2.2.3 are applicable only for elements of materials having a sharp yield point and buckling locally in the yield plateau between yield strain and strain hardening strain.

The influence of initial imperfections on the inelastic local buckling of unstiffened elements has not so far been studied satisfactorily. An analytical solution to this problem is complicated by the introduction of non-linear material properties in the non-linear equations. The postbuckling reserve strength of elements from materials having an yield plateau is negligible beyond the local buckling in the plastic range, and can be disregarded. However, when local buckling takes place in the elastic range, there is a postbuckling reserve strength and an analytical investigation of this will be presented in the next section.

2.3 Elastic Postbuckling Behavior

The elastic local buckling of a plate represents an interchange from one stable form, when the plate is flat,

to another stable form having a deflection normal to the plane. This behavior of plates is different from that of columns, which undergo considerable deflection after buckling, leading to inelastic deformation and failure with very little increase in the load carrying capacity; and that of shells which commonly experience an unstable postbuckling deformation. This postbuckling strength of plates is due to the presence of membrane tensile and shear stresses after local buckling. Since the collapse load of a plate can be many times higher than the local buckling load, any design based on the ultimate strength should take into consideration the postbuckling strength of plates. An analytical solution to the elastic postbuckling behavior of unstiffened compression elements is presented in this section, assuming an approximate wave form.

The large deflection equations of thin plates were first derived by Von Karman and were extended to plates with initial curvature by Marguerre⁴². These equations have been used by many researchers to investigate the postbuckling behavior of stiffened compression elements. Approximate solutions were obtained by Shnadel⁴³, Cox⁴⁴, Timoshenko⁴ and Marguerre⁴⁵. Levy⁴⁶ used Marguerre's equations to theoretically solve the postbuckling behavior of a simply supported rectangular plate under edge

compression in one direction, with all edges constrained to remain straight and parallel. Coan¹⁶ solved the same problem when unloaded edges were stress free. Yamaki¹⁸ extended the solution to obtain numerical results for deflection, stiffness, and the effective width of stiffened plates subject to edge compression in one direction and a variety of boundary conditions. Sayed¹⁷ has derived effective width equations for stiffened plates, with stress free and straightly held unloaded edges, using Galerkin's approximation. An effective width equation for stiffened elements based on Sayed's analytical solution will be compared with the Winter's effective width equation (eqn. 1.2.2) in Appendix A. Dawson¹⁹ has studied the effect of different generalized imperfection parameters on the effective width. All these investigators confine their attention to plates supported on all four edges against deflection normal to the plate (stiffened elements). A theoretical solution to the postbuckling behavior of unstiffened elements, which are plates with one of the unloaded edges free to move normal to the plane, will be derived using the large deflection equations of plates with initial curvature.

The large deflection equations of thin plates with initial curvature under compression, derived by Marguerre, are

$$\nabla^4 F = E (Z^2_{,xy} - Z_{,xx} Z_{,yy} + 2Z_{,xy} Z_{0,xy} - Z_{,xx} Z_{0,yy} - Z_{,yy} Z_{0,xx}) \quad (2.3.1a)$$

$$\nabla^4 Z = \frac{t}{D} (F_{,yy} (Z+Z_0)_{,xx} + F_{,xx} (Z+Z_0)_{,yy} - 2F_{,xy} (Z+Z_0)_{,xy}) \quad (2.3.1b)$$

where Z_0 is the initial out of plate deflection of the element, Z is the additional out of plate deflection due to uniform compression, and F is the stress function defined as

$$\sigma_{xx} = F_{,yy}; \quad \sigma_{yy} = F_{,xx}; \quad \sigma_{xy} = -F_{,xy}$$

$$\text{and } \nabla^4 = \left(\frac{\partial^4}{\partial x^4} + 2 \frac{\partial^4}{\partial x^2 \partial y^2} + \frac{\partial^4}{\partial y^4} \right) \quad (2.3.2)$$

In the above equations, subscripts preceded by a comma indicate a partial differential with respect to the subscripted variable. Coordinate directions and the origin of the unstiffened element are as shown in fig. 2.1.1. The deflected shape is assumed as

$$Z = A_1 f(x) \sin(\pi y/L) = A_1 \sum_{n=1}^4 C_n \left(\frac{x}{w}\right)^n \sin \frac{\pi y}{L} \quad (2.2.4)$$

where L is the length of the local buckling waves and the constants C_1 through C_4 can be obtained, by satisfying boundary conditions, from equation 2.2.5. The amplitude of the waving increases in proportion to the parameter

A_1 to be determined by the Galerkin's procedure. The effect of initial imperfection is maximum when it has the same form as the deflection due to loading, and therefore the initial imperfection is assumed to be

$$Z_0 = A_0 \sum_{n=1}^4 C_n \left(\frac{x}{w}\right)^n \sin \frac{\pi y}{L} \quad (2.3.3)$$

Substituting the assumed deflected shapes Z , Z_0 from eqs. 2.2.4 and 2.3.3 in eqn. 2.3.1a

$$\nabla^4 F = A \left[(f_{,x}^2 + ff_{,xx}) + (f_{,x}^2 - ff_{,xx}) \cos \frac{2\pi y}{L} \right] \quad (2.3.4)$$

where

$$A = E\pi^2 (A_1^2 + 2A_1 A_0) / 2L^2$$

Particular solution to equation 2.3.4 can be written as

$$F_p = A \left[G_0(x) + G_1(x) \cos \frac{2\pi y}{L} \right] \quad (2.3.5)$$

Substituting eqn. 2.3.5 in eqn. 2.3.4 for $F = F_p$, then

$$\frac{d^4 G_0(x)}{dx^4} = (f_{,x}^2 + ff_{,xx}) \quad (2.3.6a)$$

or

$$\frac{d^2 G_0(x)}{dx^2} = \frac{1}{2} f^2 \quad (2.3.6b)$$

and

$$\left(\frac{d^4 G_1}{dx^4} - \frac{8\pi^2}{L^2} \frac{d^2 G_1}{dx^2} + \frac{16\pi^4}{L^4} G_1 \right) = (f_{,xx}^2 - f_{,xx}) \quad (2.3.6c)$$

Solving eqn. 2.3.6b

$$G_0(x) = w^2 \sum_{n=4}^{10} C_{0n} \left(\frac{x}{w}\right)^n \quad (2.3.7a)$$

where

$$C_{04} = C_1^2/12, \quad C_{05} = C_1 C_2/20, \quad C_{06} = (C_2^2 + 2C_1 C_3)/60,$$

$$C_{07} = (C_1 C_4 + C_2 C_3)/42, \quad C_{08} = (C_3^2 + 2C_2 C_4)/112,$$

$$C_{09} = C_3 C_4/72, \quad C_{010} = C_4^2/180 \quad (2.3.7b)$$

Substituting

$$G_1(x) = w^2 \sum_{n=0}^{10} C_{1n} \left(\frac{x}{w}\right)^n \quad (2.3.8)$$

in eqn. 2.2.6c yields

$$\begin{aligned} & \frac{1}{w} \sum_{n=0}^{10} \left[\frac{(n+4)!}{n!} C_{1(n+4)} - 2\beta^2 \frac{(n+2)!}{n!} C_{1(n+2)} + \beta^4 C_{1n} \right] \\ & = \sum_{n=1}^4 \sum_{m=1}^4 n(m-n+1) C_n C_m \left(\frac{x}{w}\right)^{(n+m-2)} \end{aligned} \quad (2.3.9)$$

where

$$\beta = 2\pi w/L, \quad C_{1n} = 0 \text{ when } n > 10$$

Equating coefficients of equal power of (x/w) in eqn.

2.3.9, the eleven constants C_{1n} ($n=0\dots 10$) can be found.

Thus particular solution to eqn. 2.3.4 is given by

$$F_p = A[G_0(x) + G_1(x) \cos \frac{2\pi y}{L}] \quad (2.3.5)$$

where

$$G_0(x) = w^2 \sum_{n=4}^{10} C_{0n} (x/w)^n \quad (2.3.7a)$$

$$B_1(x) = w^2 \sum_{n=0}^{10} C_{1n} \left(\frac{x}{w}\right)^n \quad (2.3.8)$$

C_{0n} and C_{1n} can be obtained from eqs. 2.3.7b and 2.3.9.

Let the homogenous solution to eqn. 2.3.4 be

$\bar{F}(x,y)$

Then

$$F = F_p(x,y) + \bar{F}(x,y) \quad (2.3.10a)$$

where \bar{F} should satisfy

$$\nabla^4 F = 0 \quad (2.3.10b)$$

Assuming

$$\bar{F} = A G_2(x) \cos \frac{2\pi y}{L} + A G_3(x) \quad (2.3.11)$$

from eqn. 2.3.10a

$$\left(\frac{d^4 G_2}{dx^4} - \frac{8\pi^2}{L^4} \frac{d^2 G_2}{dx^2} + 16 \frac{\pi^4}{L^4} G_2 \right) = 0 \quad (2.3.12a)$$

and

$$\frac{d^4 G_3}{dx^4} = 0 \quad (2.3.12b)$$

The solution to eqn. 2.3.12a is

$$G_2(x) = w^2 \left[C_{21} \cosh \frac{2\pi x}{L} + C_{22} \sinh \frac{2\pi x}{L} + C_{23} \frac{2\pi x}{L} \cosh \frac{2\pi x}{L} + C_{24} \frac{2\pi x}{L} \sinh \frac{2\pi x}{L} \right] \quad (2.3.13)$$

Substituting eqs. 2.3.12a and 2.3.12b in eqn. 2.3.10

$$F = A \left[(G_1(x) + G_2(x)) \cos \frac{2\pi y}{L} + G_0(x) + G_3(x) \right] \quad (2.3.14)$$

where G_0, G_1, G_2 , and G_3 are functions of x .

Membrane stresses in the buckled unstiffened element are given by eqs. 2.3.2. Substituting eqn. 2.3.14 in eqn. 2.3.2,

$$\sigma_{xx} = F_{,yy} = -\frac{4\pi^2 A}{L^2} \left[(G_1 + G_2) \cos \frac{2\pi y}{L} \right] \quad (2.3.15a)$$

$$\sigma_{yy} = F_{,xx} = A \left[(G_1 + G_2)_{,xx} \cos \frac{2\pi y}{L} + (G_0 + G_3)_{,xx} \right] \quad (2.3.15b)$$

$$\sigma_{xy} = -F_{,xy} = \frac{2\pi A}{L} \left[(G_1 + G_2)_{,x} \cos \frac{2\pi y}{L} \right] \quad (2.3.15c)$$

There are two possible boundary conditions along the unloaded supported edge of an unstiffened element in the postbuckling range. They are (1) the edge constrained to remain straight or, (2) the edge free of membrane stresses. A membrane stress-free supported edge is the condition often encountered in cold-formed structural members. Hence, only this type of supported edge will be treated.

Consequently, shear and normal stresses are zero at the unloaded edges. These boundary conditions are

$$\begin{aligned} \sigma_{xy} &= 0 \\ \sigma_{xx} &= 0 \end{aligned} \quad \text{at } x=0, W \quad (2.3.16)$$

Substituting eqs. 2.3.15a and 2.3.15c in eqn. 2.3.16, the following set of four simultaneous equations are obtained, and constants C_{21} through C_{24} are evaluated by solving the equations.

$$\begin{bmatrix} 0 & \beta & \beta & 0 \\ \beta \sinh \beta & \beta \cosh \beta & \beta (\cosh \beta + \beta \sinh \beta) & \beta (\sinh \beta + \beta \cosh \beta) \\ 1 & 0 & 0 & 0 \\ \cosh \beta & \sinh \beta & \beta \cosh \beta & \beta \sinh \beta \end{bmatrix} \begin{bmatrix} C_{21} \\ C_{22} \\ C_{23} \\ C_{24} \end{bmatrix} = \begin{bmatrix} -C_{11} \\ -\sum_{n=0}^{10} C_{1n} \\ -C_{10} \\ -\sum_{n=0}^{10} C_{1n} \end{bmatrix}$$

where $\beta = 2\pi w/L$

$$(2.3.17)$$

Boundary conditions at $y = 0, L$ are (1) membrane shear stress is zero, (2) in plane compressive deformation is uniform and (3) resultant of normal membrane stress is equal to the average applied stress (σ_{av}). Corresponding equations are

$$\sigma_{xy} = 0 \quad (2.3.18a)$$

$$v = \text{Constant} \quad (2.3.18b)$$

$$\sigma_{av} = (1/w) \int_0^w \sigma_{yy} dx \quad (2.3.19)$$

where σ_{av} is the average compressive stress applied at the loaded edges, and v is the displacement along y direction. Eqn. 2.3.18a is automatically satisfied by the stress function F . Eqn. 2.3.18b yields

$$\frac{d^2 G_3}{dx^2} = \text{Constant} \quad (2.3.20)$$

The solution to eqn. 2.3.20 can be written as

$$G_3(x) = w^2 C_{32} (x/w)^2 \quad (2.3.21)$$

which satisfies eqn. 2.3.12b. By substituting eqs. 2.3.13, 2.3.14, 2.3.15b, and 2.3.21 in eqn. 2.3.19, constant C_{32} in eqn. 2.3.21 can be evaluated to be

$$C_{32} = \frac{1}{2A} \sigma_{av} - \frac{1}{2} \sum_{n=4}^{10} C_{0n} \quad (2.3.22)$$

Hence, the stress function F is given by eqn. 2.3.13 as

$$F = A \left\{ [G_1(x) + G_2(x)] \cos \frac{2\pi y}{L} + G_0(x) + G_3(x) \right\} \quad (2.3.13)$$

where

$$G_0(x) = w^2 \sum_{n=4}^{10} C_{0n} (x/w)^n$$

$$\begin{aligned}
G_1(x) &= w^2 \sum_{n=0}^{10} C_{1n} (x/w)^n \\
G_2(x) &= w^2 \left[C_{21} \cosh \frac{2\pi x}{L} + C_{22} \sinh \frac{2\pi x}{L} \right. \\
&\quad \left. + C_{23} \frac{2\pi x}{L} \cosh \frac{2\pi x}{L} + C_{24} \frac{2\pi x}{L} \sinh \frac{2\pi x}{L} \right] \\
G_3(x) &= w^2 C_{32} (x/w)^2 \tag{2.3.13a}
\end{aligned}$$

All constants can be evaluated by equations already derived.

Substituting eqs. 2.3.13, 2.2.4, and 2.3.3. in 2.3.1b and using Galerkin's approximation, eqn. 2.3.1b becomes

$$\begin{aligned}
\int_0^L \int_0^W \nabla^4 Z f \sin \frac{\pi y}{L} dx dy &= \frac{t}{D} \int_0^L \int_0^W [F_{,yy}(Z+Z_0)_{,xx} \\
&\quad + F_{,xx}(Z+Z_0)_{,yy} - 2F_{,xy}(Z+Z_0)_{,xy}] f \sin \frac{\pi y}{L} dx dy \tag{2.3.23}
\end{aligned}$$

All the integrals can be evaluated as given below.

$$\begin{aligned}
\int_0^L \int_0^W \nabla^4 Z f \sin \frac{\pi y}{L} dx dy &= \frac{A_1}{2wL} \sum_{n=1}^4 \sum_{m=1}^4 \frac{C_{4n} C_m}{(n+m+1)} \\
&= \frac{A_1}{2wL} I_L \tag{2.3.24}
\end{aligned}$$

$$\int_0^L \int_0^W [F_{,yy}(Z+Z_0)_{,xx} + F_{,xx}(Z+Z_0)_{,yy} - 2F_{,xy}(Z+Z_0)_{,xy}]$$

$$f \sin \frac{\pi y}{L} dx dy = \frac{A\pi^2(A_1+A_0)}{2L}$$

$$\int_0^W [(G_1+G_2)(ff_{,xx}-f_{,x}^2)-(G_0+G_3)_{,xx}f^2] dx dy$$

(2.3.25)

$$\int_0^W (G_0+G_3)_{,xx} f^2(x) dx = \frac{w \sigma_{av}}{A} \sum_{n=1}^4 \sum_{m=1}^4 \frac{C_n C_m}{(n+m+1)}$$

$$+ w \sum_{p=4}^{10} \sum_{n=1}^4 \sum_{m=1}^4 \frac{p(p-2)(n+m)C_0 C_p C_n C_m}{(n+m+p-1)(n+m+1)}$$

$$= \frac{w \sigma_{av}}{A} I_3 + w I_0 \quad (2.3.26a)$$

$$\int_0^W G_1(ff_{,xx}-f_{,x}^2) = w \sum_{p=0}^{10} \sum_{n=1}^4 \sum_{m=1}^4 \frac{m(m-n+1)C_1 C_p C_n C_m}{(n+m+p-1)}$$

$$= w I_1 \quad (2.3.26b)$$

$$\int_0^W G_2(x)(ff_{,xx}-f_{,x}^2) dx = w \sum_{n=1}^4 \sum_{m=1}^4 C_n C_m m(m-n-1)(n+m-2)!$$

$$\begin{aligned}
& \times \left\{ \sinh \beta \left[\sum_{p=0,2,4}^{p_L} \frac{C_{21}^{-(p_L+1)} C_{24}}{(p_L-p)! \beta^{(p+1)}} + \sum_{p=1,3,5}^{p_L} \frac{(p_L+1) C_{23}^{-C_{22}}}{(p_L-p)! \beta^{(p+1)}} \right. \right. \\
& \quad \left. \left. + \frac{C_{23}}{p_L!} \right] + \cosh \beta \left[\sum_{p=0,2,4}^{p_L} \frac{C_{22}^{-(p_L+1)} C_{23}}{(p_L-p)! \beta^{(p+1)}} \right. \right. \\
& \quad \left. \left. + \sum_{p=1,3,5}^{p_L} \frac{(p_L+1) C_{24}^{-C_{21}}}{(p_L-p)! \beta^{(p+1)}} + \frac{C_{24}}{p_L} \right] \right. \\
& \quad \left. + [((C_{21} - (p_L=1) c_{24}) \div \beta^{(p_L+1)}) \text{ if } p_L \text{ is odd}] \right. \\
& \quad \left. + [(((p_L+1) C_{23}^{-C_{22}}) \div \beta^{(p_L+1)}) \text{ if } p_L \text{ is even}] \right\} \\
& \hspace{20em} (2.3.26c)
\end{aligned}$$

where $p_L = (n+m-2)$

Substituting eqs. 2.3.24, 2.3.25, 2.3.26a, b and c in eqn. 2.3.23.

$$\frac{A_1}{2wL} I_L = \frac{A\pi^2 w (A_1 + A_0)}{2L} \frac{t}{D} \left\{ I_1 + I_2 - I_0 - \frac{\sigma_{av}}{A} I_3 \right\} \quad (2.3.27)$$

This equation can be written as

$$A_1 \frac{D}{\pi^2 w^2 t} \frac{I_L}{I_3} = -A(A_1 + A_0) \left\{ (I_0 - I_1 - I_2) / I_3 \right\} - (A_1 + A_0) \sigma_{av} \quad (2.3.28)$$

Using eqn. 2.2.27, eqn. 2.3.28 can be written as

$$A_1 \sigma_{cr} = A(A_1 + A_0) I + (A_1 + A_0) \sigma_{av} \quad (2.3.29)$$

where

$$(I_0 - I_1 - I_2) / (I_3) = I$$

Let

$$\gamma = E\pi^2 I t^2 / 2L^2$$

$$\Delta_0 = A_0 / t$$

$$\Delta = A_1 / t$$

$$\phi = \sigma_{av} / \gamma$$

$$k = \sigma_{av} / \sigma_{cr} \quad (2.3.30a)$$

Eqn. 2.3.29 can be written as given below, using the parameters as defined by eqn. 2.3.30a.

$$\Delta^3 + 3\Delta_0 \Delta^2 + (2\Delta_0^2 + (k-1)\phi) \Delta + \Delta_0 k \phi = 0 \quad (2.3.30b)$$

Eqn. 2.3.30b has only one real positive root, which is the value of Δ . Having found Δ , the postbuckling analysis is complete. Value of any desired variable can be obtained by back substitution into respective equations in this section.

One of the variables in this postbuckling analysis is the length of the local buckling waves. The wave length at the local buckling load can be determined by minimizing

the buckling stress with respect to the wave length L . Experimental investigations indicate that wave length tends to reduce as the element is loaded into the postbuckling range. In order to study the effect of a reduction in the wavelength, the analysis was carried out by reducing the length of the wave at the critical load up to 25%. It was found that the change in the effective width at the advanced postbuckling range due to the reduction in the wavelength was nominal. Hence, in the ensuing investigation it has been assumed that the length of wave in the postbuckling range to be the same as the length at local buckling.

2.3.1 Postbuckling Behavior of Perfectly Flat Unstiffened Elements - Parameter Study

Equations derived in the previous sections for the postbuckling behavior of unstiffened compression elements with initial imperfections can be used to study postbuckling behavior of perfectly flat unstiffened compression elements by setting the parameter A_0 in the initial imperfection amplitude eqn. 2.3.3 to be equal to zero.

The maximum compressive stress at the supported edge of an unstiffened compression element occurs at the crest of a wave and is given by

$$\sigma_{e \max} = \sigma_{yy}|_{(0, L/2)} = \sigma_{av} - A \{ 2C_{12} + \beta^2 (C_{21} + 2C_{24}) + \sum_{m=4}^{10} C_{0m} \} \quad (2.3.31a)$$

or

$$\frac{\sigma_{e \max}}{\sigma_{cr}} = \frac{\sigma_{av}}{\sigma_{cr}} - \frac{A}{\sigma_{cr}} \{ 2C_{12} + \beta^2 (C_{21} + 2C_{24}) + \sum_{m=4}^{10} C_{0m} \} \quad (2.3.31b)$$

Fig. 2.2.4 shows the relationship between $(\sigma_{e \max}/\sigma_{cr})$ and $(\sigma_{av}/\sigma_{cr})$ of perfectly flat unstiffened elements given by eqn. 2.3.31b. It is seen that in the postbuckling range the relationship is linear and the slope of the straight line depends upon the buckling coefficient K . The equation of these straight lines can be written as

$$(\sigma_{av}/\sigma_{cr}) = (1 - B_1) + B_1 (\sigma_{e \max}/\sigma_{cr}) \quad (2.3.32)$$

where B_1 is the slope of the straight lines. Fig. 2.2.5 and Table 2.2.1 show the relationship between the slope B_1 and the buckling coefficient K . The relationship between B_1 and K can be expressed by the following equation, obtained through a regression analysis having a correlation coefficient of 0.998.

$$B_1 = 0.326 + 0.086K^2 \quad (2.3.33)$$

Ratio of the effective to the actual width is

$$b_e/w = (\sigma_{av}/\sigma_{e \max}) \quad (2.3.34)$$

Substituting eqn. (2.3.34) in eqn. 2.3.31a and rearranging

$$b_e/w = \frac{1}{1 - \frac{A}{\sigma_{av}} [2C_{12} + \beta^2 (C_{21} + 2C_{24}) + \sum_{m=4}^{10} C_{0m}]} \quad (2.3.35)$$

and substituting eqn. (2.3.34) in eqn. 2.3.32 and rearranging

$$b_e/w = \frac{(1-B_1)}{(\sigma_{e \max}/\sigma_{cr})} + B_1 \quad (2.3.36)$$

Fig. 2.2.6 shows the relationship between b_e/w and $(\sigma_{e \max}/\sigma_{cr})$ as expressed by eqn. 2.3.36. It can be seen that perfectly flat unstiffened elements remain fully effective until local buckling stress is reached and the effective width reduces with further loading. The reduction is larger for elements having a lower buckling coefficient than a higher buckling coefficient.

The maximum amplitude of the out of plane deformation is obtained by substituting value of Δ from solution of eqn. 2.3.30b in eqn. 2.2.4.

$$(Z/t)_{\max} = (Z/t)_{(w,L/2)} = \Delta \sum_{n=1}^4 C_n \quad (2.3.36)$$

Fig. 2.2.7 shows the relationship between (Z/t) and $(\sigma_{e \max}/\sigma_{cr})$. Plotting $(\sigma_{e \max}/\sigma_{cr})$ against $(Z/t)_{\max}^2$ as shown in fig. 2.2.8, there is a linear relationship of the form

$$(Z/t)_{\max}^2 = B_3 \left(\frac{\sigma_{e \max}}{\sigma_{cr}} - 1 \right) \quad (2.3.37)$$

where B_3 is a function of the buckling coefficient K .

Fig. 2.2.5 and table 2.2.1 show the relationship between B_3 and the buckling coefficient K . A functional relationship between B_3 and K , obtained through a regression analysis and having a correlation coefficient of 0.999, is given below.

$$B_3 = 2.727 + 1.135/(K-0.425) \quad (2.3.38)$$

Equations 2.3.37 and 2.3.38 indicate that the ratio of the maximum out of plane deformation to thickness $((Z/t)_{\max})$ is large at the advanced stage of postbuckling of unstiffened elements having a low buckling coefficient (hinged edge condition). However, Von-Karman's equations are valid only for the intermediate range of deflection. Consequently, the equation (eqn. 2.3.37) for computation of deflection should be used with discretion for elements

having a low buckling coefficient.

2.3.2 Postbuckling Behavior of Unstiffened Elements

With Initial Imperfections - Parameter Study

Eqs. 2.3.31a,b, 2.3.35 and 2.3.36 for stresses and displacements derived in section 2.3.1 are also valid for plates with initial imperfections.

Hence, eqn. 2.3.35 given below yields the effective width for imperfect plates, as long as initial imperfections parameter A_0 is not taken to be equal to zero.

$$b_e/w = \frac{1}{1 - \frac{A}{\sigma_{av}} [2c_{12} + \beta^2 (c_{21} + 2c_{24}) + \sum_{m=4}^{10} c_{0m}]} \quad (2.3.35)$$

Fig. 2.2.9 shows the variation in the effective width for an element having a rotational edge restraint parameter ϵ equal to 2.0 and various values of initial imperfections. Fig. 2.2.10 shows the variation in the out of plane deformation for various values of initial imperfections for the same plate. It is seen that the effect of imperfection is most pronounced around the critical buckling stress and is negligible at the advanced postbuckling stage. It can also be observed that the net out of plane deformation due to in plane compression is smaller at the advanced stage of postbuckling

for a plate with initial imperfections than for a perfectly flat plate.

2.4 Summary and Conclusions

In this chapter, an analytical investigation of elastic and inelastic local buckling and postbuckling behavior of unstiffened elements has been carried out. The local buckling stress is a function of the flat width to thickness ratio of the element and the buckling coefficient, which in turn depends upon the rotational restraint at the supported edge. A method for determining the local buckling coefficient K in "closed" form has been presented. It was shown that the plastic buckling strain coefficient K_p can be obtained by multiplying the elastic buckling coefficient K by the plasticity index η' which is a function of the rotational edge restraint coefficient ϵ , the tangent modulus and the secant modulus.

In the elastic postbuckling range, the reduced effective width was shown to be a function of the maximum stress at the supported edge, the local buckling coefficient K , the flat width w , and the thickness t of the unstiffened element. It was observed that the load carrying capacity of an element is essentially reached when maximum stress at the supported edge reaches the yield stress

of the material. When the local buckling takes place in the inelastic range, it was observed that any increase in load carrying capacity beyond this is very limited and often neglected. Plots and equations giving the relationship between various parameters of the postbuckling equations have been presented.

In conclusion, it is important to reemphasize that due to the approximate nature of the assumed deflected shape, equations derived may not give a good solution in the advanced stages of the postbuckling range (large value of $\sigma_{e \max} / \sigma_{cr}$), out of plane deflection may be large and the wave form along the length may be very different from the assumed simple sinusoidal curve. However, for the range of interest in this investigation, it is expected that the analytical solution should give results of sufficient accuracy.

CHAPTER 3

EXPERIMENTAL INVESTIGATION OF UNSTIFFENED ELEMENT BEHAVIOR

3.1 General

A study of unstiffened compression element buckling and postbuckling behavior is the first step in the proposed experimental investigation. The objective of the test is to subject an unstiffened element to axial compressive stress and investigate local buckling and postbuckling behavior as the loading progresses. It is desirable to have the support condition of such an element matching the environment encountered in practice. One of the easiest and most commonly used methods of testing an element in uniform compression is to subject a member composed of such elements to uniform axial compression. This test, often referred to as the stub column test, not only gives the desired information about the element behavior, but also provides information useful in the investigation of the overall flexural buckling of such a member. In this chapter, stub column tests conducted in this investigation are described and the results of the tests are evaluated. Results of stub column tests conducted by DeWolf³² are also presented in section 3.4.2.

These test results are compared with the analytical solution derived in the previous chapter, bearing in mind the derivation of an effective width equation as the ultimate goal.

3.2 Stub-Column Test

3.2.1 Material Properties

Stub columns were fabricated from ten 18 gage, 4 feet by 10 feet sheets of low carbon commercial grade steel. Three tensile coupons were tested, from each of the ten sheets to obtain the material properties, following ASTM Designation E 8-69 on "Tension Testing of Metallic Materials"⁴⁷. The mechanical properties of the three coupons from each sheet were averaged to obtain the properties of each sheet. Tension tests generally revealed a sharply yielding stress strain relationship with yield plateau. Fig. 3.2.1 shows the early portion of the stress strain curve of a tension coupon and is typical of all the coupons. The yield stress and the ultimate stress of the ten 18 gage sheets are given in Table 3.2.1. The strain hardening occurred at an average strain of 0.0135 and the average elongation of 2 inch gage lengths was 45 percent.

3.2.2 Design of Test Specimens

One of the objectives of a stub column test is to study the local buckling and postbuckling behavior of unstiffened elements in compression. In order to get a complete picture, it is desirable to design the specimens such that the whole range of variables governing the element behavior is covered. The rotational edge restraint at the supported edge and the flat width to thickness ratio (w/t) are two of the variables which influence the behavior of an unstiffened element most. The flat width to thickness ratio can be easily designed to be within any desired range, by varying the width, thickness or both. The rotational edge restraint at the supported edge depends upon the relative stiffnesses of the supporting and supported elements, and often cannot be varied at will, because of other constraints such as the premature local buckling of the supporting element and the restrictions of the forming process.

Five H sections, as shown in Fig. 3.2.2, were designed for the stub column tests. Two specimens were tested corresponding to each section. The dimensions of the ten stub column specimens (SC) are given in Table 3.2.2. The widths of the unstiffened elements were varied to obtain a w/t ratio in the range of 30 to 60. This ensured an

elastic local buckling. Unstiffened elements having w/t ratios between 16 and 30 were tested by DeWolf³², and the results of his tests will also be used in this chapter. It is desirable to have webs that do not buckle locally prematurely and provide rotational edge restraint to the unstiffened flanges. Therefore, the webs were designed to remain fully effective until the yield stress was reached. Even though the local buckling of flanges introduced waving in the webs, webs were stiff enough to resist this with a negligible reduction in the effective width. Consequently, only local buckling of the unstiffened elements affects the stub column test results.

The lengths of the stub column specimens are also given in table 3.2.2 and the tolerance was within one tenths of an inch. Stub columns need to be as short as possible to avoid the overall buckling of the columns. However, in order to avoid the dependence of the local buckling stress of the unstiffened elements on the aspect ratio (L/w) of the elements, it is desirable to have as long a column as possible. These two conditions dictate bounds on the length of a stub column. The specification for Design of Cold-Formed Steel Structural Members² recommends the length to be bounded between twenty and fifteen times the least radius of gyration. As the loading

progresses into the postbuckling range, the radius of gyration decreases and hence, the limit based on the radius of gyration is difficult to apply. Heimerl⁴⁸ suggests a length of stub column such that the buckling pattern has at least three half-waves. The lengths of the stub column specimens were chosen, taking into account both these recommendations.

3.2.3 Fabrication and Instrumentation

Sections were cut from the 18 gage low carbon steel sheets and cold-formed into channel shapes by press braking with a sharp die so that the inside radius was negligibly small. In all subsequent computations, the inside radius has been assumed to be zero. The flatness of the plate elements was checked at random in the specimens and the maximum amplitude of the distortion was found to be of the order of two-tenths of the thickness of the sheet. The general quality of the forming was good. Each stub column specimen was fabricated out of two such channel sections from the same steel sheet. Channels were cut slightly longer than the desired final length of the test specimen. Matching holes were drilled in the web of the channel sections as shown in fig. 3.2.2. Surfaces to be joined were then cleaned with a solvent. A thin layer of Epon 907, an epoxy grout, was spread over

the surfaces to be joined together. Wires having a 0.009 inch diameter were used as spacers between the channel sections to avoid the complete squeezing out of the glue. The channel webs were riveted to hold them together while drying and to provide additional strength to the connection during the test. After the glue had set, the ends were ground to assure a uniform bearing against a flat surface. To assure a perfectly flat bearing surface, the ends were finally lapped with a lapping compound on a perfectly flat surface.

Strain gages were glued to the specimen, parallel to the axis of the specimen at mid-height, as shown in fig. 3.2.3. Twelve 1 inch long SR-4, A-12 strain gages were glued to the four flanges, one near the intersection of the web and each flange and one on each face at the free edge of each flange. In addition to this, two 6 inch long SR-4, A-9 strain gages were glued to the web near the flange and the web intersection and one 1 inch SR-4, A-12 at the mid width of the web to insure that the strain was uniform over the web.

3.2.4 Experimental Set-Up and Procedure

"Stub Column Test Procedure"⁴⁹ of the Design Criteria for Metal Compression Members was followed to set up and test the stub columns. The ground ends of the stub col-

umns were set to bear against the ground surfaces of two 3/4" thick cold-rolled steel plates. The specimen and end plates were centered in a Tinius Olsen testing machine. A thin layer of hydrostone was spread between the machine head and the table and the bearing end plates as shown in fig. 3.2.3.

Initially, the stub columns were loaded to approximately 30% of their local buckling load in order to center the specimens. The centering was done by checking the uniformity of increase in all the strain gage readings. If they did not exhibit uniform compression, the column was recentered and a new layer of hydrostone between the top plate and the machine head was recast. After the centering was completed, the load was reduced to a small initial load to maintain the surfaces in contact.

A dial gage was located at mid-height of the stub columns to measure any overall buckling of the columns in the direction normal to the weak axis. This dial gage indicated no overall flexural buckling prior to failure.

One rigid arm was attached, using a magnetic base, to each of the end plates, with its axis parallel to the axis of the column (fig. 3.2.3). The relative displacement between the two arms during the test was directly recorded in the Olsen recorder, using a compressometer. Thus a load axial deformation plot was produced.

Testing was started from an initial load with increments such that there were at least 4 or 5 readings before the elastic local buckling. In the postbuckling range, the load increment was reduced depending upon the progress into the postbuckling range. Near the ultimate load, the axial deformation was increased in very small stages to get readings as near the ultimate load as possible.

The strain gage and dial gage readings were recorded subsequent to each load increment, after the load had settled down. In the postbuckling range, the amplitude of the local buckling waves were measured using the instrument shown in fig. 3.2.4. By sliding the dial gage in the device along the free edge of the unstiffened element, readings were taken at the trough of the wave. The difference between this and the zero reading being the wave amplitude desired.

Failure occurs when a further increase in the axial shortening is accompanied by a decrease in load resistance. Sometimes this type of load shedding was difficult to recognize, because of a drop in the load after each loading stage in the postbuckling range. In such cases, failure was assumed to have occurred when an additional small deformation does not increase the load carried by the specimen to a level higher than the previous load

level. Automatic recording of the load and deformation using a compressometer also facilitated the identification of the failure load, because at this point the load deformation curve has a horizontal tangent.

Pictures of one stub column prior to loading and all the stub columns after failure are shown in figs. 3.2.5 and 3.2.6 respectively.

3.3 Background for Evaluation of Experimental Data

3.3.1 Local Buckling

It was already pointed out that waving, and hence decrease in effective width, starts from the very beginning when an unstiffened element is loaded in compression. Hence, a bifurcation type of buckling, characteristic of an ideally flat plate, is not realized in an experimental investigation. However, it was pointed out that the local buckling stress is one of the important values desired.

A number of approximate methods have been proposed for determining the local buckling stress from experimental observations. Hu et al,¹⁵ Vann et al,⁵⁰ and Johnson⁵¹ have discussed some of these methods. Basically all methods depend upon the measurement of either the out-of-plane deformation of the unstiffened element or the compressive strains at both faces of the free edge.

Difficulty in obtaining an accurate measurement of the maximum wave amplitude and change in the location of the maximum wave amplitude in the postbuckling range make the computation of local buckling stress based on out of plane deformation unreliable. Among all the methods for finding the local buckling stress from strain measurement, the modified surface strain reversal method, described below, has been found to be most reliable by past investigators and will be used here.

When an unstiffened element is subjected to compressive stress, waving starts practically from the beginning of loading. Hence, the strain readings at the free edge of the unstiffened element are non-linear as the loading progresses, as shown in fig. 3.3.1. Compressive strain at the convex side of the element is always smaller than that at the concave side, due to the flexural stress in the plate. At a certain load, the increase in the flexural tensile stress at the convex side exceeds the compressive stress due to the increase in the axial load and there is strain reversal (point A). The modified surface strain reversal method assumes the load corresponding to this point to be the critical load of an unstiffened element. This procedure has been used throughout this investigation to determine the local buckling stress experimentally.

3.3.2 Postbuckling Behavior

At each load increment, the axial load on the stub column and the strain at the web and flange intersections were measured. Since the web has been designed to remain fully effective until the yield stress is reached, the stress throughout the web and at the corners of the web and flanges is taken to be equal to the stress in the flange at the intersection of the web and flanges.

The load resisted by the four outstanding unstiffened elements can then be computed by subtracting the load carried by the rest of the area of the cross section from the total load on the stub column. The average stress in the unstiffened elements at any load is obtained by dividing the load carried by the unstiffened elements by the total area of the unstiffened elements. The maximum stress in the unstiffened elements is the stress at the web flange intersection. The ratio of the effective width to the actual width (b_e/w) is obtained from eqn. 2.3.34b (given below) by dividing the average stress on the unstiffened element by the maximum stress on the unstiffened element.

$$b_e/w = \tau_{av}/\tau_{e \max} \quad (2.3.34b)$$

With these background information, evaluation of the experimental results will be carried out in the following section.

3.4 Evaluation of Experimental Results

3.4.1 Experimental Results

The local buckling stress of the stub columns has been computed from the experimental results as described in the previous section, and is given in table 3.4.1. The corresponding buckling coefficient K computed by substituting the buckling stress σ_{cr} in the eqn. 1.2.1a and solving for the buckling coefficient K , is also presented in table 3.4.1. The stub columns tested exhibit characteristics in between that of an H section and a single channel section, because of the discontinuity of the flanges across the web and the non-integral nature of the web. The theoretical buckling coefficient of these two extreme idealizations can be obtained from W.D. Kroll⁷ and these values are also presented for comparison in table 3.4.1. The average of these two values seems to agree reasonably well with the test values.

As already mentioned, crippling is assumed to take place when the maximum stress at the supported edge reaches the yield stress. The corresponding average compressive stress and the ratio of the effective width to

the actual width (b_e/w) has been computed as explained in the previous section. The ratio of the maximum supported edge stress to the critical stress ($\sigma_{e \max}/\sigma_{cr}$) and the ratio of the effective width to the actual width (b_e/w) at crippling, are given in table 3.4.2 for all specimens. The ratio of the out of plane wave deflection amplitude to the thickness just prior to failure is also given in table 3.4.2 for all specimens.

The axial shortening of the specimens was recorded automatically by the compressometer during the loading. This axial shortening can also be computed from the strain measured by the long gages located in the web at the intersection of the web and flanges. A typical plot of the axial load versus the axial shortening for a stub column (SC-II 1) obtained from the compressometer and the strain gages is shown in fig. 3.4.1. In the post-buckling stage, there is usually a drop in the load after each load increment and the compressometer curve has been corrected for this. There is a good agreement between the two curves. This is typical of the other stub column axial shortening curves. Attempts by previous investigators to measure the axial shortening using dial gages were not as successful, because of a larger least count of dial gages used (0.001 in.).

3.4.2 Experimental Results of DeWolf³²

In this section, the results of tests conducted by another investigator³² on stub columns with unstiffened elements in compression are presented. In subsequent sections, these results and the results of the tests conducted in this investigation will be compared with the analytical solutions.

DeWolf³² tested four stub columns with unstiffened elements having a (w/t) ratio in the range of 16 to 30. The section dimensions, material properties and test results of these four stub columns (UD 1-4) are given in table 3.4.3. The experimental and theoretical buckling coefficient (K) , and at the ultimate load the ratio of the maximum edge stress to the critical stress $(\sigma_{e \max}/\sigma_{cr})$, and the ratio of the effective width to the actual width (b_e/w) (assuming the stress at the supported edge to be equal to the yield stress at the ultimate load of the stub column) are also presented in table 3.4.3. Specimens UD-1 and UD-2 actually did not undergo local buckling before failure. Any reduction in the effective width before failure can be attributed to the effect of initial imperfections. DeWolf has computed a low value of the local buckling coefficient for these two specimens assuming the local buckling to have

occurred at failure or just prior to the failure. These low values of K (0.5 and 0.64) do not appear to be consistent, when compared with those of UD-3 and UD-4. Hence, in this investigation realistic values of the buckling coefficients have been assumed as shown in table 3.4.3, and all other computations are based on these assumed values of the buckling coefficient.

3.4.3 Comparison With the Analytical Solution

In this section, the experimental results given in the previous two sections will be compared with the analytical solution presented in section 2.3 and 2.4. An analytical equation (eqn. 2.3.35) was derived in the last chapter for the effective width of unstiffened elements in the postbuckling range. The initial measurement and test results seem to indicate the maximum value of the initial imperfection amplitude to be equal to 0.2 times the thickness of the element. Hence, only this initial imperfection amplitude will be used in the analytical representation of postbuckling behavior in this and following sections. Fig. 3.4.2 shows the variation of the ratio of the effective width to the actual width (b_e/w) as the ratio of the maximum edge stress to the critical stress ($\sigma_{e \max}/\sigma_{cr}$) is changed. There are two curves, corresponding to the two values of the buckling

coefficient K equal to 0.855 and 1.003. These two values of the buckling coefficient are used, since the buckling coefficients of the stub columns tested are within this range. Curves for zero initial imperfection amplitude are also drawn for the two values of the buckling coefficient.

For comparison, the test points evaluated in the previous sections are also plotted in this figure. It can be seen that there is a very good agreement between the test results and the analytical solution in the postbuckling range. The analytical solution has been derived in the second chapter, assuming that the supported edge parallel to the direction of applied compression is free to move in the plane of the element. However, due to symmetry of the stub columns about an axis passing through the middle of the web plate, there will be some restraint against the movement of the supported edge of the unstiffened elements in the plane of the element. In addition to this, the initial imperfection amplitude has been taken to be 0.2 times the element thickness, which may be too high for narrow flanges. The slightly conservative nature of the analytical solution in the postbuckling range can be attributed to these two reasons.

In the prebuckling range, the analytical solution is very conservative compared to the test results. The ana-

lytical solution indicates a reduction in the effective width even for a very small value of the maximum supported edge stress to critical stress ratio ($\sigma_{e \max} / \sigma_{cr}$), whereas experimental results seem to indicate that the unstiffened elements having a very small (w/t) ratio, hence a large buckling stress, remain fully effective until yield stress is reached over the entire width of the element. This can be observed in some of the test results presented here and it has also been observed by many investigators studying wide flange hot rolled beams and columns. This difference between the analytical solution and the experimental results in the prebuckling range can be attributed to many factors. Unstiffened compression elements having a small (w/t) ratio may have a very small initial imperfection amplitude and hence little reduction in the effective width before yielding is reached. Besides, it was pointed out that even though failure is assumed to occur as soon as the maximum supported edge stress reaches yield stress, elements having local buckling stress around or above the yield stress may have at failure the supported edge strain greater than the yield strain. This facilitates the spread of plastification into the element, thus increasing the ultimate load. In order to take these factors into account, the analytical solution can be modified as

given below.

In fig. 3.4.2, it can be observed that the analytical curves for perfectly flat elements and the analytical curves for elements with a small initial imperfection have the same shape in the postbuckling range ($\sigma_{e \max} / \sigma_{cr} > 1$). Hence, by shifting the curves for the perfectly flat elements horizontally a certain distance to the left (towards the vertical axis), they can be made to generally coincide (in the postbuckling range) with the analytical curves for the corresponding elements with an imperfection amplitude of 0.2 times the thickness of the element. However, in the prebuckling range ($\sigma_{e \max} / \sigma_{cr} < 1$), the shifted curves (indicated by dashed lines) deviate from the analytical curves for the corresponding elements with initial imperfections. These shifted curves intersect the line corresponding to a fully effective line ($b_e/w=1.0$) at a certain value of the abscissa ($\sigma_{e \max} / \sigma_{cr}$) different from zero. The shifted curves are still slightly conservative in the prebuckling range in comparison to the test results, though much closer to the test results in the prebuckling range than the analytical curves. Hence, an effective width equation for the unstiffened elements' elastic postbuckling behavior can be reasonably represented by the equation of the shifted curve.

The analytical curve corresponding to zero initial

imperfection has been shown to be given by the equation

$$\frac{b_e}{w} = \frac{(1-B_1)}{(\sigma_{e \max}/\sigma_{cr})} + B_1 \quad (2.3.36)$$

from which, the equation for the shifted curve can be written as

$$\frac{b_e}{w} = \frac{(1-B_1)}{\left(\frac{\sigma_{e \max}}{\sigma_{cr}} + B_2\right)} + B_1 \quad (3.4.1)$$

where B_2 is the abscissa distance $(\sigma_{e \max}/\sigma_{cr})$ by which the curve of a perfectly flat plate has to be shifted horizontally towards the vertical axis to take into consideration the effect of initial imperfection. For a given initial imperfection, the value of B_2 depends upon the buckling coefficient K . Table 3.4.4 and fig. 3.4.2 give the relationship between the parameter B_2 and the buckling coefficient K for the assumed initial imperfection of 0.2 times thickness. The functional relationship between B_2 and K can be written as given below, through a regression analysis having a correlation coefficient of 0.999.

$$B_2 = 0.378 - 0.768(K - 1.18)^4 \quad (3.4.2)$$

Hence the effective width equation of an unstiffened element can be written as

$$\frac{b_e}{w} = \frac{(1-B_1)}{\left(\frac{\sigma_{e \max}}{\sigma_{cr}} + B_2\right)} + B_1 \quad (3.4.1)$$

where

$$B_1 = 0.326 + 0.086 K^2 \quad (2.3.33)$$

and

$$B_2 = 0.378 - 0.768 (K - 1.18)^4 \quad (3.4.2)$$

3.4.4 Winter's Unstiffened Element Effective Width Equation

An effective width equation for unstiffened elements has already been proposed by Winter.¹³ This equation was derived by modifying Von Karman's effective width equation for stiffened elements to fit the test results on unstiffened compression elements. The equation can be written in a general form as

$$b_e/w = B_5 \sqrt{\sigma_{cr}/\sigma_{e \max}} (1.0 - B_6 \sqrt{\sigma_{cr}/\sigma_{e \max}}) \quad (3.4.3a)$$

Substituting eqn. 2.3.34 for ratio b_e/w in eqn. 3.4.3a, it can be written as

$$\sigma_{av}/\sigma_{cr} = B_5(\sqrt{\sigma_{e\ max}/\sigma_{cr}} - B_6) \quad (3.4.3b)$$

Eqn. 3.4.3b makes it easy to obtain constants B_5 and B_6 graphically, since this is an equation for a straight line in terms of the variables σ_{av}/σ_{cr} and $\sqrt{\sigma_{e\ max}/\sigma_{cr}}$. In order to obtain constants B_5 and B_6 , experimental and analytical investigation results are plotted in fig. 3.4.4. The two non-dimensional parameters in eqn. 3.4.3b are chosen as the ordinate and abscissa of the plot. The curve corresponding to the effective width eqn. 3.4.1, which is based on the analytical solution, is drawn in fig. 3.4.4. The buckling coefficient K equal to 0.5 is used for the curve since it yields a conservative value of the effective width for the values of K over a major range. A fully effective element curve ($\sigma_{av} = \sigma_{e\ max}$) is also presented. Using all this information, a straight line representing eqn. 3.4.3b is drawn to obtain a conservative fit. From this, the value of constants B_5 and B_6 is found to be

$$B_5 = 1.19$$

and

$$B_6 = 0.298$$

Substituting this in eqn. 3.4.3a

$$b_e/w = 1.19 \sqrt{\sigma_{cr}/\sigma_{e \max}} (1.0 - 0.298 \sqrt{\sigma_{cr}/\sigma_{e \max}}) \quad (3.4.5)$$

Comparing the coefficients B_5 and B_6 in eqn. 3.4.5 and the coefficients in eqn. 1.2.3, proposed by Winter for unstiffened elements, there is only a small difference in the value of the coefficient B_6 . Equation 3.4.5 is similar in format to the effective width eqn. 1.2.2 for stiffened elements which is given below.

$$b_e/w = \sqrt{\sigma_{cr}/\sigma_{e \max}} (1.0 - 0.22 \sqrt{\sigma_{cr}/\sigma_{e \max}}) \quad (1.2.2)$$

Equation 3.4.5 is plotted along with eqn. 3.4.1 for the two extreme values of the buckling coefficient ($K = 0.425$ and 1.277), in fig. 3.4.5. Eqn. 3.4.5 gives a conservative value of the effective width over a wide range, except in the early postbuckling range of the unstiffened elements with a low buckling coefficient K . The effective width given by eqn. 3.4.5 tends to become more and more conservative in the advanced postbuckling range.

The effective widths computed using eqn. 3.4.1 and eqn. 3.4.5 are compared with the effective widths evaluated from the experimental results in table 3.4.5. The effective width eqn. 3.4.1 yields results which vary from 4 percent on the conservative side to 7 percent on the unconservative side, when compared with the test results.

Eqn. 3.4.5 when compared with the test results, exhibits differences from 10 percent on the conservative side to 9 percent on the unconservative side. Both the equations seem to indicate a good correlation with the test results, except in the advanced postbuckling range, where the eqn. 3.4.5 becomes more conservative.

The ultimate and the preultimate test points are plotted in fig. 3.4.6 in terms of the parameters σ_{av}/σ_{cr} and $\sqrt{\sigma_{e\ max}/\sigma_{cr}}$. Curves corresponding to the effective width equation 3.4.1, for two values of the buckling coefficient K (0.855, 1.003), and the effective width equation 3.4.5 are also plotted in this figure for comparison. Preultimate points generally fall on the conservative side of the effective width equations, which can be attributed to the measurement of the average rather than the maximum supported edge strain by the strain gages. The ultimate load points do exhibit a good correlation with the effective width equations. A reasonably good correlation between the effective width equations and stub column test results indicates the validity of the effective width equations. These equations will be checked with the postbuckling behavior of the unstiffened compression flanges of flexural members, in the fifth chapter.

3.4.4 Out of Plane Deformation

Even though the existence of the postbuckling reserve of unstiffened elements was recognized long ago, there has been some reluctance about using this to the full extent with a uniform factor of safety, as in the case of stiffened elements. This has been mainly due to the objection to the unsightly waving of elements in the service load range. One of the objectives of this investigation has been to measure the amplitude of the out of plane deformation of unstiffened elements in the postbuckling range to get an idea of the magnitude of the waving.

The out of plane deformation of the unstiffened elements was measured during the test, as indicated in the test procedure. The amplitude of the out of plane deformation just prior to failure is given in table 3.4.2. These test points are also plotted in fig. 3.4.7. An analytical solution to the out of plane deformation amplitude of perfectly flat plates, given by eqn. 2.3.37, is also plotted for the values of the buckling coefficient K equal to 0.855 and 1.003.

All the test points fall on the conservative side of the analytical solution. There is considerable scatter in the test points and one could attribute this to the

effects of initial imperfection and the normal experimental scatter. It is important to realize that real elements will have out of plane deformation even before the local buckling stress is reached, whereas a perfectly flat plate equation does not give any out of plane deflection prior to the local buckling. However, the deflection prior to buckling is usually very small and is not of any interest. Hence, equation 2.3.37 can be used to compute the amplitude of the out of plane deflection. It can be seen that the amplitude of the out of plane deformation of unstiffened elements is not very high, even at the advanced postbuckling range, as long as there is some rotational edge restraint, however small it may be (fig. 2.2.7). Most of the unstiffened elements, with the exception of equal angles and cruciform sections under compression, have at least a small rotational restraint at the supported edge. Consequently, one should be able to use the available postbuckling strength of such sections, without any concern about the excessive waving.

3.5 Summary and Conclusions

Stub column experiments, conducted in the course of studying the buckling and postbuckling behavior of unstiffened elements, have been presented in this chapter.

Material and section properties, test set-up and procedure, and test results are presented in the first part of the chapter. The results of the stub column tests conducted by another investigator³² are also included. The test results have been compared with the analytical solution to arrive at an effective width equation for the unstiffened element postbuckling behavior. Two equations, one based on the analytical solution of the previous chapter and the other having a format similar to the effective width equation for stiffened elements, have been examined (eqs. 3.4.1, 3.4.5).

It is shown in this section that the buckling coefficient computed from the experiments, using the modified surface strain reversal method, compare well with the theoretical solution. An analytical solution, using a value of the initial imperfection amplitude equal to 0.2 times the thickness of the element, seems to exhibit a good agreement with the test results in the postbuckling range. However, in the prebuckling range, the analytical solution was conservative, and had to be modified to account for the progression of plastification into the element (eqn. 3.4.1). The effective width eqn. (3.4.5), having the same format as the effective width equation for stiffened elements, was obtained by a conservative fit of experimental and analytical results, and

is essentially the same as the Winter's equation for unstiffened elements (eqn. 1.2.3). This equation (eqn. 3.4.5) is generally conservative when compared to the effective width equation based on the analytical solution (eqn. 3.4.1), except in the early postbuckling range of elements with a low buckling coefficient K .

Eqn. 2.3.37 gives a conservative result for the amplitude of out of plane deflection in the range of interest, namely for stresses above critical stress. Consequently, this equation can be used to get an idea of the out of plane deflection of unstiffened elements. It was observed that the waving of the unstiffened elements may not be objectionable as long as there is at least some rotational edge restraint at the supported edge parallel to the direction of loading.

CHAPTER 4

INTERACTION OF THE LOCAL AND THE OVERALL BUCKLING IN COMPRESSION MEMBERS

4.1 General

Economical design of compression members requires that the material in a column cross section be distributed as far away from the centroid of the column as possible. This often results in compression members having thin component elements. It is commonly assumed in the study of the flexural and torsional instability of hot-rolled columns that the shape of the cross section remains unchanged. However, thin plate elements of a cold-formed column may buckle locally before the overall buckling of the column. This distortion of the column cross section reduces the effective stiffness of the column and the load at which the column becomes unstable. Consequently, it is important to consider the local buckling of thin plate elements while studying the overall buckling of columns in compression. In this chapter the effects of the local buckling of the unstiffened elements on the overall flexural buckling of cold-formed steel columns will be treated. Before venturing further into the study of the interaction behavior, it is appropriate to review briefly the flexural instability of the

columns.

4.1.1 The Flexural Instability of Columns

A centrally loaded ideally straight column transmits the compressive force passing through the centroidal axis without any lateral bending, as long as the applied force is less than the critical value known as the buckling load. When the load reaches the critical value, the column can be in equilibrium either in a straight configuration or a slightly bent configuration, as long as the cross section is such as to preclude the torsional buckling prior to the flexural buckling. This lateral buckling can take place either at a constant load or with a load gradient, depending upon whether the buckling is elastic or inelastic. Because of initial imperfections in the column geometry and the eccentricity of the applied load, the strength of a column, in practice, is usually less than the critical load of an ideal column having the same section and mechanical properties. However, the critical load is of interest since it can be visualized as being asymptotically approached as the imperfections tend to zero. In the current design practice^{1,49} the reduction in the strength due to the initial imperfections is taken care of by an appropriate factor of safety and a proper modification of the design curves.

The critical load at which a linearly elastic, initially straight and concentrically loaded column will buckle was derived by Euler as

$$P_e = \pi^2 EI/L^2 \quad (4.1.1)$$

where P_e is known as the Euler buckling load. Upon substituting for the moment of inertia I in terms of the area A and the radius of gyration r of the cross section, the formula for the stress σ_e at the Euler buckling load is obtained,

$$\sigma_e = \frac{\pi^2 E}{(L/r)^2} \quad (4.1.2)$$

These equations have been derived for the columns with the hinged-end condition and are usually extended to the other end conditions by substituting the effective length (KL) in the place of the actual length L . In order to avoid any possible confusion between the buckling coefficient and the effective length factor K , in all the column equations the length L instead of KL will be taken to mean the effective length of the column.

The flexural buckling stress of columns of shorter length may exceed the proportional limit of the material. Consequently, for these columns, the Euler equation derived for the elastic range is not directly applicable.

A detailed review of theories proposed for column buckling beyond the proportional limit can be found in the Guide to Design Criteria for Metal Compression Members.⁴⁹

A column loaded beyond the proportional limit without buckling will start to bend, as the load increases, at an average stress σ_t obtained by substituting the tangent modulus E_t of the material in the place of the elastic modulus E in eqn. 4.1.2.

$$\sigma_t = \frac{\pi^2 E_t}{(L/r)^2} \quad (4.1.3)$$

Even though the initial bifurcation in the inelastic range takes place at the tangent modulus stress (eqn. 4.1.3), the lateral deflection increases with an increase in the average compressive stress, and the upper bound on the failure stress is given by the reduced modulus stress σ_r

$$\sigma_r = \frac{\pi^2 E_r}{(L/r)^2} \quad (4.1.4)$$

where E_r is the reduced modulus, which is a function of the Youngs modulus E and the tangent modulus E_t , depending upon the cross section.

Structural steel coupons tested in tension exhibit a nearly linear stress-strain behavior up to the yield

stress. If this were to be the behavior of compression members, then one would expect the columns to develop full yield stress for values of the slenderness ratio (L/r) less than $(L/r)_y$ where

$$(L/r)_y = \sqrt{\pi^2 E / \sigma_y} \quad (4.1.5)$$

and the buckling stress would be given by the Euler stress (eqn. 4.1.2) for a value of the slenderness ratio larger than that given by eqn. 4.1.5. However, when a stub column is tested to ascertain the stress strain characteristics in compression, it is found that the proportional limit is lower than the yield stress, which is attributable to the presence of residual stresses, work hardening, and the variation in the yield stress over the cross section of the column. Fitting a parabola which joins the Euler buckling curve tangentially, and gives a conservative estimate of the major and minor axis flexural buckling stress of wide-flange columns having a maximum residual stress of $0.3\sigma_y$, the Column Research Council proposed the following equation for the buckling stress (σ_c) of hot rolled steel columns beyond the proportional limit.

$$\sigma_c = \sigma_y - \frac{\sigma_y^2}{4\pi^2 E} (L/r)^2 \quad (4.1.6)$$

Extensive research carried out to determine the strength of hot rolled steel columns is reviewed by the Guide to Design Criteria for Metal Compression Members.⁴⁹ These investigations treat analytically and experimentally the effects of the residual stresses and the initial curvature. One of the general conclusions that can be drawn from these studies is that the effects of the initial imperfections and the residual stress are most pronounced around the slenderness ratio, given by eqn. 4.1.5, where the Euler buckling stress is equal to the yield stress of the material. Having gone through the general equations governing flexural buckling, a cursory treatment of the research carried out by various investigators in the area of the interaction of the local and overall buckling of the compression members will be presented in the succeeding section.

4.1.2 The Flexural Buckling Strength of Compression Members With Locally Buckling Elements

The effective areas of the thin compression elements of cold-formed steel columns decrease with an increase in the compressive stress. If the columns are very slender, they may become unstable even before the effective area of component elements begins to decrease. The buckling stress of such columns may be obtained by using

the Euler eqn. 4.1.2 as long as the stress is below the proportional limit. The cold-formed steel compression members also exhibit a gradually yielding stress strain curve in compression. This can be attributed to the non-linearity of the basic material property before the yield, the cold work in the process of forming, and the local buckling. The reduction in the effective area of thin elements in compression due to local buckling, reduces the average compressive stress at failure of stub columns with thin elements to a value less than the yield stress, whereas a fully effective stub column will have an average compressive stress at failure nearly equal to the yield stress. Consequently, the flexural buckling stress of the compression members with component elements buckling locally, cannot be obtained directly from the equations derived for hot rolled sections designed to remain fully effective until failure.

The ultimate load of a stub column having thin compression elements that buckle locally can be written as

$$P_u = A_{eff} \sigma_y = A \sigma_y Q = P_y Q \quad (4.1.7)$$

where Q is known as the form factor, introduced to take into account the reduction in the effective area, P_u is the ultimate load, A_{eff} is the effective area, A is the total area and P_y is the load at failure of the fully

effective section. The main difference between the strength of stub columns with thin elements, and that of a fully effective section, is the factor $Q\sigma_y$ instead of σ_y . The Specification for the Design of Cold-Formed Steel Structural Members² recommends the use of the following equation to determine the flexural buckling strength of the cold-formed structural steel compression members beyond the proportional limit.

$$\sigma_c = Q\sigma_y - \frac{(Q\sigma_y)^2}{4\pi^2 E} (L/r)^2 \quad (4.1.8)$$

The equation has been obtained by replacing the yield stress σ_y in the Column Research Council equation (4.1.6) with $Q\sigma_y$ to account for the reduced effective area. This equation, however, does not consider the reduction in the radius of gyration as a result of the local buckling. The buckling strength of slender cold-formed columns is calculated using the Euler equation (eqn. 4.1.2).

Bijlaard et al²⁷ were among the earliest investigators to study the buckling strength of compression members with component plate elements in the postbuckling range. They derived an analytical solution for the flexural buckling strength of columns in the intermediate range of the slenderness ratio. The flexural buckling strength before the local buckling of the elements was

taken to be equal to the Euler buckling stress in their derivation. In the plastic range, the buckling strength was represented by a Johnson's parabola. The authors compared their analytical solution with the experimental results on aluminum tubular and H column specimens and indicated good agreement. However, they failed to recognize the reduction, due to initial imperfections, in effective area even before local buckling. This reduction has been found to be discernable in the case of steel members with thin elements. Various other investigators^{14,52,53,54,31} have compared their semi-empirical solutions for the interaction in the postbuckling range with the test results. Many of these solutions are applicable only in the elastic range.

Graves Smith²⁸ has presented a theoretical analysis for the flexural buckling strength of rectangular tubes in the postbuckling range of the component plates. He has included the large deflection due to the local buckling and the plastification of plate elements in his development. He indicates good comparison between his analytical solution and the results of tests he conducted using square aluminum tube columns.

DeWolf³² conducted tests using cold-formed steel compression members with stiffened and unstiffened elements. He has compared the results of these tests with theo-

retical curves obtained using the effective moment of inertia in the tangent modulus eqn. 4.1.3. These effective moments of inertia were arrived at by distributing the effective area of buckled elements properly about the neutral axis. He shows good correlation between the test results and theoretical curves. The theoretical method proposed by DeWolf will be discussed in further detail later in this chapter (section 4.4.3).

4.2 Experimental Investigation of Compression Members

An experimental investigation of compression members was conducted to study the interaction of the flexural buckling of the compression members and the local buckling of the unstiffened elements. The objective of this investigation was to determine the effects of the local buckling of the unstiffened elements on the overall or flexural buckling of compression members.

4.2.1 Material Properties

The 18 gage sheets used in fabricating the stub column specimens were also used in forming the long compression specimens. Consequently, the mechanical properties of the specimens determined, as detailed in sec-

tion 3.2.1, are given in table 3.2.1.

4.2.2 Design of the Specimens

The cross section dimensions of the compression specimens were the same as those used for the stub column specimens of the previous chapter. There were five different H-sections, having the ratio of the flat width to thickness (w/t) of unstiffened elements in the range of 30 to 60. Three columns of different lengths, corresponding to each of the cross sections, were tested. The lengths of the specimens were chosen so that the columns buckle in the postbuckling range of the unstiffened elements. The measured dimensions of the specimens, the section properties, and the sheets from which they were fabricated are given in table (4.2.1).

DeWolf³² tested four different sections having similar cross sections, but the (w/t) ratios of the unstiffened elements were in the range of 16 to 30. The results of his tests will also be presented in this chapter to encompass the entire range of interest of the w/t ratio.

4.2.3 Fabrication and Instrumentation

The column specimens (H section) were fabricated by gluing, back to back, two channel sections from the same sheet, which were cold formed by press braking. The form-

ing and the glueing processes have been described in section 3.2.3.

One cold-rolled 3/4" end plate was welded to each plane end of the finished column such that they were perpendicular to the axis of the column. The welding of the end plates to the column was carried out in a particular order, so that there was no residual compressive stress at the free edge of the unstiffened elements due to welding. This was done to ensure that the columns would not fail prematurely due to the crippling of the unstiffened elements locally at an end of the column, as a result of the superposition of the applied and the residual compressive stresses at the free edge of the unstiffened elements.

Twelve SR-4, A12 and two SR-4, A9 strain gages were glued to the specimens at mid-height, similar to the stub columns as shown in fig. 3.2.2. These gages were used to center the columns during the set-up and also to get an idea of the axial stiffness of the columns during the test.

4.2.4 Experimental Set-Up and Procedure

The column tests were performed using the ASTM Designation STP 4.19, "The Testing of Pinned-End Steel Columns",⁵⁵ as a guide. The columns were tested as pinned-end columns, using the fixtures developed at Cornell for

another series of pinned column tests.⁵⁶ The end plates of the column were set against the ground plates in the end bearing fixtures. Fig. 4.2.1 shows sections drawn through the end fixtures. The columns were oriented in the fixtures such that the weak axis of the columns was parallel to the knife edge. Thus the supports were free to rotate about the knife edge while the column was buckling about the weak axis.

The end plates of the columns were secured by four bolts in each direction, provided in the box of the end fixtures. Using the set of eight bolts, the column ends could be moved horizontally in either direction. The boxes could also be rotated about a horizontal axis perpendicular to the knife edge by adjusting the wedges under the knife edge using a lower set of four bolts. By using both sets of bolts, any eccentricity of the axial load on the columns could be corrected.

Seven dial gages were used to measure the transverse deflection of the columns, as indicated in fig. 4.2.2. Four of these dial gages were used to measure the transverse deflections in the direction of the strong axis at the ends and the center section of the columns, and the other three were used to measure the deflection parallel to the weak axis at these sections. Dial gages were also provided to measure any displacement of the

end fixtures during the test.

The tests were conducted in a Baldwin testing machine and a picture of the whole set-up is shown in fig. 4.2.3. The columns were initially loaded to approximately thirty percent of their local buckling load for the purpose of centering. The eccentricity of the applied load was checked using the strain gages and the dial gages at the mid-height of the columns. Any displacement of the end fixtures was also recorded. The uniformity of increase in the strain over the cross section of the specimen and the lack of any transverse deflection, indicated that the load was concentric. In a few of the instances, it was difficult to achieve uniform compression as measured by the strain gages and in such cases only the dial gages were relied upon for the purpose of centering the columns. If the applied load was found to be eccentric, the load was reduced to about 200 pounds and the column eccentricity was corrected by adjusting the two sets of bolts provided for this purpose in the end fixtures. Once the column had been centered, the load was reduced to a small initial load of about 200 pounds to keep all the surfaces in contact and thus maintain the alignment and from this load the test was begun.

The load was increased during the test by small increments, so that the readings could be taken as close to the failure as possible. Prior to the local buckling of the elements, the strain gage and dial gage readings were recorded after the loading valves were shut off and the load had stabilized. In the postbuckling range, it was difficult to obtain the stability of load this way, and the readings were taken by maintaining the load constant at a particular level by operating the valves. Near the flexural buckling load, the transverse deflection of the column increased at a faster rate and the failure took place following the formation of permanent kinks in the unstiffened elements on the concave side of the buckled column. After failure, the transverse deflection increased with a decrease in the axial load, indicating instability. Fig. 4.2.4 shows a picture of all the columns after failure.

The procedure for the evaluation of the test results and the results of the compression tests will be presented in the following sections.

4.3 Background for Evaluation of Experimental Data

4.3.1 Determination of the Elastic Flexural Buckling Load From Experiments

While an ideal column in the linear elastic range exhibits bifurcation buckling at the Euler buckling load,

an actual column, when loaded in compression, does not undergo bifurcation buckling due to the effects of imperfections in the geometry and the loading. The real columns withstand the compression with very little increase in transverse deflection in the early stages, and the deflection grows at an increasing rate near the Euler buckling load.

Southwell⁵⁷ proposed a method for obtaining the theoretical flexural buckling stress of a column from the experimental result of the column with initial imperfections. He derived the following equation for the lateral deflection of an elastic column subject to compression.

$$w_m = P_{cr} \frac{w_m}{P} - \bar{w} \quad (4.3.1)$$

where w_m is the increase in the deflection at the center of the column due to the axial load P , \bar{w} is the initial deflection at the same section, and P_{cr} is the theoretical flexural buckling load. Equation 4.3.1 defines a straight line in terms of the variables w_m and w_m/P which are obtained from the elastic range of the column test in which P is a reasonably large fraction of P_{cr} . Eqn. 4.3.1 has been derived for compression members having a constant moment of inertia as the load is increased, whereas, the moment of inertia of columns, with locally buck-

ling unstiffened element, changes due to a change in the effective area. If the change in the moment of inertia is taken into account, eqn. 4.3.1 reduces to

$$w_m = \frac{I_e}{I_{ecr}} \times P_{cr} \frac{w_m}{P} - \bar{w} \quad (4.3.2)$$

where I_e is the effective inertia at the load P and I_{ecr} is the effective inertia at the load P_{cr} . Plotting the results of compression tests in terms of the variables w_m and w_m/P at loads near the critical load, test points lie nearly in a straight line. The slope of the straight line is nearly equal to the critical load P_{cr} , since at loads near the critical load $\frac{I_e}{I_{ecr}}$ is nearly equal to 1. Test points falling on a straight line gives some validity to this assumption. Plotting the result of a test in terms of the variable in eqn. 4.3.1., (fig. 4.3.1) the slope of the straight lines gives the theoretical elastic buckling load.

This procedure was used to determine the flexural buckling load of all the test specimens. In some of the tests the failure was very sudden, and in such cases the buckling load has been taken to be equal to the failure load. In the next section, the results of the column tests evaluated in this manner will be presented and will

be compared with various analytical solutions.

4.4 Evaluation of the Experimental Results

4.4.1 Experimental Results

Results of the long column tests conducted in this investigation, and the relevant results of similar tests conducted by a few other investigators, will be presented in this section. The ultimate load and the theoretical flexural buckling load, computed as described in the previous section, are presented in table 4.4.1 for all fifteen specimens tested in this investigation. The average flexural buckling stress obtained by dividing the buckling load by the total area is also given in the table. The slenderness ratio calculated from the effective length of the column and the radius of gyration of the total cross section are other values of interest in the table.

DeWolf³² tested pinned-end compression members similar in shape to the specimens in this investigation (fig. 3.2.2). The w/t ratios of the unstiffened elements of the specimens were in the range of 16 to 30. The length of the specimens were chosen so as to have the overall flexural buckling occur in the postbuckling range of the component unstiffened elements. The test set-up and procedure were the same as described in Section 4.2.4. The

flexural buckling loads have been assumed to be nearly the same as the corresponding ultimate load given by DeWolf³². The specimens' dimensions, properties, and the results of the tests conducted by DeWolf are given in table 4.4.2. The numbering of the specimens has been changed from U- in DeWolf's report to UD- in this report.

Bijlaard and Fisher²⁷ have presented the results of compression tests on extruded H sections of 75S-76 aluminum alloy. They tested three different H sections having a flat width to thickness ratio (w/t) of unstiffened elements equal to 10.3, 14.3 and 18.14. Corresponding to each of these three sections (J, K and L), columns of different lengths having a flexural buckling stress in the postbuckling range of the component unstiffened elements were tested. A detailed outline of the tests and results can be obtained from their publication.²⁷ The dimensions and the section properties of their specimens are presented in table 4.4.3 and fig. 4.4.1. The test results are given in table 4.4.4.

All the test results have been presented in the tables in a format suitable for comparison to the analytical solutions to be presented in the following sections.

4.4.2 Comparison of Test Results to AISI Specification Procedure

In this section, the results of the column tests will

be compared to the flexural buckling strength of locally buckling columns determined using the procedure suggested by the AISI Specification for the Design of Cold-Formed Steel Structural Members. According to the specification, the buckling strength is given by the two following equations as discussed in section 4.1.2.

$$\sigma_c = Q\sigma_y - \frac{(Q\sigma_y)^2}{4\pi^2 E} \left(\frac{L}{r}\right)^2 \quad \text{when } \frac{L}{r} \leq \sqrt{\frac{2\pi^2 E}{Q\sigma_y}}$$

and

$$\sigma_c = \sigma_e = \frac{\pi^2 E}{(L/r)^2} \quad \text{when } \frac{L}{r} > \sqrt{\frac{2\pi^2 E}{Q\sigma_y}} \quad (4.4.1)$$

where Q is the form factor defined in section 4.1.2.

Substituting for $\sqrt{\pi^2 E/\sigma_y}$ in equations 4.4.1 from 4.1.5.

$$\sigma_c / \sigma_y = P/P_y = Q - \frac{Q^2}{4} \frac{(L/r)^2}{(L/r)_y^2} \quad \text{when } \frac{L}{r} \leq \sqrt{\frac{2}{Q}} \left(\frac{L}{r}\right)_y$$

and

$$\sigma_c / \sigma_y = P/P_y = \frac{(L/r)_y^2}{(L/r)^2} \quad \text{when } \frac{L}{r} > \sqrt{\frac{2}{Q}} \left(\frac{L}{r}\right)_y \quad (4.4.2)$$

In eqn. 4.4.2 $(L/r)_y$ is the slenderness ratio of the columns for which the Euler buckling stress is equal to

the yield stress of the material, P is the flexural buckling load and P_y is the load on the specimen if the total area of the cross section yields without buckling locally. For the stub columns tested the ratio of the ultimate load to the yield load (P_u/P_y), which is taken equal to the form factor Q as in the case of columns with stiffened elements, and the ratio of the slenderness ratios $(L/r)/(L/r)_y$ are given in table 4.4.5. The values of Q given in this table are computed from the stub column test results. In table 4.4.6, the values of the same variables are given for the slender columns tested in this investigation. Column curves corresponding to eqn. 4.4.2 are plotted in figs. 4.4.2 through 4.4.6 for the five values of the form factor Q obtained from the five different size stub columns tested. The results of the stub column and the slender column tests are also plotted in the corresponding figures.

The AISI curves, plotted using the Q values from the test results, are generally unconservative compared to the slender column test results. The difference between the theoretical value and the test results increases as the flat width to thickness ratio of the unstiffened element increases. The error on the unconservative side is about 55 percent for sections having unstiffened elements with

a w/t ratio of about 60 and decreases to about 4 percent for the sections having unstiffened elements with a w/t ratio of about 30. It is important to realize that the curves are drawn for the Q values obtained from the test results, whereas the Q values calculated on the basis of the AISI recommendation will be much smaller, because of the limited use of the postbuckling strength of the unstiffened elements. AISI curves using the Q values suggested by the AISI² are also plotted in figs. 4.4.2 through 4.4.6 to indicate the conservative nature of the existing AISI design procedure.

The AISI eqn. 4.4.1 has been derived from the Column Research Council (CRC) equation (eqn. 4.1.6) by taking into account only the reduction in the effective area through the introduction of the form factor Q . Whereas, as discussed earlier, the reduction in the effective area leads also to a reduction in the effective radius of gyration. This has not been taken into consideration in the eqn. 4.4.1. Any reduction in the radius of gyration in eqn. 4.4.1 leads to a reduction in the buckling stress. Hence, when the reduction in the effective radius of gyration is neglected, one should expect to obtain results of an unconservative nature. An increase in the w/t ratio is accompanied by an increase in the postbuckling range and

hence a larger decrease in the effective radius of gyration. Consequently, the AISI equation using the Q values from the test results should give a more unconservative result as the (w/t) ratio of the unstiffened element increases. This reasoning explains the discrepancy between the AISI curves obtained using the test Q values and the test results in figs. 4.4.2 through 4.4.6.

In the following sections, theoretical solutions for the determination of the flexural buckling stress will be presented which will take into consideration the reduction in the effective area, as well as the reduction in the effective radius of gyration due to local buckling. These theoretical solutions will be compared to the results of the tests presented in tables 4.4.1 through 4.4.4.

4.4.3 Comparison of Test Results to Theoretical Solutions

In the second chapter of this report, an analytical solution was presented for the elastic postbuckling behavior of unstiffened elements. As an extension of this, a method for determining flexural buckling strength will be presented in this section. The flexural buckling strength, calculated using some simplifying assumptions regarding the distribution of the effective area of the unstiffened elements in the postbuckling range, will also be presented subsequent to this.

4.4.3.1 Flexural Buckling Strength from Analytical

Solution

The membrane stress in the postbuckling range of the unstiffened elements, in the direction of the applied compressive stress (y direction), is given by eqn.

2.3.15b .

$$\sigma_{yy} = A \{ (G_1 + G_2)_{,xx} \cos \frac{2\pi y}{L_w} + (G_0 + G_3)_{,xx} \} \quad (2.3.15b)$$

where L_w is the length of the local buckling waves. A and the functions G_0 , G_1 , G_2 , and G_3 are defined in the second chapter. It was observed in that chapter that the effective cross section of the unstiffened elements in the postbuckling range varies along the length of the wave. The average effective section over the length of a whole wave should be used to calculate the flexural buckling strength. The flexural buckling strength was computed for one column section using the average effective section and the least effective section at $y=L_w/2$ and it was found that the difference between the two flexural buckling strengths was small. Since the effective width equations in the third chapter have been derived for the section $y=L_w/2$, the effective area corresponding to this section will be used in the derivation of the flexural buckling strength.

The normal membrane stress at section $y=L_w/2$ is

$$\sigma_{yy} \Big|_{y=L_w/2} = \sigma = A \{ (G_0 + G_3)_{,xx} - (G_1 + G_2)_{,xx} \} \quad (4.4.3)$$

The stress at the supported edge is

$$\sigma_{e \max} = \sigma \Big|_{x=0} = (\sigma_{av})_e e^{-A \{ \sum_{n=4}^{10} n c_{0n} + 2c_{12} + \beta^2 (c_{21} + 2c_{24}) \}} \quad (2.3.31a)$$

where constants C_{0n} , C_{1n} , C_{2n} are defined in the second chapter, $\beta = 2\pi w/L_w$ and $(\sigma_{av})_e$ is the average membrane stress over the total area of the element. The ratio of the membrane stress σ to the maximum stress $\sigma_{e \max}$ can be obtained from eqs. 4.4.3 and 2.3.31a. This ratio is shown in fig. 4.4.7 for a typical unstiffened element. The typical redistribution of stress due to local buckling from the free edge to the supported edge can be seen here. The redistribution towards the supported edge increases as the loading progress into the postbuckling range. The effective section properties of an element about any axis can be obtained by using an effective cross section in which the thickness is varied according to the ratio of the membrane stress σ to the maximum supported edge stress $\sigma_{e \max}$. Thus

$$t_{\text{eff}} = \frac{t\sigma}{\sigma_{e \text{ max}}} = \frac{tA}{\sigma_{e \text{ max}}} \{G_0 + G_3 - G_1 - G_2\},_{xx} \quad (4.4.4)$$

In fig. 4.4.8b, the effective thickness given by equation 4.4.4 is shown for a typical unstiffened element. Using this equivalent cross section, the effective section properties and hence the flexural buckling column curves can be found, following the steps given below.

- 1) Assume an average stress over the unstiffened elements $((\sigma_{\text{av}})_e)$
- 2) Calculate the maximum supported edge stress $(\sigma_{e \text{ max}})$, distribution of the effective thickness (t_{eff}) , the effective area (A_{eff}) and the effective moment of inertia (I_{eff}) , using eqn. 4.4.4.
- 3) Multiplying the effective area (A_{eff}) by the maximum edge stress $(\sigma_{e \text{ max}})$, the total load (P) can be obtained, from which the average stress over the cross section $(\sigma_{\text{av}} = P/A_{\text{total}})$ can be found.
- 4) The effective length L corresponding to the load P can be obtained from the equation

$$L = \sqrt{\frac{\pi^2 E_t I_{\text{eff}}}{P}} = \sqrt{\frac{\pi^2 E_t I_{\text{eff}}}{\sigma_{\text{av}} A_{\text{total}}}} \quad (4.4.5a)$$

In eqn. 4.4.5a E_t is the tangent modulus and A_{total} is the total area of the cross section. If the mechanical properties vary over the cross section, as in the case of cold-formed members, eqn. 4.4.5a can still be used by

introducing the summation of the effective section properties, E_{ti} , and $I_{i,eff}$ of the corner and flat elements. Eqn. 4.4.5a becomes

$$L = \sqrt{\frac{\pi^2 \sum_{i=1}^n E_{ti} I_{i,eff}}{\sigma_{av} A_{total}}} \quad (4.4.5b)$$

In eqn. 4.4.5b, all the properties with subscript i correspond to the i^{th} element and the summation is over all the elements in the cross section. The tangent moduli E_{ti} of the elements are calculated at a strain equal to $e_{e\ max}$, where $e_{e\ max}$ is the strain at the supported edge of the unstiffened element. In the specimens tested, the corners were sharp bends. Consequently, the effect of strain hardening due to cold working has been neglected.

The tangent modulus in eqs. 4.4.5a and 4.4.5b had to be computed before these equations could be used. This was done using the Ramberg-Osgood⁵⁸ equations to model the stress-strain curve of the material. The equation expressing the relationship between the stress and the strain could be written as

$$e = \frac{\sigma}{E} + K_1 \left(\frac{\sigma}{E}\right)^n \quad (4.4.6a)$$

where e is the strain at the stress σ , E is the modulus of elasticity of the material, and constants K_1 and n

were chosen to suit the material stress strain curve.

The constant K_1 is defined by Ramberg-Osgood as,

$$K_1 = 3/7 \left(\frac{\sigma_1}{E} \right)^{1-n} \quad (4.4.6b)$$

where σ_1 is the stress at the intercept of the material stress strain curve and a line through the origin with a slope of 0.7 times the Young's modulus E .

For the steel specimens of this investigation and DeWolf's investigation³², σ_1 has been taken as the yield stress of the material and n has been taken to be equal to 75, since the materials had essentially sharp yield points. The value of σ_1 and n for Bijlaard and Fisher's aluminum specimen were found by curve fitting and are given in table 4.4.3. The yield stress of these specimens and the modulus of elasticity are also given in the table. Following the procedure outlined, the column curves for all the specimens were derived. These curves will be compared in section 4.4.3.3 to the other approximate solutions to be presented in the next section and the test results in tables 4.4.1 through 4.4.4.

4.4.3.2 Flexural Buckling Strength from Effective Width Equations

The analytical procedure outlined in the proceeding

section for obtaining column curves is long and time consuming, and is not a feasible method for routine design. In this section a procedure for obtaining column curves using the effective width equations will be presented. Certain simplifying assumptions regarding the membrane stress distribution in the unstiffened elements is made, thus reducing the cumbersome computation with very little loss of accuracy.

DeWolf³² assumed two types of effective cross sections to compute the effective section properties of compression members with unstiffened elements. (a) In the first case, the thickness of the element was assumed to vary linearly from the actual thickness at the supported edge, to a reduced thickness at the free edge such that the effective area was equal to the effective area obtained from an effective width equation. (b) In the second case, the whole effective area of an unstiffened element was assumed to be distributed over a width equal to the effective width adjacent to the supported edge of the unstiffened element and the thickness was maintained uniform and equal to the actual thickness.

In fig. 4.4.8a, the actual stress distribution over the width of an unstiffened element and the two assumed equivalent stress distributions are shown. When the flex-

ural buckling of a member in the postbuckling range of the component unstiffened elements takes place about an axis perpendicular to the unstiffened elements and near the supported edge (e.g. weak axis of an H section), the former assumption (case a) regarding stress distribution tends to overestimate the effective stiffness of the member, whereas the latter assumption (case b) tends to underestimate the effective stiffness of the member. Figs. 4.4.9b and 4.4.9a show the distribution of the effective area of the unstiffened elements in columns according to the two assumptions. In figs. 4.4.9a and 4.4.9b, it has been assumed that the web remains fully effective until failure. However, any reduction in the effective area of the web due to local buckling can be easily accounted for. The flexural buckling stress calculated on the basis of the distribution of the effective area as in the case (a) provides an upper bound and that of case (b) provides a lower bound to the flexural buckling stress based on the actual stress distribution.

The column curves based on the two assumed equivalent cross sections can be obtained by following the steps given below.

- 1) Select a uniform longitudinal compressive strain ϵ ;
- 2) From the stress strain relationship of the material (eqn. 4.4.6a) determine the tangent modulus E_{ti} and

the stress σ_i for the flat and corner elements as outlined in the last section.

- 3) Determine the effective area of the flat elements using an effective width equation.
- 4) Determine the effective moment of inertia of the sub elements based on the assumed distribution of the effective area.
- 5) Compute the effective area ($A_{\text{eff}} = \sum A_{i,\text{eff}}$) of the column cross section.
- 6) Compute the total force on the column cross section ($P = \sum \sigma_i A_{i,\text{eff}}$) and the average stress ($\sigma_{\text{av}} = P/A$).
- 7) Find the length (L) of the column that experiences the flexural buckling at the load P from eqn. 4.4.5b.
- 8) Find the L/r from the length L and the radius of gyration of the total cross section r.

Following the procedure outlined above, the flexural buckling stress curves for all the specimens were derived assuming the two equivalent stress distributions (figs. 4.4.9a and 4.4.9b) and using the two effective width equations (eqs. 3.4.1 and 3.4.5) derived in the third chapter. In the next section, the results of the tests presented in the tables 4.4.1 through 4.4.4 will be compared to the theoretical solutions presented in this section and the preceding section.

4.4.3.3 Comparison of Test Results

In figs. 4.4.10 through 4.4.33, the column curves obtained using the theoretical procedures presented in sections 4.4.3.1 and 4.4.3.2 are plotted for the test specimens in tables 4.4.1 through 4.4.4, along with the corresponding test results. In these figures, the curves marked "analytical solution" correspond to those obtained following the procedure outlined in section 4.4.3.1. Flexural buckling curves have been derived for all the specimens following the procedure discussed in section 4.4.3.2 using the two effective width equations (eqs. 3.4.1 and 3.4.5) derived in the third chapter. The effective width equation used is indicated in the title of the corresponding figure. The stress distributions assumed for obtaining the effective inertia are indicated in the plots by referring to corresponding distributions in fig. 4.4.9. The curve corresponding to the Euler equation 4.1.2 is also drawn in these figures.

The analytical solution curves in figs. 4.4.10 through 4.4.18 do not join the Euler curve within the range of the figures because, according to the analytical solution, the decrease in the effective width of the unstiffened elements begins from the very onset of compressive stress. The analytical solution curves, however, become asymptotically very close to the Euler curves within the range of the

plots. The effective width solution curves, using eqn. 3.4.1 are also plotted in the same figures (figs. 4.4.10 through 4.4.21). There are two curves corresponding to the two assumed distributions (fig. 4.4.9) of the effective area of the unstiffened elements (figs. 4.4.10 through 4.4.21). Generally, the analytical solution curves lie between these two curves corresponding to the effective width equations, since the actual effective radius of gyration lies between the two effective radii of gyration obtained using the two assumed distributions of the unstiffened elements' effective area. The analytical solution curves fall outside the bounds of the curves based on the assumed distribution of the effective area in some regions. This can be attributed to the conservative nature of the effective width equations, when compared to the effective width from the analytical solution. In general, the analytical solution curve falls nearer to the curve obtained by assuming a linear variation of the effective area (fig. 4.4.9b).

Since, according to the effective width eqn. 3.4.1, the reduction in the effective width begins only after the applied compressive stress exceeds a limiting value, the flexural buckling curves obtained using this equation merge with the Euler curve above a particular slenderness ratio. This is true with the curves obtained using the

effective width eqn. 3.4.5, though in this case the limiting value of the slenderness ratio is higher (figs. 4.4.22 through 4.4.33).

In general, the results of the compression tests fall between the two curves corresponding to the two assumed effective area distributions and are usually nearer to the curve corresponding to the rectangular distribution (fig. 4.4.9a). Consequently, the flexural buckling stress computed using this effective area distribution (fig. 4.4.9a) can be expected to yield a conservative and reasonable estimate of the flexural buckling strength of the compression members in general.

There are certain cases where even this theoretical result yields an unconservative value of the buckling strength, as indicated by some of the test points falling below the curve corresponding to the rectangular distribution of the effective area of unstiffened elements (fig. 4.4.9a). This happens only for such columns which have a theoretical flexural buckling stress very nearly equal to the yield stress of the material. All the theoretical solutions have considered only the membrane stresses in the unstiffened elements and have disregarded the bending stress due to the local buckling of the elements. A superposition of the membrane and the bending compressive stresses in the unstiffened elements may lead to the yielding of the unstiffened elements at some point

different from the supported edge, even before the stress at the supported edge reaches the yield stress. In such a case, the stiffness of the yielded portion of the unstiffened element drops to a very low value, whereas this has not been considered in the theoretical analysis. In addition to this, the bending of columns below the flexural buckling load, due to initial imperfections, will lead to an increase in the load on the unstiffened elements on the concave side of the columns, and this could reduce the stiffness of the column to a value less than that computed on the basis of the uniform compression of the column. The reduction in the flexural buckling stress, when the theoretical flexural buckling stress is nearly equal to the yield stress, can be attributed to these two reasons. It is difficult, if not impossible, to take into consideration these effects theoretically. A procedure to approximately accommodate these effects in the computation of the flexural buckling stress will be presented in the chapter 6, which deals with the design method of compression members.

Some of the test specimens of Bijlaard and Fisher buckle at the Euler buckling stress, whereas the theoretical solutions indicate a flexural buckling stress less than the Euler buckling stress (figs. 4.4.19 - 4.4.21, 4.4.31 - 4.4.33). This can be attributed to a lower value of the amplitude of initial imperfection of

specimens' unstiffened elements, whereas a value of 0.2 t was assumed in the derivation of the theoretical solution and effective width equations.

4.5 Summary and Conclusions

The results of compression tests on members with unstiffened elements were presented. This included the results of the tests conducted in this investigation and the results of the tests on similar specimens by other investigators.

An analytical solution to obtain the column curves of members with unstiffened compression elements buckling locally, was developed. Theoretical solutions, based on two types of distribution of the effective area of the unstiffened elements obtained from the effective width equations, were also presented. The theoretical solutions were compared with the results of the tests on compression members.

It can be concluded that the flexural buckling stresses based on the rectangular distribution of the effective area of the unstiffened elements adjacent to the supported edge (fig. 4.9.9a) are generally in good agreement with the test results. The flexural buckling stress based on the effective width equation 3.4.5 is

more conservative in the early postbuckling range than that obtained using eqn. 3.4.1, due to the conservative nature of eqn. 3.4.5 in this range.

In Appendix 2 another method for obtaining the flexural buckling stress of slender columns with thin unstiffened elements is presented, which is a modified form of the CRC procedure.

CHAPTER 5

EFFECT OF LOCAL BUCKLING ON FLEXURAL MEMBERS

5.1 General

Flexural members, subjected either to a uniform bending moment or bending with a moment gradient, are commonly encountered in structural applications. Generally, such members fail either by local buckling of the flanges in compression or by lateral buckling. The lateral buckling of thin walled members depends upon the unbraced length and the radius of gyration of the compression flanges about an axis perpendicular to the direction of the lateral deflection. By choosing these two factors properly, failure due to lateral buckling can be avoided, and in such cases local buckling of compression flanges initiates the failure. In this chapter, failure of flexural members only due to local buckling of the unstiffened compression flanges will be studied.

Hot-rolled steel sections are proportioned to avoid the local buckling of compression flanges in the elastic range. In fact, compact hot-rolled sections can sustain compression strain up to the strain hardening range of the material. These sections can be used in the plastic

design of indeterminate structures requiring a large inelastic rotation capacity at maximum moment sections in the structure. M.G. Lay et al^{33,34} have presented an analytical study of wide-flange beams under uniform moment and moment gradient. They have investigated both the local buckling of compression flanges and the lateral buckling. Local buckling of a plate in the inelastic and the strain hardening ranges has been investigated by Haaijer^{26,59}. An experimental investigation of the post-elastic behavior of wide flange beams has been conducted by Sawyer³⁵ and an experimental investigation of beams under moment gradient has been carried out by Lukey et al.³⁷ Experimental and analytical investigations to study the lateral buckling and the postbuckling strength of wide-flange beams were performed by Lee and Galambos.^{60,61} All these investigations were carried out to study the behavior of the hot-rolled steel beams.

The compression elements of cold-formed flexural members are usually thin. Consequently, these elements often buckle locally in the elastic range, and rarely do they withstand compression strain in the strain hardening range. Therefore, the local buckling is of interest only in the elastic range and the early stages of the inelastic range (prior to strain hardening), in the design of the cold-formed flexural members. In this chapter, the

results of tests conducted on cold-formed flexural members with unstiffened elements in compression will be presented and will be compared with the analytical and effective width equations already derived in the second and third chapters.

5.2 Flexural Member Tests

5.2.1 Material Properties


Eleven beam specimens were fabricated from four 4 feet by 10 feet sixteen gage high strength steel sheets to obtain a large elastic postbuckling range. Seven other beam specimens were formed using two 4 feet by 10 feet twelve gage low carbon commercial grade steel sheets. Three tensile coupons were tested from each of the six sheets to obtain the material properties, following the ASTM Procedure E8-69 on "Tension Testing of Metallic Materials."⁴⁷ Tension coupons were also made from the undisturbed portions of the tested specimens to check the material properties. The mechanical properties of the six steel sheets are given in table 5.2.1. The tension tests generally revealed a sharp yielding stress strain relationship with yield plateau. Some of the tension coupons had a proportional limit around two thirds of the yield stress. However, the departure from linearity was very small until the yield stress was reached. Strain

hardening started at an average strain of 0.02 in./in. for sheets I through IV and at an average strain of 0.017 in./in. for the sheets V and VI. The average elongation of a two inch gage length was about 40 per cent.

Hans Peter Reck, a former researcher at Cornell University, tested beams with unstiffened elements in compression. Results of these tests, not reported so far, are also included in this chapter. The yield stress of these specimens are presented in table 5.4.1 along with the test results.

5.2.2 Design of Experimental Specimens

One of the objectives of the beam tests is to study the elastic and the inelastic local buckling of the unstiffened compression elements in flexural members. The beam specimens were designed so that the unstiffened elements in the members were subjected to compression.

The beam specimens (B-1 through B-18) designed for this investigation were inverted hat sections () shown in fig. 5.2.1. The specimens were designed to avoid failure due to lateral buckling, and local buckling of webs as a result of the combined shear and flexural compressive stress. The webs were also designed to withstand the loads without local crippling. The tension and

compression flanges were designed to minimize the effects of curling as a result of the beam curvature. The dimensions of the specimens, from direct measurement, are listed in table 5.2.2. Reck's specimens (UP-9 through UP-12) were I sections, the geometry of which is shown in fig. 5.2.1b and the measured dimensions are listed in table 5.2.2. The dimensions are the average of the measurements at various sections along the length of the beams. The thickness of the specimens varied slightly over the length of the specimens. All the other dimensions also varied over the length of the beam due to the forming process. All the inverted hat specimens were formed using a sharp die and the inside radius of the bends has been taken to be zero. The radius of the bend of Reck's specimens is listed along with the other dimensions in table 5.2.2.

5.2.3 Fabrication and Instrumentation

The inverted hat specimens were fabricated by press braking steel sheets of proper dimensions to the desired shape. The I sections were fabricated by riveting two press brake formed channel sections back to back. All the specimens were formed with their axes parallel to the rolling direction of the sheets. The specimens were cut to lengths a few inches longer than the center to center

distances L , of the supports given in table 5.2.2.

Diaphragm stiffeners were welded to the specimens at the load and support points as shown in fig. 5.2.1. The specimens were loaded with two equal concentrated loads equidistant from the supports. The distances from the support center line to the load center line (LS) are also given in table 5.2.2. The length of the uniform moment region was chosen to minimize the effect of restraint at the load points, on the local buckling of the unstiffened compression flanges. When required, diaphragm stiffeners were provided also in the uniform moment region of the inverted hat sections, to prevent lateral buckling prior to failure.

Strain gages were glued to the specimens, parallel to the longitudinal direction of the beams, as shown in fig. 5.2.1c. In the case of specimens failing in the elastic range, two pairs of SR-4 A9 gages (6 inch gage length) were glued to the tension and compression flanges near the intersection of the webs and the flanges at the center section of the beams. Six pairs of SR-4 A12 gages (1 inch gage length) were glued to the tension and compression flanges near the intersection of the webs and flanges in the uniform moment zone, for specimens failing in the inelastic range, to determine the distribution

of strains along the length of the beams in the uniform moment region. In all the specimens, a few pairs of SR-4 A12 strain gages were glued to both faces of the unstiffened elements in the uniform moment region near the free edges, as shown in fig. 5.2.1. These gages were used to center the specimens in the testing machine and to determine the local buckling load.

5.2.3 Experimental Set-Up and Procedure

The beam specimens prepared as described in the preceding section were tested in a Baldwin hydraulic testing machine. The beams were subjected to a uniform bending moment in the middle using two concentrated loads at equal distance from the supports. The two concentrated loads were transmitted through a centrally loaded spreader beam. A diagram of the test set-up is shown in fig. 5.2.2.

Initially, the beams were loaded to approximately one third to one half the local buckling load or yield load, whichever was lower, in order to check the centering of the specimens. The symmetry of the loading was confirmed by the uniformity of increase in the strains at different sections in the uniform moment region. After the centering was completed, the load was reduced to a small value of 200 pounds to start the test.

The specimens were instrumented to measure the deflection at mid span and any settlement at the supports as shown in fig. 5.2.2. The slopes of the beams at two sections near the two load points were measured using two inclinometers as indicated in fig. 5.2.2. These inclinometers were a combination of a small level and a micrometer. In addition to the instrument shown in fig. 3.2.4, dial gages were also located at the center section near the free edges of the unstiffened elements, to measure the maximum amplitude of the elastic local buckling waves.

The beams were loaded in small increments. All the dial gage, strain gage and inclinometer readings were recorded after each load increment. In spite of the low rate of the load increment, a certain relaxation, indicated by a drop in the load after the loading valves were shut, was inevitable in the advanced postbuckling stages and in the inelastic range. During the relaxation, there was little change in the dial gage readings and the strain gage readings changed slightly. When the test was continued, the load drop was immediately recovered. The load was increased by a smaller amount near elastic local buckling and near failure to determine these values as accurately as possible. Failure was defined as the attain-

ment of a maximum load and the onset of load shedding. There were about twelve sets of readings taken before failure and one set of readings was taken soon after the load shedding.

A picture of the loading set-up is shown in fig.

5.2.3. Evaluation of the test results will be presented in the following sections.

5.3 Background for Evaluation of Experimental Data

Before evaluation and discussion of the experimental results, background information for the evaluation of the experimental data will be presented in this section. This will cover the procedures for determining the local buckling stress, the effective width in the elastic post-buckling range and at the ultimate load, from the experimental data.

The local buckling stresses were determined using the strain gages located at the free edge of the unstiffened compression flanges, following the modified surface strain reversal method. This method assumes the load corresponding to the reversal of compressive strain increment in the gages on the convex side of the unstiffened element local buckling waves to be the local buckling load. A more detailed description of this method is presented in section 3.3.1.

At the center section of the beams, the bending moment (M), the tensile strain (e_t) and the compressive strain (e_c) in the flanges near the intersection with the webs, can be determined from the test data. An effective width can be calculated using any two of the three values. Consequently, one can compute three values for the effective width from the three sets of independent values corresponding to each loading stage. Due to experimental error, the three values of the effective width are not the same. Since the tensile strain is usually insensitive to a change in the effective width of the compression flange, the effective width based on the moment (M) and the tensile strain (e_t) is unreliable. Among the other two combinations (e_c - M and e_c - e_t) whichever indicated an effective width nearly equal to the full width in the early loading stages was used to obtain the experimental effective width of the unstiffened compression elements in the postbuckling range. The stiffness of beams B-1 and B-2 at the early stages of loading, calculated using experimental data, was smaller than the theoretical stiffness based on the measured dimensions. This difference could not be attributed wholly to the reduction in the effective width of the unstiffened compression elements due to initial waving. Consequently, all the measured dimensions of these two beams were re-

duced by four percent. These revised dimensions, and not the measured dimensions, are given in table 5.2.1.

Although smaller load increments were used near the ultimate load, it was usually difficult to take readings right at the ultimate load. Therefore, readings were taken just prior to the ultimate load and at the early stage of load shedding. The strain and dial gage readings at the ultimate load were obtained from the readings at these two adjacent loads, by interpolation.

Strain gages were glued at three sections in the uniform moment region, in the case of beams with compression elements buckling locally in the inelastic range (fig. 5.2.1d). Even though in the early stages of loading, the strain increments in these gages were uniform, indicating a uniform moment region, just prior to the failure the strains at sections near the load points generally increased at a faster rate than the strains at the center section. Finally, the failure took place near one of the load points by the formation of a permanent kink in the compression element. This faster rate of strain increment near the load points can be attributed to the local effects of the concentrated load. In such cases, the strain at the center section has been used as the ultimate strain in the evaluation.

5.4 Evaluation of the Experimental Results

5.4.1 Experimental Results:

Moment Curvature Relationship

Figs. 5.4.1 and 5.4.2 show the typical moment curvature relationship at the center section of two beams B-4 and B-16 respectively. Beam B-4 has a local buckling stress less than the yield stress and an elastic post-buckling range in which the effective width of the unstiffened compression flanges is less than the actual width. In the early prebuckling range, the theoretical curve based on the full section, and the experimental curve coincide. However, above a certain moment the experimental curve becomes non-linear, due to a reduction in the effective stiffness of the cross section, and departs from the fully effective section curve. The experimental stiffness decreases monotonically as the bending moment increases. Failure takes place when the compressive stress near the flange web intersection, which is the maximum compressive stress in the locally buckled compression flange, is nearly equal to the yield stress of the material. The maximum moment at failure is less than the yield moment of the fully effective section, and at failure the flexural stiffness of the beam is zero. This has been found typical of all beams having an elastic postbuckling

range, though the reduction in stiffness just prior to failure is more drastic in the case of beams with a larger (w/t) ratio.

Beam B-16 has an unstiffened compression flange of a low (w/t) ratio, and consequently has a theoretical local buckling stress larger than the yield stress of the material. The unstiffened compression element buckles locally in the inelastic range at a strain less than the strain hardening strain, and the section can withstand bending moments larger than the yield moment of the fully effective section (fig. 5.4.2). Increase in the load carried by the beam beyond the local buckling of the unstiffened compression flange in the inelastic range is negligible, because the load shedding begins almost immediately after the local buckling. Since an inelastic deformation of the order of the strain hardening strain is required before the plastic moment capacity M_p of the section can be developed, the moment at failure is less than the plastic moment capacity of the section (M_p). The theoretical moment curvature relationship of the fully effective section is also drawn in fig. 5.4.2. The experimental curve deviates from the theoretical curve just prior to the yield moment, indicating a reduction in the experimental stiffness. This can be attributed to the effects of initial imperfections, and the non-linearity of

the stress strain relationship prior to the yield stress. The flexural stiffness decreases monotonically with increase in the bending moment and becomes zero at failure. This behavior has been typical of beams with compression elements buckling in the inelastic range.

The theoretical yield moment (M_y), the theoretical plastic moment capacity (M_p) and the experimental ultimate moment (M_u) are given in table 5.4.1 for all the beam specimens. Except for the beams B-17 and B-18, all the beams have an ultimate moment M_u less than the plastic moment capacity M_p . The beams having an elastic post-buckling range fail even before reaching the yield moment M_y of the fully effective beam sections. The ultimate moment of the beam B-17 is four percent higher than the plastic moment capacity of the specimen, and that of B-18 is 8 percent higher than the corresponding plastic moment capacity. The effect of increase in the yield stress of corners due to cold-forming has been neglected in all calculations so far, on the basis of the assumption that the area of corners is small. Whereas, in the case of beams B-17 and B-18, the ratio of the area of corners to the area of compression flanges is nearly equal to 10 percent. The ultimate moment (M_u) of these beams having a value greater than the ultimate moment capacity of the beams (M_p) can be due to a combination of increase in the

yield stress at corners as a result of cold-forming and general experimental scatter.

Load Deflection Relationship

A typical load deflection curve of a beam (B-15) is shown in fig. 5.4.3. Here again, the stiffness of the beam is linear in the elastic range and is equal to the stiffness of the fully effective section. However, the experimental curve departs from the theoretical line before the yield load is reached, which is attributable to the effects of initial imperfections and the non-linearity of the stress strain curve just prior to yielding. The stiffness continues to decrease in the inelastic range and becomes zero at the failure load, which is reached almost immediately after the local buckling of the unstiffened elements in the inelastic range. Loads corresponding to the beginning of yielding in the uniform moment region and the formation of a plastic hinge ($M = M_p$) are also indicated in fig. 5.4.3.

Local Buckling and Postbuckling Properties

The experimental local buckling coefficient K for beams having an elastic postbuckling range, computed as discussed in the previous section, are given in table 5.4.2. The stress at the supported edge of the unstiffened elements and the effective width of the elements at the ul-

timate load are also given for these specimens in table 5.4.2. The compressive strain (e_{cu}) at failure in the unstiffened elements of the beam specimens are presented in table 5.4.3. These experimental results, along with the subultimate effective widths computed from the experiments, will be compared with the analytical solutions in the following sections.

5.4.2 Elastic Local Buckling and Postbuckling Behavior of Unstiffened Compression Flanges

In this section, the experimental local buckling and postbuckling behavior of the unstiffened compression flanges in the beam specimens will be compared with the analytical solutions derived in chapters 2 and 3.

It was shown that the local buckling stress of the unstiffened elements depends upon the rotational edge restraint provided by the supporting elements. It was easy to compute the rotational edge restraint for the compression members, because of a uniform stress distribution over the cross section. In the case of flexural members, only that area of the section on the compression side of the neutral axis is subjected to compression. Consequently, the rotational edge restraint based on a uniform compression over the whole cross section will be somewhat conservative for beams since the compressive

stress reduces the stiffness of the supporting elements. The rotational edge restraint based on no compressive stress at all on the supporting elements will yield an unconservative value of the rotational edge restraint, since the compressive stress on part of the web is disregarded. However, for specimens in this investigation, the effect of the compressive stress on the web will be negligible, since the webs were designed to be sufficiently stiff under the compressive stress gradient. The length of the local buckling waves is another factor influencing the stiffness of the supporting elements. Although the stiffness increases with a decrease in the wave length, it has been found²⁵ that assuming the wave length to be infinity in the computation of the rotational edge restraint, has a negligible effect on the value of the buckling coefficient of the unstiffened elements. This assumption on the conservative side is partly offset by the slightly unconservative result of disregarding the compressive stress on the supporting elements. Hence, an infinite length of the local buckling waves and no compressive stress on the supporting elements are assumed in computing the rotational edge restraint at the supported edge of the unstiffened compression flanges. Based on this assumption, the rotational edge restraint factor ($\epsilon_R = (w/D') \times (M_s / \theta_s)$) for hat sections can be shown

to be equal to

$$\epsilon_R = \frac{2BC(3BT+2D)}{D(2BT+D)} \quad (5.4.1)$$

where all the dimensions are indicated in fig. 5.2.1a. Variables M_s and θ_s are the moment and the corresponding rotation at the supported edge of the element and D' is the flexural rigidity of the unstiffened element. Similarly, for an ideal I section of dimensions shown in fig. 5.2.1b and having an integral web, the rotational edge restraint factor can be derived to be

$$\epsilon_{I_{ideal}} = 12xBC/D \quad (5.4.2a)$$

The rotational edge restraint factor of unstiffened elements in the individual channel sections, of which the I sections are made, is given by

$$\epsilon_C = 3xBC/D \quad (5.4.2b)$$

The rotational edge restraint factor of the actual I section has been taken to be the average of an ideal I section rotational edge restraint factor $\epsilon_{I_{ideal}}$ and a channel edge restraint factor ϵ_C .

$$\epsilon_I = (\epsilon_{I_{ideal}} + \epsilon_C)/2 = 7.5BC/D \quad (5.4.2c)$$

For a perfectly flat unstiffened element, as long as the local buckling stress is in the elastic range, one can calculate the local buckling coefficient K assuming a completely elastic behavior, either from equation 2.2.8b or from the curve K_e in fig. 2.2.2. However, in an actual unstiffened element, having an elastic local buckling stress near the yield stress of the material, the superposition of the flexural compressive stress due to initial imperfections and the membrane compressive stress may cause a partial yielding of the unstiffened element. In such cases, the buckling coefficient of the element will be given by a value in between the elastic value (K_e) and the plastic value (K_p), given by eqn. 2.2.20 and fig. 2.2.2. In table 5.4.2, both the elastic and the plastic buckling coefficients K_e , K_p of the unstiffened compression flanges of test specimens are presented. The experimental buckling coefficient is nearer to the theoretical elastic buckling coefficient K_e for larger values of the ratio of the yield stress to the critical stress (σ_y/σ_{cr}), and as the local buckling stress approaches the yield stress of the material, the experimental local buckling coefficient K approaches the theoretical plastic buckling coefficient K_p . The specimen UP-12 has a low buckling coefficient due to some inexplicable reason, and this test result has been dropped from further consideration.

Ratios of the effective width to the actual width (b_e/w), the yield stress to the local buckling stress (σ_y/σ_{cr}), and the average compressive stress in the unstiffened element to the local buckling stress (σ_{av}/σ_{cr}) at the ultimate load of the beam specimens are presented in table 5.4.2. These values were also computed at the subultimate loads for all the specimens and are plotted in fig. 5.4.4 along with the values at the ultimate load. The ordinate in the figure is the ratio of the average compressive stress in the unstiffened compression flange to the local buckling stress (σ_{av}/σ_{cr}) and the abscissa is the ratio of the maximum supported edge stress in the unstiffened flange to the local buckling stress ($\sqrt{\sigma_{e\ max}}/\sigma_{cr}$).

The two effective width equations derived in the third chapter for unstiffened elements are given below.

$$\frac{b_e}{w} = \frac{(1-B_1)}{\left(\frac{\sigma_{e\ max}}{\sigma_{cr}} + B_2\right)} + B_1 \quad (3.4.1)$$

where

$$B_1 = 0.326 + 0.086K^2$$

$$B_2 = 0.378 - 0.768(K-1.18)^4$$

and

$$\frac{b_e}{w} = 1.19\sqrt{\sigma_{cr}/\sigma_{e\ max}} (1.0 - 0.298\sqrt{\sigma_{cr}/\sigma_{e\ max}}) \quad (3.4.5)$$

Expressing b_e/w in terms of σ_{av}/σ_{cr} using eqn. 2.3.34b in the above two equations, we obtain two equations in terms of σ_{av}/σ_{cr} and $\sqrt{\sigma_{e\ max}/\sigma_{cr}}$. Curves corresponding to these two equations are also plotted in fig. 5.4.4 for comparison with the test results. Two curves corresponding to eqn. 3.4.1 are plotted for two values of the buckling coefficient K ($K = 0.95$ and 0.6), because the buckling coefficients of the unstiffened elements in the test specimens were in this range. All the subultimate points in the plot are on the conservative side of the two effective width equations. This can be attributed to the average nature of the subultimate supported edge strain measured from the experiments, whereas the effective width equations have been derived for the section having the maximum edge strain in the element. The test points at the ultimate load are generally located nearer to the curves corresponding to the two effective width equations.

In fig. 5.4.5, the curves corresponding to the two effective width equations are again plotted with the ratio of the effective width to the actual width (b_e/w) as ordinate and the ratio of the maximum edge stress to the critical stress ($\sigma_{e\ max}/\sigma_{cr}$) as abscissa. The test points at the ultimate load are also plotted in this figure. In general, there is a reasonably good correlation between the test results and the two effective width equations.

In table 5.4.2, the theoretical effective widths of the test specimens at the ultimate load, computed using the two effective width equations, have been presented for comparison with the experimental results. The effective width eqn. 3.4.1, based on the analytical solution of Chapter 2, overestimates the effective width by about 15 percent for unstiffened elements with a large w/t ratio and underestimates the effective width by about 1 percent for unstiffened elements with a small w/t ratio. The effective width equation 3.4.5, having a format similar to the AISI equation for the stiffened elements, underestimates the effective width of the unstiffened elements having a large w/t ratio by about 6 percent and overestimates the effective width by about 4 percent for unstiffened elements with a small w/t ratio.

As the flat width to thickness ratio (w/t) of unstiffened elements decreases the local buckling stress (σ_{cr}), hence the ratio of the effective width to the actual width (b_e/w) at ultimate load increases. Below a particular value of the w/t ratio, the elements remain fully effective up to the yield stress and this limiting value of the w/t ratio will be discussed in the following section.

5.4.3 Limiting Flat Width to Thickness Ratio

When the ratio of the flat width to the thickness

(w/t) of unstiffened elements is less than a limiting value, the elements can withstand a compressive stress up to the yield stress without any perceptible reduction in the effective width of the element. This can be observed in table 5.4.1, where beam specimens having a low w/t ratio fail at moments higher than the corresponding yield moment. Since the beam specimens have been designed to yield in the compression flange first, a value of the ultimate moment higher than the yield moment indicates the complete yielding of the compression elements without any appreciable reduction in the effective width.

The limiting value of the w/t ratio can be obtained from the effective width equations by setting the ratio b_e/w equal to one, substituting σ_y for $\sigma_{e \max}$, and substituting for the local buckling stress σ_{cr} the following equation

$$\sigma_{cr} = \frac{K\pi^2 E}{12(1-\mu^2)(w/t)^2} \quad (1.2.1a)$$

From eqn. 3.4.1

$$(w/t)_{lim} = \sqrt{\pi^2 E(1-B_2)/12(1-\mu^2)} \sqrt{K/\sigma_y} \quad (5.4.3)$$

Similarly, from eqn. 3.4.5

$$(w/t)_{lim} = \sqrt{0.354\pi^2 E/12(1-\mu^2)} \sqrt{K/\sigma_y} \quad (5.4.4)$$

In fig. 5.4.6, the ratio of the ultimate moment to the yield moment (M_u/M_y) is plotted against the parameter $((w/t)\sqrt{\sigma_y/K})$ for all the test points. When the ratio (M_u/M_y) is greater than one, the unstiffened compression element is fully effective even up to the yield stress, since the yielding begins in the compression flange. The limiting values of the parameter $((w/t)\sqrt{\sigma_y/K})$, computed using eqs. 5.4.3 and 5.4.4 are also plotted in fig. 5.4.6. The limit corresponding to eqn. 5.4.3 seems to agree reasonably with the test results, and the limit corresponding to the eqn. 5.4.4 is conservative.

Members having the unstiffened elements in compression can be designed for the yield strength of the total cross section, as long as the w/t ratio of the unstiffened elements is less than the limiting value of the w/t ratio. If the w/t ratio is larger than the limiting value, the strength of the effective cross section obtained using the effective width equation is to be used in the design. Unstiffened compression elements, having w/t ratio less than the limiting ratio $(w/t)_{lim}$, can withstand inelastic strain before failure due to local buckling. The inelastic strain capacity of unstiffened compression elements will be discussed in the next section.

5.4.4 Inelastic Strain Capacity of Unstiffened Compression Elements

It was observed that due to low width to thickness

ratio, unstiffened compression elements in hot rolled steel sections can in general withstand compressive strains as high as the strain hardening strain, whereas unstiffened elements in cold-formed steel members generally buckle locally in the elastic range, or in the inelastic range at strains far less than the strain hardening strain. In the last section, expressions for the limiting value of the w/t ratio, below which the unstiffened elements remain fully effective up to the yield stress, were derived. In steel flexural members having unstiffened elements with w/t ratios less than the limiting value, local buckling takes place in the plastic range and the ultimate moment is larger than the yield moment of the section, as a result of the partial plastification of the webs. Flexural members in table 5.4.1 with the unstiffened compression elements having a w/t ratio of about 8, fail at a moment as high as fifty percent above the yield moment. At moments larger than the yield moment, beam sections experience inelastic rotation, and this could also be used to redistribute moments from the maximum moment section to other sections in indeterminate structures. In order to use this reserve load carrying capacity beyond the yield load, one needs to know the extent of inelastic strain that can be sustained by the unstiffened elements before failure. In this sec-

tion, the plastic strain capacity of the unstiffened elements in steel flexural members will be discussed.

The compressive strain in unstiffened flanges near the intersection of webs and flanges of beam specimens at the ultimate load is given in table 5.4.3. If an unstiffened element buckles locally in the elastic range, then the failure is assumed to occur when the maximum strain at the supported edge of the element is nearly equal to the yield strain of the material. However, it can be seen from the results presented in table 5.4.1, that when the elastic local buckling strain is nearly equal to the yield strain, the strain at the supported edge at failure can be larger than the yield strain of the material. This has also been observed by other researchers.³¹

It was perceived during the tests that the beams fail almost immediately after local buckling in the inelastic range. Consequently, there should be some correlation between the plastic local buckling strain and the ultimate strain capacity of the unstiffened compression flanges in the beam specimens. In the second chapter, an expression was derived for the plastic buckling strain of unstiffened elements having an elastic perfectly plastic stress strain relationship. The equations for the plastic buckling strain is

$$(e_{cr})_p = K_p \frac{\pi^2}{12(1-\mu^2)(w/t)^2} \quad (2.2.14)$$

Two curves representing the equation for two limiting values of Poisson's ratio ($\mu = 0.3, 0.5$) are plotted in fig. 5.4.7 in terms of the variables $(e_{cr})_p/K_p$ and (w/t) . The ultimate compressive strain capacity of the test specimens, given in table 5.4.3, is also plotted in fig. 5.4.7 in terms of the same variables. The test points generally fall on the conservative side of the curve corresponding to a value of Poisson's ratio of 0.3. The degree of conservatism increases as the inelastic buckling strain approaches the yield strain of the material. This may be attributed to the larger difference between the ultimate strain and the local buckling strain in the early stages of the inelastic range. However, the effect of initial imperfection is also larger in this region. Consequently, based on the limited experimental evidence, eqn. 2.2.19 with a value of Poisson's ratio of 0.3, seems to yield a realistic and conservative value of the inelastic strain capacity for elements having a (w/t) ratio below the limiting value. Elements having a (w/t) ratio larger than the limiting value can be assumed to fail when the supported edge strain is equal to the yield strain of the material.

5.5 Summary and Conclusions

The effect of elastic and inelastic local buckling in flexural members has been dealt with in this chapter. Results of beam tests with unstiffened flanges in compression have been presented.

The test results have been compared with the two effective width equations derived in the third chapter. Expressions for the limiting value of the flat width to thickness ratio $((w/t)_{lim})$ were derived and compared with the test results. The inelastic compressive strain capacity of beams with the unstiffened compression flanges buckling locally in the inelastic range has been compared with the theoretical plastic buckling strain of the unstiffened elements.

The two effective width equations were found to yield a conservative and reasonable result in the pre-ultimate range of the postbuckling behavior of the test specimens and they were found to exhibit a reasonably good correlation at the ultimate load. The expressions for the limiting value of the (w/t) ratio agreed well with the test results, eqn. 5.4.4 yielding a more conservative limit. The plastic buckling strain calculated using the value of Poisson's ratio of 0.3 in eqn. 2.2.19 yields a conservative, yet reasonable, value of the plastic strain capacity of the unstiffened elements buck-

ling in the inelastic range.

CHAPTER 6
POSSIBLE DESIGN METHOD

6.1 General

Based on the analytical equations derived in the preceding chapters and the comparison of these equations to the test results, design formulations for members having unstiffened elements in compression will be presented in this chapter.

The Specification for the Design of Cold-Formed Steel Structural Members² recommends a limiting compressive stress on the unstiffened elements in order to prevent excessive out of plane deformations in the postbuckling range. The stiffened elements on the other hand, are designed using an effective width equation which makes complete use of the available postbuckling strength with a factor of safety.

On the basis of the evidence given in the preceding chapters, effective width equations will be presented for the design of the unstiffened elements. An equation will also be presented for computing the maximum amplitude of the out of plane deformation of the unstiffened elements in the postbuckling range. On the basis of the experimental and analytical evidence, it can be stated

that the amplitude of the out of plane deformation of elements having a small or moderate w/t ratio is inconsequential as long as there is a small rotational edge restraint available at the supported edge of the unstiffened elements.

Procedures for the design of flexural and compression members using the effective width equations will also be presented in this chapter.

6.2 Local Buckling of Unstiffened Element

6.2.1 General

A bifurcation type of local buckling is encountered only in the case of ideally flat elements. Unstiffened elements in practice begin to experience out of plane waving even before the applied compressive stress exceeds the theoretical local buckling stress. However, it was demonstrated that the amplitude of the local buckling waves increases at a faster rate only near the theoretical local buckling stress. Besides, the theoretical local buckling stress has been found to be an important parameter in the representation of elastic postbuckling behavior. Moreover, local buckling of unstiffened elements in the plastic range is almost immediately followed by the failure of the unstiffened

elements. Consequently, computation of the theoretical local buckling stress is the first step in the design of members with unstiffened elements in compression.

The theoretical elastic and inelastic local buckling stresses are functions of the flat width to thickness ratio (w/t) of the unstiffened elements and a parameter K , known as the local buckling coefficient (eqn. 1.2.1a). The local buckling coefficient K , in turn, is a function of the rotational edge restraint factor ϵ as illustrated in fig. 2.2.2. The derivation of the relationship between K and ϵ is given in section 2.2.1 and 2.2.2. The rotational edge restraint factor depends upon the relative stiffness of the supporting elements and the unstiffened element and consequently on the dimensions of the cross section and the stress on the component elements. In the following section, a procedure for computing the value of the rotational edge restraint factor will be presented.


6.2.2 Rotational Edge Restraint Factor

In the derivation of the equation for the local buckling stress of unstiffened elements (sec. 2.2.1 and 2.2.2), the moment at the supported edge of the element M_r , and the angle of rotation ϕ_r were assumed to be proportional and the coefficient of proportionality ($C_r = M_r / \phi_r$) was assumed to depend on the dimensions of the

restraining elements. However, it was not mentioned that the coefficient of proportionality C_r also depends upon the compressive stress acting on the restraining element. It is obvious that if both the restraining element and the unstiffened element buckle at the same stress, there is no rotational restraint, and the elements behave as plates simply supported along the common unloaded supported edges. The effect of the compressive stress on the stiffness of the restraining element diminishes rapidly as the stiffness of the restraining element increases.

An exact solution to the stability problems is possible, though very tedious. Applying the principles of the moment distribution method to long plate assemblies, Lundquist, Stowell and Schuette⁶² have developed a procedure for the solution of the stability of plate assemblies. An approximate method of obtaining the rotation edge restraint, presented by Bleich²⁵, is based on the assumptions that the edges where the plates join remain straight and all plates joining at an edge rotate by an equal angle during local buckling. Bleich derives equations for the rotational restraint of supporting elements, initially disregarding the effect of compressive stress and later makes proper adjustment for the compressive stress by means of a correction

factor. This procedure will be used in this section to determine the rotational edge restraint of unstiffened elements.

The restraining element may either be a stiffened element as in the case of channel, I and inverted hat () sections, or an unstiffened element as in the case of angle and T sections. Consequently, the problem is one of deriving equations for the rotational restraint provided by stiffened and unstiffened elements, which will be done in the following sections.

6.2.2.1 Channel and I Sections Subjected to Uniform Compression

In this section, the rotational edge restraint factor of unstiffened elements, due to the restraint from the stiffened elements in I and channel sections subjected to uniform compression, is derived. The buckled configuration and the free body diagrams of the individual elements under this deformed state of I and channel sections are shown in fig. 6.2.1a, assuming that the unstiffened flanges are restrained by the web. Disregarding the effect of compressive stress on the restraining element stiffness, the coefficient of proportionality C_r between the moment M_r and the angle of rotation ϕ_r at the supporting edge is given by

$$C_r = M_r / \phi_r = 2D_r / B_r \quad (6.2.1)$$

where D_r and B_r are the flexural rigidity and width of the restraining element. The value C_r obtained from eqn. 6.2.1 is conservative, since the buckling wave length has been assumed to be infinity. The rotational edge restraint factor ($\epsilon = C_r \times B_b / D_b$) of the unstiffened elements can be calculated using eqs. 6.2.1 and 2.2.5 as

$$\epsilon = \frac{C_r B_b}{N_b D_b} = \frac{2}{N_b} \frac{D_r}{D_b} \frac{B_b}{B_r} = \frac{2}{N_b} \left(\frac{t_r}{t_b} \right)^3 \frac{B_b}{B_r} \quad (6.2.2)$$

where B_b , D_b and t_b are respectively the width, flexural rigidity and the thickness of the buckling element, t_r is the thickness of the restraining element and N_b is the number of locally buckling unstiffened elements of equal stiffness joining at the junction. For example, the value of N_b is equal to one in the case of Z and channel sections and is equal to two in the case of I sections. In eqn. 6.2.2, the effect of compressive stress on the restraining element has been disregarded. If the local buckling stress of the restraining element is equal to the local buckling stress of the buckling element, then the rotational edge restraint is zero. Consequently, the effect of the compressive stress on the restraining element can be approximately taken into

account by multiplying eqn. 6.2.2 by a correction factor r which becomes zero when the local buckling stress of the restraining and the buckling element is the same.²⁵ The local buckling stress of the restraining and buckling elements are given by

$$(\sigma_{cr})_r = \frac{K_r \pi^2 E}{12(1-\mu^2)(B_r/t_r)^2} \quad (6.2.3a)$$

$$(\sigma_{cr})_b = \frac{K_b \pi^2 E}{12(1-\mu^2)(B_b/t_b)^2} \quad (6.2.3b)$$

where K_r and K_b are the buckling coefficients of restraining and buckling elements respectively. The correction factor r , which has to satisfy the following condition

$$r = 0$$

when $(\sigma_{cr})_b / (\sigma_{cr})_r = 1$

and $r \rightarrow 1$

as $(\sigma_{cr})_b / (\sigma_{cr})_r \rightarrow 0$ (6.2.3c)

can be written as

$$\begin{aligned} r &= 1 - \frac{(\sigma_{cr})_b}{(\sigma_{cr})_r} \\ &= 1 - (K_b/K_r) (t_b^2 B_r^2 / t_r^2 B_b^2) \quad (6.2.3d) \end{aligned}$$

For the hinged support condition

$$K_r = 4.0$$

and $K_b = 0.425$ (6.2.3e)

Substituting the values of the buckling coefficients from eqn. 6.2.3e in 6.2.3d, the correction factor r for this case becomes²⁵

$$r = 1 - (0.425/4.0) (t_b^2 B_r^2 / t_r^2 B_b^2) \quad (6.2.3f)$$

Thus the equation for the rotational edge restraint factor ϵ corrected for the effect of compressive stress on the restraining element can be written using eqs. 6.2.2 and 6.2.3f as

$$\epsilon = \frac{2}{N_b} (t_r/t_b)^3 (B_b/B_r) [1 - 0.106 (t_b/t_r)^2 (B_r/B_b)^2] \quad \text{when } r \geq 0 \quad (6.2.4)$$

Eqn. 6.2.4 is valid only when the local buckling stress of the restraining element is greater than or equal to the local buckling stress of the unstiffened element, that is, when the correction factor r given by eqn. 6.2.3 is greater than or equal to zero. Even though

this investigation is concerned only with sections in which the unstiffened elements are restrained by a stiffened element, for the sake of completeness the rotational edge restraint factor, when the stiffened elements buckle first, will also be presented. An approximate equation for the value of ϵ , when $r \leq 0$ can be written as²⁵

$$\epsilon = - \frac{2\pi}{N_b} \frac{B_b}{B_r} [1 - 9.4(t_r/t_b)^2 (B_b/B_r)^2] \quad (6.2.5)$$

when

$$r \leq 0$$

Bleich²⁵ shows that the local buckling stress calculated using these approximate values of the rotational edge restraint factor ϵ given by eqs. 6.2.4 and 6.2.5 compare well with the more exact solution of Lundquist et al.⁶²

Following the same procedure, an equation for the rotational edge restraint factor ϵ of unstiffened elements in flexural members will be derived in the following section.

6.2.2.2 Channel and I Sections Subjected to Uniform Bending

In the preceding section, equations for the rotational edge restraint factor ϵ were derived for I and

channel sections subjected to a uniform compressive stress, as in columns under axial load. Following the procedure outlined by Bleich²⁵ for uniformly compressed member, equation for the rotational edge restraint factor ϵ , when these cross sections are subject to a uniform bending moment causing a uniform compressive stress in the unstiffened elements, is derived in this section.

The distribution of the flexural stress over the cross sections, the distorted shapes due to local buckling and the freebody diagrams of the elements indicating moments at the common edges are shown in fig. 6.2.1b. The unstiffened compression flanges are assumed to be restrained by the web elements. The effect of the moment at the intersection of the tension flange and web on the rotational edge restraint factor ϵ of the unstiffened compression element is very small, and is disregarded. Assuming conservatively the buckling wave length to be infinity, the coefficient of restraint C_r of the web not including the effect of compressive stress on the web is

$$\begin{aligned} C_r &= M_r / \phi_r \\ &= 3D_r / B_r \end{aligned} \quad (6.2.6a)$$

where D_r and B_r are the flexural rigidity and the width

of the restraining element respectively. Using eqn. 6.2.6a, the rotational edge restraint factor ϵ of the unstiffened element, not including the effect of compressive stress on the web, can be written as

$$\begin{aligned}\epsilon &= C_r B_b / N_b D_b \\ &= 3D_r B_b / N_b D_b B_r \\ &= (3/N_b) (t_r/t_b)^2 (B_b/B_r)\end{aligned}\quad (6.2.6b)$$

where all the dimensions are shown in fig. 6.2.1b and N_b is the number of locally buckling unstiffened flanges of equal stiffness restrained by the web at the junction.

Again the effect of compressive stress on the restraining web can be taken into account approximately by using the correction factor given by eqn. 6.2.3d. The buckling coefficient K_b of a hinged unstiffened element is equal to 0.425 once again. The buckling coefficient K_r of the restraining web subjected to a stress gradient as in fig. 6.2.1b can be conservatively taken to be equal to 7.8, which is the buckling coefficient of a hinged stiffened element subjected to a compressive stress gradient varying linearly from zero

at one edge to a maximum value at the other edge⁴.

(In a beam experiencing a bending moment, part of the web is subject to tensile stress, thus increasing its local buckling coefficient to a value greater than 7.8. However, it will be shown that for the beams tested in this investigation the effect of assuming the local buckling coefficient of the web to be 7.8 conservatively, is negligible. Table (6.2.2)). Substituting the value of K_r and K_b in eqn. 6.2.3d, the correction factor r becomes

$$r = (0.425/7.8)(t_b/t_r)^2(B_r/B_b)^2 \quad (6.2.7)$$

Using the correction factor given by eqn. 6.2.7 and eqn. 6.2.6b, the rotational edge restraint factor ϵ of the unstiffened elements in a beam can be written as

$$\epsilon = \frac{3}{N_b} (t_r/t_b)^3 [1 - 0.054(t_b/t_r)^2(B_r/B_b)^2] \quad (6.2.8)$$

In the preceding two sections, equations for the rotational edge restraint factor ϵ of the unstiffened elements restrained by stiffened elements, were derived. The rotational edge restraint factor ϵ of unstiffened elements restrained by unstiffened elements, will be presented in the following section.

6.2.2.3 Edge Rotational Restraint Factor of Miscellaneous Sections Subject to Uniform Compression

Bleich²⁵ has derived equations for rotational edge restraint factors of various other sections subject to a uniform compression. Results for sections with unstiffened elements under a uniform compression will be presented here.


A T section is shown in fig. 6.2.2a. A conservative equation for the rotational edge restraint provided by the flanges to the local buckling of the web, when such a section is subject to a uniform compression, has been derived as²⁵

$$\epsilon = 2 \left(\frac{t_r}{t_b} \right)^3 \left(1 - \left(\frac{t_b}{t_r} \right)^2 \left(\frac{B_r}{B_b} \right)^2 \right) \quad (6.2.9)$$

where all the dimensions are shown in fig. 6.2.2a.

An angle section is shown in fig. 6.2.2b. When the width and thickness of the legs are the same, the rotational edge restraint factor is equal to zero for uniform compression. However, when the legs are not equal, the narrow leg restrains the local buckling of the wider unstiffened leg. When the ratio of the width of the legs (B_r/B_b) is less than 2/3, the buckling coefficient

of the wider leg is larger than 0.504 for long angles.²⁵

Any practical cross section can be either realistically or conservatively idealized to one of the cases for which an equation for the rotational edge restraint has been presented. For example, a Z section can be idealized as a channel section. The rotational edge restraint factor ϵ of an unstiffened element under compression in an inverted hat section () can be conservatively assumed as that of the unstiffened element in a channel section, having the width of both unstiffened elements equal to the width of the unstiffened element of the inverted hat section. Having computed, using the equations presented, a conservative yet realistic value of the rotational edge restraint factor of the unstiffened elements in most common sections, one can determine the buckling coefficient of the unstiffened elements following the procedure to be outlined in the next section.

6.2.3 Elastic and Inelastic Local Buckling

A procedure for calculating the local buckling coefficient and the local buckling stress of unstiffened elements will be presented in this section, using the equations for the rotational edge restraint factor derived in the preceding sections and the equations for

the elastic and plastic local buckling coefficients in sections 2.2.1 and 2.2.2.

The elastic local buckling coefficient K_e , of an unstiffened element having a high aspect ratio (L/w) and given rotational edge restraint factor ϵ can be obtained from eqn. 2.2.8b or fig. 2.2.2. Similarly, the plastic buckling coefficient K_p of the element, which is always less than or equal to the elastic buckling coefficient K_e , can be obtained using eqn. 2.2.20 or fig. 2.2.2. The theoretical local buckling coefficient K of the element depends upon whether the local buckling takes place in the elastic or inelastic range of the material.

The local buckling strain (e_{cr}) of an element can be written as

$$e_{cr} = K\pi^2 / (12(1-\mu^2)(w/t)^2) \quad (6.2.10a)$$

The local buckling coefficient K_y corresponding to the yield strain e_y , for a given (w/t) ratio, can be obtained from eqn. 6.2.10a by substituting e_y for e_{cr} .

$$K_y = 12(1-\mu^2)(w/t)^2 e_y / \pi^2 \quad (6.2.10b)$$

The local buckling coefficient K of an ideally flat

element depends upon the relative values of the buckling coefficients K_y , K_e and K_p , as given below.

$$\text{If } K_y > K_e \quad \text{then } K = K_e \quad (6.2.11a)$$

$$\text{If } K_p > K_y \quad \text{then } K = K_p \quad (6.2.11b)$$

$$\text{If } K_e > K_y > K_p \quad \text{then } K_e > K > K_p \quad (6.2.11c)$$

As in eqn. 6.2.11a, the local buckling coefficient of an ideally flat unstiffened element K is equal to the elastic buckling coefficient K_e , if the local buckling strain obtained by substituting the elastic buckling coefficient K_e in eqn. 6.2.10a is less than the yield strain e_y . On the other hand, if the local buckling strain obtained by using the plastic buckling coefficient K_p in eqn. 6.2.10 is greater than the yield strain e_y , then the local buckling coefficient K is equal to the plastic buckling coefficient K_p (eqn. 6.2.11b). However, in the intermediate range where the local buckling strain corresponding to the elastic buckling coefficient is greater than the yield strain and that corresponding to the plastic buckling coefficient is less than the yield strain, the local buckling coefficient K of the ideally flat element has a value between the elastic and plastic buckling coefficients.

In general, an unstiffened element of a structural

member, as a result of initial imperfections, experiences flexural stresses in addition to the applied compressive stress even before local buckling of the element. Consequently, superposition of the membrane and the flexural stress may cause yielding somewhere in the element before the local buckling of the element, when the elastic local buckling stress of the element is near the yield stress of the material. Thus, the plastification of an unstiffened element starts at a lower stress in the case of a real element when compared to an ideally flat element. As a result, the local buckling coefficient K of a real unstiffened element starts to reduce from the value of the elastic local buckling coefficient K_e , at an earlier stage than the limit set by eqn. 6.2.11a, and reduces to the value of the plastic buckling coefficient K_p earlier than the limit set by eqn. 6.2.11b.

In order to obtain the limits in the case of actual unstiffened elements, the elastic and inelastic local buckling coefficients K_e and K_p of the unstiffened elements in the compression and flexural specimens are compared with the experimental values of the local buckling coefficient K_{expt} in tables 6.2.1 and 6.2.2. The ratio of the theoretical local buckling coefficient limit K_y to the elastic buckling coefficient K_e is also

given in these tables. In figure 6.2.3, the results of the compression and flexural specimens of table 6.2.1 and 6.2.2 are plotted in terms of the parameters $(K_{\text{expt.}} - K_p) / (K_e - K_p)$ and K_y / K_e . The experimental points, especially those of the built up I sections, are scattered over a wide range. This can be attributed to the following reasons. The definition of the local buckling of an unstiffened element in an experimental specimen (chapter 3) is arbitrary because of the lack of a bifurcation type of buckling. The effect of initial imperfections is most pronounced near the local buckling stress, especially when the local buckling takes place near the yield stress of the material. The effectiveness of connecting two channel sections to form an I or H section can vary in a random way. The scatter of the experimental points can be due to some combination of these reasons. The parameter $(K_{\text{expt.}} - K_p) / (K_e - K_p)$ also tends to exaggerate the scatter of the test points.

A straight line originating from $K=K_p$ at the value of $K_y / K_e = 1$ and reaching the value of $K=K_e$ at $K_y / K_e = 5$, seems to give a conservative lower limit of the experimental points. An equation for the local buckling coefficient K , based on this fit, can be written as

$$\begin{aligned}
K &= K_p && \text{when } K_y < K_e \\
K &= K_p + (K_e - K_p)(K_y - K_e) / 4K_e && \text{when } K_e < K_y < 5K_e \\
K &= K_e && \text{when } 5K_e < K_y
\end{aligned}
\tag{6.2.12}$$

Eqn. 6.2.12 yields in general a conservative value of the local buckling coefficient when compared to eqn. 6.2.11a, b, c, as expected.

The theoretical local buckling coefficients K_{theory} calculated using eqn. 6.2.12 are presented in table 6.2.1 and 6.2.2 for comparison. In general, the theoretical values are conservative when compared to test values by margins as high as 28 percent. Only a few of the theoretical results are unconservative, the maximum difference on the unconservative side being 4 percent. The mean difference between the experimental and theoretical values of the buckling coefficient is 12.8 percent on the conservative side and the coefficient of variation is 0.723. This information can be qualitatively inferred from fig. 6.2.3, using which eqn. 6.2.12 was deduced.

In order to obtain the rotational edge restraint factor ϵ for all the beams tested, the distribution of compressive stress in the web has been assumed to vary from zero stress at the bottom to the maximum compressive stress at the top. This, however, is a conservative

assumption. So as to check the effect of such an assumption, the buckling coefficients of two beams (B-1 and UP-11) have been calculated using the actual distribution of the stress in the webs. The results of this evaluation is presented at the end of table 6.2.2. It is seen that the effect of assuming the conservative stress distribution in the webs makes about only one percent difference in the theoretical local buckling coefficient K of the unstiffened flanges.

As long as the w/t ratio of the unstiffened elements is larger than the limiting value $(w/t)_{lim}$, governed by eqn. 5.4.3 or 5.4.4, there is a reduction in the effective width of the unstiffened elements and failure is assumed to occur when the maximum compressive stress in the element, at the supported edge parallel to the direction of compression, reaches the yield stress of the material. However, if the (w/t) ratio of an unstiffened element is smaller than the limiting value $(w/t)_{lim}$, the element remains fully effective until the whole width of the element yields in compression. In such cases, the elements can undergo additional plastic strain before failure. It was observed in the fifth chapter that the failure of the unstiffened elements, in the plastic range, takes place almost immediately after local buckling. Consequently, it was

suggested that the plastic buckling strain given by eqn. 2.2.19 can be taken as the inelastic strain capacity of the unstiffened elements having a (w/t) ratio less than the limiting value $(w/t)_{lim}$.

In table 6.2.3, the limiting value of the (w/t) ratio of the unstiffened elements in the flexural specimens are given. These values have been computed using eqn. 5.4.3 presented below.

$$(w/t)_{lim} = \pi \sqrt{(1-B_2)E / (12(1-\mu^2))} \sqrt{K/\sigma_y} \quad (5.4.3)$$

where $B_2 = 0.378 - 0.768 (K - 1.18)^4$. The inelastic strain capacity (e_{cu}) obtained from experimental results are also given in table 6.2.3. Theoretical values of the inelastic strain capacity are given in table 6.2.3 for comparison. The theoretical values have been taken to be equal to the yield strain when the (w/t) ratios of the elements are greater than the limiting values $(w/t)_{lim}$. When the (w/t) ratios are less than the limiting values $(w/t)_{lim}$, the theoretical inelastic strain capacity of the unstiffened elements have been taken as the plastic buckling strain given by eqn. 2.2.19.

$$(e_{cr})_p = K_p \pi^2 / (12(1-\mu^2) (w/t)^2) \quad (2.2.19)$$

The theoretical values are generally on the conservative side of the experimental values. The mean difference between the experimental and theoretical values of the ultimate strain capacity is 23.3 percent on the conservative side and the coefficient of variation is 0.91. The difference is maximum (about 57 percent) for the elements having a (w/t) ratio around the $(w/t)_{lim.}$ value

It has been assumed that as long as the (w/t) ratio is greater than $(w/t)_{lim.}$, the ultimate strain of the element is equal to the yield strain. However, the strain at the supported edge of an unstiffened element having a value of the (w/t) ratio near the limiting value $(w/t)_{lim.}$ can be higher than the yield strain³¹. This accounts for the larger difference between the experimental and theoretical values of the ultimate strain in this range of the (w/t) ratio. The ultimate strain at this range is very sensitive to initial imperfections. Consequently, using a more conservative theoretical value in this range is justifiable. Using inelastic strain capacity of the unstiffened elements given by eqn. 2.2.19, one can obtain the ultimate moment capacity of a given section and the inelastic rotation capacity at a plastic hinge following the procedure presented by Reck.⁶³

When local buckling stress of unstiffened elements

is less than the yield stress, the elements can sustain an additional load in the postbuckling range. The elastic postbuckling behavior of unstiffened elements will be treated in the next section.

6.3 Elastic Postbuckling Behavior of Unstiffened Elements

The effective width of an unstiffened element begins to decrease prior to failure, when the (w/t) ratio of the element is less than the limiting value given by eqn. 5.4.3 or 5.4.4. Beyond the elastic local buckling, the elements can sustain additional load until the maximum stress at the supported edge parallel to the direction of compression is nearly equal to the yield stress of the material.

Two equations for computing the effective width of unstiffened elements, one based on an analytical derivation and the other empirical equation based on experimental results, were given in the third chapter. These equations are

$$\frac{b_e}{w} = \frac{(1-B_1)}{\left(\frac{\sigma_{e \max}}{\sigma_{cr}} + B_2\right)} + B_1 \quad (3.4.1)$$

where

$$B_1 = 0.326 + 0.086 K^2$$

$$B_2 = 0.378 - 0.768 (K-1.18)^4$$

and

$$\frac{b_e}{w} = 1.19 \sqrt{\sigma_{cr} / \sigma_{e \max}} (1.0 - 0.298 \sqrt{\sigma_{cr} / \sigma_{e \max}}) \quad (3.4.5)$$

where $\sigma_{e \max}$ is the maximum compressive stress at the supported edge parallel to the direction of compression, σ_{cr} is the local buckling stress, b_e is the effective width, w is the actual width of the unstiffened element, and K is the local buckling coefficient.

The theoretical effective width of unstiffened elements in the compression and flexural members tested in this investigation, computed using the theoretical values of the buckling coefficient in eqs. 3.4.1 and 3.4.5, are compared with the experimental effective width at the ultimate load of the elements, in table 6.3.1 and 6.3.2. In general, the theoretical equations give reasonably good results. The theoretical results obtained using eqn. 3.4.1 differ from the test values by a margin of up to 19 percent on the conservative side and 13 percent on the unconservative side. The mean difference between the experimental and theoretical values of the effective widths is 5.1 percent on the conservative side and the coefficient of variation is 1.57. Eqn. 3.4.5 yields results which differ from the test values up to 17 percent on the conservative side and 16

percent on the unconservative side. The mean difference between the experimental and theoretical values of the effective widths is 6.55 percent on the conservative side and the coefficient of variation is 1.11. The difference is attributable to both experimental scatter and theoretical approximation. These two effective width equations were shown to give sufficiently conservative theoretical values of the effective width at the subultimate loads also (figs. 3.4.6, 5.4.4).

Since the variation of the constants B_1 and B_2 even for the extreme values of the buckling coefficient K is small, they can be conservatively taken as

$$\begin{aligned} B_1 &= 0.326 \\ B_2 &= 0.378 \end{aligned} \quad (6.3.1)$$

for all values of the buckling coefficient K .

The theoretical effective widths of the unstiffened elements in the test specimens computed using eqn. 3.4.1 and the simplified constants given by eqn. 6.3.1, are presented along with the experimental effective widths in tables 6.3.3 and 6.3.4. The theoretical results differ from the experimental values up to 22 percent on the conservative side and 7 percent on the unconservative side. The mean difference and the coefficient of

variation are 10.9 percent and 0.63 respectively. The simplified constants given by eqn. 6.3.1 being conservative, the effective widths computed using this value of the constants are generally more conservative.

An equation for the maximum amplitude of out of plane deformation of the unstiffened elements was derived in the third chapter and is presented below.

$$z/t = \sqrt{B_3 \left(\frac{\sigma_{e \max}}{\sigma_{cr}} - 1 \right)} \quad (2.3.37)$$

where $B_3 = 2.727 + 1.135/(K-0.425)$.

This equation, was derived for a perfectly flat element and was found (fig. 3.4.7) to give conservative yet realistic results for the amplitude of the deformation of experimental elements in the range of interest (post critical range).

The derivation of analytical equations was accomplished through an approximation solution of VonKarman's plate equations, which are valid only in the intermediate range of out of plane deflection. Consequently the analytical equation derived should not be used in the case of unstiffened elements having a large width to thickness ratio and a large postbuckling range. However, for the

specimens tested which have unstiffened elements with a width to thickness ratio of up to 60, the analytical solution exhibits a good correlation with the test results.

Short compression members and flexural members can be designed using the procedures outlined so far. A design procedure for long compression members which fail as a result of overall flexural buckling will be presented in the next section.

6.4 Analysis of Compression members

Compression members fail by local crippling when they are short and there is very little overall bending of the members. As the length of the compression members increases, the theoretical flexural buckling load decreases and when the flexural buckling load is less than the local crippling load, the members fail due to flexural buckling.

Hot-rolled compression members retain the shape of their cross section, and can be designed using the tangent modulus equation (eqn. 4.1.3) or the Column Research Council (CRC) equation (eqn. 4.1.6). On the other hand, cold-formed compression members usually have thin plate elements in compression, which may buckle locally

before the columns fail due to flexural buckling. The local buckling of the elements leads to a reduction in the effective section properties of the columns and hence, a reduction in the flexural buckling load of the columns. Consequently, computation of the strength of cold-formed compression members should take into consideration the effect of local buckling of the plate elements. In this section, a procedure for the analysis of cold-formed steel compression members, with locally unstable unstiffened elements, will be presented.

Effective section properties of compression members at any axial strain can be calculated following the steps given below.

1. Select a uniform longitudinal compressive strain e .
2. From the stress strain relationship of the material (eqn. 4.4.6a) determine the tangent modulus E_{t1} , and the stress σ_1 of the flat and corner elements at the strain e .
3. Determine the effective area of the flat elements using an effective width equation.
4. Determine the effective moment of inertia I_{eff} of the subelements about the axis of overall buckling of the section, assuming that the effective area of the unstiffened elements is distributed adjacent to the supported edge as

shown in fig. 4.4.9a.

5. Calculate the total effective area ($A_{eff} = \sum A_{i,eff}$) of the column.
6. Compute the total force on the column ($P = \sum \sigma_i A_{i,eff}$) and the average stress ($\sigma_{av} = P/A_{total}$) from the stress σ_i and the effective area $A_{i,eff}$ of the subelements.

Having obtained the average stress σ_{av} and the section properties of the column at this stress, the effective length L of the column which will experience overall buckling at this average stress σ_{av} can be calculated using eqn. 4.4.5b

$$L = \sqrt{\frac{\pi^2 \sum_{i=1}^n E_{ti} I_{i,eff}}{\sigma_{av} A_{total}}} \quad (4.4.5b)$$

In eqn. 4.4.5b, L is the effective length of the column, A_{total} is the total cross sectional area of the column. This equation is based on the tangent modulus equation for column flexural buckling.

Column curves are derived for the nine sets of test columns (LC-I through LC-V and UD-1 through UD-4). A computer program written by DeWolf³², which follows the steps outlined above, was used with some modification of the effective width equation and distribution of the effective area to arrive at the column curves. There are

three sets of column curves (figs. 6.4.1 through 6.4.9) for each column corresponding to three of the effective width equations used to calculate the section properties. They are: (curve b) obtained using effective width eqn. 3.4.1 in which the coefficients B_1 and B_2 are taken as functions of the local buckling coefficient K ; (curve c) obtained using eqn. 3.4.1 and simplified values of B_1 and B_2 as given in eqn. 6.3.1; (curve d) obtained using the effective width eqn. 3.4.5. In all these cases, theoretical buckling coefficients calculated as detailed in section 6.2.3 are used (Table 6.3.1).

Column test points are also plotted in figs. 6.4.1 through 6.4.9 for a comparison with corresponding theoretical column curves. The theoretical curves compare well with the test results, yielding somewhat conservative yet realistic values for the column buckling stresses. These theoretical curves are more conservative than those derived in chapter 4 (figs. 4.4.10 through 4.4.30), because the theoretical buckling coefficients used in this chapter are conservative when compared to the experimental values used in chapter 4.

On the basis of this comparison, it can be concluded that the flexural buckling strength of columns can be calculated using the tangent modulus equation in which the effective section properties, obtained from any one

of the effective width equations, are used.

Another procedure, based on a modified version of the Column Research Council method, is presented in appendix 2. A step by step method for calculating the flexural buckling strength of a column using the tangent modulus method and modified CRC method is also enumerated in appendix 2. An example showing the method of calculating the flexural buckling strength following the step by step procedure is also presented in appendix 2.

6.5 Summary and Conclusions

Procedures for calculating the strength of members with unstiffened elements in compression have been presented. Theoretical equations for calculating the local buckling stress in the elastic range and the strain capacity in the plastic range were presented. Equations for computing the reduced effective width of unstiffened elements in the elastic postbuckling range were also presented. Short compression members and flexural members can be designed using these equations.

Equations were presented for calculating the overall flexural buckling strength of compression members. These equations take into account the reduction in the effective stiffness of the compression members, due to local buckling.

The equations presented, realistically model the local buckling and the postbuckling behavior of unstiffened elements, and the effect of local buckling on the flexural and compression member behavior.

CHAPTER 7

SUMMARY AND CONCLUSIONS

7.1 Summary and Conclusion

The elastic and inelastic local buckling and the postbuckling behavior of unstiffened compression elements have been investigated analytically and experimentally. The effect of local buckling on the overall flexural buckling of columns and the bending of beams with unstiffened compression elements, has been studied. Methods for the design of cold-formed steel structural members with unstiffened compression elements have been presented on the basis of the analytical and experimental investigations.

In the first chapter a qualitative description of the elastic and inelastic behavior of the unstiffened elements was presented. The behavior of members with unstiffened elements in compression was also discussed. A brief outline of the purpose and the scope of the investigation was presented.

An analytical solution to the elastic and inelastic local buckling and the postbuckling behavior of unstiffened elements was presented in the second chapter. The large deflection equations of Von Karman were solved by assuming an approximate wave form for the deflected shape of the

unstiffened elements. The amplitude of the wave was obtained using Galerkin's method. Closed form equations were derived for the effective width and the maximum amplitude of deflection of the ideally flat unstiffened element. The inelastic local buckling strain of the unstiffened elements having an elasto-plastic stress strain relationship was obtained using Stowell's²³ equations.

The results of the stub column tests were presented in the third chapter and were compared with the analytical solution derived in the second chapter. On the basis of this comparison an effective width equation for unstiffened elements with initial imperfections was presented. Another effective width equation having a format similar to the AISI effective width equation for stiffened elements was derived. Both effective width equations compared well with the results of tests on stub columns. The analytical equation for the maximum amplitude of the out of plane deformation of an ideally flat unstiffened element compared well with the out of plane deflection of the test specimens at the ultimate load.

The flexural buckling strength of compression members with unstiffened elements was investigated in the fourth chapter. For compression members the AISI specification design approach was quite conservative. This is primarily

due to the limit that the specification places on the compressive stress on the unstiffened elements in order to limit excessive out of plane distortions. Test results indicated that the distortion of the unstiffened elements in the postbuckling range was not objectionable. Procedure was presented for obtaining the flexural buckling strength curves for compression members with unstiffened elements, using the tangent modulus equation. In this equation the effective section property was substituted to obtain the flexural buckling strength.

The effect of the local buckling of unstiffened elements on the bending of beams was studied in the fifth chapter. It was found that the proposed effective width equations realistically modeled the elastic postbuckling behavior of the beams. The theoretical plastic strain at the local buckling was found to give a conservative estimate of the inelastic strain capacity of unstiffened elements, buckling in the plastic range.

Procedures for the analysis of the strength of short and long compression members and beams with unstiffened elements in compression were presented in the sixth chapter. The theoretical values obtained using these procedures compared well with the test results. On the basis of this it can be concluded that the procedures

presented could be used to calculate the strength members with unstiffened compression elements, taking full advantage of the postbuckling strength of the elements.

In appendix A an analytical effective width equation (A .1) is derived for stiffened elements which is based on Sayed's work. This analytical equation is compared with Winter's effective width equation for stiffened elements (eqn. 1.2.3). In appendix B Winter's effective width equation for stiffened elements (eqn. 1.2.3) is compared with the effective width equation for unstiffened elements (eqn. 3.4.5) and the test results. A procedure for obtaining column flexural buckling curves based on a modified form of the Column Research Council equation is also presented in appendix B and compared with the test results and the tangent modulus column curves. Finally a step by step procedure and an example are presented in appendix B for calculating the flexural buckling strength of columns using the tangent modulus and modified CRC methods.

7.2 Scope for Future Investigation

In this investigation it was assumed that the unstiffened elements subjected to compression were always restrained from rotation by the adjoining elements, the limiting condition being a zero restraint. In some appli-

cations, as in the case of edge stiffeners, the adjoining elements may buckle before the unstiffened element, in which case the unstiffened element behaves as a restraining element. The effect of this negative restraint on the local buckling behavior of the unstiffened element needs to be investigated.

The unstiffened compression flanges in this investigation were braced at sufficiently close intervals to avoid lateral buckling of the beams. The effect of local buckling on the maximum unbraced length and on the lateral buckling strength of beams is an area which warrants further research.

The effect of local buckling on the bending of beams and the flexural buckling of columns was separately investigated. Beam columns are one of the most commonly encountered members in practice. The effect of local buckling on the behavior of beam columns is an area of interest requiring further attention. The effect of local buckling on torsional flexural buckling of columns is another area of practical application and has to be looked into.

These are a few areas of interest where the local buckling of the unstiffened elements affects the behavior of a member and hence require further research.

APPENDIX A

EFFECTIVE WIDTH EQUATIONS FOR STIFFENED ELEMENTS

An effective width equation for stiffened elements derived by Winter^{12,13} is given below.

$$b_e/w = \sqrt{\sigma_{cr}/\sigma_{e\ max}} - 0.22 \sigma_{cr}/\sigma_{e\ max} \quad (1.2.2)$$

where b_e is the effective width, w is the actual flat width, $\sigma_{e\ max}$ is the maximum compressive stress in the loaded direction at the unloaded supported edge and σ_{cr} is the local buckling stress of the stiffened elements. Sayed¹⁷ has presented an analytical method for calculating the effective width of stiffened elements in the elastic postbuckling range, following a procedure similar to that given here in the second chapter for an effective width equation of unstiffened elements. Below an effective width equation for stiffened elements, based on Sayed's analytical solution and having the same format as eqn. 3.4.1 derived for unstiffened elements, will be presented.

Using eqn. 46c in reference 17, the effective width equation of perfectly flat stiffened elements with simply supported unloaded edges free to move in the plane of the element can be written as

$$b_e/w = \frac{0.746}{\sigma_{e \max}/\sigma_{cr}} + 0.254 \quad (\text{A.1})$$

where all the variables are defined above.

Using eqs. 71 and 73 in reference 17, the post-buckling behavior of stiffened elements with initial imperfections can be analyzed. Effective width equation (eqn. A.1) for a perfectly flat plate can be modified to take into account initial imperfections, as explained in section 3.4.3 of this report. The modified form of the effective width equation for a stiffened element, having an amplitude of initial imperfection equal to 0.2 times the thickness of the element (a value which apparently yields a close agreement with test results-ref. 17), can be written as

$$b_e/w = \frac{0.746}{\left(\frac{\sigma_{e \max}}{\sigma_{cr}} + 0.55\right)} + 0.254 \quad (\text{A.2})$$

Effective width eqs. 1.2.2 and A.2 are compared in fig. A .1. The analytical eqn. A.2 and eqn. 1.2.2, on which the present AISI design equation is based, compare well over a large range of the postbuckling behavior.

APPENDIX B
COMPARISON OF EFFECTIVE WIDTH EQUATIONS
AND POSSIBLE DESIGN PROCEDURES

B.1 General

Winter¹² proposed an effective width equation (eqn. 1.2.2) for the postbuckling behavior of stiffened elements, currently being used in the AISI Specification for the Design of Cold-Formed Steel Structural Members.² In Chapter 3 an effective width equation for unstiffened elements (eqn. 3.4.5) was presented which is essentially the same as the effective width equation for unstiffened elements (eqn. 1.2.3) proposed by Winter¹³ on the basis of a research report by Miller.⁶⁴ In the following sections, the effective width equations for stiffened elements (eqn. 1.2.2) will be compared with the effective width equation for unstiffened elements (eqn. 3.4.5) in the light of test results.

A procedure, based on the tangent modulus method, for calculating the flexural buckling strength of columns with locally buckling unstiffened elements was presented in chapter 4. A modified form of the Column Research Council method will be derived in this chapter for calculating the flexural buckling strength of colu

and will be compared with the tangent modulus method and test results. Finally a step by step method for calculating the flexural buckling strength of columns with locally buckling unstiffened elements, based on the two methods, will be presented and an example will be worked out.

B.2 Comparison of Effective Width Equations and Test Results of Stub Columns and Beams

Winter¹³ on the basis of a research conducted by Miller⁶⁴ presented the following effective width equation for the postbuckling behavior of unstiffened elements.

$$b_e/w = 0.8t\sqrt{E/\sigma_{e \max}} (1-0.202(t/w)\sqrt{E/\sigma_{e \max}}) \quad (\text{B.2.1})$$

Eqn. 1.2.3 is obtained¹⁴ from eqn. B.2.1 by using 0.5 for the value of local buckling coefficient (K) in the equation for the local buckling stress (eqn. 1.2.1a).

$$b_e/w = 1.19\sqrt{\sigma_{cr}/\sigma_{e \max}} (1.0-0.3\sqrt{\sigma_{cr}/\sigma_{e \max}}) \quad (\text{1.2.3})$$

In chapter 3 on the basis of test results and analytical solution, an effective width equation (eqn. 3.4.5) was derived which is essentially the same as eqn. 1.2.3, but for a small variation in one of the two constants. Eqn.

3.4.5, given below, will be referred to as Winter's unstiffened element equation (WU).

$$b_e/w = 1.19\sqrt{\sigma_{cr}/\sigma_{e\ max}}(1.0-0.298\sqrt{\sigma_{cr}/\sigma_{e\ max}}) \quad (3.4.5)$$

Winter¹² presented an effective width equation for stiffened elements which can be rewritten as shown in eqn. 1.2.2. Eqn. 1.2.2, given below, will be referred to as Winter's stiffened element equation (WS).

$$b_e/w = \sqrt{\sigma_{cr}/\sigma_{e\ max}}(1.0-0.22\sqrt{\sigma_{cr}/\sigma_{e\ max}}) \quad (1.2.2)$$

WU equation (eqn. 3.4.5) and WS equation (eqn. 1.2.2) are plotted in fig. B.2.1. The ratio of effective width to actual width (b_e/w) is the ordinate and the ratio of maximum edge stress to critical stress ($\sigma_{e\ max}/\sigma_{cr}$) is the abscissa in fig. B.2.1. The test results (at failure) of stub columns (from tables 3.4.2 and 3.4.3) and beams (from table 5.4.2) are also plotted in fig. B.2.1. The test results are scattered around Winter's unstiffened element (WU) equation, whereas Winter's stiffened element (WS) equation is generally conservative for unstiffened elements tested.

In tables B.2.1 and B.2.2, the experimental effective widths at failure of stub columns and beams are compared with the effective widths given by the two

(WU and WS) equations. The mean error of the effective widths given by WU equation is 1.6 percent and the standard deviation is 7.5 percent. The effective widths obtained using WS equation have a mean error of 10.9 percent and a standard deviation of 7.0 percent. On the basis of fig. B.2.1 and tables B.2.1 and B.2.2, it can be concluded that Winter's unstiffened element (WU) equation (eqn. 3.4.5) yields a more accurate value of the effective width of unstiffened elements in the postbuckling range than Winter's stiffened element (WS) equation (eqn. 1.2.2).

It should be noted, however, that the difference is most pronounced for large values of $\sigma_{e \max} / \sigma_{cr}$, i.e., for large w/t ratios. In the range of most practical w/t ratios for unstiffened elements, the WS equation is seen to be usable, though somewhat conservative.

B.3 Flexural Buckling Strength of Columns

The theoretical flexural buckling strength of columns can be calculated using the two effective width equations to obtain the effective section properties. In this section, the theoretical flexural buckling strengths, calculated using the two procedures:

- (1) the tangent modulus method presented in section 4.4.3,
- and (2) a modified form of the Column Research Council

Method, will be compared with the column test results.

B.3.1 Tangent Modulus Method

A procedure for calculating the flexural buckling strength of columns was presented in section 4.4.3, which uses the effective section properties and the tangent modulus equation. The column curves obtained following this procedure, in which the effective section properties are calculated using effective width equations WU (eqn. 3.4.5) and WS (eqn. 1.2.2), are shown in figs. B.3.1 through B.3.9. In these figures, the average stress (P/A) versus the slenderness ratio (L/r) is plotted for the nine different column sections tested. The column test results in tables 4.4.2 and 4.4.3 are also plotted in these figures.

The figures indicate that the column curves derived using WU equations compare well with the test results but for a few short column test results, whereas the column curves based on WS equations are generally conservative for the columns with unstiffened elements. Again, the differences are more significant for the unstiffened elements with a large w/t ratio, say $w/t \geq 35$.

B.3.2 Modified Column Research Council Method

The Column Research Council Guide to Design Cri-

teria for Metal Compression Members⁴⁹ proposed a procedure to calculate the flexural buckling strength of hot-rolled steel columns, taking into consideration nonlinearity due to residual stresses.

According to the CRC method, the flexural buckling strength of a slender column is given by the Euler equation (eqn. 4.1.2) in the range of stress less than half the yield stress, and above this stress the flexural buckling stress is given by a parabolic equation. The two equations can be written as given below.

$$\sigma_{cr} = \frac{\pi^2 E}{(L/r)^2} \quad \text{when } L/r \geq \sqrt{2}(L/r)_y \quad (\text{B.3.1})$$

and

$$\sigma_{cr} = \sigma_y - \frac{\sigma_y^2}{4\pi^2 E} (L/r)^2 \quad \text{when } L/r \leq \sqrt{2}(L/r)_y \quad (\text{B.3.2})$$

where

$$(L/r)_y = \sqrt{\pi^2 E / \sigma_y} \quad (4.1.5)$$

and σ_{cr} is the flexural buckling stress of columns.

Eqs. (B.3.1) and (B.3.2) can be modified to take into consideration the effects of local buckling, encountered before flexural buckling in cold-formed steel structural columns, by introducing the effective section properties instead of total section properties and in-

interpreting σ_{cr} as the stress (σ_{eff}) on the effective area (A_e) of the column cross section at the flexural buckling load. The stress on the effective area (σ_{eff}) can be written as

$$\sigma_{eff} = \sigma_{av} \frac{A}{A_{eff}} \quad (B.3.3)$$

where σ_{av} is the average stress on the total area at the flexural buckling load. Using eqn. B.3.3 and modifications necessary to account for reduction in effective section as a result of local buckling, eqs. B.3.1 and B.3.2 can be rewritten as

$$\sigma_{av} = \frac{A_e}{A} \frac{\pi^2 E}{(L/r_e)^2} \quad (B.3.4)$$

and

$$\sigma_{av} = \frac{A_e}{A} \sigma_y - \frac{\sigma_y^2}{4\pi^2 E} (L/r_e)^2 \quad (B.3.5)$$

The limiting value of the effective slenderness ratio $(L/r_e)_{lim}$, above which eqn. B.3.4 is to be used can be obtained by equating the average stress (σ_{av}) given by the two equations (eqs. B.3.4 and B.3.5) and is given by

$$(L/r_e)_{lim} = \sqrt{2\pi^2 E/\sigma_y} = \sqrt{2}(L/r)_y \quad (B.3.6)$$

where $(L/r)_y$ is defined in eqn. 4.1.5. Eqs. B.3.4 and

B.3.5 are the desired modified form of the CRC equations and give the average flexural buckling stress of cold-formed structural steel columns. It can be easily shown that eqn. B.3.4 reduces to Euler equation when the flexural buckling occurs at a stress below σ_{lim} . (the limiting stress below which a compression element is fully effective). The procedure outlined above will be referred to as the modified Column Research Council procedure (modified CRC procedure).

Using the two effective width equations (WU and WS eqns.) and the modified CRC procedure, column curves for the nine different sections tested have been computed and are shown in figs. B.3.10 through B.3.18. The ordinate and abscissa in these figures are the average stress (P/A) and slenderness ratio (L/r) respectively. Corresponding column test results are also shown in these figures. Column curves obtained using the WU equation compare well with the test results, whereas the WS equation is conservative compared to the test results.

The theoretical values of the flexural buckling stress from the tangent modulus method using WU eqn. have good correlation in the case of sections UD-2 and UD-3 and are unconservative for at least one column in the case of all other sections. The modified CRC method

using WU eqn. generally yields theoretical values which indicate good correlation with the test results but for one column each in the case of sections LC-I and LC-IV. For columns with unstiffened elements having a low value of w/t ratio ($w/t \leq 30$) the modified CRC method tends to be conservative. On the basis of the figs. B.3.1 through B.3.18 and the discussion above it appears that the modified CRC method indicates a better correlation with the test results, especially in the case of shorter columns in each section which have the flexural buckling stresses on the effective areas ($\sigma_{eff} = P/A_{eff}$) nearly equal to the yield stress of the material.

In the next section validity of the modified CRC method for columns with stiffened elements will be investigated using the test results of DeWolf³².

B.3.3 Columns With Locally Buckling Stiffened Elements

In the previous section, theoretical methods for calculating the flexural buckling strength of cold-formed steel columns were presented, and the column curves obtained using these procedures were compared with the results of tests on columns with unstiffened elements. In this section, flexural buckling strength curves for columns with locally buckling stiffened elements will be arrived at using the modified Column Research Council

procedure and compared with the stiffened column test results of DeWolf.³²

DeWolf³² tested columns with stiffened elements in axial compression. The shape of the cross sections is shown in fig. B.3.19a. The section dimensions and properties of the eighteen columns of four different cross section dimensions are given in table B.3.1. The test results of the eighteen columns are presented in table B.3.2.

The effective width equation for stiffened elements, referred to as WS equation in the last section, gives the postbuckling effective width of stiffened elements in compression. This equation is written in terms of the maximum stress at the supported edge ($\sigma_{e \max}$) and the local buckling stress (σ_{cr}) as shown below.

$$b_e/w = \sqrt{\sigma_{cr}/\sigma_{e \max}} (1.0 - 0.22\sqrt{\sigma_{cr}/\sigma_{e \max}}) \quad (1.2.2)$$

The effective width of stiffened elements can be distributed as shown in fig. B.3.19b to obtain the effective flexural stiffness of stiffened sections about the minor axis. Using the effective stiffness thus computed and the modified CRC procedure outlined in the last section, column curves for stiffened sections could be obtained.

Column curves for the four sections in table B.3.1

are shown in figs. B.3.20 through B.3.23. In addition to the curves corresponding to the Euler and yield stress, there are three column curves for each section. Two of these curves are drawn for the maximum and minimum values of the local buckling coefficient of stiffened elements ($K = 4.0$ and 6.97). The third curve is drawn for the experimental value of the buckling coefficient, obtained by DeWolf. There is a good correlation between the column curves corresponding to the experimental values of the buckling coefficient and the test results, indicating the validity of the modified CRC procedure for stiffened columns also. Value of the local buckling coefficient of stiffened elements is usually assumed to be equal to 4.0 in design. In general, the column curves corresponding to the lowest value of the local buckling coefficient ($K = 4.0$) is slightly conservative.

DeWolf compared the flexural buckling strength of columns having stiffened elements with the tangent modulus column curves (figs. 6.12-6.15, ref. 32). These four figures are compared with figs. B.3.20-B.3.23 to evaluate the relative merit of the modified CRC method. The modified CRC curves exhibit good correlation in the case of all the column test results, whereas, the tangent modulus method yields unconservative values in the

case of columns having the flexural buckling stress on the effective area ($\sigma_{\text{eff}}=P/A_{\text{eff}}$) nearly equal to the yield stress.

B.3.4 Computation of Flexural Buckling Strength of Columns

Procedures for drawing the column curves for a given section were presented so far. In this section, an iterative method for calculating the flexural buckling strength of a slender cold-formed steel column of a given section and effective length will be presented. The procedure will also be illustrated numerically using one of the columns tested.

Steps for Calculating the Flexural Buckling Strength of Columns with Locally Buckling Unstiffened Elements:

1. Calculate the total area, total moment of inertia and effective length of the column. Calculate the local buckling stress of flat elements substituting the relevant values of the local buckling coefficient (K). For stiffened elements, the local buckling coefficient K could be assumed conservatively to be equal to 4.0. The local buckling coefficient of unstiffened elements could be calculated theoretically as described in section 6.2.

2. Assume a reasonable value of stress on the effective area ($\sigma_{eff} = P/A_{eff}$) corresponding to the flexural buckling of the column, as an initial estimate. This can be the flexural buckling stress of the column section, computed using any one of the present methods (AISI method for example).

3. Calculate the stresses and tangent moduli of the flat and corner elements at the assumed stress on the effective area, using the stress strain relationship of the elements.

4. Calculate the effective width of the flat elements using the proper effective width equation (eqn. 1.2.2 for stiffened elements and eqn. 3.4.5 for unstiffened elements).

5. Distribute the effective width of stiffened and unstiffened elements adjacent to the supported edges as shown in figs. B.3.19b, 4.4.9a. Calculate the effective area (A_{eff}), effective moment of inertia (I_{eff}) and effective tangent modulus stiffness ($\sum_i E_{ti} I_{i,eff}$).

6. Determine the stress on the effective area (σ_{eff}) at the flexural buckling using the modified CRC formula or modified tangent modulus formula given below.

Modified CRC Formula:

$$\sigma_{\text{eff}} = \frac{\pi^2 E}{(L/r_e)^2} \quad \text{when } (L/r_e) \geq \sqrt{2}(L/r)_y \quad (\text{A2.3.6})$$

$$\sigma_{\text{eff}} = \sigma_y (1 - \sigma_y (L/r_e)^2 / 4\pi^2 E) \quad \text{when } (L/r_e) \leq \sqrt{2}(L/r)_y \quad (\text{A2.3.7})$$

Modified Tangent Modulus Formula:

$$\sigma_{\text{eff}} = \frac{\pi^2 \sum (E_{ti} I_{i,\text{eff}})}{A_{\text{eff}} L^2} \quad (\text{A2.3.8})$$

7. Compare the σ_{eff} calculated in step 6 with the σ_{eff} assumed in step 2. If the difference is more than an acceptable limit, assume a new value of the σ_{eff} equal to the average of the assumed and calculated values from the preceding iteration and repeat steps 3 through 7.

8. If the difference between the assumed and calculated values of the σ_{eff} is within an acceptable error margin, calculate the effective stress on all elements using the stress strain curve of the elements. The theoretical flexural buckling load of the column is given by

$$P_{\text{cr}} = \sum_I A_{i,\text{eff}} \sigma_{i,\text{eff}} \quad (\text{A2.3.9})$$

Using the steps enumerated, a numerical computation of the flexural buckling strength of a slender column, tested in this investigation, is presented below.

Numerical example: (Specimen LC - II)

Step 1. section dimensions and properties:
(fig. 3.2.2)

$$B = 2.50 \text{ in.}, D = 4.007 \text{ in.}, t = 0.0492 \text{ in.},$$

$$L = 57.19 \text{ in.}, w = 2.451 \text{ in.}, w/t = 49.81,$$

$$\sigma_y = 30.26 \text{ ksi}$$

Total area:

$$\begin{aligned} A &= (4 \times w \times t) + (2(D - 2 \times t) + \pi t^2) \\ &= (4 \times 2.451 \times .0492) + (2 \times (4.007 - 2 \times .0492) \\ &\quad + (\pi \times .0492^2)) \end{aligned}$$

$$\underline{A = 0.875 \text{ in}^2}$$

Total moment of inertia:

$$\begin{aligned} I &= (D \times \frac{(2t)^3}{12}) + (4 \times t \times \frac{w^3}{12}) + 4 \times w \times t \\ &\quad \times (\frac{w}{2} + t)^2 = (4.007 \times \frac{(2 \times .0492)^3}{12}) \\ &\quad + (4 \times .0492 \times \frac{2.451^3}{12}) + 4 \times 2.451 \times .0492 \\ &\quad \times (\frac{2.451}{2} + .0492)^2 \end{aligned}$$

$$\underline{I = 1.027 \text{ in}^4}$$

$$r = \sqrt{I/A} = \sqrt{1.027/0.875}$$

$$\underline{r = 1.085 \text{ in}}$$

$$L/r = 57.19/1.085$$

$$\underline{L/r = 52.71}$$

Local buckling coefficient:

$$K = 0.820 \quad (\text{from table 6.3.1})$$

$$\underline{K = 0.820}$$

$$\begin{aligned} \sigma_{cr} &= \frac{K\pi^2 E}{12(1-\mu^2)(w/t)^2} \\ &= \frac{0.820 \times \pi^2 \times 29500}{12 \times 0.91 \times 49.81^2} \end{aligned}$$

$$\underline{\sigma_{cr} = 8.81 \text{ ksi}}$$

$$\begin{aligned} (L/r)_y &= \sqrt{\pi^2 E / \sigma_y} \\ &= \sqrt{\pi^2 \times 29500 / 30.26} \end{aligned}$$

$$\underline{(L/r)_y = 98.1}$$

Step 2. Assume a value of σ_{eff}

Computations of starting σ_{eff} value using the present AISI method.

$$\text{At } \sigma_{e \max} = \sigma_y$$

unstiffened elements:

$$\begin{aligned} b_{e,u} &= w_u \times 1.19 \sqrt{\sigma_{cr} / \sigma_{e \max}} (1 - 0.297 \sqrt{\sigma_{cr} / \sigma_{\max}}) \\ &= 2.451 \times 1.19 \sqrt{\frac{8.81}{39.26}} (1 - 0.297 \sqrt{\frac{8.81}{30.26}}) \end{aligned}$$

$$\underline{b_{e,u} = 1.322 \text{ in}}$$

stiffened elements:

$$b_{e,s} = w_s = (4.007 - 2 \times .0492)$$

$$\underline{b_{e,s} = 3.909 \text{ in}}$$

$$A_{\text{eff}} = 0.653 \text{ in}^2$$

$$A = \frac{A_{\text{eff}}}{A} = \frac{0.653}{0.857}$$

$$Q = \underline{0.746}$$

$$\sigma_{\text{eff}} \approx Q \sigma_y \left[1 - \frac{\sigma_y (L/r)^2}{4\pi^2 E} \right]$$

$$= 0.746 \times 30.26 \left[1 - \frac{30.26 \times 52.71^2}{4 \times \pi^2 \times 29500} \right]$$

$$\sigma_{\text{eff}} = \underline{21.65 \text{ ksi}} \quad \text{assumed}$$

initial guess

Modified CRC Method:

Iteration No.	Step 2,7	Step 3	Step 4		Step 5			Step 6
	Assumed σ_{eff} (ksi)	$(\sigma_{e\ max})_{flat} = \sigma_{corner}$ (ksi)	b_e (in)		A_{eff} (in ²)	r_{eff} (in)	L/r_{eff}	Calculated σ_{eff} (ksi)
			unstiffened	stiffened				
1	20.9	20.9	1.529	3.909	0.693	0.610	93.7	23.4
2	22.1	22.1	1.496	3.909	0.687	0.594	96.3	22.9
3	22.5	22.5	1.486	3.909	0.685	0.592	96.6	22.6

$$P_{cr} = (A_{eff,i} \sigma_{i,eff})$$

$$= 0.685 \times 22.6 = 15.54 \text{ kips}$$

$$(\sigma_{av})_{theory} = P_{cr}/A = \frac{15.54}{0.875} = 17.8 \text{ ksi}$$

$$(\sigma_{av})_{expt.} = 18.48 \text{ ksi} \quad (\text{from table 4.4.1})$$

$$\text{error} = 3.8 \% \quad (\text{conservative})$$

Modified Tangent Modulus Method:

Iteration No.	Step 2,7	Step 3	Step 4		Step 5			Step 6
	Assumed σ_{eff} (ksi)	$(\sigma_{e\ max})_{flat} = \sigma_{corner}$ (ksi)	b_e (in)		A_{eff} (in ²)	r_{eff} (in)	L/r_{eff}	Calculated σ_{eff} (ksi)
			unstiffened	stiffened				
1	20.9	20.9	1.529	3.909	0.693	0.610	93.7	33.1
2	27.0	27.0	1.383	3.909	0.664	0.539	106.1	25.8
3	26.4	26.4	1.395	3.909	0.667	0.544	105.1	26.4

$$P_{cr} = \sum_i A_{i,eff} \sigma_{i,eff}$$

$$= 0.667 \times 26.4 = 17.61 \text{ ksi}$$

$$(\sigma_{av})_{theory} = \frac{P_{cr}}{A} = \frac{17.61}{0.875} = 20.12 \text{ ksi}$$

$$(\sigma_{av})_{expt.} = 18.48 \text{ ksi} \quad (\text{from table 4.4.1})$$

$$\text{error} = -8.9\% \quad (\text{unconservative})$$

B.4 Summary and Conclusions

Theoretical values of strength of beams and columns with unstiffened elements in compression were calculated using the effective width equations for unstiffened elements (WU eqn., eqn. 3.4.5) and stiffened elements (WS eqn., eqn. 1.2.2). The column flexural buckling strength curves were derived using the tangent modulus method and modified Column Research Council method. Beam and column test results were compared with the theoretical values. Column curves for DeWolf's columns³² with stiffened elements, derived using the modified Column Research Council method, were also compared with his test results. Finally a step by step procedure for calculating the flexural buckling strength of a column was given and a numerical example was presented.

Winter's effective width equation derived for stiffened elements (WS eqn. 1.2.2) is generally conservative if compared with the experimental effective width of unstiffened elements. Whereas, Winter's effective width equation for unstiffened elements (WU eqn. 3.4.5) indicates a good correlation with the test results. However the difference between the two equations is marginal in the case of unstiffened ele-

ments having a smaller postbuckling range (elements having a smaller w/t ratio). The column curves obtained using the modified Column Research Council method exhibits a better correlation with the column test results than the tangent modulus curves, especially when the flexural buckling stress on the effective area of the column ($\sigma_{\text{eff}} = P/A_{\text{eff}}$) is nearly equal to the yield stress of the material.

Note from the project directors: While Mr. Kalyanaraman states his preference for the C.R.C. Column Curve over the Tangent Modulus Method, which is his perfect right as investigator, we as project directors wish to add that the degree of accuracy of the two methods to us appears to be about the same. Therefore the choice between the two methods for specification and design use could well be made on the basis of greater generality or practicality.

T. P. and G. W.

LIST OF REFERENCES

1. AISC Specification for the Design Fabrication and Erection of Structural Steel for Buildings, American Institute of Steel Construction, New York, N.Y., 1970.
2. Specification for the Design of Cold-Formed Steel Structural Members, American Iron and Steel Institute, New York, N.Y., 1968.
3. Bryan, G.H., "On the Stability of a Plane Plate Under Thrusts in Its Own Plane with Applications on the "Buckling" of the Sides of a Ship," Proc. London Math. Soc., 1891, P51.
4. Timoshenko, S.P., and Gere, J.M., Theory of Elastic Stability, McGraw-Hill, New York, N.Y., 1961.
5. Lundquist, E.E., Stowell, E.Z., "Critical Compressive Stress for Outstanding Flanges," NACA Report 734, 1942.
6. Chilver, A.H., "A Generalized Approach to the Local Instability of Certain Thin-Walled Struts," Aeronautical Quarterly, Vol. IV, Aug. 1953.
7. Kroll, W.D., Fisher, G.P., Heimerl, G.J., "Charts for the Calculation of the Critical Stresses for the Local Instability of Columns with I-, Z-, Channel, and Rectangular-Tube Section," NACA L-429, 1943.
8. Stowell, E.Z., Lundquist, E.E., "Local Instability of Columns with I-, Z-, Channel and Rectangular-Tube Sections," NACA TN-743, 1939.
9. Walker, A.C., "Local Instability in Plates and Channel Struts," J. Structural Div. ASCE Vol. 92 No. ST3, June, 1966.
10. Bleustein, J.L., Gjelsvik, A., "Rational Design of Light Gage Beams," J. Structural Div., ASCE Vol. 96 No. ST7, July 1970.
11. Gerard, G., "Handbook of Structural Stability-Part IV: Failure of Plates and Composite Elements," NACA TN 3784, 1957.

12. Winter, G., "Strength of Thin Steel Compression Flanges," Transactions, ASCE, Vol. 112, 1947.
13. Winter, G., "Strength of Thin Steel Compression Flanges," Reprint No. 32, Engineering Experiment Station, Cornell University, Ithaca, N.Y.
14. Jombock, J.R., Clark, J.W., "Postbuckling Behavior of Flat Plates," J. Structural Div., ASCE Vol. 87, No. ST5, June 1961.
15. Hu, P.C., Lundquist, E.E., Batdort, S.B., "Effects of Small Deviations From Flatness on Effective Width and Buckling of Plates in Compression," NACA TN 1124, 1946.
16. Coan, J.M., "Large Deflection Theory for Plates with Small Initial Curvature Loaded in Edge Compression," J. Applied Mechanics, Vol. 18, Trans. ASME Vol. 73, 1951.
17. Abdel-Sayed, G.A., "Effective Width of Thin Plates in Compression," J. Structural Div., ASCE, Vol. 95 No. ST10, October 1969.
18. Yamaki, N., "Postbuckling Behavior of Rectangular Plates with Small Initial Curvature Loaded in Edge Compression," J. Applied Mech., Vol. 26, 1959, Vol. 27, 1960.
19. Dawson, R.G., Walker, A.C., "Postbuckling of Geometrically Imperfect Plates," J. Structural Div., ASCE, Vol. 98 No. ST1, Jan. 1972.
20. Ros, M., Eichinger, Final Report, 1st Congress, IABSE, Paris 1932.
21. Bijlaard, P.P., "Theory of Plastic Stability of Thin Plates," Pubs. International Association of Bridge and Structural Engineers Vol. VI, 1940-41.
22. Ilyushin, A.A., "The Elastic-Plastic Stability of Plates," Translation in NACA, TM 1188.
23. Stowell, E.Z., "A Unified Theory of Plastic Buckling of Columns and Plates," NACA TN 1556, 1958.
24. Stowell, E.Z., Pride, R.A., "Plastic Buckling of Extruded Composite Sections in Compression," NACA TN 1971, 1949.

25. Bleich, F., Buckling Strength of Metal Structures, McGraw-Hill Book Co., New York, N.Y. 1952.
26. Haaijer, G., "Plate Buckling in the Strain Hardening Range," J. Engineering Mechanics Div., ASCE, Vol. 83 No. EM2, April 1957.
27. Bijlaard, P.P., Fisher, G.P., "Column Strength of H-Sections and Square Tubes in Postbuckling Range of Component Plates," NACA TN 2994, 1963.
28. Graves Smith, T.R., "The Ultimate Strength of Locally Buckled Columns of Arbitrary Length," Thin Walled Steel Structures, Eds. Rockey and Hill, Crosby Lockwood, London, 1969.
29. Wang, S.T., "Post-Local-Buckling Behavior of Thin-Walled Columns," Second Speciality Conference on Cold-Formed Steel Structures, Dept. of Civil Eng., Univ. Missouri, Rolla.
30. Sharp, M., "Strength of Beams or Columns With Buckled Elements," J. Structural Div., ASCE, Vol. 96 No. ST5, May 1970.
31. Skaloud, M., and Zornerova, M., "Experimental Investigation into the Interaction of the Buckling of Compressed Thin-Walled Columns with the Buckling of Their Plate Elements," ACTA Technica, CSAV.
32. DeWolf, J., "Local and Overall Buckling of Cold-Formed Compression Members," Report No. 354, Dept. of Structural Eng., Cornell Univ., Ithaca, N.Y. 1973.
33. Levy, M.G., and Galambos, T.V., "Inelastic Steel Beams Under Uniform Moment," J. Structural Div., ASCE, Vol. 91 No. ST6, December 1965.
34. Lay, M.G., and Galambos, T.V., "Inelastic Beams Under Moment Gradient," J. Structural Div., ASCE, Vol. 91 No. ST6, December 1965.
35. Sawyer, H.A., Jr., "Post-Elastic Behavior of Wide-Flange Steel Beams," J. Structural Div., ASCE, Vol. 87 No. ST8 December 1961.

36. Adams, P.F., Lay, M.G., and Galambos, T.V., "Experiment on High Strength Steel Members," Welding Research Council Bulletin No. 110, November, 1965.
37. Lukey, A.F., Smith, R.J., Hosain, M.V., and Adams, P.F., "Experiments on Wide-Flange Beams Under Moment Gradient," Welding Research Council Bulletin No. 142, July 1969.
38. Johnson, A.L., and Winter, G., "The Structural Performance of Austenitic Stainless Steel Members," Report No. 327, Dept. of Structural Eng., Cornell Univ., Ithaca, N.Y. 1967.
39. Rhodes J., and Harvey, J.M., "The Local Buckling and Post-Local-Buckling of Thin-Walled Beams," Aeronautical Quarterly, Vol. XXII, November, 1971.
40. Wang, S.T., "Nonlinear Analysis of Thin-Walled Continuous Beams," Second Speciality Conference on Cold-Formed Steel Structures, Dept. of Civil Eng., Univ. of Missouri, Rolla.
41. Stanley, F.R., "Inelastic Column Theory," J. Aeronautical Sciences, Vol. 14, May 1947.
42. Marguerre, K., "Zur Theorie der Gekrummten platte Grosser Formanderung," Proc. Fifth International Congress for Applied Mechanics, Cambridge, England, 1938.
43. Schnadel, G., "Die Uberschreitung der Knickgrenze bei dunnen platten," Proc. Third International Congress for Applied Mechanics, Stockholm, Vol. 3, 1930.
44. Cox, H.L., "The Buckling of Thin Plates in Compression," Technical Rep. of the Aeronautical Committee 1933-34.
45. Marguerre, K., "Die Mittrangende Breite der Gedruckten Platte," Luftfahrtforschung, Vol. 14, 1937.
46. Levy, S., "Bending of Rectangular Plates With Large Deflections," NACA Report No. 737, 1942.
47. "Tension Testing of Metallic Materials", ASTM Designation: E 8-61 T, 1965.

48. Heimerl, G.J., Roy, A.J., "Determination of Desirable Lengths of Z and Channel-section Columns for Local Instability Tests," NACA, WR L-180, 1944.
49. Johnson, B.G., ed., Design Criteria for Metal Compression Members, John Wiley & Sons, New York, N.Y. Second Edition, 1966.
50. Vann, P.W., Sehested, J., "Experimental Techniques for Plate Buckling," Second Speciality Conference on Cold-Formed Steel Structures, Department of Civil Engineering, University of Missouri, Rolla.
51. Johnson, A.L., "The Structural Performance of Austenitic Stainless Steel Members," Report No. 327, Dept. of Structural Eng., Cornell Univ., Ithaca, N.Y. 1966.
52. Scidenfaden, J. "Interaction in the Post-Buckled Range for the Channel Section," Z.P. Flugwiss, Vol. 2, 1954.
53. Bulson, P.S., "Local Stability and Strength of Structural Sections," Thin Walled Steel Structures, Their Design and Use in Building, Crosby Lockwood and Son, London, 1969.
54. Kloppel, K., Schmied, R., and Schubert, J., "Die Traglast mittig und aussermittig gedruckter Stutzen mit kastenformigem Querschnitt im uberkritischen Bereich unter Verwendung der nichtlinearen Beultheorie, Teil II. Experimentelle Untersuchungen, Vergleich der experimentellen and theoretischen Ergebnisse, "Der Stahlbau, Vol. 38, 1969.
55. Pekoz, T.B. "Torsional-Flexural Buckling of Thin-Walled Sections Under Eccentric Load," Dept. of Structural Engineering, Report No. 329, Cornell University, April 1967.
56. Estuar, F.R., and Lambert Tall, "Testing of Pinned-End Steel Columns," Test Methods for Compression Members, ASTM STP, 419, American Society of Testing Materials, 1967.
57. Southwell, R.V., "On the Analysis of Experimental Observations in Problems of Elastic Stability," Proc. Royal Society (London), Ser. A, Vol. 135, April 1932.

58. Ramberg, W., and Osgood, W.R., "Description of Stress Strain Curves by Three Parameters," NACA Tech. Note 902, 1943.
59. Haaijer, G., Thurlimann, B., "On Inelastic Buckling in Steel," J. Eng. Mech. Div., ASCE, Vol. 84, No. #M2, April 1958.
60. Lee, G.C., Galambos, T.V., "Post-Buckling Strength of Wide-Flange Beams," J. Eng. Mech. Div., ASCE, Vol. 88, No. EM1, February 1962.
61. Galambos, T.V., "Inelastic Lateral Buckling of Beams," J. Structural Div., ASCE, Vol. 89, No. ST5, October 1963.
62. Lundquist, E.E., Stowell, E.Z., Schuette, E., "Principles of Moment Distribution Applied to Stability of Structures Composed of Bars and Plates," NACA, Wartime Report L-326.
63. Peck, H.P., "Inelastic Reserve Capacity of Cold-Formed Beams with Stiffened Compression Elements," Report No. 356, Department of Structural Engineering, Cornell University, Ithaca, N.Y. 1974.
64. Miller, E.A., "A Study of the Strength of Short Thin Walled Steel Studs," Ph.D. thesis, School of Engineering, Cornell University, Ithaca, N.Y., October 1943.

TABLE 2.2.1
 LOCAL BUCKLING AND POSTBUCKLING PARAMETERS
 OF UNSTIFFENED ELEMENTS

ϵ	K_e	η'	K_p	B_1	B_3
0.0	0.428	1.000	0.425	0.354	---
0.05	0.504	0.908	0.456	0.354	17.602
0.10	0.535	0.867	0.464	0.354	13.216
0.20	0.578	0.832	0.481	0.356	10.426
0.50	0.663	0.781	0.518	0.362	7.383
1.00	0.748	0.744	0.557	0.372	6.372
1.50	0.813	0.725	0.589	0.380	5.680
2.00	0.855	0.712	0.609	0.387	5.435
3.00	0.919	0.697	0.641	0.398	5.054
5.00	1.003	0.684	0.686	0.414	4.676
10.00	1.100	0.672	0.740	0.433	4.328
20.00	1.173	0.668	0.783	0.448	4.156
50.00	1.235	0.666	0.822	0.460	4.029
∞	1.287	0.665	0.856	0.469	3.965

ϵ Rotational edge restraint factor
 K_e Elastic local buckling coefficient
 η' Modified plasticity index (e_p/e_e)
 K_p Plastic local buckling coefficient
 B_1, B_3 Constants in postbuckling behavior equations

TABLE 3.2.1
MECHANICAL PROPERTIES OF HOT ROLLED STEEL
SHEETS FOR COLUMN SPECIMENS

SHEET NO.	σ_y (ksi)	σ_u (ksi)
1	31.59	46.71
2	30.73	47.05
3	30.63	46.07
4	30.26	45.93
5	25.68	43.22
6	31.11	46.13
7	31.29	47.69
8	30.50	45.98
9	31.05	46.32
10	33.18	48.25

TABLE 3.2.2
STUB COLUMN SPECIMEN DIMENSIONS^a

Specimen	Sheet No.	BC(in)	D(in)	t(in)	w/t	Area (in ²)	L(in)
SC - I 1	1	2.873	4.031	0.0490	57.63	0.9485	20.0
SC - I 2	2	2.871	4.032	0.0489	57.71	0.9463	20.0
SC - II 1	5	2.505	3.988	0.0477	51.52	0.8493	17.0
SC - II 2	4	2.498	4.009	0.0489	50.08	0.8711	17.0
SC - III 1	7	2.126	3.998	0.0484	42.93	0.7892	14.0
SC - III 2	6	2.127	4.000	0.0484	42.95	0.7896	14.0
SC - IV 1	7	1.751	2.997	0.0483	35.25	0.6185	12.0
SC - IV 2	8	1.727	3.034	0.0480	34.98	0.6136	12.0
SC - V 1	10	1.497	3.011	0.0487	29.74	0.5754	10.0
SC - I 2	9	1.501	3.003	0.0488	29.76	0.5766	10.0

a - refer to fig. 3.2.2

TABLE 3.4.1
LOCAL BUCKLING COEFFICIENT FROM STUB COLUMN TESTS

Specimen	w/t	(D-T)/BC	Experimental		Theoretical ^a		
			σ_{cr} (ksi)	K	I	C	Average
SC - I 1	57.63	1.39	8.35	1.040	1.11	0.84	0.975
SC - I 2	57.71	1.39	7.72	0.964	1.11	0.84	0.975
SC - II 1	51.52	1.57	9.54	0.949	1.10	0.84	0.970
SC - II 2	50.08	1.59	9.69	0.912	1.10	0.81	0.955
SC - III 1	42.93	1.86	13.72	0.948	1.10	0.75	0.925
SC - III 2	42.95	1.86	13.81	0.955	1.10	0.75	0.925
SC - IV 1	35.25	1.68	21.14	0.985	1.10	0.78	0.940
SC - IV 2	34.98	1.73	21.48	0.986	1.10	0.78	0.940
SC - V 1	29.74	2.06	26.40	0.876	1.10	0.73	0.915
SC - V 2	29.76	1.97	25.52	0.848	1.10	0.73	0.915

a - From REF. 7

TABLE 3.4.2
EXPERIMENTAL EFFECTIVE WIDTH AT ULTIMATE LOAD

Specimen	(w/t)	P _u (K)	$\sigma_{e \max} = \sigma_y$ (ksi)	σ_{av} (ksi)	σ_{cr} (ksi)	$\frac{\sigma_{e \max}}{\sigma_{cr}}$	$\frac{\sigma_{av}}{\sigma_{cr}}$	b _{e/w}	(Z/t) _{max}
SC - I 1	57.63	23.35	31.59	17.54	8.35	3.78	2.10	0.556	2.15
SC - I 2	57.71	21.95	30.73	17.34	7.72	3.98	2.25	0.565	1.91
SC - II 1	51.52	19.38	25.68	15.74	9.54	2.69	1.65	0.613	1.82
SC - II 2	50.08	21.78	30.26	17.35	9.69	3.12	1.79	0.574	1.36
SC - III 1	42.93	19.78	31.29	19.08	13.72	2.28	1.39	0.610	1.16
SC - III 2	42.95	21.70	31.11	19.33	13.81	2.25	1.40	0.622	1.21
SC - IV 1	35.25	17.58	31.29	23.25	21.14	1.48	1.10	0.743	0.96
SC - IV 2	34.98	16.80	30.50	22.12	21.48	1.42	1.03	0.725	0.83
SC - V 1	29.74	17.70	33.18	26.40	26.40	1.27	1.00	0.787	0.53
SC - V 2	29.76	16.63	31.05	22.46	25.52	1.22	0.88	0.721	0.52

TABLE 3.4.3

STUB-COLUMN SPECIMEN DIMENSIONS^{a,b}

Specimen	BC(in)	D(in)	t(in)	w/t	Area(in ²)	L(in)	(D-t)/BC
UD - 1	1.00	3.00	0.058	16.2	0.565	7.4	2.94
UD - 2	1.25	3.00	0.058	20.55	0.623	9.0	2.35
UD - 3	1.50	3.00	0.058	24.86	0.681	9.0	1.96
UD - 4	1.75	3.00	0.058	29.17	0.739	9.0	1.68

EXPERIMENTAL RESULTS

Specimen	Experimental		Theoretical ^d			P _u (k)	σ _{e max} (ksi)	σ _y (ksi)	σ _{av} (ksi)	σ _{e max} σ _{cr}	σ _{av} σ _{cr}	b _e w
	σ _{cr} (ksi)	K	I	C	Avg.							
UD - 1	71.12 ^c	0.700	1.098	0.635	0.784	24.7	41.9	46.63	0.58	0.66	1.100	
UD - 2	49.69 ^c	0.787	1.099	0.716	0.867	25.8	41.9	40.80	0.84	0.82	0.973	
UD - 3	35.60	0.825	1.100	0.788	0.908	27.0	41.9	37.29	1.18	1.05	0.890	
UD - 4	26.90	0.858	1.095	0.472	0.944	27.4	41.9	32.78	1.56	1.22	0.782	

a - Tested by John DeWolf (Ref. 32)

b - Refer to Fig. 3.2.2

c - Based on the assumed buckling coefficient

d - From Ref. 7

TABLE 3.4.4
INITIAL IMPERFECTION PARAMETER IN
EFFECTIVE WIDTH EQUATION

K	B_2
.504	0.214
.535	0.248
.578	0.279
.663	0.325
.748	0.350
.813	0.361
.855	0.366
.919	0.375
1.003	0.379
1.100	0.381
1.173	0.379
1.235	0.378
1.287	0.376

TABLE 3.4.5
COMPARISON OF EFFECTIVE WIDTHS OF STUB
COLUMN UNSTIFFENED FLANGES

Specimen	w/t	EXPERIMENTAL			Eqn. 3.4.1		Eqn. 3.4.5	
		K	$\frac{\sigma_{e/\max}}{\sigma_{cr}}$	b_e/w	b_e/w	% diff.	b_e/w	% diff.
SC-I 1	57.63	1.040	3.78	0.556	0.558	-0.5	0.518	6.8
SC-I 2	57.71	0.964	3.98	0.565	0.542	4.0	0.508	10.2
SC-II 1	51.52	0.949	2.69	0.613	0.598	2.4	0.594	3.1
SC-II 2	50.08	0.912	3.12	0.574	0.570	0.7	0.560	2.4
SC-III 1	42.93	0.940	2.28	0.610	0.627	-2.8	0.633	-3.7
SC-III 2	42.95	0.955	2.25	0.622	0.631	-1.5	0.636	-2.3
SC-IV 1	35.25	0.982	1.48	0.743	0.727	2.1	0.739	0.5
SC-IV 2	34.98	0.986	1.42	0.725	0.738	-1.8	0.749	-3.4
SC-V 1	29.74	0.876	1.27	0.787	0.762	3.1	0.777	1.2
SC-V 2	29.76	0.848	1.22	0.721	0.773	-7.2	0.787	-9.2
UD-1	16.20	0.700	0.58	1.100	1.000	9.00	0.952	13.4
UD-2	20.55	0.787	0.84	0.973	0.897	7.80	0.877	9.9
UD-3	24.86	0.825	1.18	0.890	0.783	12.1	0.796	10.6
UD-4	29.17	0.858	1.56	0.782	0.706	9.7	0.726	7.2

a - Using experimental K values

TABLE 4.2.1
DIMENSIONS* AND SECTION PROPERTIES OF COMPRESSION SPECIMENS

Specimen	Sheet No.	D (in.)	BC (in.)	T (in.)	w/t	Col. Length (in.)	L (in.)	Area (in. ²)	I min. (in. ⁴)
LC-11	1	4.024	2.866	0.0489	57.61	60.00	63.25	0.9425	1.542
LC-12	1	4.031	2.869	0.0492	7.31	89.00	92.25	0.9495	1.556
LC-13	2	4.006	2.876	0.0488	57.93	120.00	123.25	0.9408	1.555
LC-I	4	4.007	2.500	0.0492	50.81	53.94	57.19	0.8745	1.030
LC-II2	4	4.018	2.501	0.0487	50.36	86.95	90.20	0.8670	1.021
LC-II3	5	4.008	2.509	0.0489	50.31	120.00	123.25	0.8711	1.035
LC-III1	7	4.039	2.113	0.093	41.86	47.94	51.19	0.8031	0.624
LC-III2	6	4.015	2.120	0.0483	42.89	84.00	87.25	0.7861	0.617
LC-III3	5	3.990	2.126	0.0488	42.57	120.00	123.25	0.7928	0.629
LC-IV1	9	3.018	1.743	0.0474	35.77	47.97	51.22	0.6057	0.337
LC-IV2	8	3.004	1.726	0.0483	34.74	68.61	71.86	0.6123	0.334
LC-IV3	7	3.015	1.742	0.0492	34.41	90.00	93.25	0.6277	0.349
LC-V1	10	3.029	1.488	0.0489	29.43	41.90	45.15	0.5757	0.217
LC-V2	3	2.996	1.502	0.0492	29.53	53.88	57.13	0.5786	0.224
LC-V3	10	3.027	1.490	0.0491	29.35	72.00	75.25	0.5782	0.219

* - Refer to Fig. 3.2.2

TABLE 4.4.1
TEST RESULTS OF COMPRESSION SPECIMENS

Specimen	w/t	L (in)	area (in ²)	r min. (in)	P _{ult.} (kip)	P _{cr.} (kip)	P _{cr./area} (ksi)	L/r _{min.}
LC-II1	57.61	63.25	0.943	1.279	14.00	14.96	15.86	49.45
LC-II2	57.31	92.25	0.950	1.280	13.80	14.07	14.81	72.07
LC-I3	57.93	123.25	0.941	1.286	11.00	11.00	11.69	95.84
LC-III1	50.81	57.19	0.875	1.085	16.00	16.17	18.48	52.71
LC-II2	50.36	90.20	0.868	1.085	12.80	13.16	15.18	83.13
LC-II3	50.31	123.25	0.871	1.090	9.73	9.95	11.42	113.07
LC-III1	41.86	51.19	0.803	0.881	16.10	16.49	20.54	58.10
LC-III2	42.89	87.25	0.786	0.886	11.00	11.66	14.83	98.48
LC-III3	42.57	123.25	0.793	0.891	8.70	8.83	11.13	138.33
LC-IV1	35.77	51.22	0.606	0.746	11.96	12.19	20.12	68.66
LC-IV2	34.74	71.86	0.612	0.738	10.50	11.29	18.45	97.37
LC-IV3	34.41	93.25	0.628	0.746	8.90	8.96	14.27	125.00
LC-V1	29.43	45.15	0.576	0.614	14.55	14.63	25.40	73.53
LC-V2	29.53	57.13	0.579	0.623	12.20	12.65	21.85	91.70
LC-V3	29.35	75.25	0.578	0.615	10.75	10.75	18.60	122.36

TABLE 4.4.2

SECTION PROPERTIES AND TEST RESULTS OF DeWOLF'S COMPRESSION SPECIMENS

Specimen	w/t	Area (in. ²)	I min. (in.)	r min. (in.)		P _u (kips)	P _u /A (ksi)	L/r
UD-11	16.2	0.5637	0.0778	0.3715	4.8	24.7	43.82	12.92
UD-12	16.2	0.5637	0.0778	0.3715	20.7	21.4	37.96	55.72
UD-13	16.2	0.5637	0.0778	0.3715	33.1	20.4	36.19	89.10
UD-14	16.2	0.5637	0.0778	0.3715	43.2	12.2	21.64	116.29
UD-21	20.5	0.6217	0.1516	0.4938	5.9	25.4	40.86	11.95
UD-22	20.5	0.6217	0.1516	0.4938	5.9	26.1	41.98	11.95
UD-23	20.5	0.6217	0.1516	0.4938	26.2	24.0	38.60	53.06
UD-24	20.5	0.6217	0.1516	0.4938	42.2	20.4	32.81	85.46
UD-25	20.5	0.6217	0.1416	0.4938	53.1	15.0	24.13	107.53
UD-31	24.8	0.6797	0.2617	0.6205	5.9	27.0	39.72	9.51
UD-32	24.8	0.6797	0.2617	0.6205	26.2	23.6	34.72	42.22
UD-33	24.8	0.6797	0.2617	0.6205	48.2	22.8	33.54	77.68
UD-34	24.8	0.6797	0.2617	0.6205	59.1	18.0	26.48	95.25
UD-41	29.1	0.7377	0.4152	0.7503	5.9	27.4	37.14	7.86
UD-42	29.1	0.7377	0.4152	0.7503	33.1	23.4	31.72	44.12
UD-43	29.1	0.7377	0.4152	0.7503	69.1	20.0	27.25	92.10

a - From reference 32.

TABLE 4.4.3

DIMENSIONS AND SECTION PROPERTIES OF BIJLAARD'S ALUMINUM COMPRESSION SPECIMENS^a

Spec.	D (in.)	BC (in.)	TF (in.)	TW (in.)	w/TF	Area (in.)	K	σ_y (ksi)	E (ksi)	N	σ_1
J	1.875	1.406	0.128	0.125	10.50	0.922	0.741	83.0	10430	28	85.75
K	2.500	1.906	0.129	0.122	14.30	1.257	0.727	84.0	10430	30	86.38
L	3.000	2.313	0.124	0.126	18.14	1.494	0.760	82.0	10430	25	84.95

a - From reference 27.

TABLE 4.4.4
SECTION PROPERTIES AND TEST RESULTS OF BIJLAARD'S
ALUMINUM COMPRESSION SPECIMENS^a

Specimen	L (in)	L/r	P_u/A (ksi)
J-1	17.62	25.0	62.50
J-2	21.16	30.0	61.00
J-3	24.65	35.0	59.20
J-4	28.84	40.8	56.30
J-5	29.84	42.5	54.85
J-6	29.84	42.5	55.20
J-7	35.20	50.0	41.75
K-1	24.15	25.0	49.90
K-2	29.03	30.0	47.60
K-3	33.84	35.0	42.60
K-4	38.70	40.0	39.20
K-5	43.53	45.0	36.15
K-6	48.37	50.0	33.80
L-1	29.23	25.0	41.30
L-2	41.10	35.0	32.40
L-3	46.86	40.0	28.80
L-4	52.27	44.9	26.20
L-5	64.48	55.0	23.80
L-6	72.66	62.0	20.65
L-7	72.66	62.0	21.60
L-8	80.97	69.1	20.35
L-9	93.80	80.0	15.60

a - from reference 27.

TABLE 4.4.5

SECTION PROPERTIES AND TEST RESULTS OF STUB COLUMN SPECIMENS

Specimen	w/t	A (in. ²)	σ_y (ksi)	P_y (kips)	P_u (kips)	Q Test $=P_u/P_y$	Q AISI	P_u/A (ksi)	(L/r)
SC-I1	57.63	0.9485	31.59	29.96	23.35	0.779	0.130	24.61	7.80
SC-I2	57.71	0.9463	30.73	29.08	21.95	0.755	0.130	23.19	7.81
SC-III1	51.52	0.8493	25.68	21.81	19.38	0.889	0.196	22.82	7.81
SC-II2	50.08	0.8711	30.26	26.36	21.78	0.826	0.176	25.00	7.84
SC-III1	42.93	0.7892	31.29	24.69	19.78	0.801	0.232	25.06	7.86
SC-III2	42.95	0.7896	31.11	24.56	21.70	0.884	0.233	27.48	7.86
SC-IV1	35.25	0.6185	31.29	19.35	17.58	0.909	0.344	28.42	7.94
SC-IV2	34.98	0.6136	30.50	18.71	16.80	0.898	0.358	27.38	8.14
SC-V1	29.74	0.5754	33.18	19.09	17.70	0.927	0.455	30.76	8.07
SC-V2	29.76	0.5766	31.05	17.90	16.63	0.929	0.486	28.84	8.04

TABLE 4.4.6

SECTION PROPERTIES AND TEST RESULTS OF SLENDER COMPRESSION SPECIMENS

Specimen	w/t	Q	P_y (ksi)	P_{cr} (kips)	A (in. ²)	P/P_y	$(L/r)_y$	(L/r)	$\frac{L/r}{(L/r)_y}$
LC-II1	57.61	0.767	31.59	14.96	0.9425	0.5025	96.00	49.45	0.515
LC-II2	57.31	0.767	31.59	14.07	0.9495	0.4691	96.00	72.07	0.751
LC-I3	57.93	0.767	30.73	11.00	0.9408	0.3805	97.34	95.84	0.985
LC-III1	50.81	0.858	30.26	16.17	0.8745	0.6111	98.09	52.71	0.537
LC-II2	50.36	0.858	30.26	13.16	0.8670	0.5016	98.09	83.13	0.848
LC-II2	50.31	0.858	25.68	9.95	0.8711	0.4448	106.48	113.07	1.062
LC-III1	41.86	0.843	31.29	16.49	0.8031	0.6562	96.46	58.10	0.602
LC-III2	42.98	0.843	31.11	11.66	0.7861	0.4768	96.74	98.48	1.018
LC-III3	42.57	0.843	25.68	8.83	0.7928	0.4337	106.48	138.33	1.299
LC-IV1	35.77	0.904	31.05	12.19	0.6057	0.6482	96.83	68.66	0.709
LC-IV2	34.74	0.904	30.50	11.29	0.6123	0.6045	97.70	97.37	0.997
LC-IV3	34.41	0.904	31.29	8.96	0.6277	0.4562	96.46	125.00	1.296
LC-V1	29.43	0.928	33.18	14.63	0.5757	0.7659	93.67	73.53	0.785
LC-V2	29.53	0.928	30.63	12.65	0.5786	0.7138	97.50	91.70	0.941
LC-V3	29.35	0.928	33.18	10.75	0.5782	0.5603	93.67	122.36	1.306

TABLE 5.2.1
MATERIAL PROPERTIES OF HOT ROLLED STEEL SHEETS
FOR BEAM SPECIMENS

Sheet No.	σ_y (ksi)	σ_u (ksi)
I	51.0	65.5
II	53.8	69.5
III	51.3	65.8
IV	50.2	64.5
V	35.9	50.0
VI	33.8	48.5

TABLE 5.2.2
DIMENSIONS OF BEAM SPECIMENS

Specimen	Sheet No.	BC (in.)	BT (in)	D (in)	t (in)	RC (in)	w/t	LS (in)	L (in)
B-1	I	4.360	7.744	4.047	0.0708	0.00	60.5	19.0	73.0
B-2	II	3.847	7.683	4.023	0.0711	0.00	53.1	19.0	70.0
B-3	II	3.410	8.140	4.198	0.0750	0.00	44.5	19.0	70.0
B-4	I	2.840	6.139	3.189	0.0750	0.00	36.9	19.0	58.0
B-5	III	2.278	6.094	3.272	0.0740	0.00	29.8	19.0	
B-6	III	1.868	6.069	3.194	0.0756	0.00	23.7	19.0	58.0
B-7	III	1.529	4.125	2.180	0.0748	0.00	19.4	16.0	52.0
B-8	IV	1.310	4.151	2.188	0.0735	0.00	16.8	16.0	48.0
B-9	IV	1.074	4.163	2.182	0.0753	0.00	13.3	16.0	48.0
B-10	IV	0.870	4.157	2.177	0.0755	0.00	10.5	16.0	48.0
B-11	IV	0.654	4.150	2.160	0.0755	0.00	7.7	16.0	48.0
B-12	V	2.211	5.971	2.996	0.0994	0.00	21.2	19.0	56.0
B-13	V	2.044	5.891	3.006	0.0997	0.00	19.5	19.0	56.0
B-14	V	1.761	4.963	2.498	0.0998	0.00	16.6	15.0	45.0
B-15	VI	1.510	4.969	2.500	0.1002	0.00	14.1	15.0	45.0
B-16	VI	1.364	5.102	1.995	0.0993	0.00	12.7	16.0	45.0
B-17	VI	1.129	3.999	1.990	0.0997	0.00	10.3	16.0	45.0
B-18	VI	0.887	3.969	2.000	0.1001	0.00	7.9	16.0	45.0
UP-9 ^a	--	1.680	1.671	3.978	0.0600	0.062	26.0	21.0	60.0
UP-10 ^a	--	1.220	1.241	4.013	0.0350	0.062	32.1	20.0	60.0
UP-11 ^a	--	1.417	1.446	4.005	0.0347	0.062	38.0	20.0	60.0
UP-12 ^a	--	1.616	1.648	4.001	0.0355	0.062	42.8	20.0	60.0

a - Reck's Specimens

TABLE 5.4.1
THEORETICAL AND EXPERIMENTAL MOMENTS
OF BEAM SPECIMENS

Specimen	w/t	M_y (in-K)	M_p (in-K)	M_u (in-K)	K^a	M_u/M_y	σ_y (ksi)	w/t $\sqrt{\sigma_y/K}$
B-1	60.5	138.7	145.0	81.7	0.961	0.589	51.0	441
B-2	53.1	132.3	144.5	80.9	0.934	0.611	53.8	403
B-3	44.5	134.7	156.1	81.2	0.831	0.603	53.8	358
B-4	36.9	77.6	87.6	54.3	0.791	0.699	51.0	296
B-5	29.8	67.7	81.7	52.3	0.798	0.773	51.3	238
B-6	23.7	58.4	74.2	52.4	0.584	0.897	51.3	222
B-7	19.4	29.5	36.1	25.8	0.619	0.875	51.3	177
B-8	16.8	25.7	32.8	26.4	0.604	1.027	50.2	153
B-9	13.3	23.0	30.8	27.0	0.586	1.174	50.2	123
B-10 ^a	10.3	20.0	28.1	25.7	0.568	1.285	50.2	97
B-11 ^a	7.7	17.0	25.1	24.9	0.550	1.465	50.2	74
B-12	21.2	54.3	66.2	50.6	0.620	0.932	35.9	161
B-13	19.5	51.6	64.1	51.2	0.616	0.992	35.9	149
B-14	16.6	35.9	44.6	34.7	0.618	0.967	35.9	127
B-15	14.1	30.6	39.5	34.4	0.604	1.124	33.8	105
B-16	12.7	21.0	27.7	25.8	0.618	1.229	33.8	94
B-17	10.3	17.9	23.8	24.9	0.600	1.391	33.8	77
B-18	7.9	15.5	21.6	23.5	0.580	1.156	33.8	60
UP-9 ^c	26.0	44.0	51.1	36.9	0.747	0.839	42.0	195
UP-10 ^c	32.1	18.2	21.8	14.3	0.666	0.786	36.0	236
UP-11 ^c	38.0	20.0	23.5	15.5	0.804	0.775	36.0	254

a - Experimental K in the elastic range and theoretical K_p in the plastic range.

b - Specimen failed due to lateral buckling.

c - Reck's Specimens

TABLE 5.4.2

ELASTIC LOCAL BUCKLING AND POSTBUCKLING TEST RESULTS OF BEAM SPECIMENS

Specimen	Experimental					Theoretical				Experimental				Theoretical			
	w/t	σ_{cr} (ksi)	K	K_e	K_p	σ_y (ksi)	$\frac{\sigma_y}{\sigma_{cr}}$	$\frac{\sigma_{av}}{\sigma_{cr}}$	$\frac{b_e}{w}$	Eqn. 3.4.1		Eqn. 3.4.5		Eqn. 3.4.1		Eqn. 3.4.5	
										$\frac{b_e}{w}$	%error	$\frac{b_e}{w}$	%error	$\frac{b_e}{w}$	%error	$\frac{b_e}{w}$	%error
B-1	60.5	6.99	0.961	0.948	0.660	51.0	7.30	3.06	0.419	.480	-14.6	.392	6.4				
B-2	53.1	8.82	0.920	0.926	0.646	53.8	6.10	2.84	0.466	.491	- 5.4	.424	13.6				
B-3	44.5	11.21	0.831	0.901	0.632	53.8	4.80	2.40	0.500	.504	- 0.8	.469	6.9				
B-4	36.9	15.52	0.791	0.916	0.640	51.0	3.29	1.69	0.514	.549	- 6.8	.549	0.0				
B-5	29.8	23.54	0.798	0.874	0.624	51.3	2.18	1.21	0.555	.624	-12.4	.644	-3.5				
B-6	23.7	27.70	0.584	0.844	0.604	51.3	1.85	1.10	0.595	.658	-10.6	.684	-3.9				
UP-9 ^a	26.0	29.53	0.747	0.930	0.650	42.0	1.42	1.05	0.739	.728	1.4	.749	-2.9				
UP-10 ^a	32.1	17.26	0.666	0.875	0.620	36.0	2.09	1.30	0.622	.628	1.0	.654	-4.1				
UP-11 ^a	38.0	14.81	0.804	0.900	0.632	36.0	2.43	1.48	0.609	.603	1.0	.618	-2.5				
UP-12 ^a	42.8	8.11	0.560	0.925	0.645	-	-	-	-	-	-	-	-				

a - Reck's Specimens

TABLE 5.4.3
 ULTIMATE COMPRESSIVE STRAIN OF BEAM SPECIMEN

Specimen	w/t	K ^a	$e_{cu} \times 1000$	$\frac{e_{cu} \times 1000}{K}$	e_{cu}/e_y
B-1	60.5	0.961	1.889	1.966	1.09
B-2	53.1	0.934	1.828	1.957	1.00
B-3	44.5	0.831	1.771	2.131	0.97
B-4	36.9	0.791	2.108	2.665	1.22
B-5	29.8	0.798	2.256	2.827	1.30
B-6	23.7	0.584	3.127	5.354	1.80
B-7	19.4	0.619	3.160	5.105	1.82
B-8	16.8	0.604	3.820	6.325	2.24
B-9	13.3	0.586	4.500	7.679	2.64
B-10 ^b	10.3	0.568	3.636	--	--
B-11 ^b	7.7	0.550	3.280	--	--
B-12	21.2	0.620	2.780	4.484	2.28
B-13	19.5	0.616	2.826	4.588	2.32
B-14	16.6	0.618	3.776	6.110	3.10
B-15	14.1	0.604	3.840	6.358	3.35
B-16	12.7	0.618	4.590	7.427	4.01
B-17	10.3	0.600	5.845	9.742	5.10
B-18	7.9	0.580	8.600	14.828	7.51
UP-9 ^c	26.0	0.747	1.424	1.906	1.04
UP-10 ^c	32.1	0.666	1.220	1.832	0.87
UP-11 ^c	38.0	0.804	1.220	1.517	0.91

a - Experimental K in the elastic range and theoretical K_p in the plastic range.

b - Specimen failed due to lateral buckling

c - Reck's Specimens

TABLE 6.2.1

LOCAL BUCKLING COEFFICIENT OF UNSTIFFENED ELEMENTS IN SHORT COMPRESSION MEMBERS

Spec.	(w/t)	σ_y (ksi)	B_b/B_r	ϵ	K_e	K_p	K_y	K_y/K_e	$K_{expt.}$	$\frac{K_{expt.} - K_p}{K_e - K_p}$	K_{theory}	% diff.
SC-I 1	57.6	31.6	0.713	5.41	1.028	0.702	3.94	3.83	1.040	1.037	0.932	10.3
SC-I 2	57.7	30.7	0.721	5.40	1.028	0.702	3.83	3.73	0.964	0.804	0.925	4.1
SC-II 1	51.5	25.7	0.628	4.69	0.992	0.682	2.56	2.58	0.949	0.861	0.804	15.3
SC-II 2	50.1	30.3	0.623	4.64	0.990	0.680	2.85	2.88	0.912	0.748	0.825	9.5
SC-III 1	42.9	31.3	0.532	3.86	0.962	0.664	2.17	2.25	0.940	0.926	0.757	19.5
SC-III 2	43.0	31.1	0.532	3.86	0.962	0.664	2.16	2.24	0.955	0.977	0.756	20.8
SC-IV 1	35.3	31.3	0.584	4.31	0.982	0.674	1.46	1.49	0.982	1.000	0.711	27.6
SC-IV 2	35.0	30.5	0.569	4.18	0.978	0.670	1.40	1.43	0.986	1.026	0.703	28.7
SC-V 1	29.7	32.2	0.497	3.55	0.950	0.660	1.10	1.16	0.876	0.745	0.671	23.3
SC-V 2	29.8	31.1	0.500	3.58	0.952	0.662	1.03	1.08	0.848	0.641	0.668	21.2
UD-1*	16.2	41.9	0.333	2.03	0.858	0.610	0.52	0.48	-	-	0.610	-
UD-2*	20.6	41.9	0.417	2.83	0.914	0.640	0.58	0.73	-	-	0.640	-
UD-3*	24.9	41.9	0.500	3.58	0.952	0.662	0.97	1.02	0.825	0.562	0.663	19.6
UD-4*	29.2	41.9	0.583	4.30	0.982	0.674	1.34	1.36	0.858	0.597	0.702	18.2

* DeWolf's specimens

TABLE 6.2.2
LOCAL BUCKLING COEFFICIENT OF UNSTIFFENED ELEMENTS IN FLEXURAL MEMBERS

Spec.	(w/t)	σ_y (ksi)	B_b/B_r	ϵ	K_e	K_p	K_y	K_y/K_e	$K_{expt.}$	$\frac{K_{expt.} - K_p}{K_e - K_p}$	K_{theory}	% Diff.
B1	60.5	51.0	1.077	3.06	0.924	0.640	7.00	7.58	0.961	1.130	0.924	3.9
B2	53.1	53.8	0.956	2.70	0.906	0.638	5.69	6.28	0.920	1.052	0.906	1.6
B3	44.5	53.8	0.812	2.24	0.874	0.620	3.99	4.57	0.831	0.831	0.847	-1.9
B4	36.9	51.0	0.891	2.50	0.890	0.628	2.61	2.93	0.791	0.622	0.754	4.7
B5	29.8	51.3	0.696	1.86	0.842	0.604	1.71	2.03	0.798	0.815	0.665	16.6
B6	23.7	51.3	0.585	1.49	0.810	0.586	1.08	1.33	0.584	0.000	0.605	-3.5
UP-9 [†]	26.0	42.0	0.422	4.69	0.990	0.682	1.07	1.08	0.747	0.211	0.651	12.8
UP-10 [†]	32.1	36.0	0.304	3.13	0.930	0.644	1.40	1.50	0.666	0.077	0.639	4.1
UP-11 [†]	38.0	36.0	0.354	3.80	0.962	0.662	1.95	2.03	0.804	0.473	0.698	13.2
UP-12 [†]	42.8	36.0	0.404	4.46	0.984	0.680	2.47	2.51	-	-	0.560	-
B-1*	60.5	51.0	1.077	3.20	0.930	0.648	7.0	7.53	0.961	1.102	0.930	3.2
		($K_r=33.0$)										
UP-11*	38.0	36.0	0.354	4.10	0.970	0.670	1.95	2.01	0.804	0.446	0.706	12.2
		($K_r=23.9$)										

* Rotational restraint by the web calculated using the actual stress distribution in the web.

† Peter Reck's specimens.

TABLE 6.2.3
STRAIN CAPACITY OF UNSTIFFENED ELEMENTS IN FLEXURAL
SPECIMENS

Spec.	$(w/t)^K$	K_{theory}	σ_y	$(w/t)_{lim}$	$(\epsilon_{cu})_{expt}$	$(\epsilon_{cu})_{theory}$	% Diff
B1	60.5	0.924	51.0	17.4	1889	1729	8.5
B2	53.1	0.906	53.8	16.8	1828	1824	0.2
B3	44.5	0.847	53.8	16.3	1771	1824	-3.0
B4	36.9	0.754	51.0	16.0	2108	1729	18.0
B5	29.8	0.665	51.3	15.3	2256	1739	22.9
B6	23.7	0.605	51.3	14.9	3127	1739	44.4
B7	19.4	0.604	51.3	14.9	3160	1739	45.0
B8	16.8	0.588	50.2	15.0	3820	1702	55.5
B9	13.3	0.565	50.2	14.8	4500	2903	35.5
B10*	10.3	0.542	50.2	14.7	3636	4615	-
B11*	7.7	0.502	50.2	14.5	3280	7623	-
B12	21.2	0.590	35.9	17.7	2780	1218	56.2
B13	19.5	0.582	35.9	17.6	2826	1218	56.9
B14	16.6	0.604	35.9	17.8	3776	1970	47.8
B15	14.1	0.588	33.8	18.2	3840	2685	30.1
B16	12.7	0.602	33.8	18.3	4590	3354	26.9
B17	10.3	0.584	33.8	18.2	5845	4952	15.3
B18	7.9	0.555	33.8	18.0	8600	8117	5.6
UP-1	26.0	0.651	42.0	16.8	1424	1424	0.0
UP-2	32.1	0.639	36.0	18.0	1220	1220	0.0
UP-3	38.0	0.698	36.0	18.5	1220	1220	0.0
UP-4	42.8	0.560	36.0	17.5	1220	1220	0.0

* - Specimen failed due to lateral buckling.

Peter Reck's specimens.

TABLE 6.3.1

EFFECTIVE WIDTHS OF UNSTIFFENED ELEMENTS IN SHORT COMPRESSION MEMBERS

Specimen	w/t	σ_y (ksi)	K_{theory}	σ_{cr} (ksi)	$\frac{\sigma_y}{\sigma_{cr}}$	$\left(\frac{b_e}{w}\right)_{expt}$	Eqn. 3.4.1		Eqn. 3.4.5	
							b_e/w	%diff.	b_e/w	%diff.
SC-I 1	57.6	31.6	0.932	7.5	4.222	0.556	0.531	4.5	0.495	10.9
SC-I 2	57.7	30.7	0.925	7.4	4.150	0.565	0.532	5.8	0.499	11.7
SC-II 1	51.5	25.7	0.804	8.1	3.180	0.613	0.556	9.3	0.556	9.3
SC-II 2	50.1	30.3	0.825	8.8	3.450	0.574	0.546	4.9	0.538	6.3
SC-III 1	42.9	31.3	0.757	11.0	2.857	0.610	0.570	6.6	0.580	4.9
SC-III 2	43.0	31.1	0.756	10.9	2.847	0.622	0.570	8.3	0.581	6.6
SC-IV 1	35.3	31.3	0.711	15.3	2.051	0.743	0.633	14.8	0.658	11.4
SC-IV 2	35.0	30.5	0.703	15.3	1.991	0.725	0.640	11.8	0.666	8.2
SC-V 1	29.7	33.2	0.671	20.2	1.640	0.787	0.688	12.6	0.713	9.4
SC-V 2	29.8	31.1	0.668	20.1	1.544	0.721	0.704	2.3	0.728	-1.0

cont. TABLE 6.3.1

UD-1*	16.2	41.9	0.610	62.0	0.676	1.100	1.018	7.5	0.924	16.0
UD-2*	20.6	41.9	0.640	40.4	1.037	0.973	0.835	14.2	0.827	15.0
UD-3*	24.9	41.9	0.663	28.6	1.465	0.890	0.720	19.1	0.742	16.7
UD-4*	29.2	41.9	0.702	22.0	1.905	0.782	0.650	16.9	0.676	13.5

* DeWolf's specimens

TABLE 6.3.2
EFFECTIVE WIDTHS OF UNSTIFFENED ELEMENTS IN FLEXURAL MEMBERS

Specimen	w/t	σ_y (ksi)	K_{theory}	$(w/t)_{lim}$	$\frac{\sigma_y}{\sigma_{cr}}$	$(b_e/w)_{expt.}$	Eqn. 3.4.1		Eqn. 3.4.5	
							b_e/w	% diff.	b_e/w	% diff.
B1	60.5	51.0	0.924	6.7	7.577	0.419	0.475	-13.4	0.386	8.0
B2	53.1	53.8	0.906	8.6	6.280	0.466	0.487	-4.6	0.418	10.2
B3	44.5	53.8	0.847	11.4	4.718	0.500	0.508	-1.6	0.473	5.4
B4	36.9	51.0	0.754	14.8	3.454	0.514	0.539	-4.9	0.538	-4.6
B5	29.8	51.3	0.665	20.0	2.569	0.555	0.584	5.2		
UP-9*	26.0	42.0	0.651	25.7	1.636	0.739	0.689	6.8	0.714	3.4
UP-10*	32.1	36.0	0.639	16.5	2.177	0.622	0.618	0.7	0.644	-3.5
UP-11*	38.0	36.0	0.698	12.9	2.793	0.609	0.570	6.4	0.585	3.9
UP-12*	42.8	36.0	0.560	8.2	4.417	0.500	0.491	1.8	0.486	2.8

* Peter Reck's specimens

TABLE 6.3.3
EFFECTIVE WIDTHS OF UNSTIFFENED ELEMENTS IN SHORT COMPRESSION MEMBERS

Specimen	w/t	σ_y (ksi)	K_{theory}	σ_{cr} (ksi)	$\frac{\sigma_y}{\sigma_{cr}}$	$(\frac{b_e}{w})_{expt.}$	$\frac{Eqs. 3.4.1 \ \& \ 6.3.1}{b_e/w}$	% diff.
SC-I 1	57.6	31.6	0.932	7.5	4.222	0.556	0.472	15.1
SC-I 2	57.7	30.7	0.925	7.4	4.150	0.565	0.475	15.9
SC-II 1	51.5	25.7	0.804	8.1	3.180	0.613	0.515	15.9
SC-II 2	50.1	30.3	0.825	8.8	3.450	0.574	0.502	12.5
SC-III 1	42.9	31.3	0.757	11.0	2.857	0.610	0.534	12.3
SC-III 2	43.0	31.1	0.756	10.9	2.847	0.622	0.535	14.0
SC-IV 1	35.3	31.3	0.711	15.3	2.051	0.743	0.603	18.8
SC-IV 2	35.0	30.5	0.703	15.3	1.991	0.725	0.611	15.7
SC-V 1	29.7	33.2	0.671	20.2	1.640	0.787	0.660	16.1
SC-V 2	29.8	31.1	0.668	20.1	1.544	0.721	0.677	6.1
UD-1*	16.2	41.9	0.610	62.0	0.676	1.100	0.965	12.3
UD-2*	20.6	41.9	0.640	40.4	1.037	0.973	0.802	17.6
UD-3*	24.9	41.9	0.663	28.6	1.465	0.890	0.692	22.2
UD-4*	29.2	41.9	0.702	22.0	1.905	0.782	0.628	19.7

* DeWolf's specimens

TABLE 6.3.4
EFFECTIVE WIDTHS OF UNSTIFFENED ELEMENTS IN FLEXURAL MEMBERS

Specimen	w/t	σ_y (ksi)	K_{theory}	$(w/t)_{lim.}$	$\frac{\sigma_y}{\sigma_{cr}}$	$(\frac{b_e}{w})_{expt.}$	$\frac{Eqs. 3.4.1 \& 6.3.1}{b_e/w}$	% diff.
B1	60.5	51.0	0.924	6.7	7.577	0.419	0.411	1.9
B2	53.1	53.8	0.906	8.6	6.280	0.466	0.427	8.4
B3	44.5	53.8	0.847	11.4	4.718	0.500	0.458	8.4
B4	36.9	51.0	0.754	14.8	3.454	0.514	0.502	2.3
B5	29.8	51.3	0.665	20.0	2.569	0.555	0.555	0.0
B6	23.7	51.3	0.605	28.7	1.786	0.595	0.637	-7.1
UP-9*	26.0	42.0	0.651	25.7	1.636	0.739	0.661	10.6
UP-10*	32.1	36.0	0.639	16.5	2.177	0.622	0.598	5.1
UP-11*	38.0	36.0	0.698	12.9	2.793	0.609	0.539	11.5
UP-12*	42.8	36.0	0.560	8.2	4.417	0.500	0.466	6.8

* Peter Reck's specimens.

TABLE B.2.1 COMPARISON OF EFFECTIVE WIDTHS - STUB COLUMNS

Specimen	w/t	Experiment		WU eqn.		WS eqn.	
		$\frac{\sigma_{e \max}}{\sigma_{cr}}$	b_e/w	b_e/w	% error	b_e/w	% error
SC I1	57.6	3.78	0.556	0.518	6.8	0.456	18.0
SC I2	57.7	3.98	0.565	0.508	10.2	0.446	21.1
SC III1	51.5	2.69	0.613	0.594	3.1	0.528	13.9
SC II2	50.1	3.12	0.574	0.560	2.4	0.496	13.6
SC III1	42.9	2.28	0.61	0.633	-3.7	0.566	7.2
SC III2	43.0	2.25	0.622	0.636	-2.3	0.569	8.5
SC IV1	35.3	1.48	0.743	0.739	0.5	0.673	9.4
SC IV2	35.0	1.42	0.725	0.749	-3.4	0.684	5.7
SC V1	29.7	1.27	0.787	0.777	1.2	0.714	9.3
SC V2	29.8	1.22	0.721	0.787	-9.2	0.725	0.5
UD-1*	16.2	0.58	1.100	0.952	13.4	0.934	15.1
UD-2*	20.6	0.84	0.973	0.877	9.9	0.829	14.8
UD-3*	24.9	1.18	0.890	0.796	10.6	0.734	17.5
UD-4*	29.2	1.56	0.782	0.726	7.2	0.660	15.6

* - DeWolf test results.³²

TABLE B.2.2 COMPARISON OF EFFECTIVE WIDTHS - BEAMS

Specimen	w/t	Experiment		WU eqn.		WS eqn.	
		$\frac{\sigma_{e \max}}{\sigma_{cr}}$	b_e/w	b_e/w	% error	b_e/w	% error
B1	60.5	7.30	0.419	0.392	6.4	0.340	18.9
B2	53.1	6.10	0.466	0.424	9.0	0.369	20.8
B3	44.5	4.80	0.500	0.469	6.2	0.411	17.8
B4	36.9	3.29	0.514	0.549	-6.8	0.484	5.8
B5	29.8	2.18	0.555	0.644	-16.0	0.576	-3.8
B6	23.7	1.85	0.595	0.684	-15.0	0.616	-3.5
UP-9*	26.0	1.42	0.739	0.749	1.4	0.684	7.4
UP-10*	32.1	2.09	0.622	0.654	-4.3	0.590	4.3
UP-11*	38.0	2.43	0.609	0.618	-1.5	0.551	9.5
UP-12*	42.8	4.44	0.500	0.485	3.0	0.425	15.0

* - Peter Reck test results.

TABLE B.3.1
 DIMENSIONS¹ AND SECTION PROPERTIES OF COLUMNS WITH STIFFENED ELEMENTS²

Specimen ^a	B (in)	D (in)	T (in)	Width- Thickness ^b Single Thickness Element	Width- Thickness Double Thickness Element	Area of Full Cross- Section (in ²)	Radius of Gyration About Weak Axis (in)	Experi- mental Buckling Coeffi- cient
S-1	2.0	3.5	0.058	57.2	16.7	0.86	0.799	4.85
S-2	2.0	5.0	0.058	83.0	16.7	1.03	0.836	5.37
S-3	2.0	7.0	0.058	117.4	16.7	1.26	0.869	6.11
S-4	2.0	9.0	0.058	151.8	16.7	1.49	0.890	6.90

1 - see fig. A2.3.19a

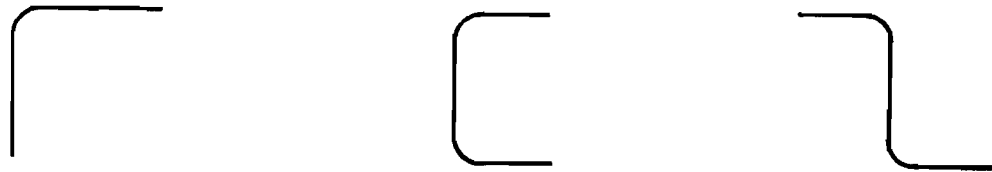
2 - DeWolf's Specimen³²

TABLE B.3.2

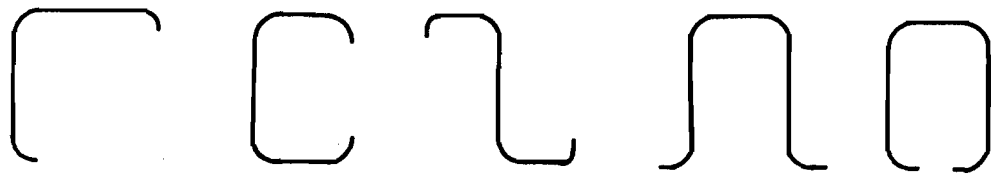
TEST RESULTS OF COLUMNS WITH STIFFENED ELEMENTS*

Specimen	Test Column Length (in)	Effective Length (in)	Slender-ness Ratio= $\frac{\text{Eff.Length}}{\text{Rad. of Gyration}}$	Ultimate Load (kips)	Ultimate Stress= $\frac{\text{Ult.Load}}{\text{Full Area}}$ (ksi)
S-1	10.5	6.8	8.5	34.6	40.5
	27.9	31.1	39.0	32.0	37.4
	52.0	55.2	69.1	29.6	34.6
	88.0	91.2	114.1	17.9	20.9
S-2	15.0	9.8	11.7	34.8	33.9
	52.0	55.2	66.0	28.0	27.2
	82.0	85.2	102.0	21.3	20.8
	99.9	103.1	123.5	17.7	17.2
S-3	18.1	11.8	13.6	37.0	29.3
	22.0	25.2	29.0	35.2	27.8
	92.0	95.2	109.8	19.6	15.5
	92.0	95.2	109.8	19.0	15.1
	92.0	95.2	109.8	18.2	14.4
S-4	18.9	12.3	13.8	36.7	24.6
	34.8	38.0	42.6	33.6	22.6
	55.0	58.2	65.5	29.3	19.6
	100.0	103.2	116.0	17.6	11.8
	119.9	123.1	138.2	13.75	9.2

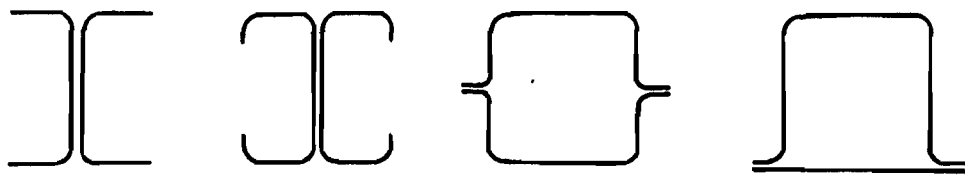
* - DeWolf's test results.³²



Open Sections

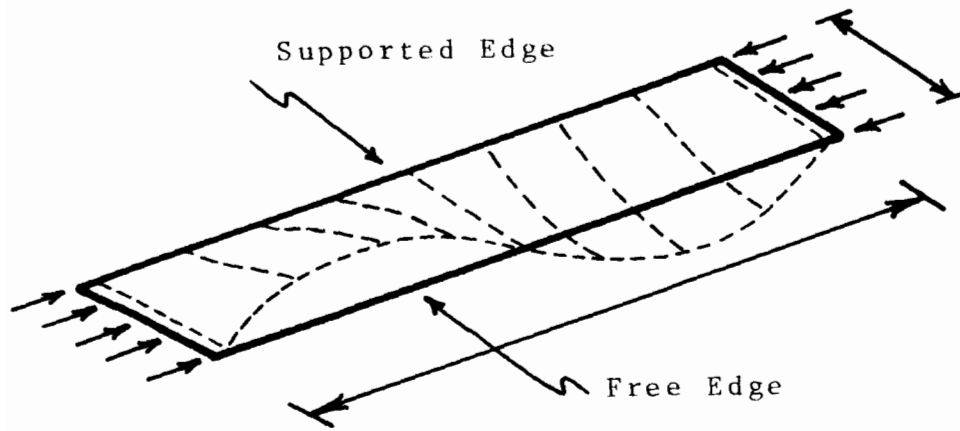


Lipped Sections



Built-up Sections

Fig. 1.1 COMMON COLD-FORMED STRUCTURAL SHAPES



Local Buckling of Unstiffened Element



Section Schematic

Fig. 1.2 UNSTIFFENED ELEMENT IDEALIZATION

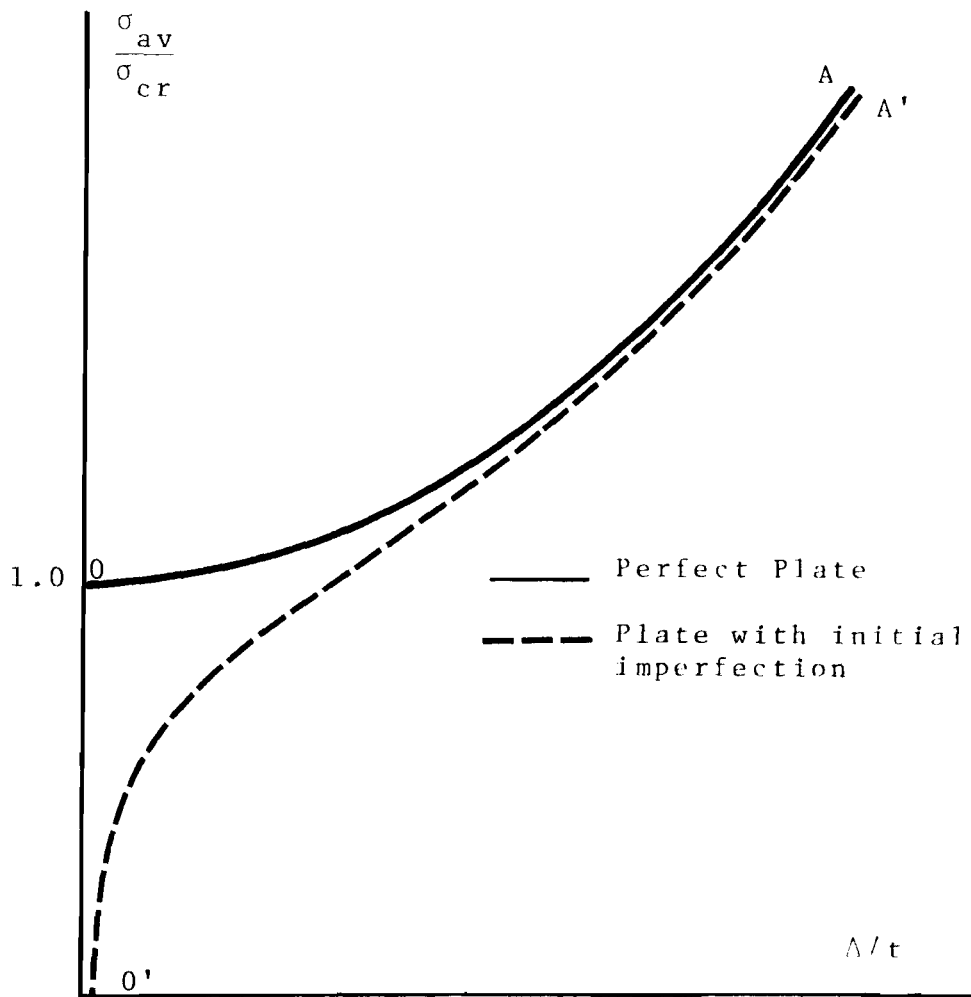


Fig. 1.3 OUT OF PLANE DEFORMATION DUE TO LOCAL BUCKLING OF UNSTIFFENED COMPRESSION ELEMENT

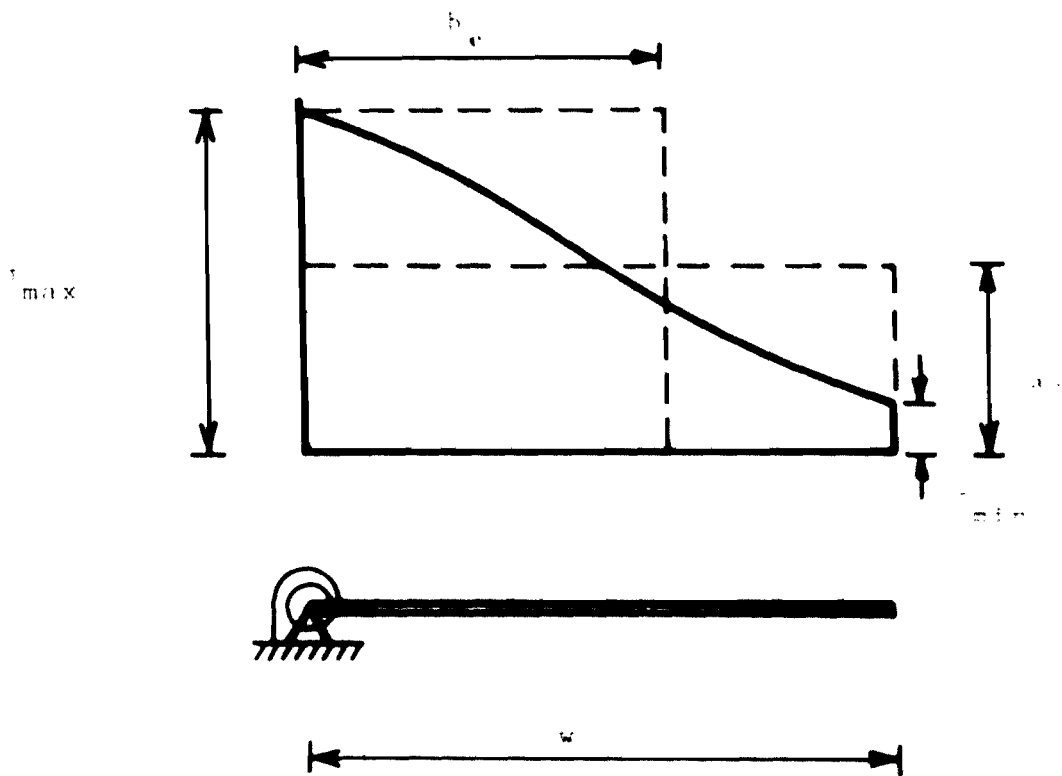


FIG. 1.4 STRESS DISTRIBUTION IN UNSTIFFENED ELEMENT IN THE POST-BUCKLING RANGE

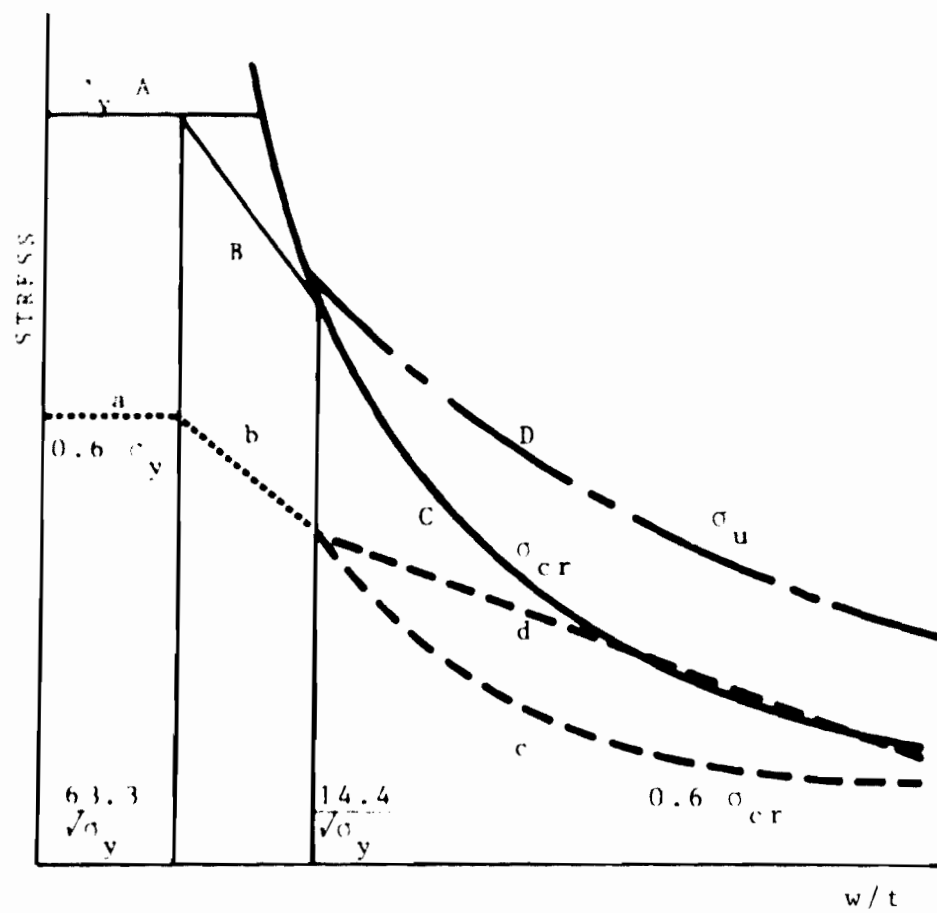


Fig. 1.5 AISI DESIGN CURVE - UNSTIFFENED ELEMENTS

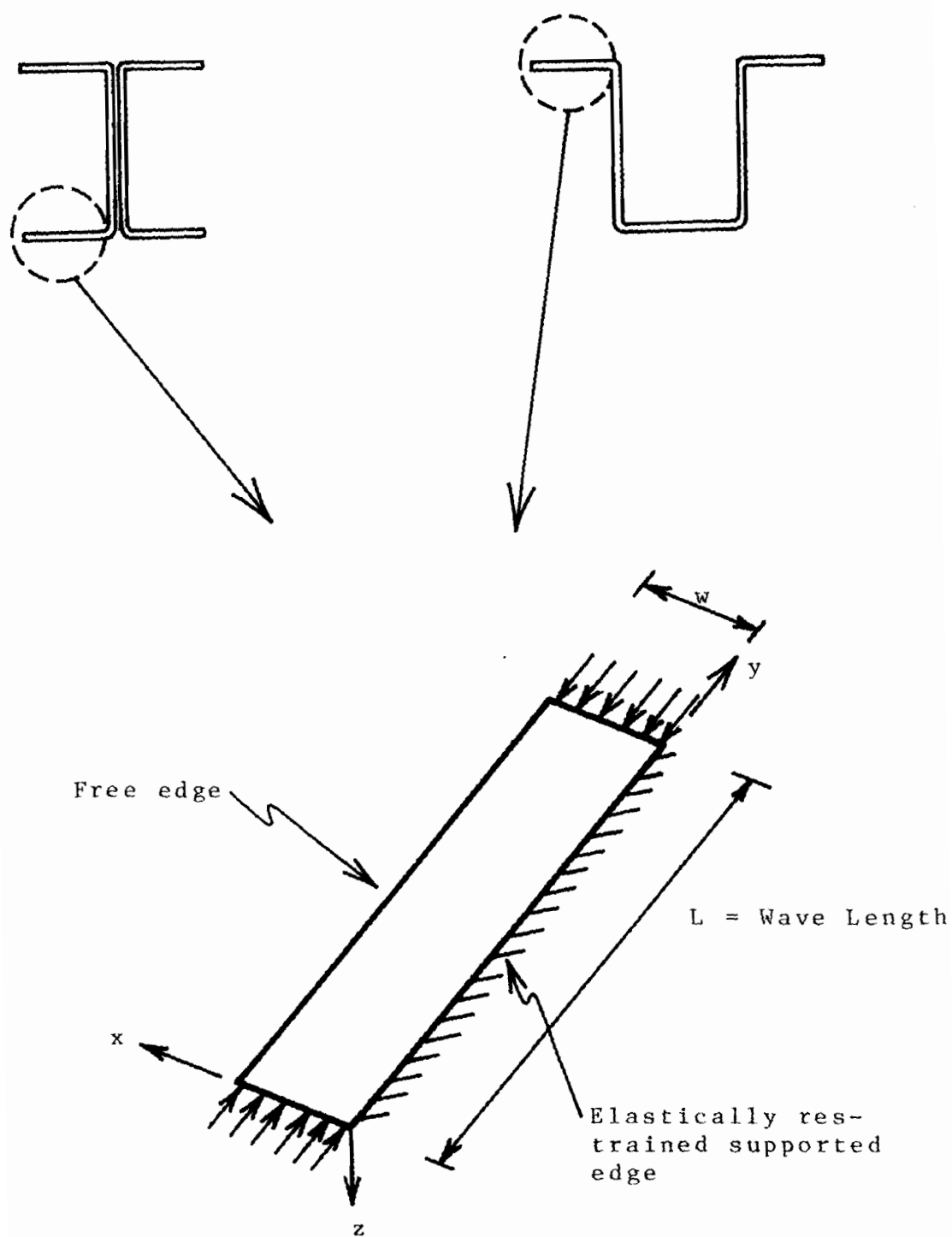


Fig. 2.2.1 UNSTIFFENED ELEMENT IDEALIZATION

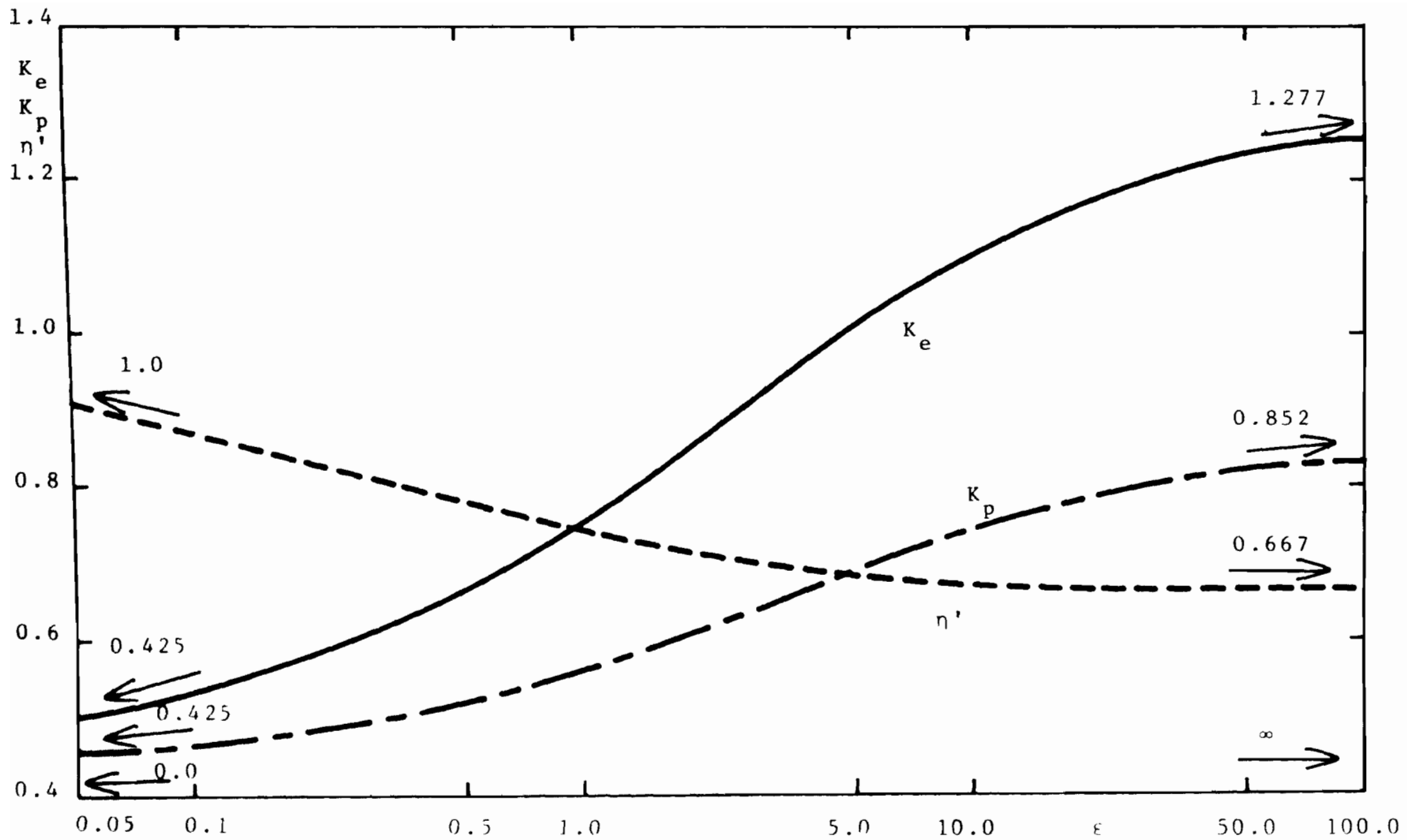


Fig. 2.2.2 ELASTIC AND INELASTIC LOCAL BUCKLING COEFFICIENTS

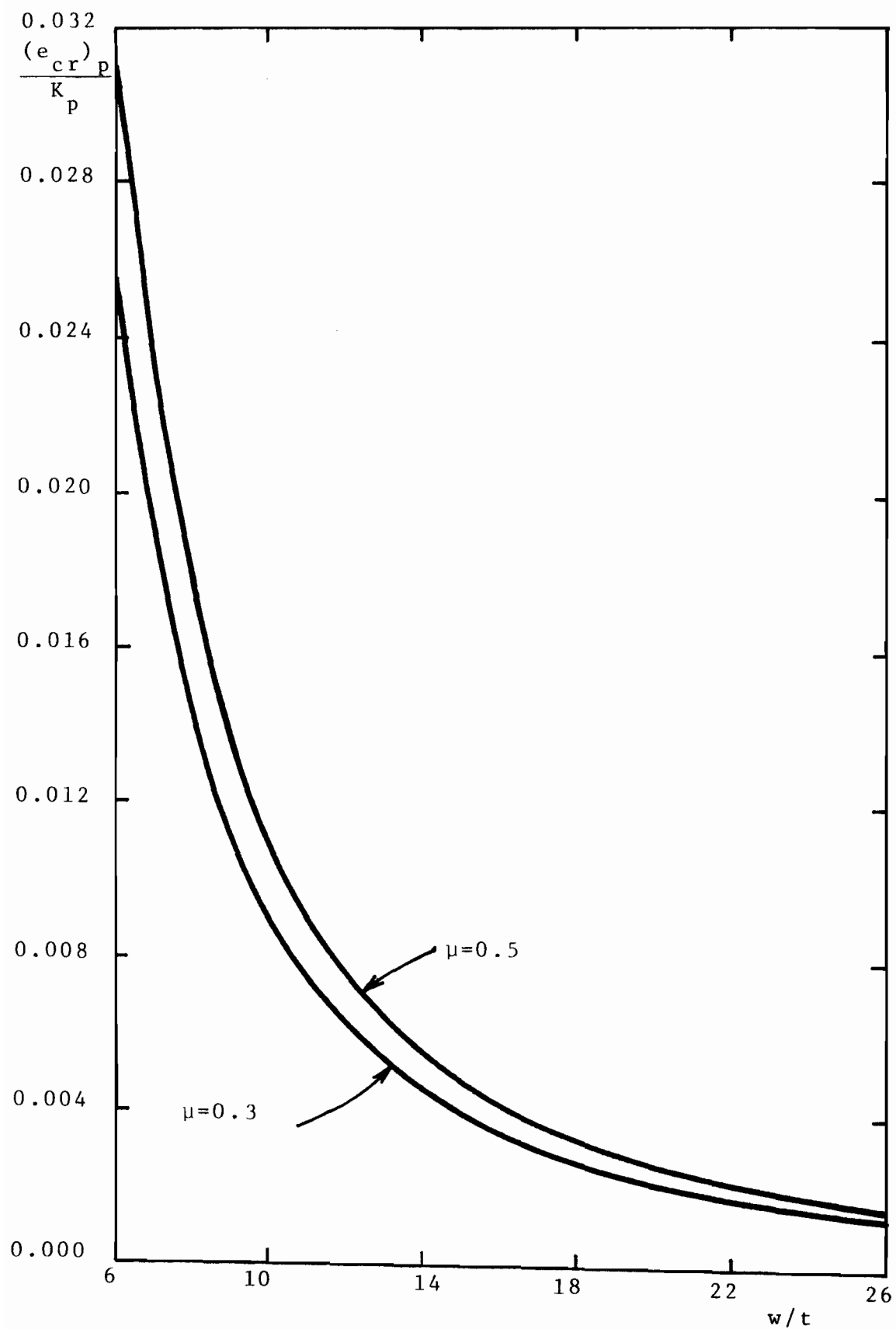


Fig. 2.2.3 PLASTIC BUCKLING STRAIN VS. w/t RATIO OF UNSTIFFENED ELEMENTS

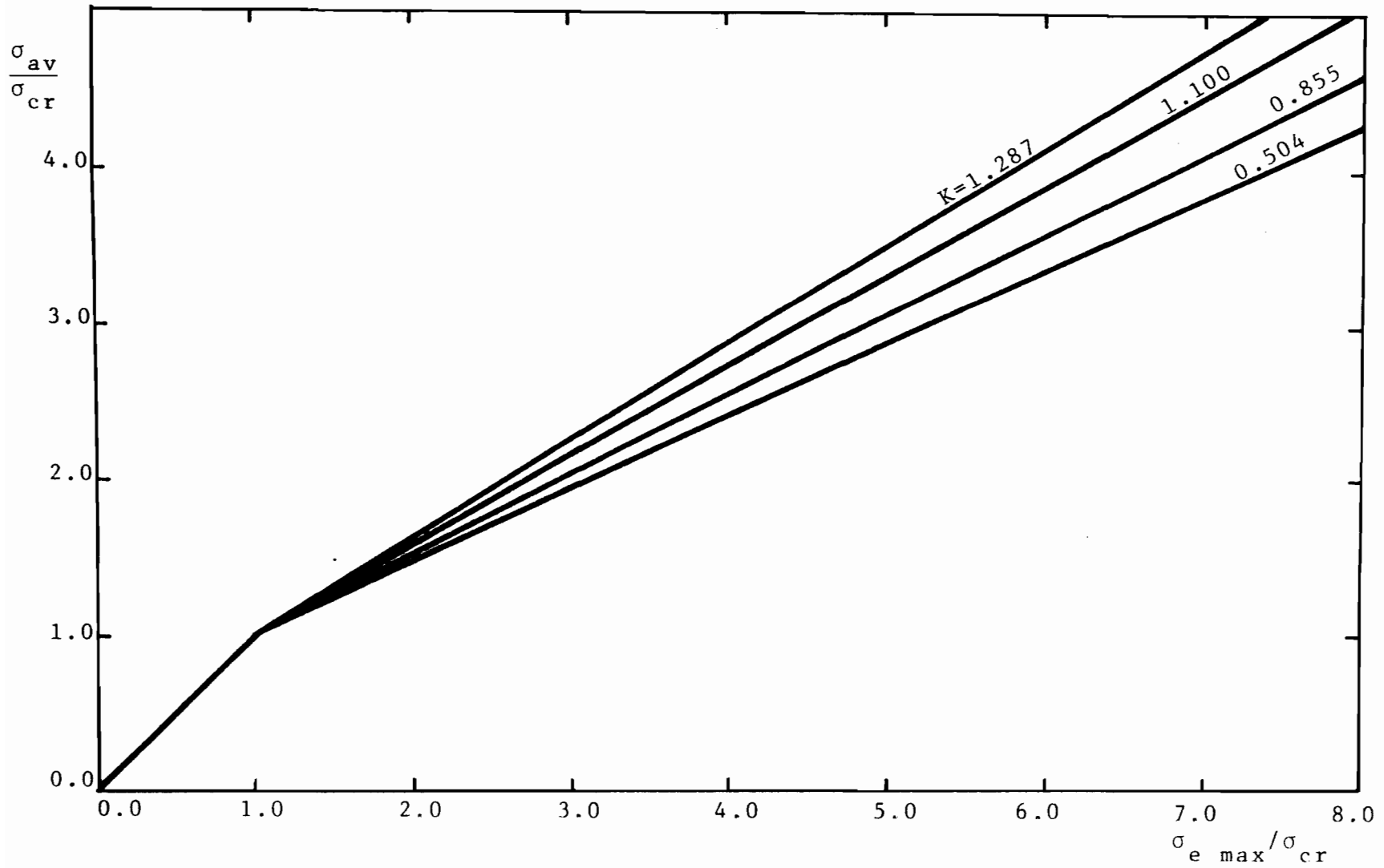


Fig. 2.2.4 AVERAGE STRESS VS. MAXIMUM SUPPORTED EDGE STRESS - PERFECTLY FLAT UNSTIFFENED ELEMENTS

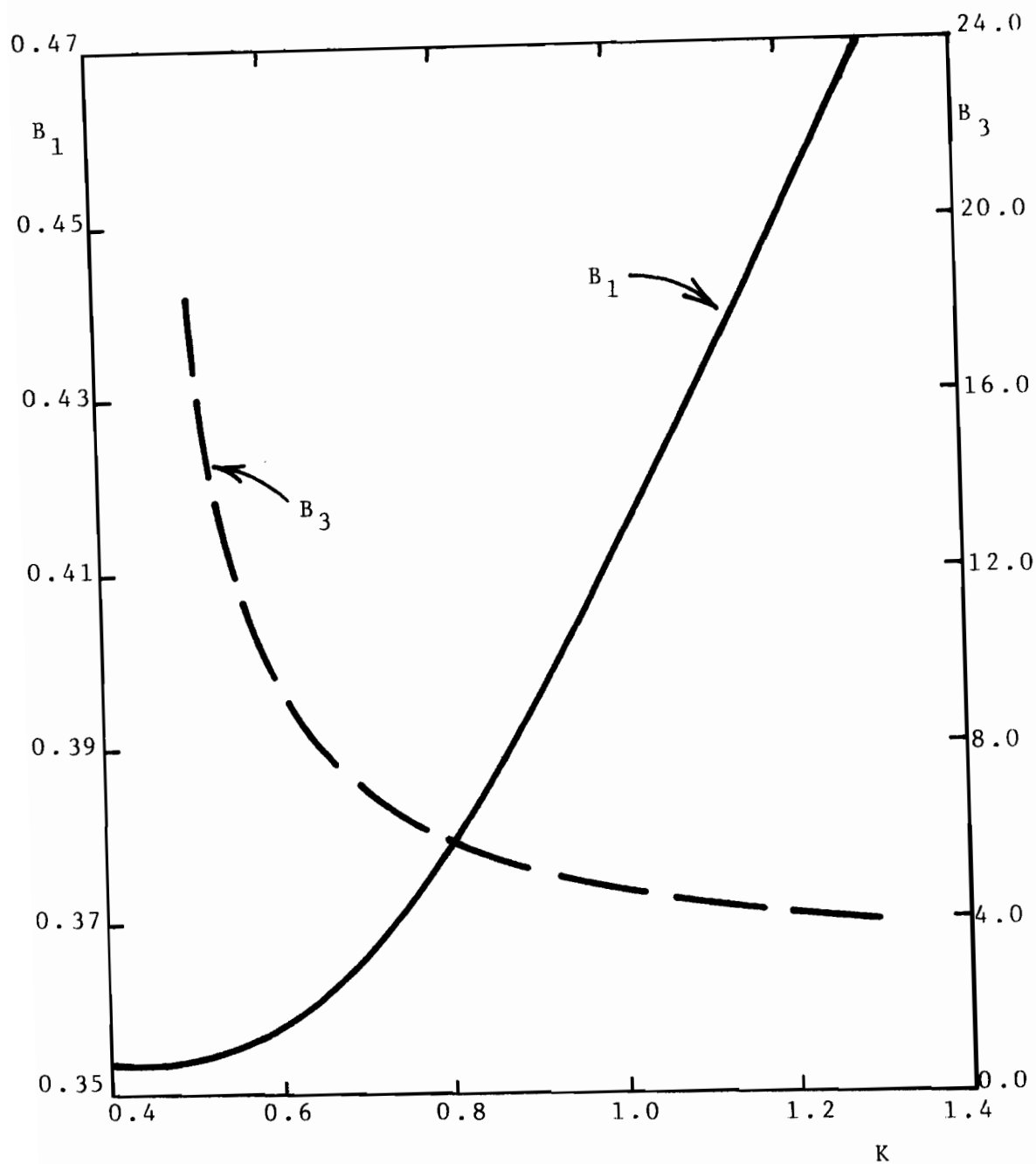


Fig. 2.2.5 POSTBUCKLING PARAMETERS VS. BUCKLING COEFFICIENT - UNSTIFFENED ELEMENTS

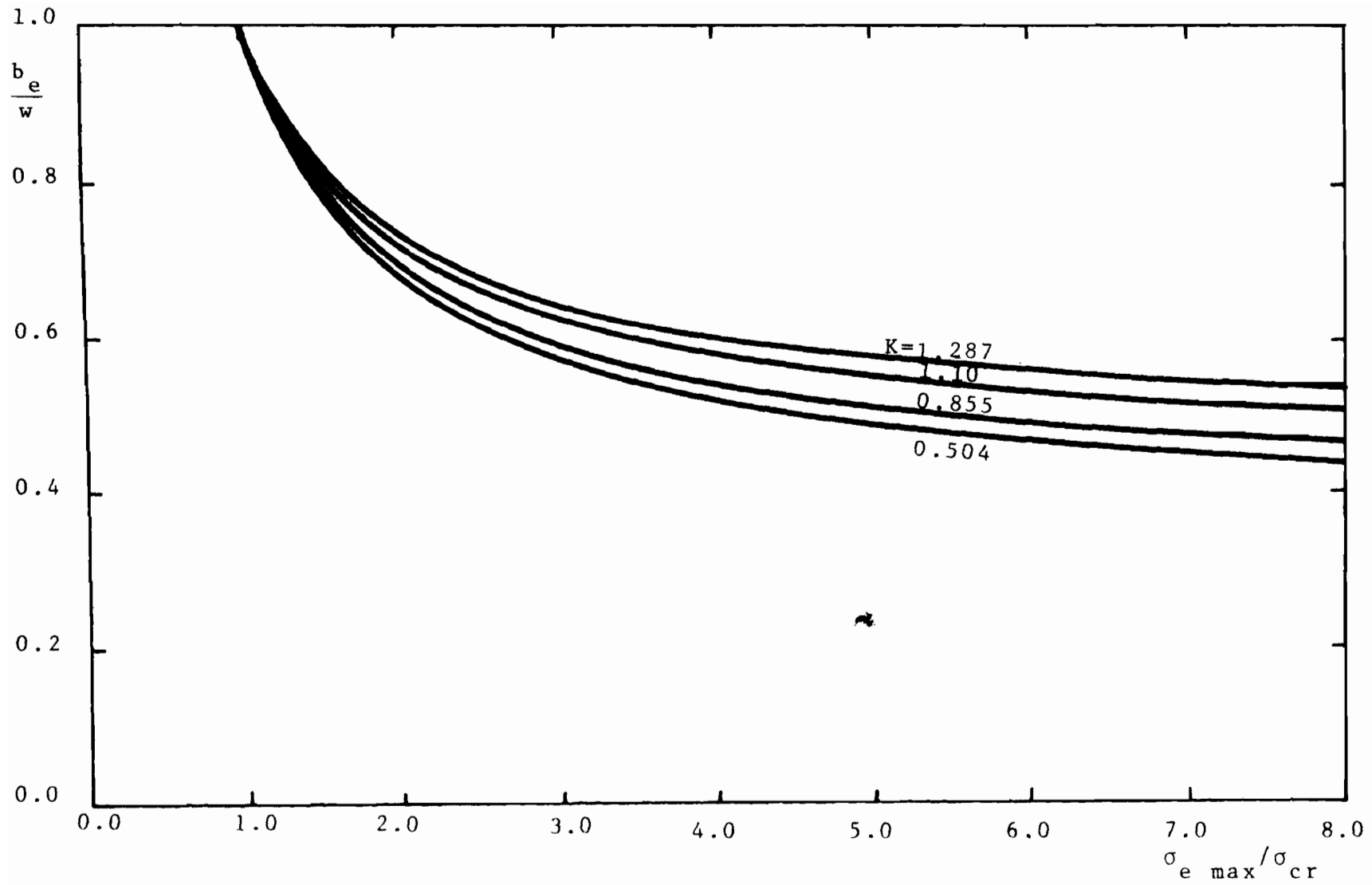


Fig. 2.2.6 EFFECTIVE WIDTH OF PERFECTLY FLAT UNSTIFFENED ELEMENTS

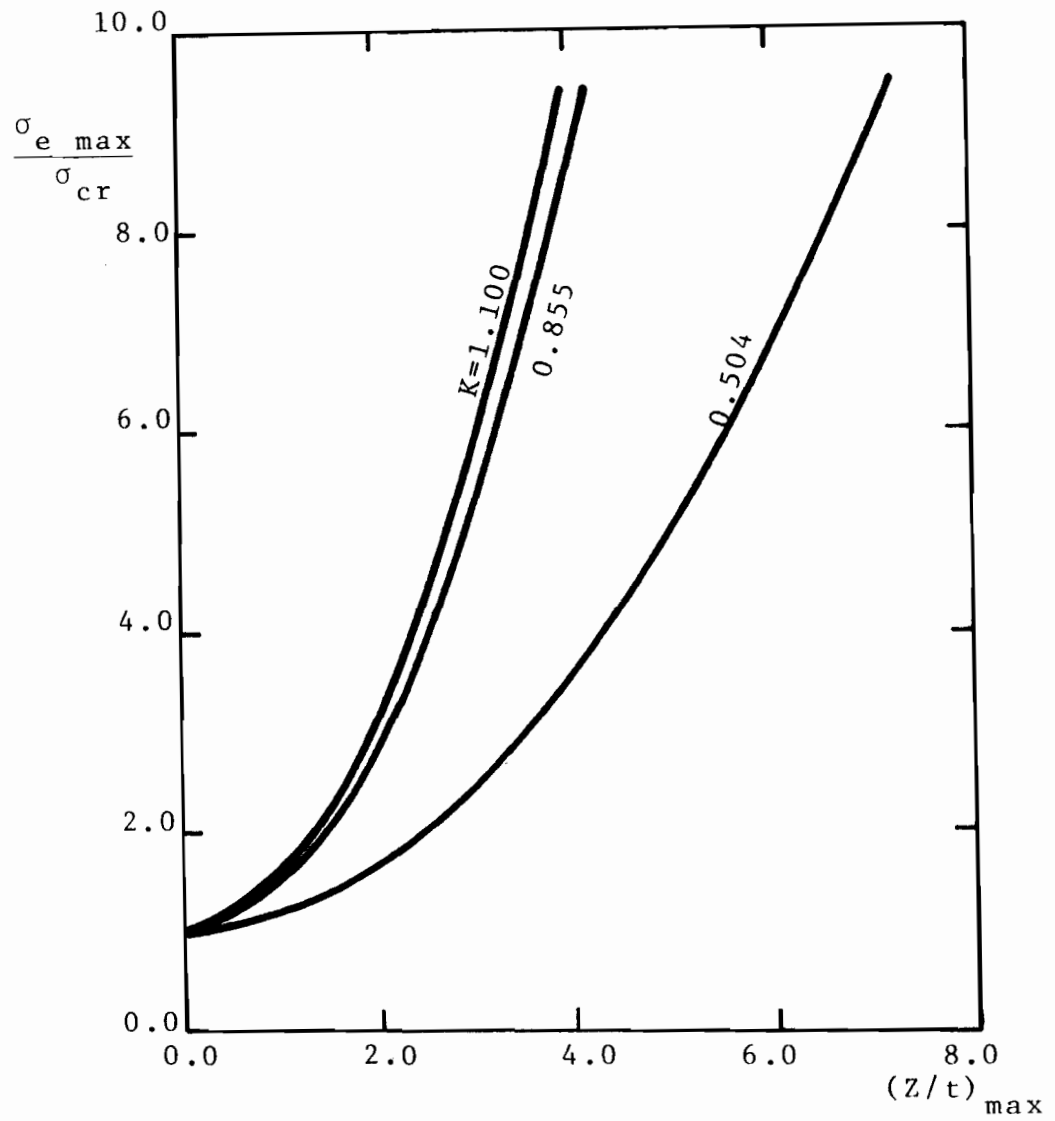


Fig. 2.2.7 POSTBUCKLING OUT OF PLANE DEFLECTION OF PERFECTLY FLAT UNSTIFFENED ELEMENTS

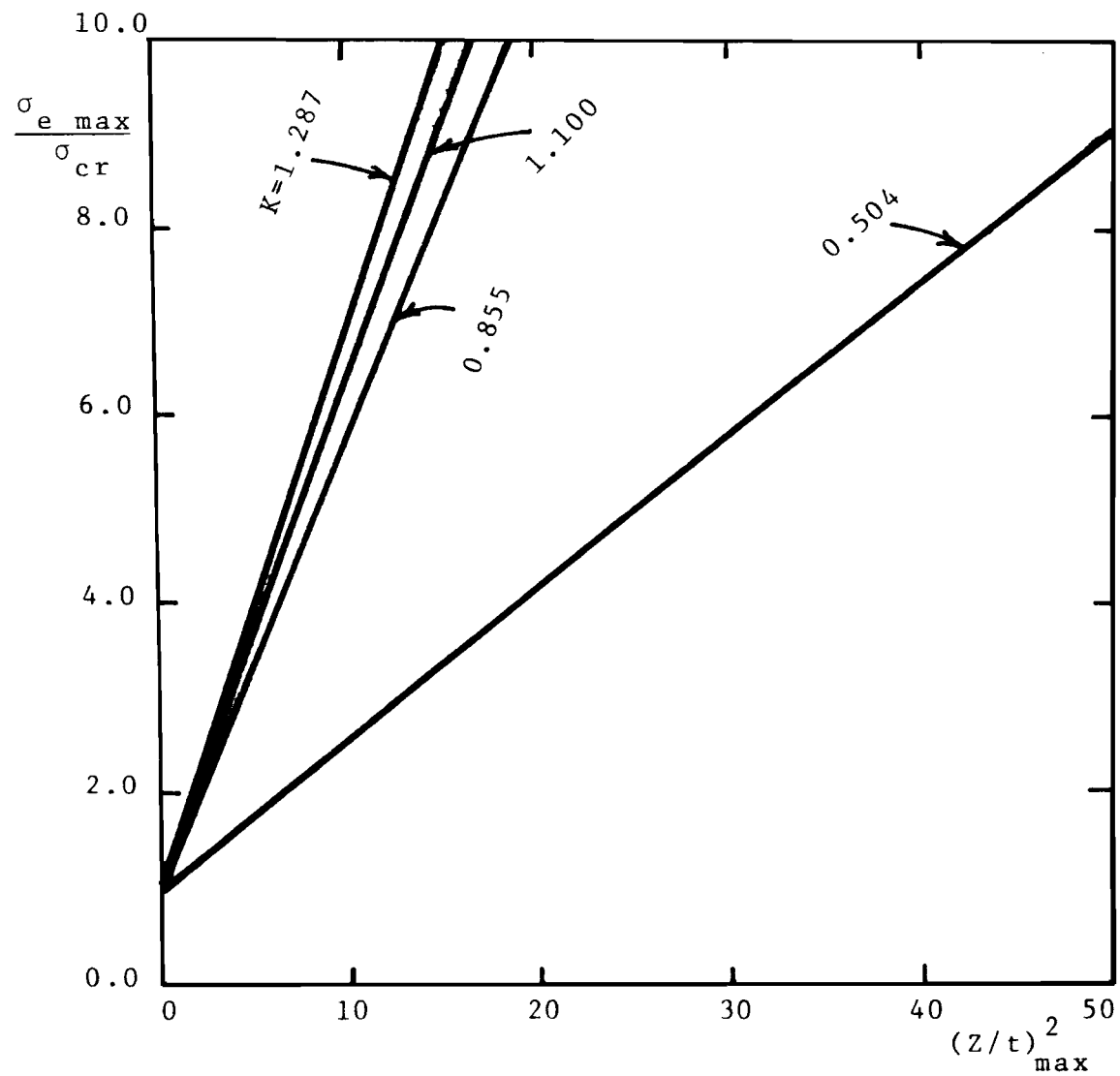


Fig. 2.2.8 POSTBUCKLING OUT OF PLANE DEFLECTION OF PERFECTLY FLAT UNSTIFFENED ELEMENTS

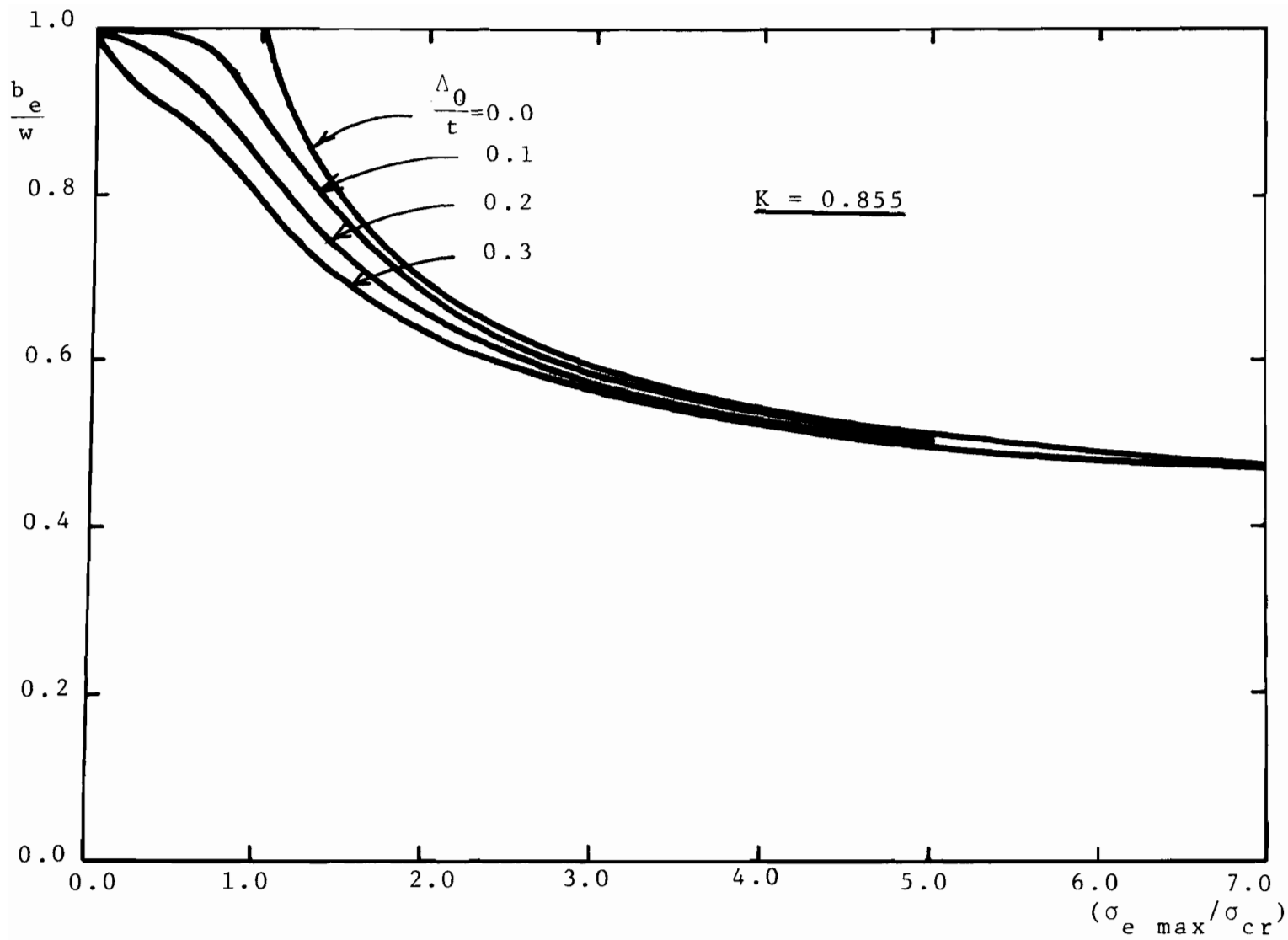


Fig. 2.2.9 EFFECTIVE WIDTH OF UNSTIFFENED ELEMENTS WITH INITIAL IMPERFECTION

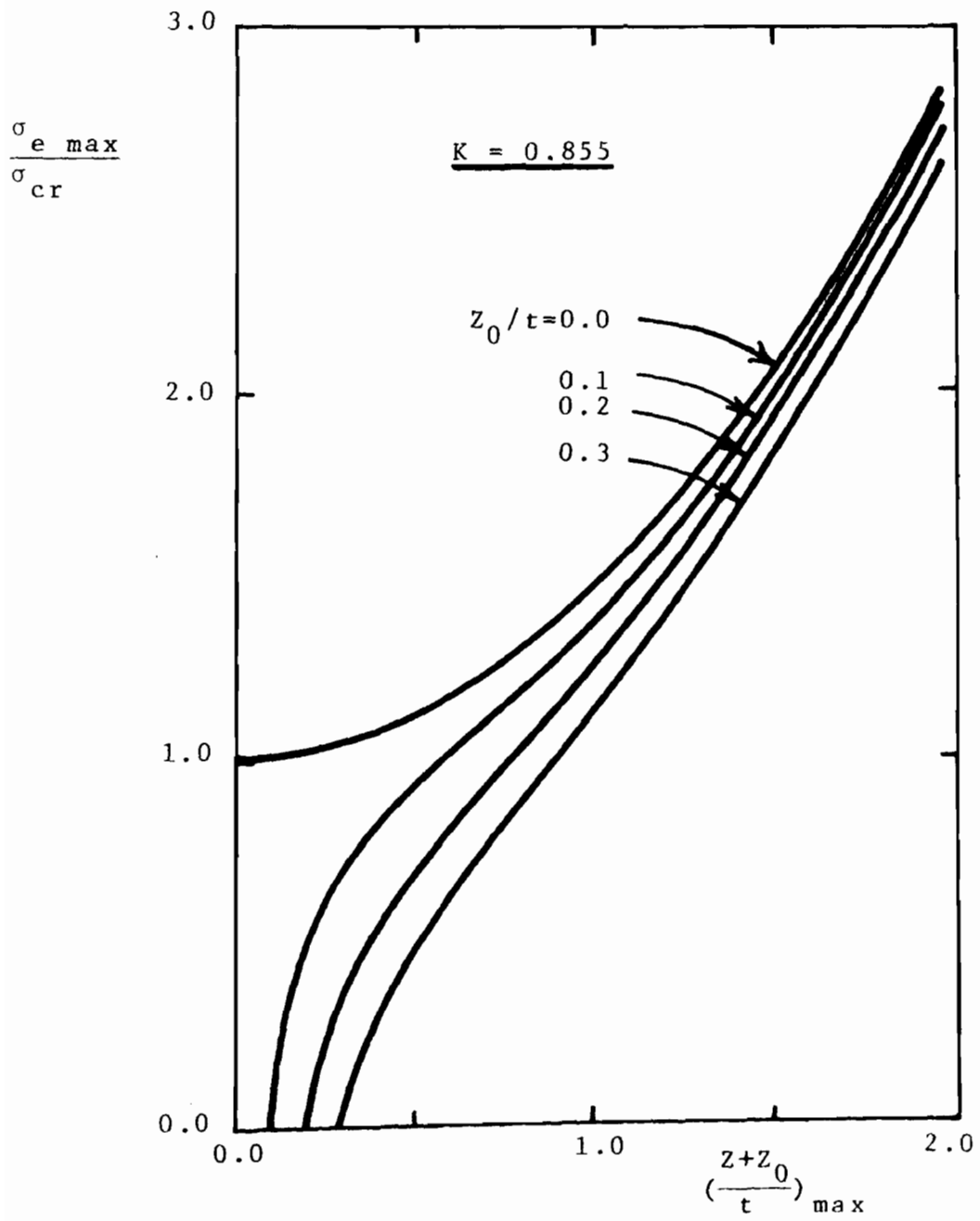


Fig. 2.2.10 POSTBUCKLING OUT OF PLANE DEFLECTION OF UNSTIFFENED ELEMENTS WITH INITIAL IMPERFECTION

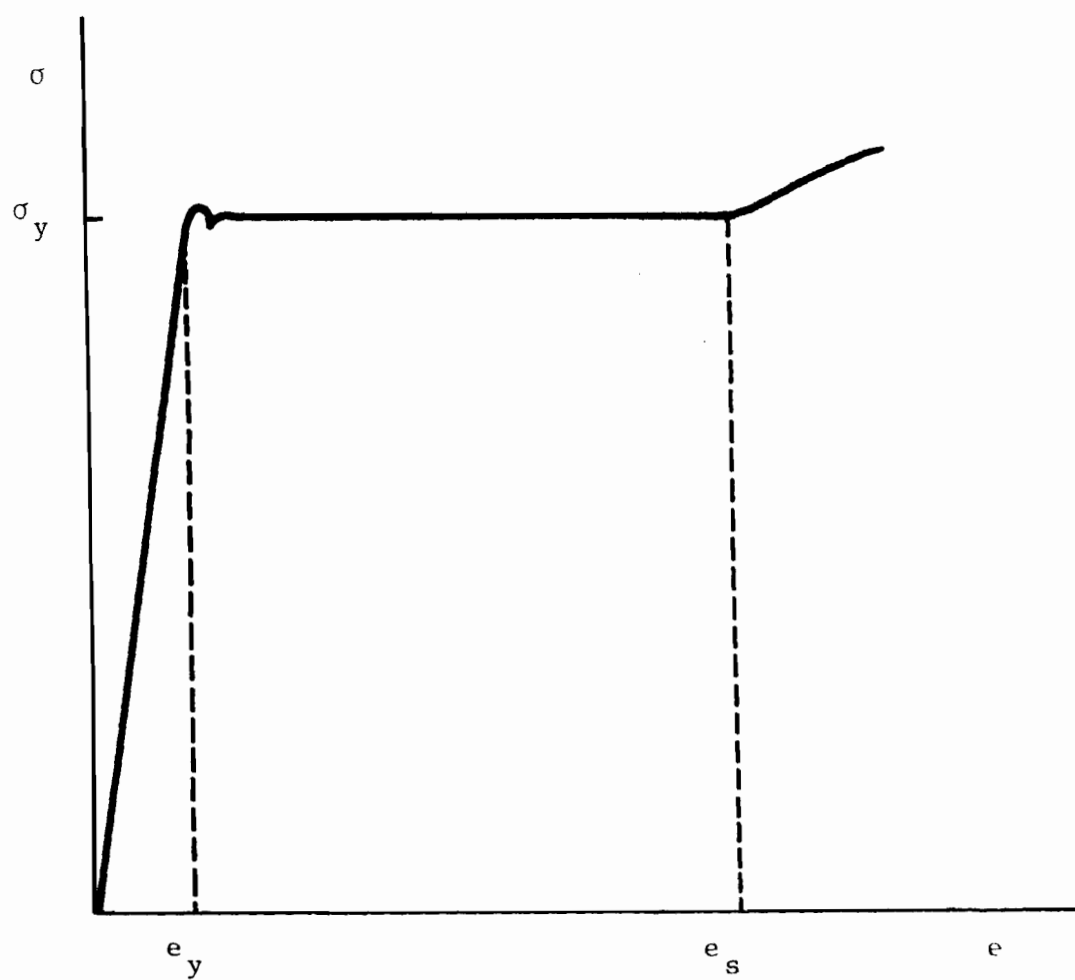


Fig. 3.2.1 TYPICAL STRESS STRAIN CURVE OF STEEL SHEETS

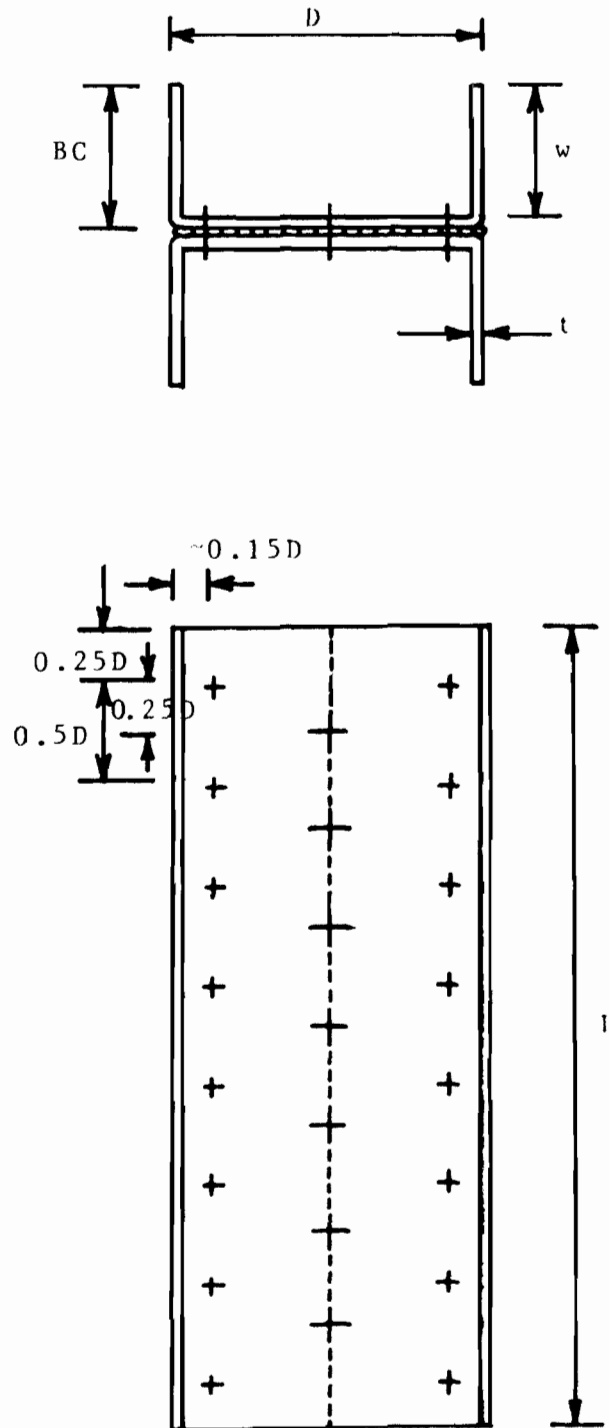
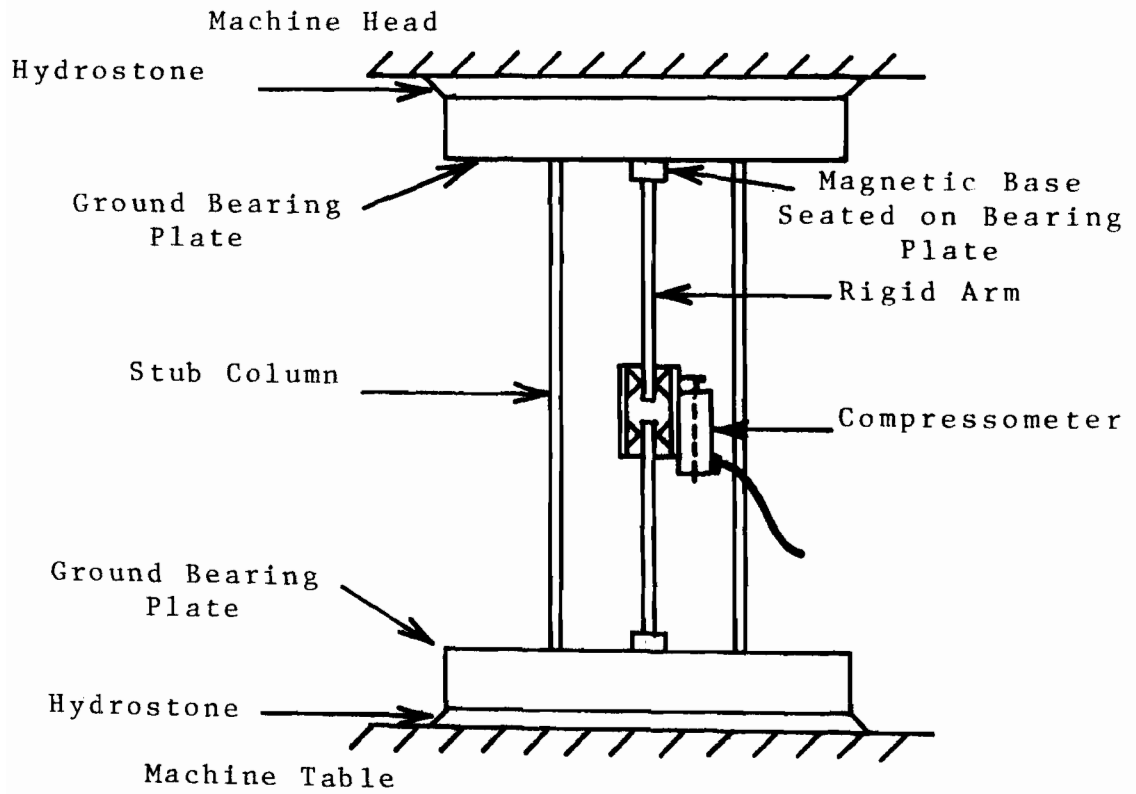
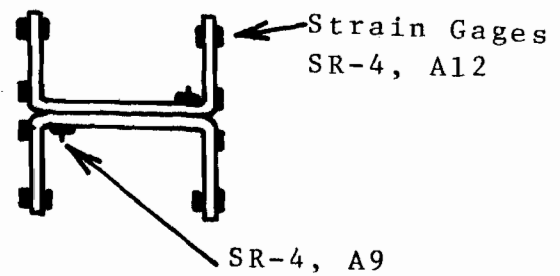


Fig. 3.2.2 STUB-COLUMN TEST SPECIMEN



a) Stub Column Test Set-Up



b) Cross-section and Strain gage location

Fig. 3.2.3 STUB COLUMN TEST SET-UP AND SPECIMEN SECTION WITH STRAIN GAGES

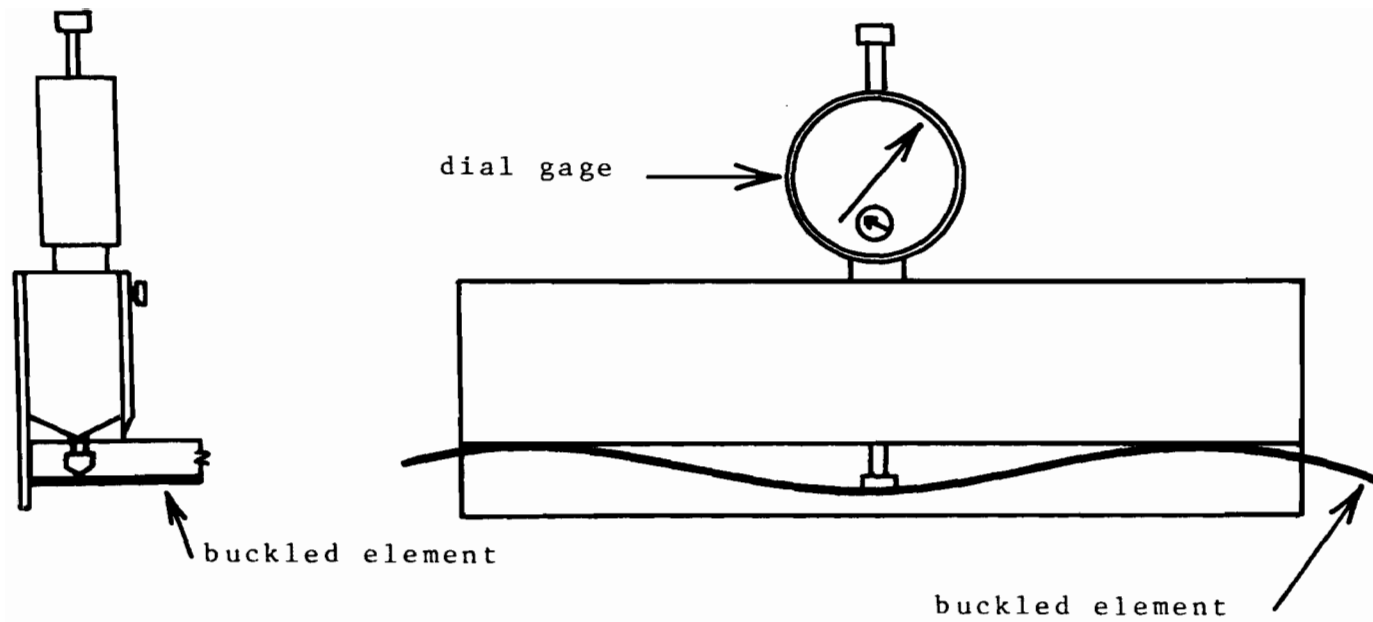


Fig. 3.2.4 WAVE AMPLITUDE MEASURING INSTRUMENT



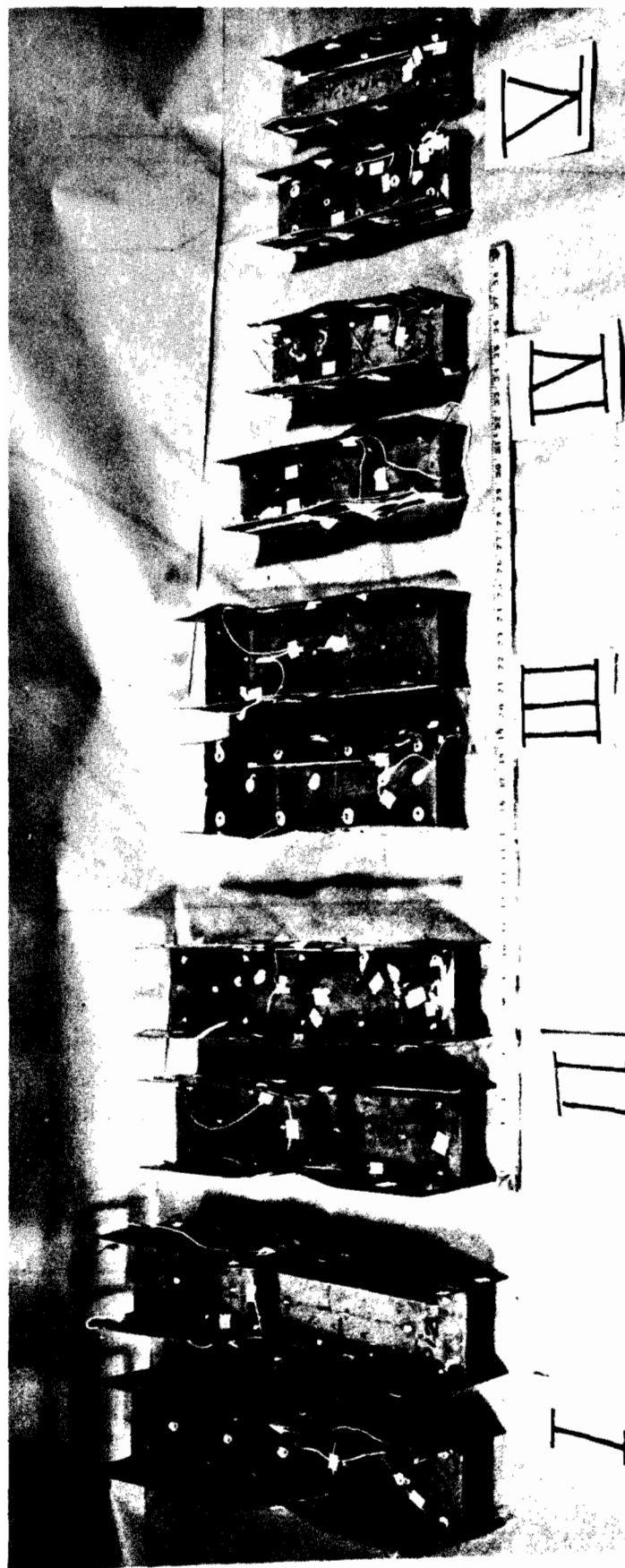


Fig. 3.2.6 STUB-COLUMN SPECIMENS - AFTER TEST

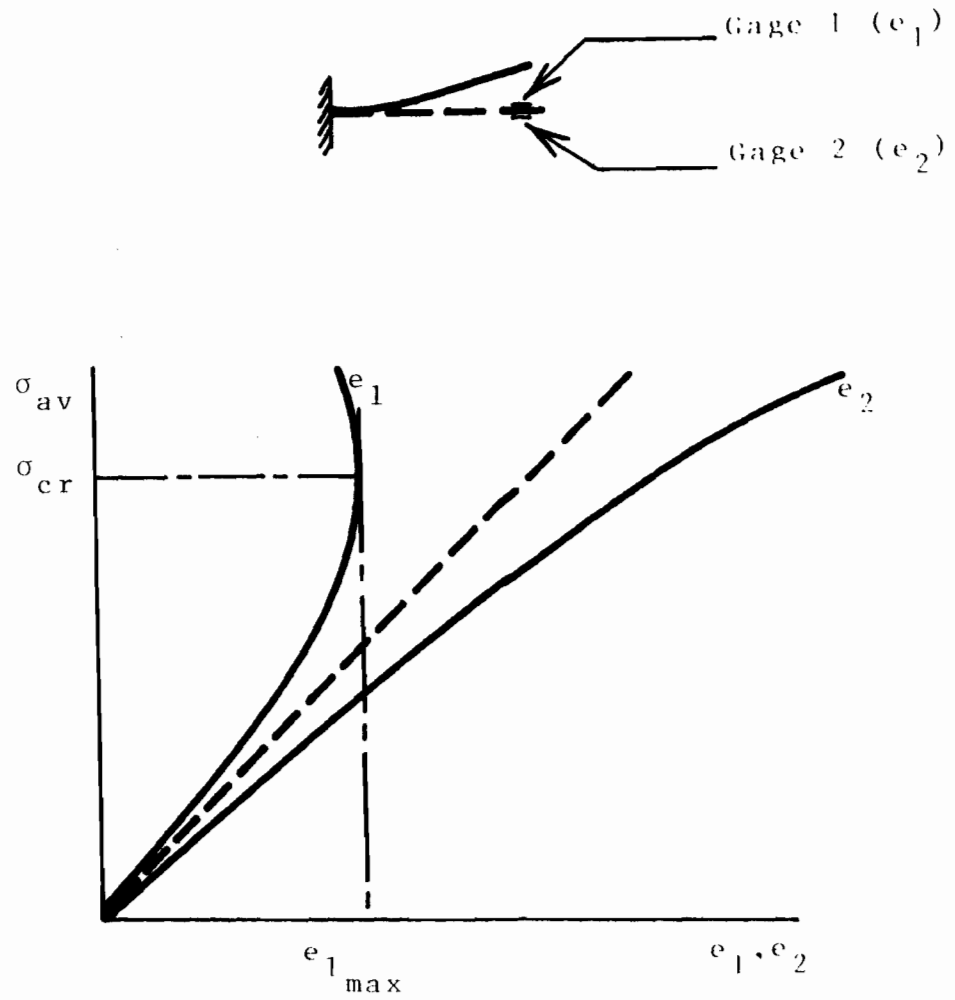


Fig. 3.3.1 DETERMINATION OF LOCAL BUCKLING STRESS - EXPERIMENTAL METHOD

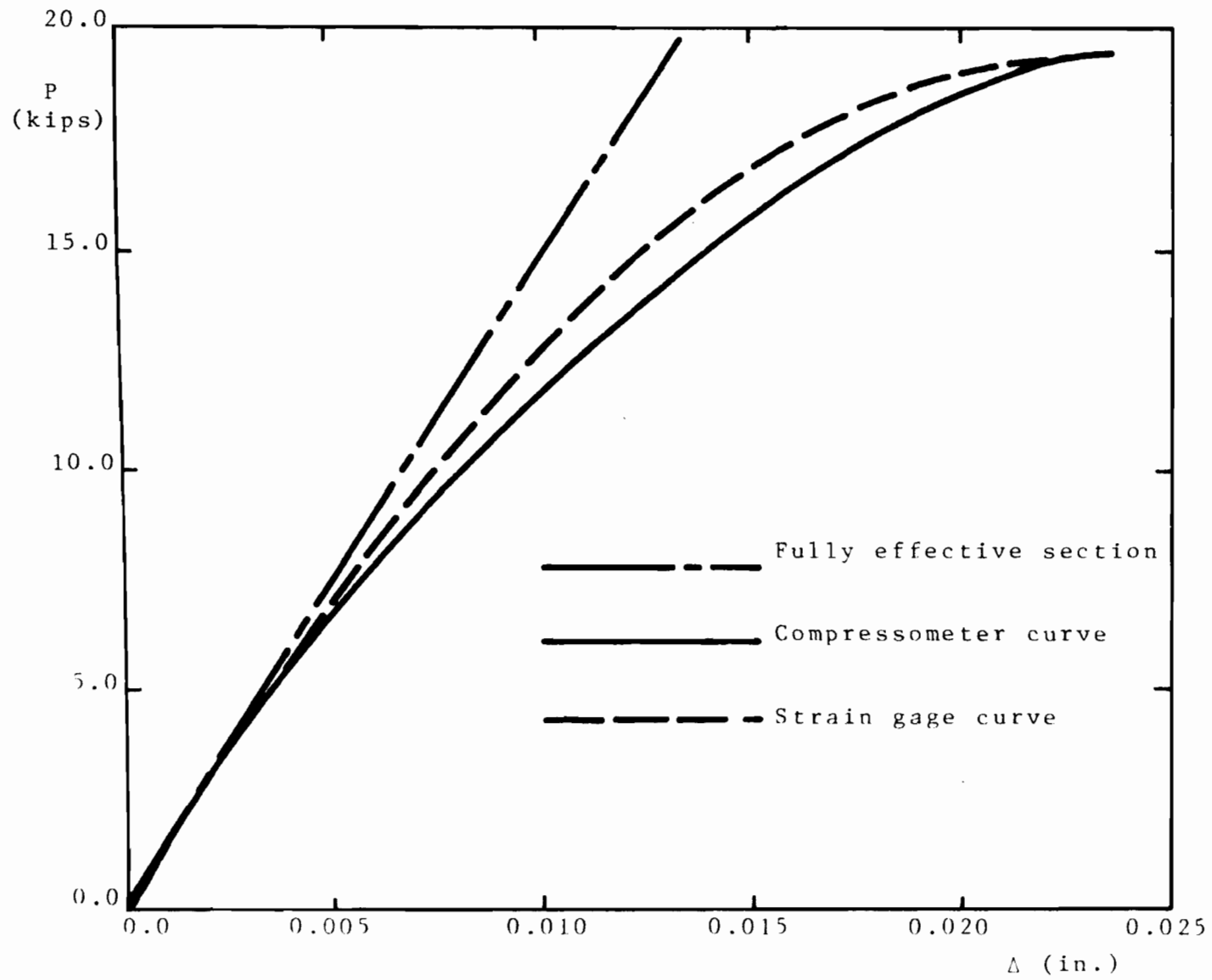


Fig. 3.4.1 AXIAL LOAD VERSUS SHORTENING OF STUB-COLUMN (SC-III)

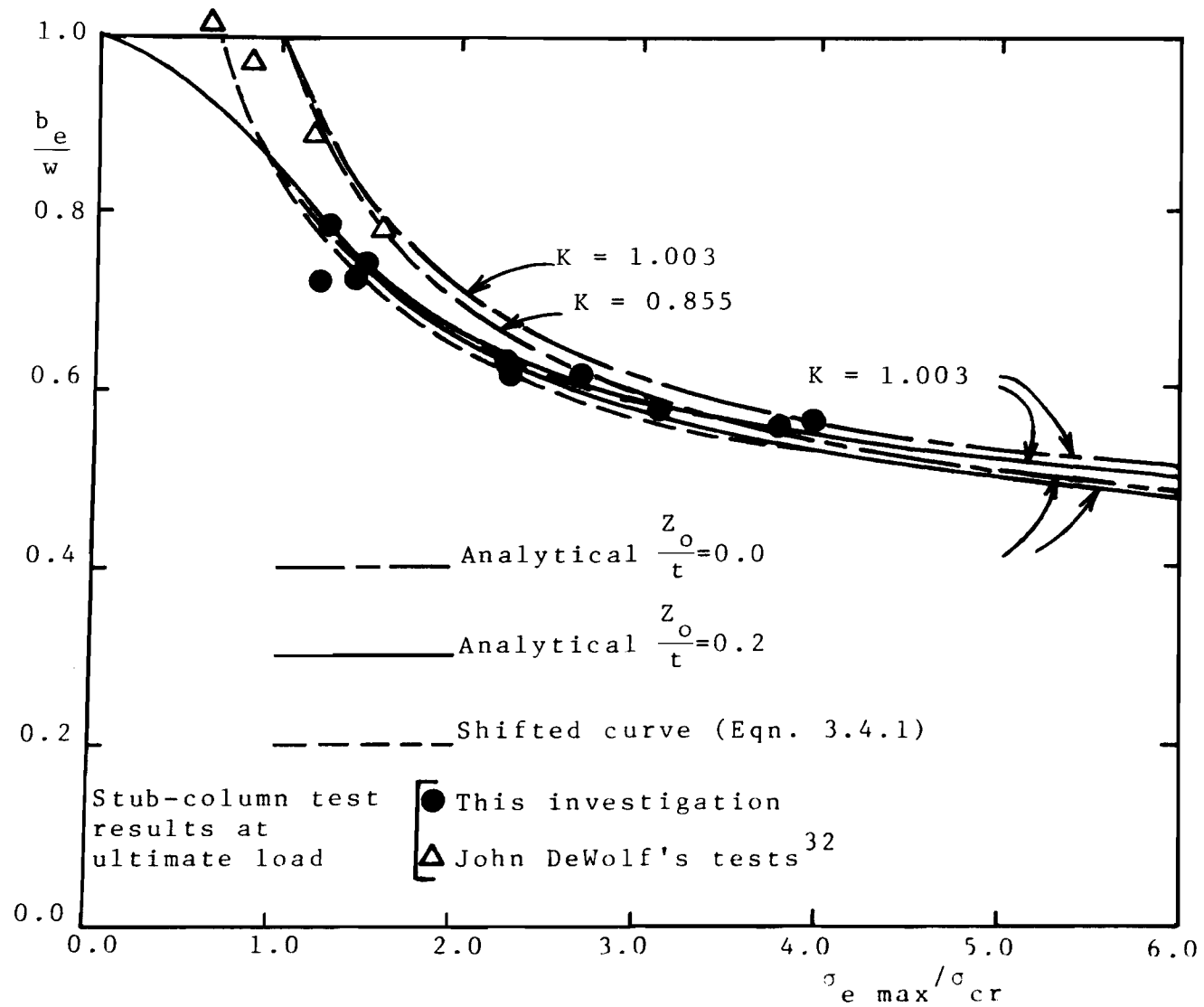


Fig. 3.4.2 COMPARISON OF EFFECTIVE WIDTH EQUATIONS AND STUB-COLUMN TEST RESULTS

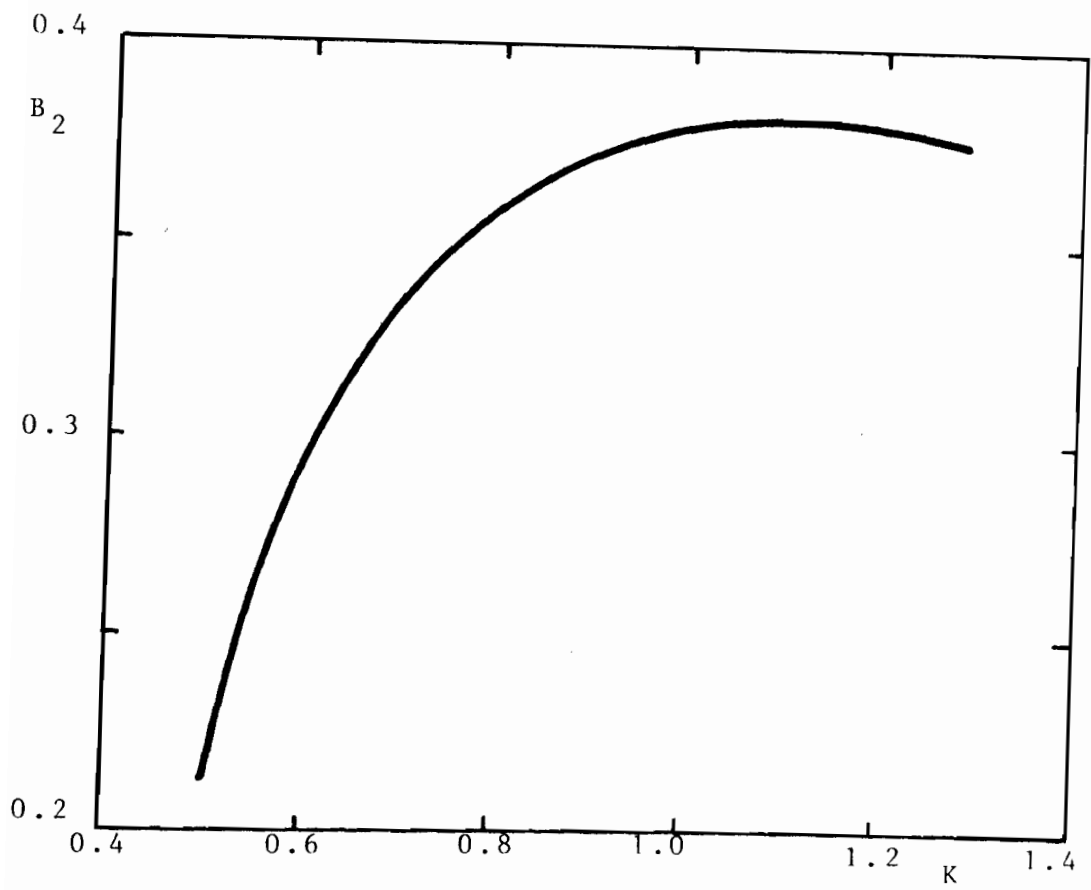


Fig. 3.4.3 EFFECTIVE WIDTH EQUATION (eqn. 3.4.1) INITIAL IMPERFECTION PARAMETER $\frac{z}{t} = 0.2$

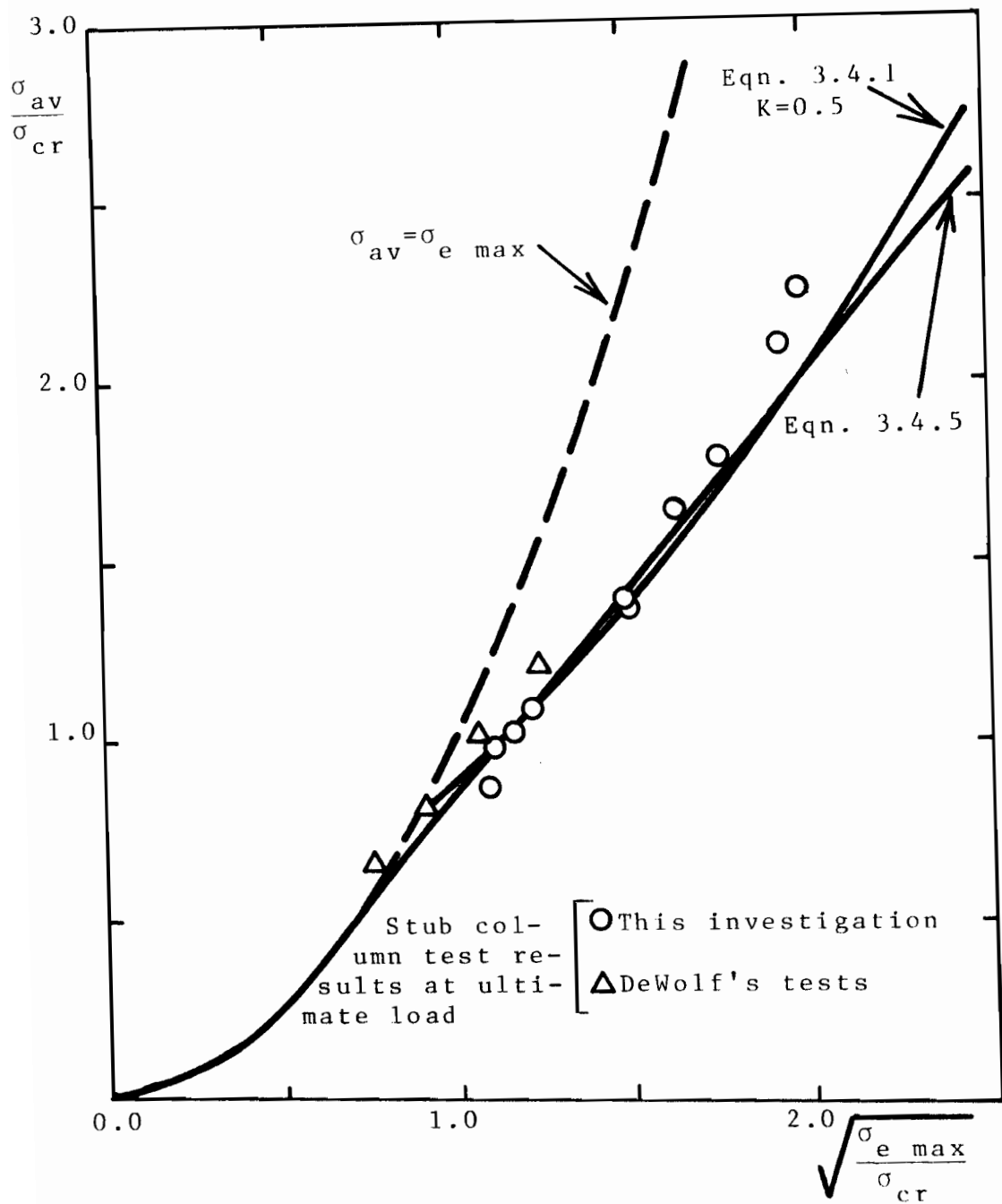


Fig. 3.4.4 AVERAGE AND MAXIMUM STRESSES AT ULTIMATE LOAD OF UNSTIFFENED ELEMENTS

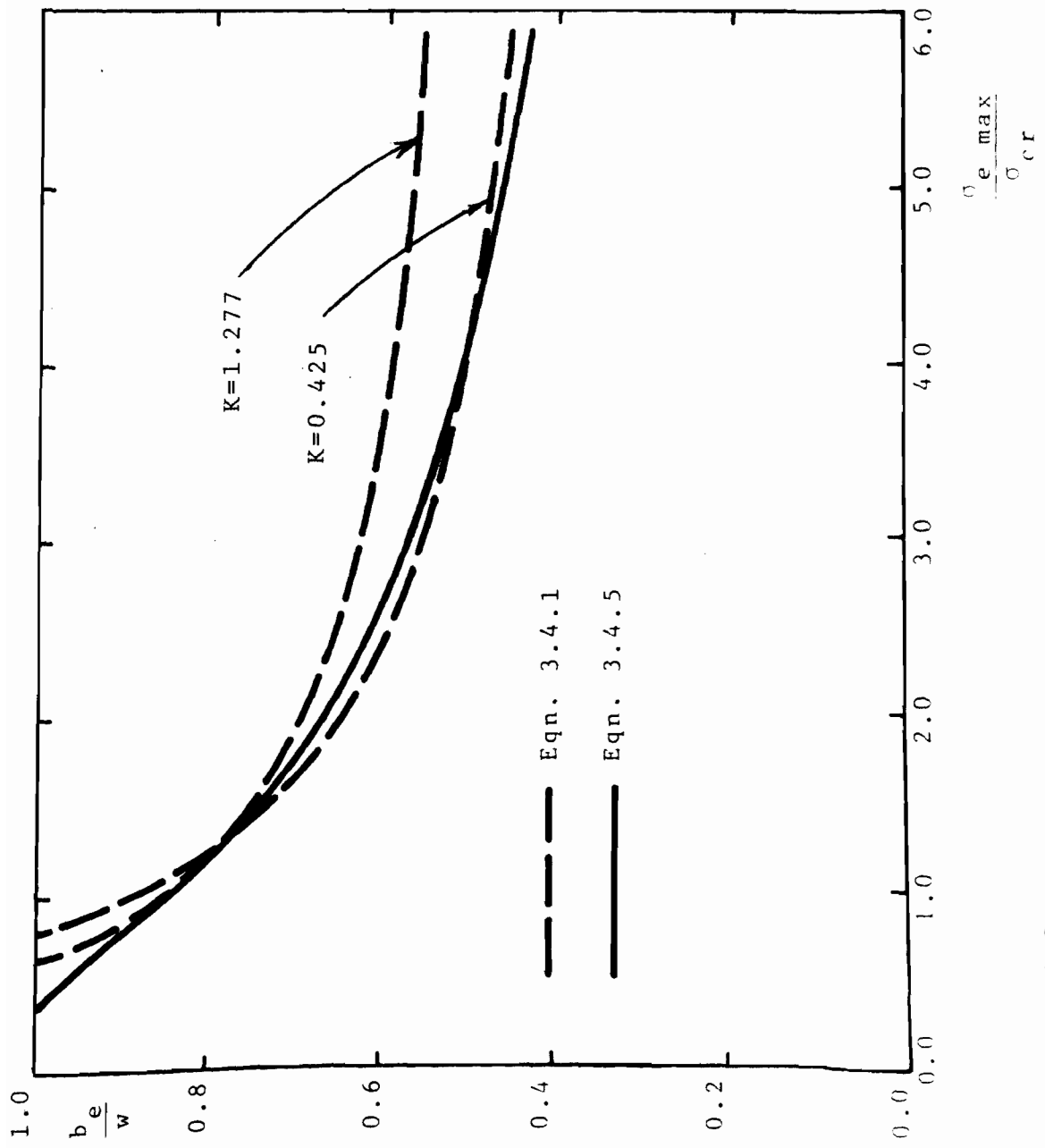


FIG. 3.4.5 COMPARISON OF EFFECTIVE WIDTH EQUATIONS

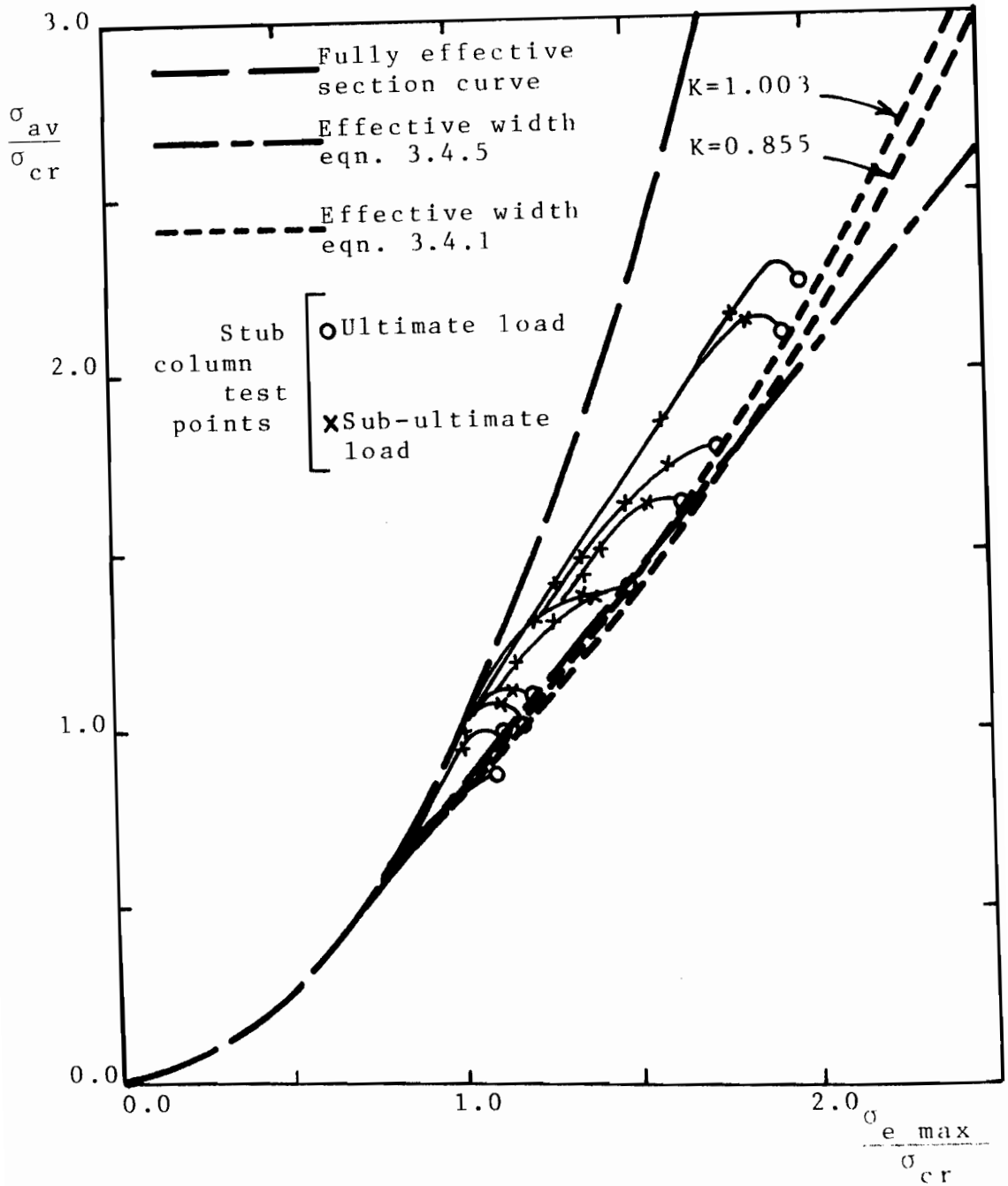


Fig. 3.4.6 COMPARISON OF SUB-ULTIMATE AND ULTIMATE TEST RESULTS AND THE EFFECTIVE WIDTH EQUATIONS

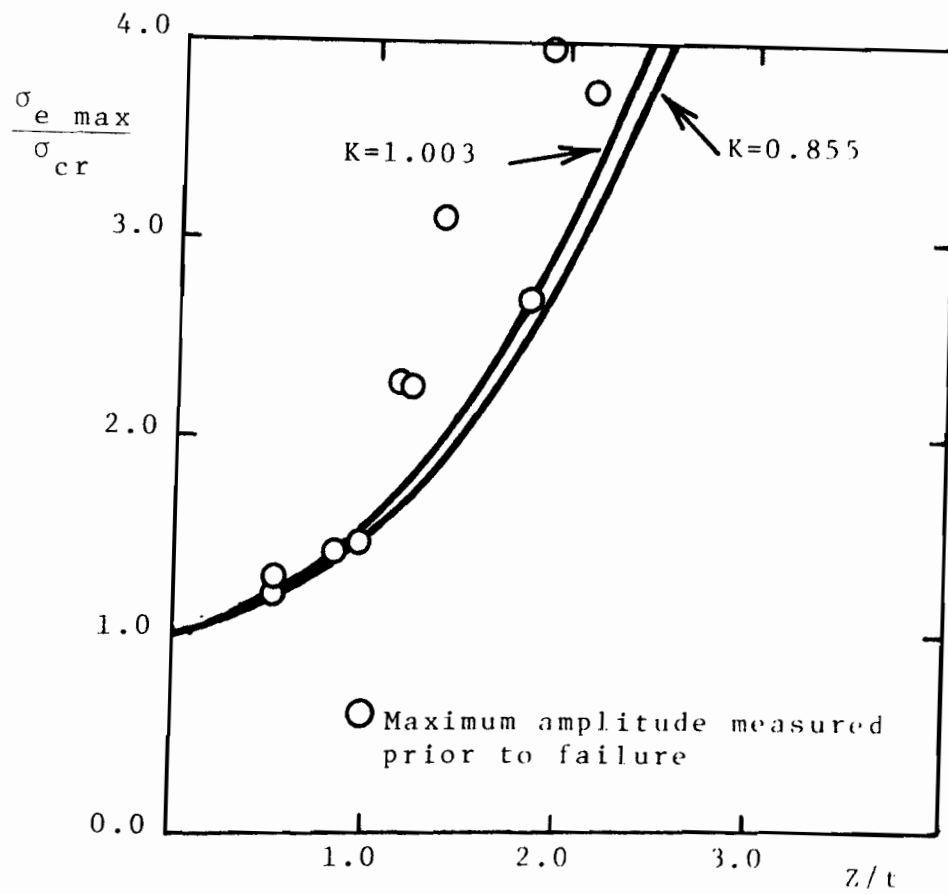
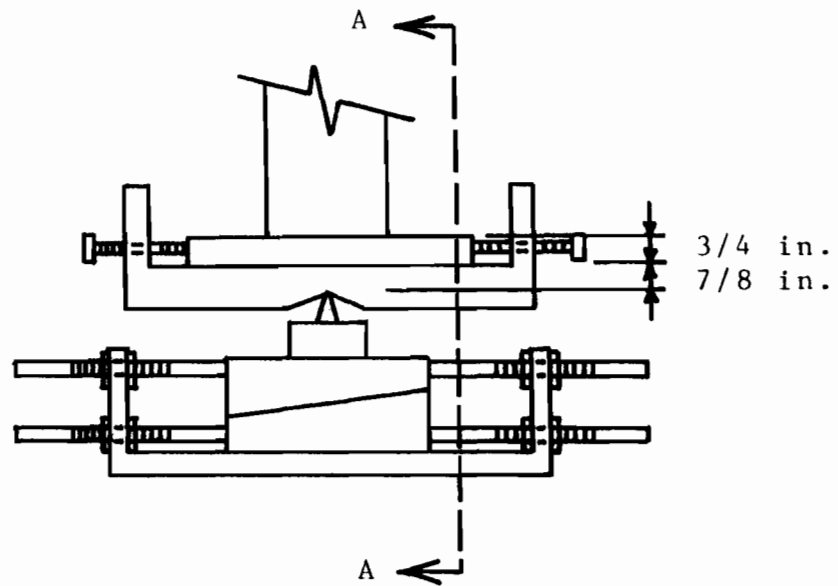
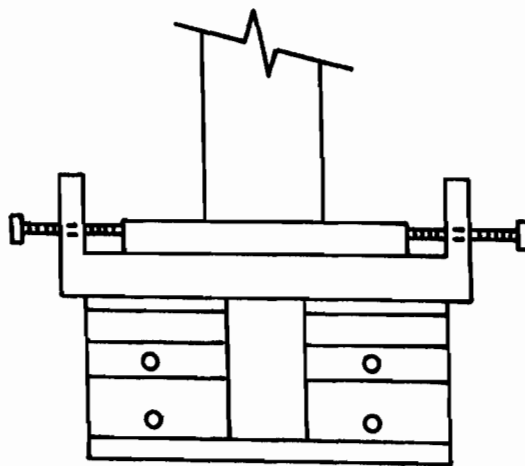


Fig. 3.4.7 MAXIMUM AMPLITUDE OF POSTBUCKLING DEFLECTION OF UNSTIFFENED ELEMENTS



(a) Section through Support in the Direction of Flexural Buckling



(b) Section A-A

Fig. 4.2.1 END FIXTURE FOR COLUMN TESTS

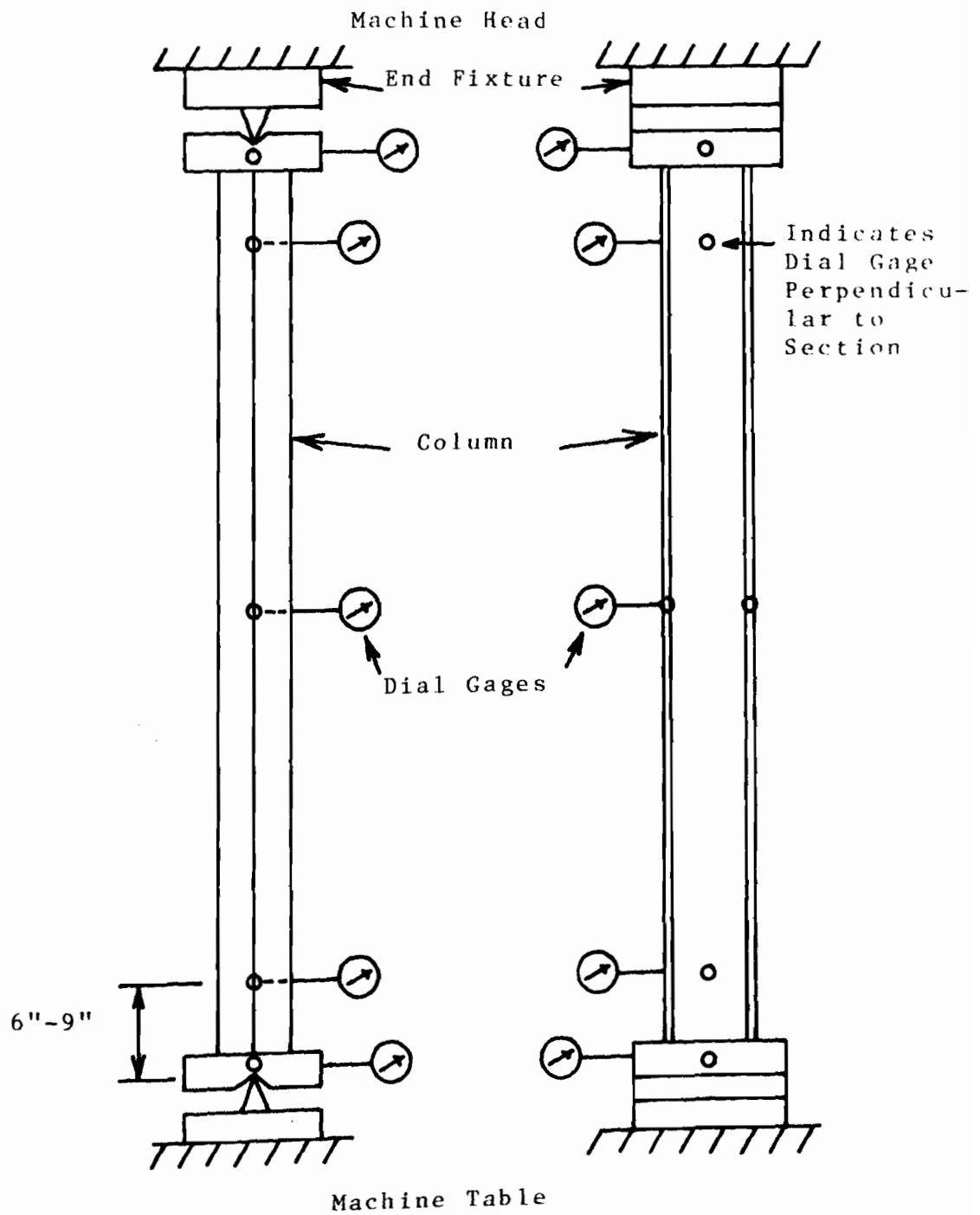


Fig. 4.2.2 LOCATION OF DIAL GAGES LONG COLUMN TESTS

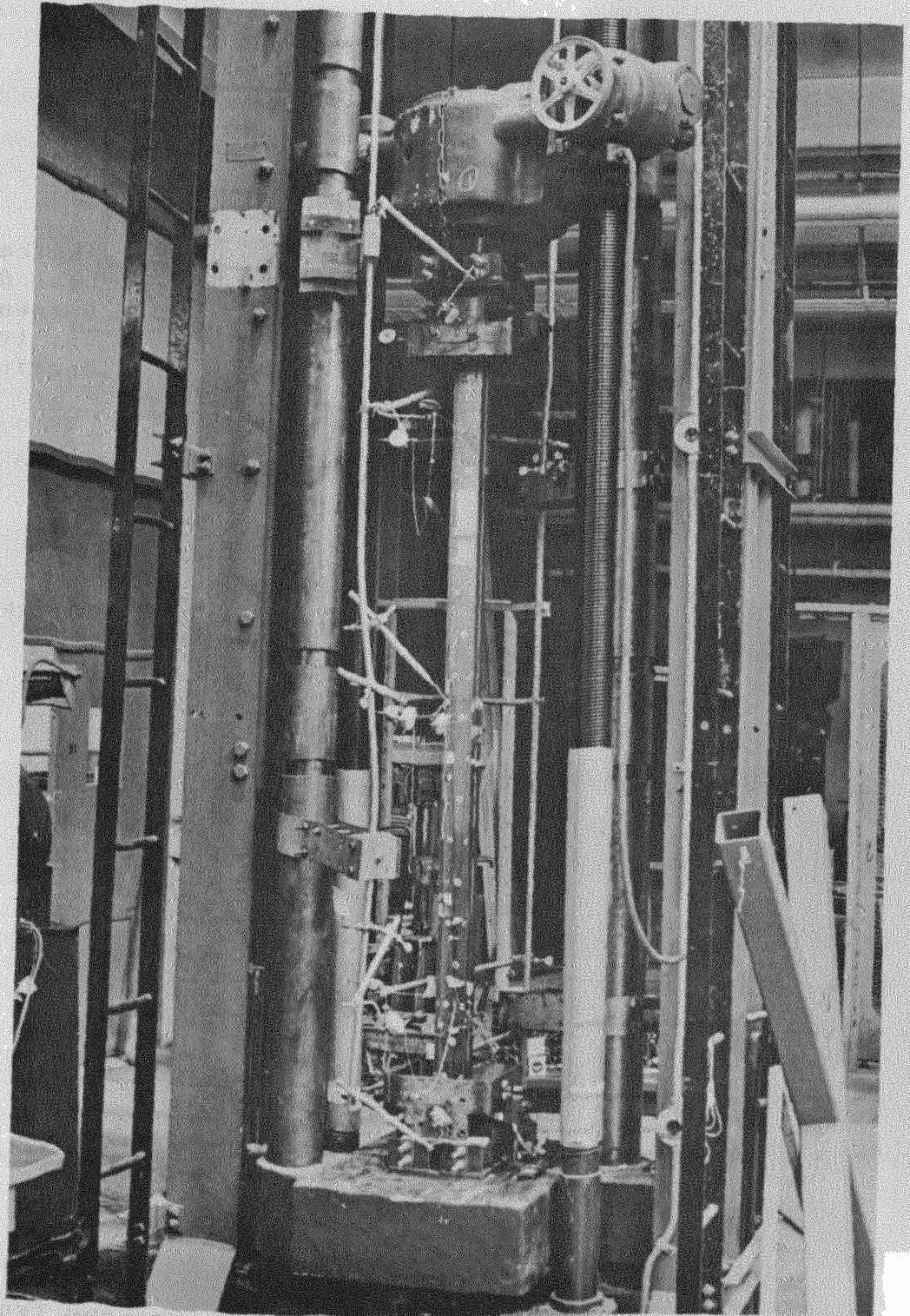


Fig. 4.2.3 COMPRESSION MEMBER TEST SET-UP

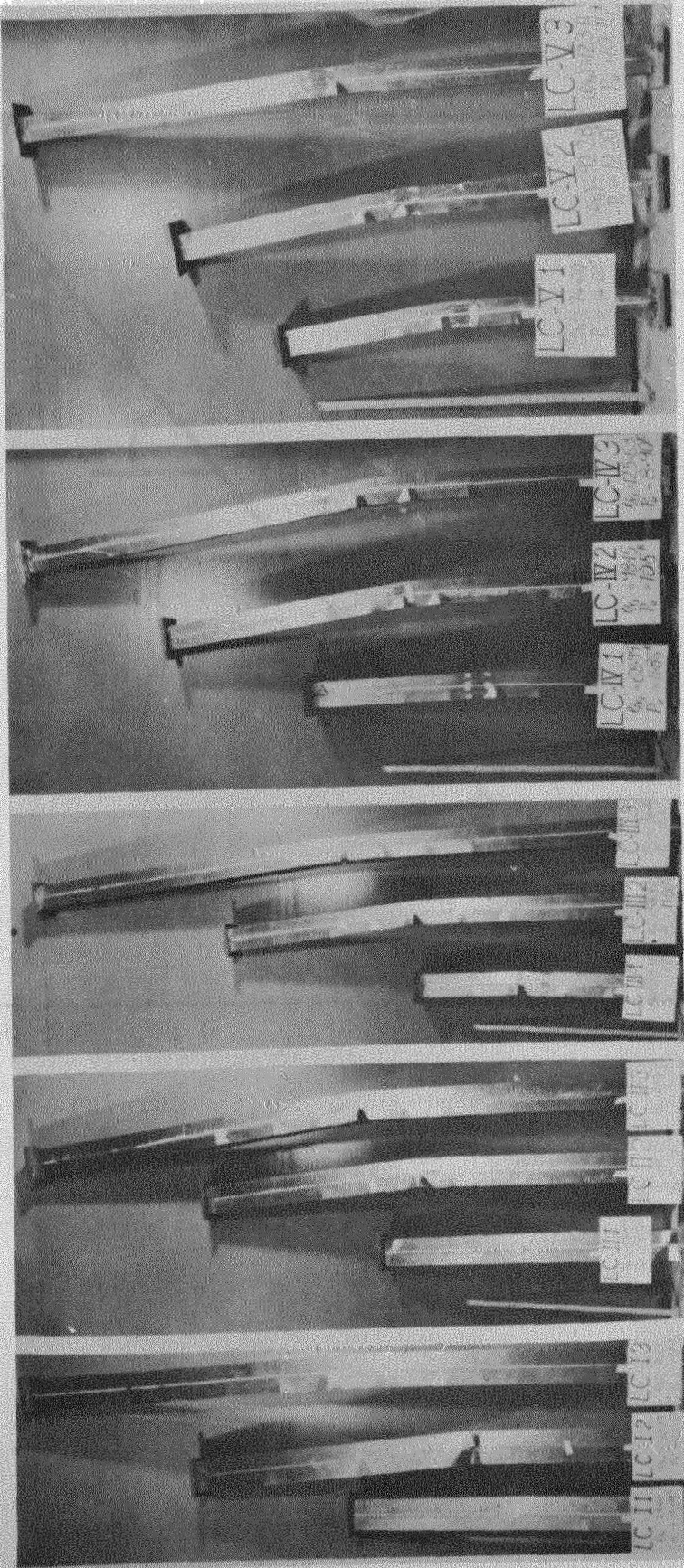


Fig. 4.2.4. COMPRESSION MEMBERS AFTER FAILURE

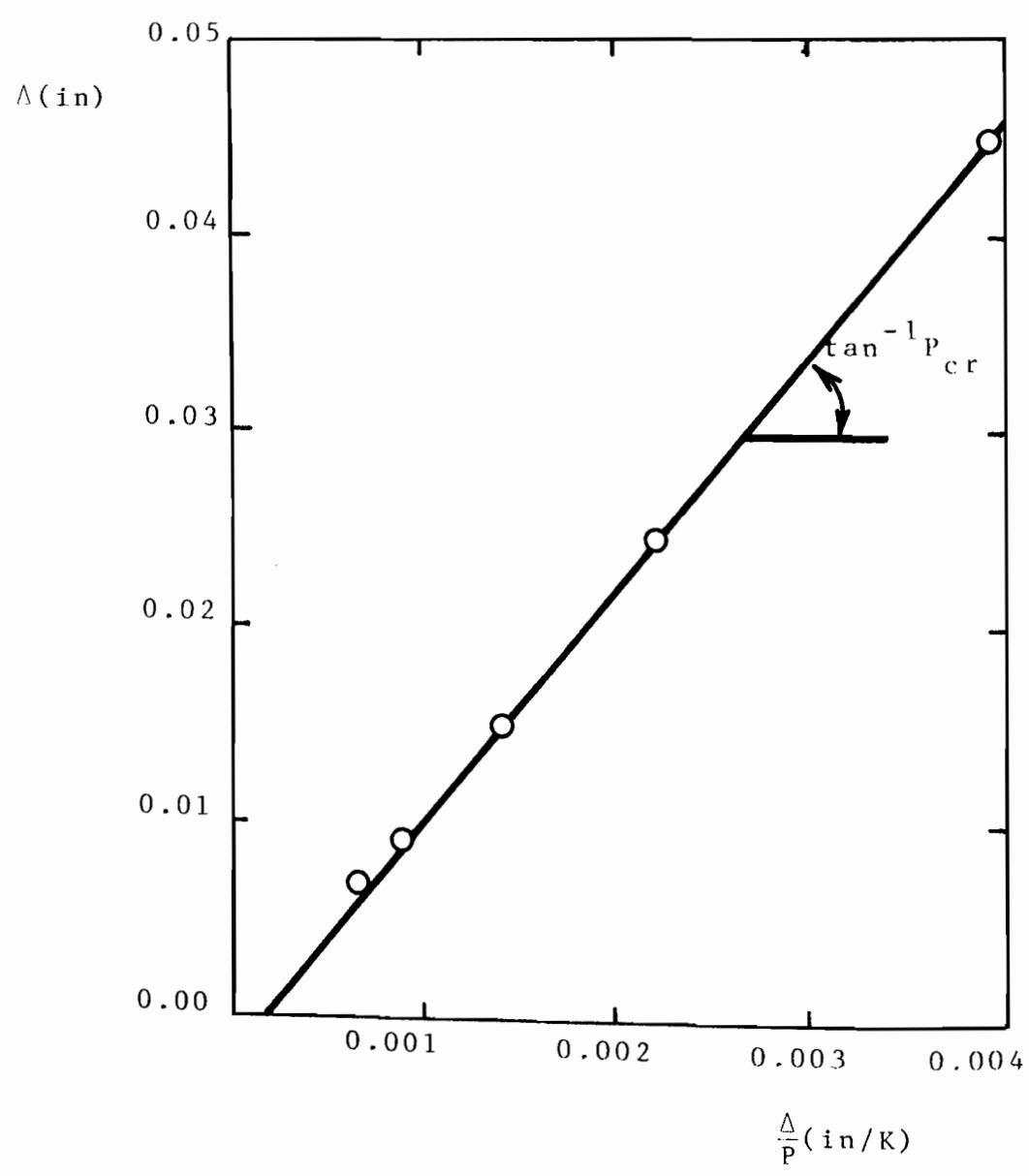


Fig. 4.3.1 A TYPICAL SOUTHWELL PLOT - SPECIMEN LC-IV

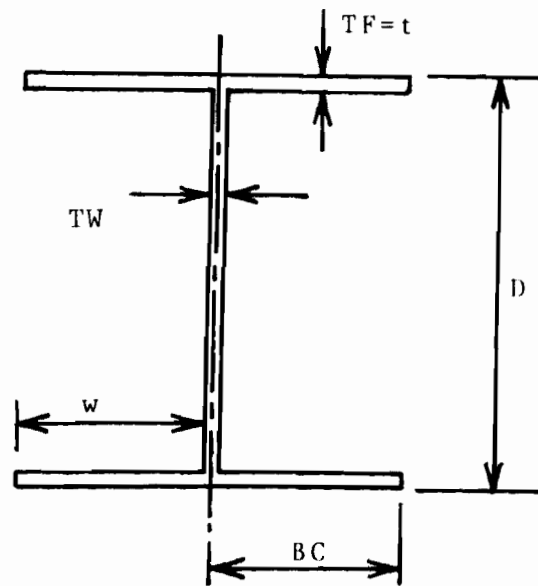


Fig. 4.4.1 BIJLAARD AND FISHER'S SPECIMEN CROSS SECTION (Ref. 27)

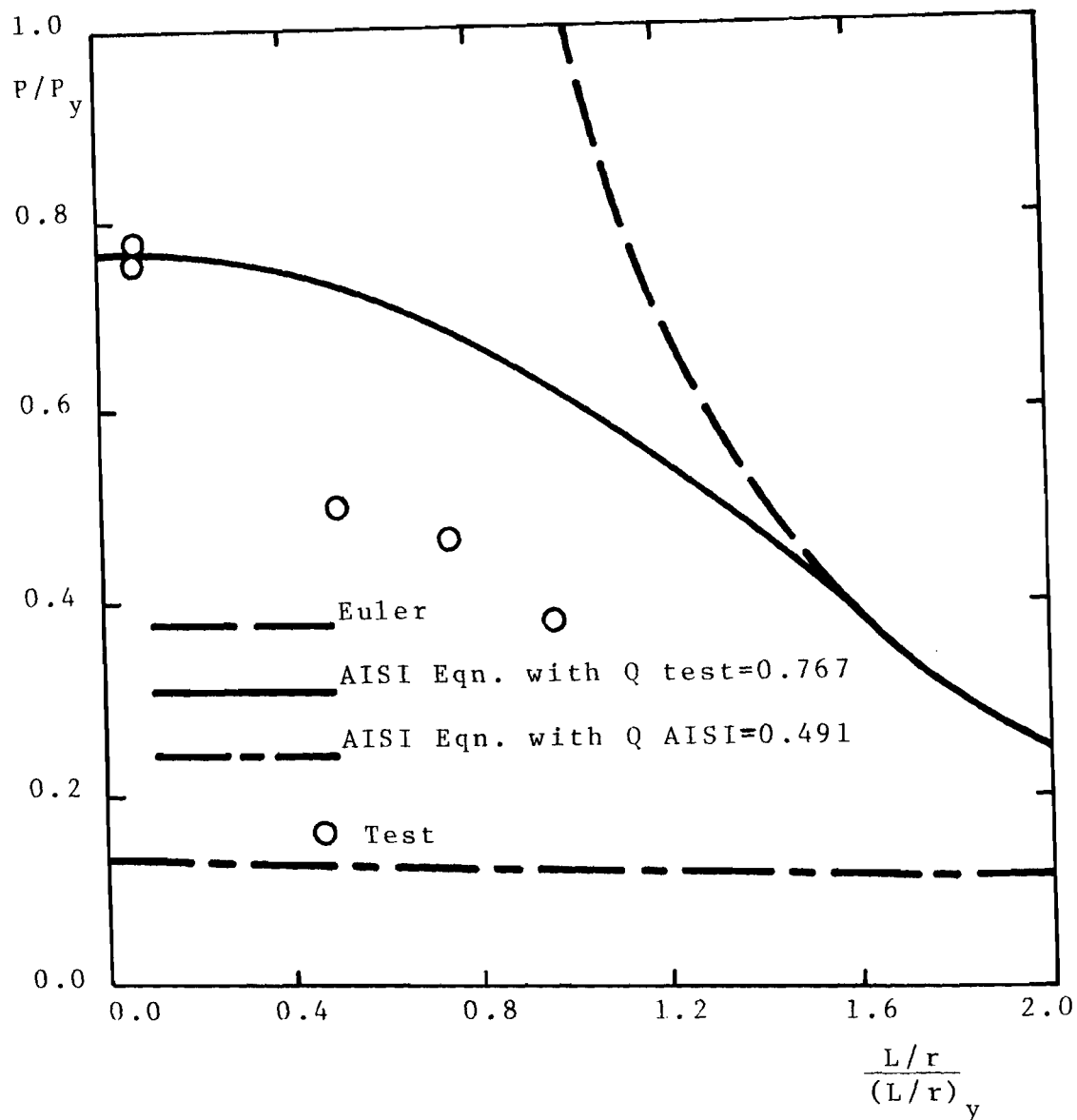


Fig. 4.4.2 COMPARISON OF TEST RESULTS AND THE AISI SPECIFICATION COLUMN CURVE - SPECIMENS LC-I ($w/t = 57.6$)

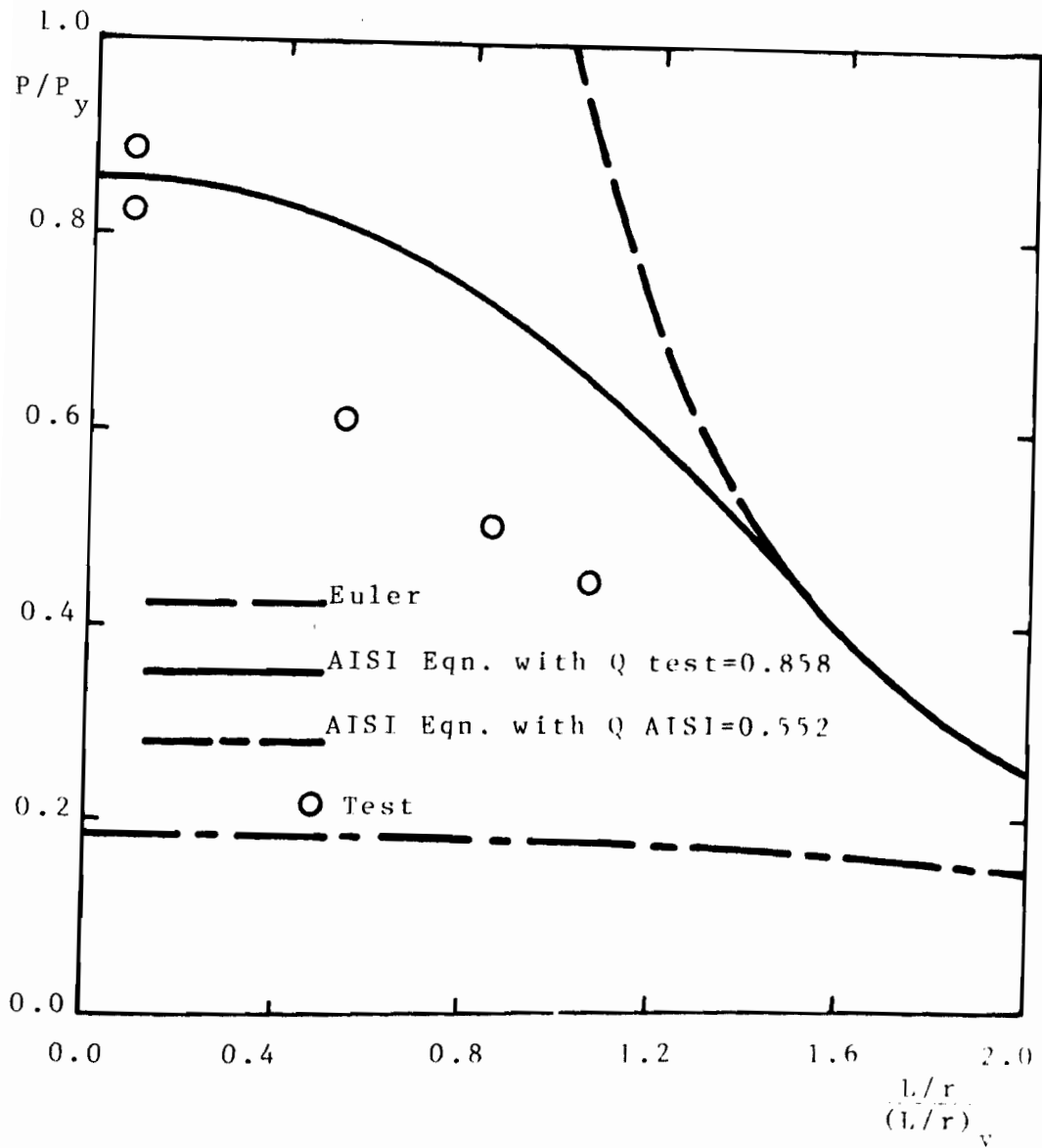


Fig. 4.4.3 COMPARISON OF TEST RESULTS AND THE AISI SPECIFICATION COLUMN CURVE - SPECIMENS LC-11 ($w/t = 57.5$)

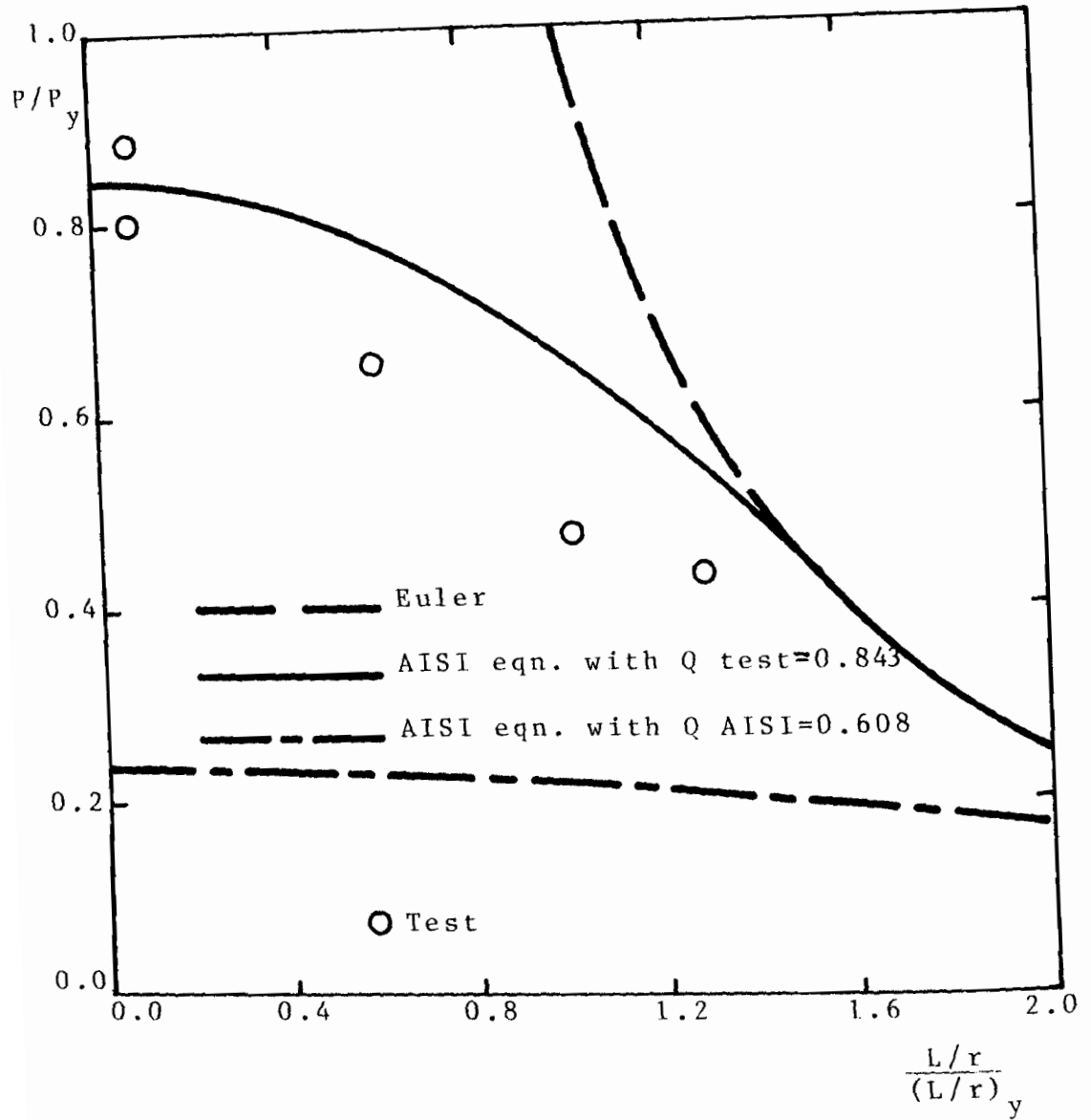


Fig. 4.4.4 COMPARISON OF TEST RESULTS AND THE AISI SPECIFICATION COLUMN CURVE - SPECIMENS LC-III ($w/t = 42.0$)

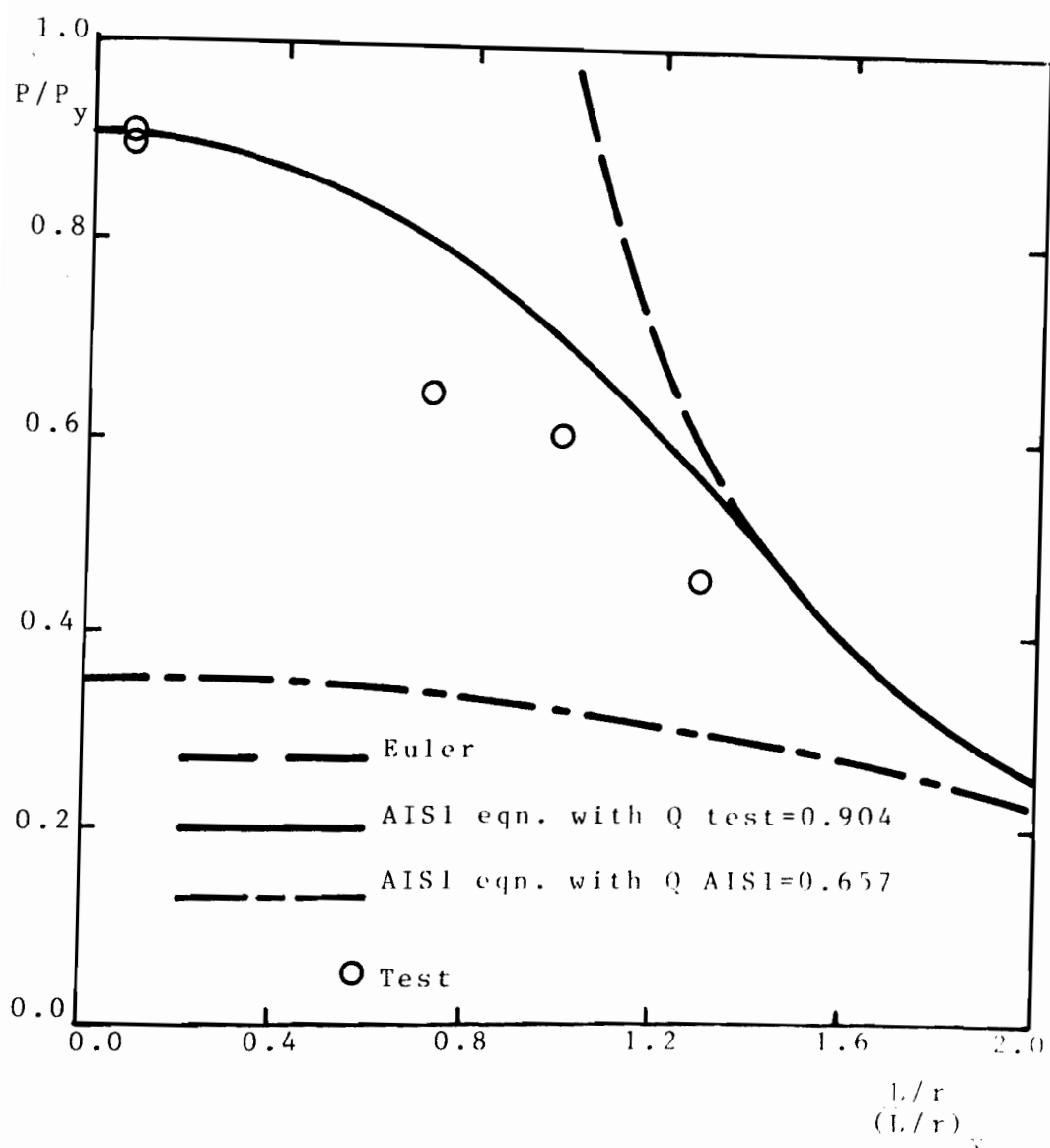


Fig. 4.4.5 COMPARISON OF TEST RESULTS AND THE AISI SPECIFICATION COLUMN CURVE - SPECIMENS LC-IV ($w/t=35.0$)

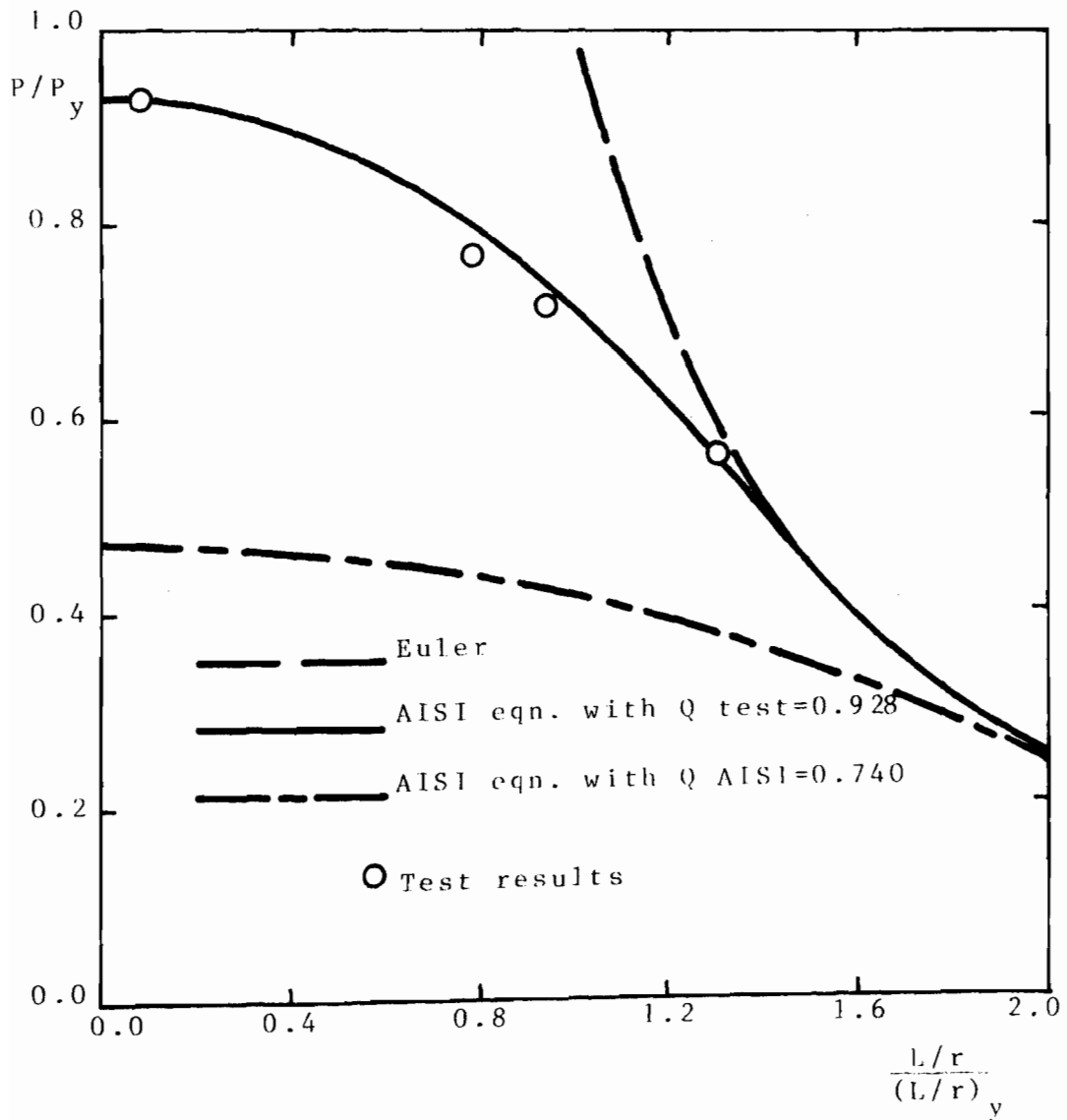


Fig. 4.4.6 COMPARISON OF TEST RESULTS AND THE AISI SPECIFICATION COLUMN CURVE - SPECIMENS LC-V ($w/t = 29.5$)

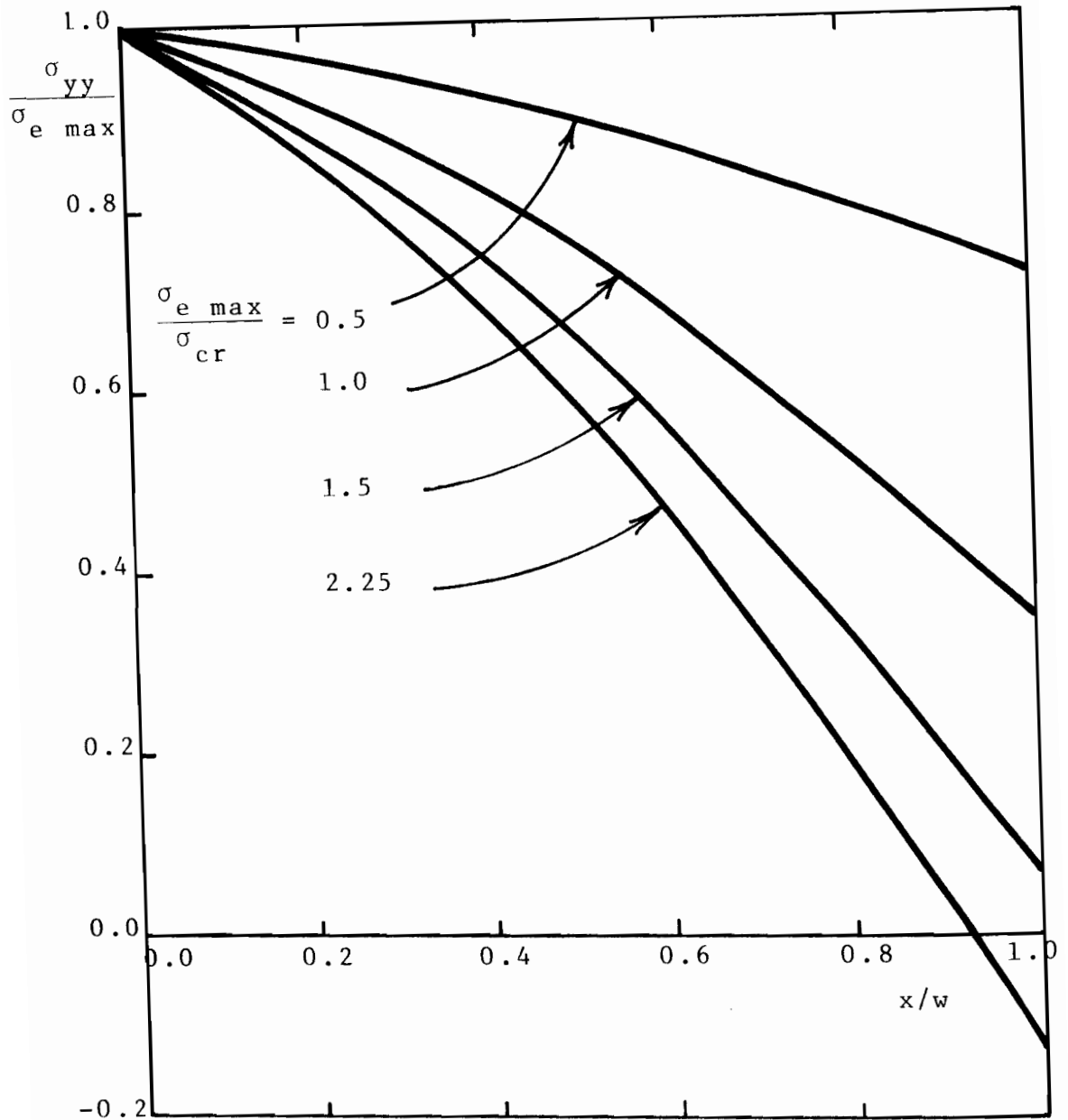
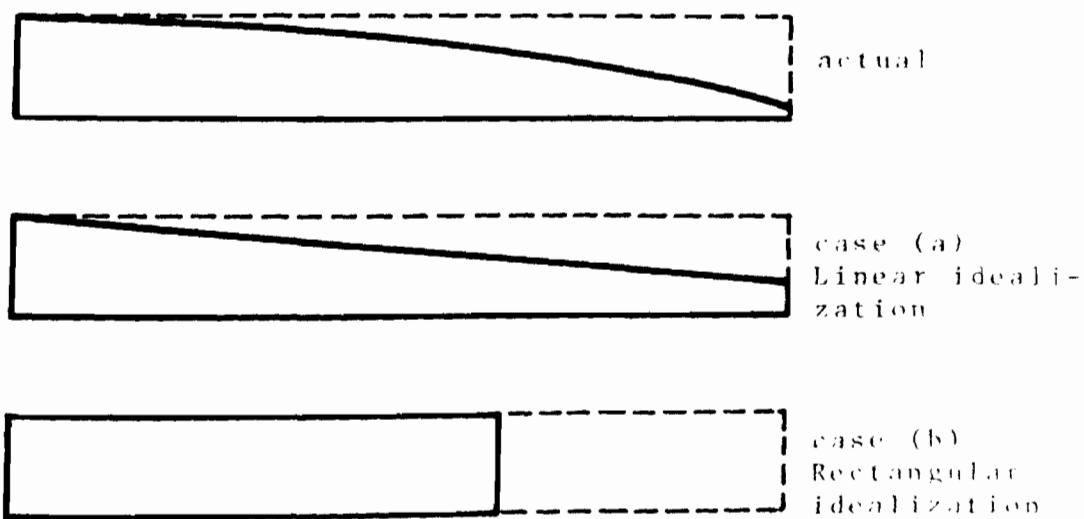
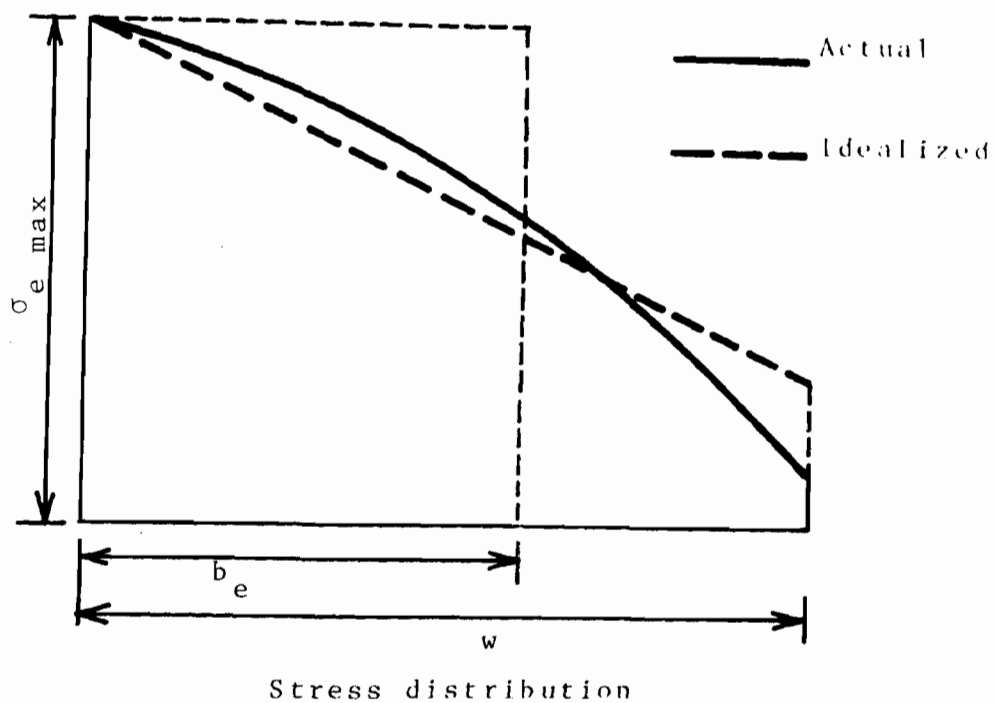
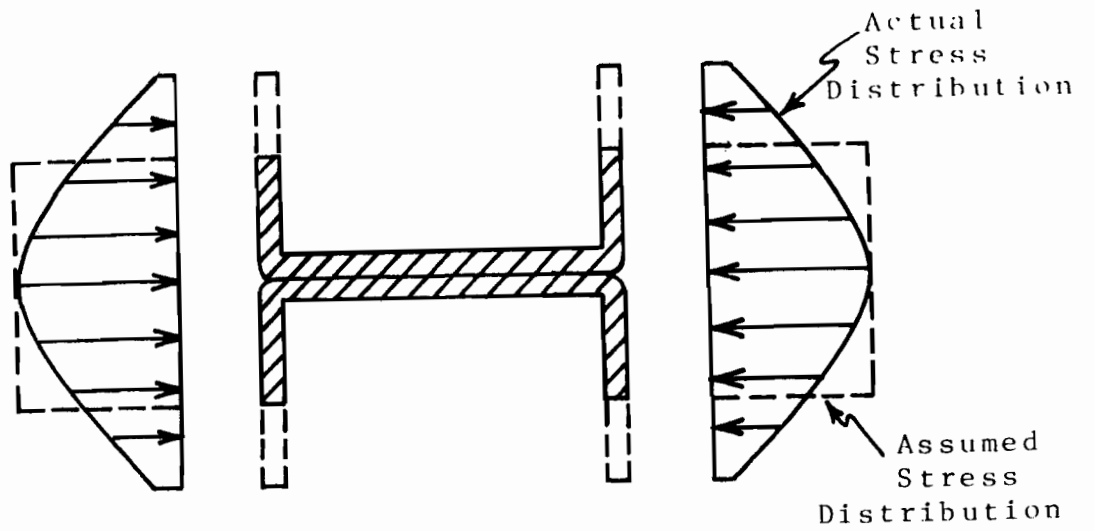


Fig. 4.4.7 TYPICAL COMPRESSIVE STRESS REDISTRIBUTION IN LOCALLY BUCKLING UNSTIFFENED ELEMENTS SPECIMEN LC-1 ($w/t = 57.5$)

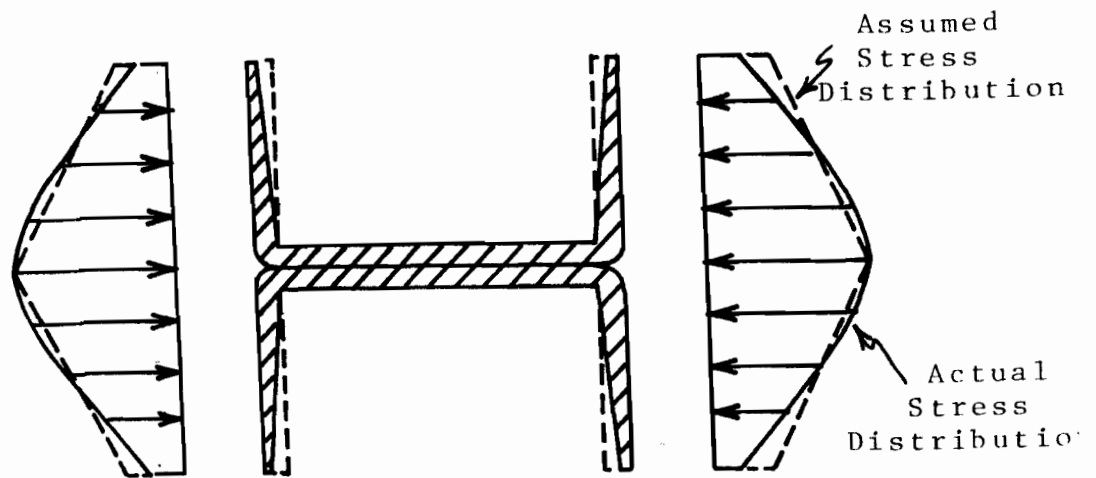


Distribution of the effective area

Fig. 4.4.8 IDEALIZATION OF EFFECTIVE AREA OF UNSTIFFENED ELEMENTS IN THE POSTBUCKLING RANGE



(a) Effective web areas located at web end of flange



(b) Effective web areas distributed linearly through web

Fig. 4.4.9 EFFECTIVE SECTIONS AND STRESS DISTRIBUTIONS FOR COLUMN SPECIMENS

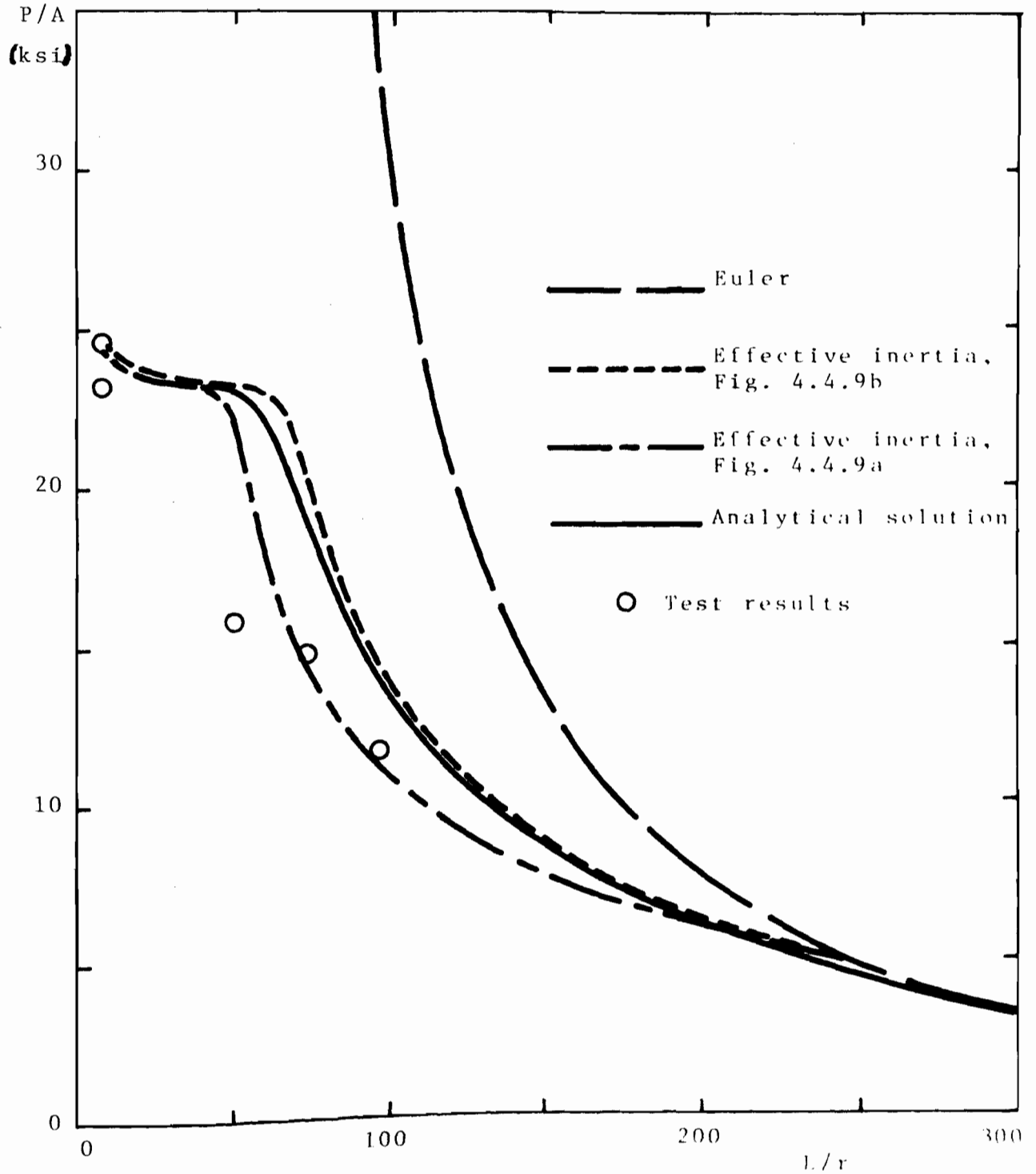


Fig. 4.4.10 COMPARISON OF TEST RESULTS, THE ANALYTICAL SOLUTION AND EFFECTIVE WIDTH EQUATION (EQN. 3.4.1) COLUMN CURVES - SPECIMENS LC-1 ($w/t = 59.5$)

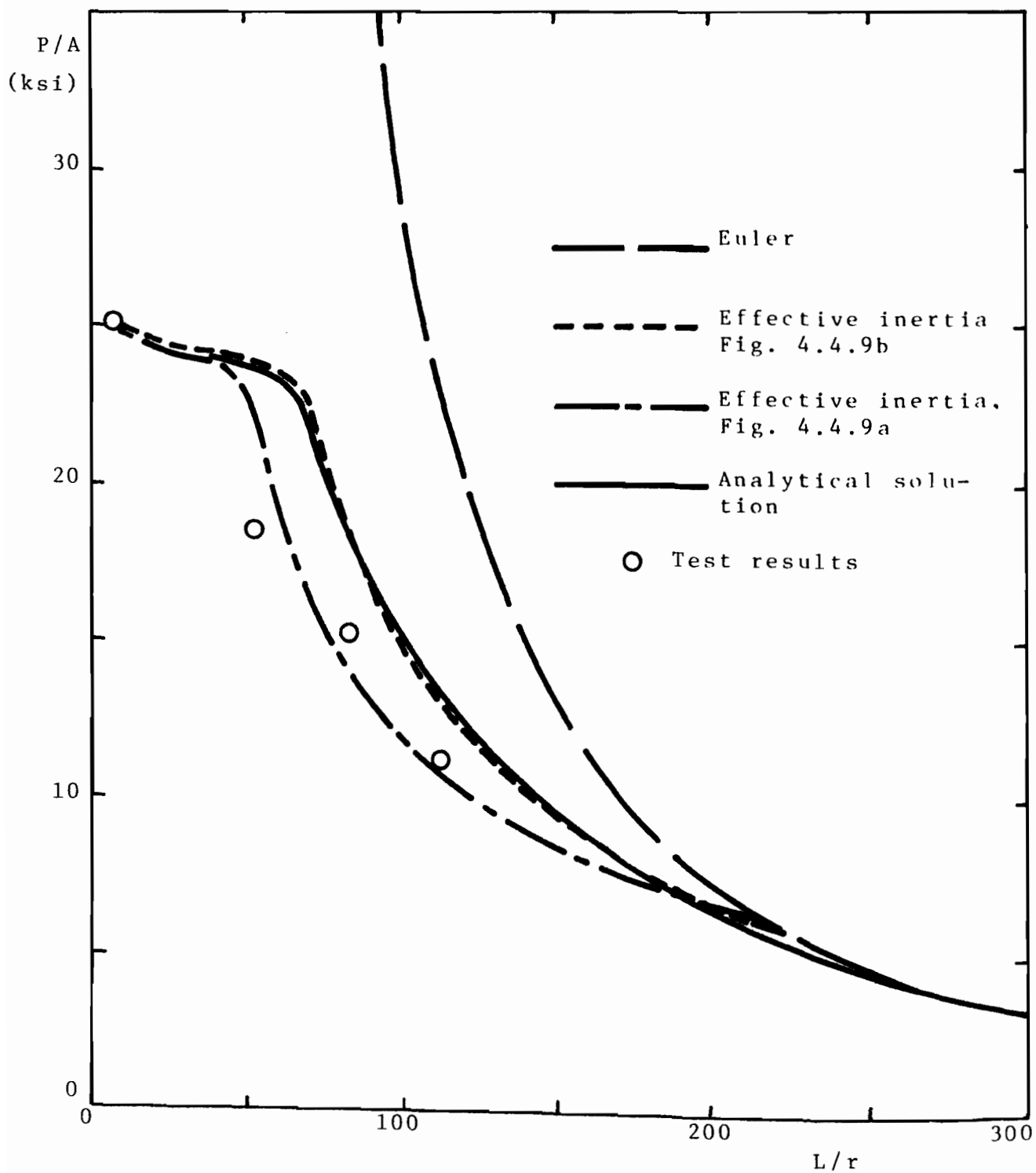


Fig. 4.4.11 COMPARISON OF TEST RESULTS, THE ANALYTICAL SOLUTION AND EFFECTIVE WIDTH EQUATION (EQN. 3.4.1) COLUMN CURVES—SPECIMENS LC-II ($w/t = 50.5$)

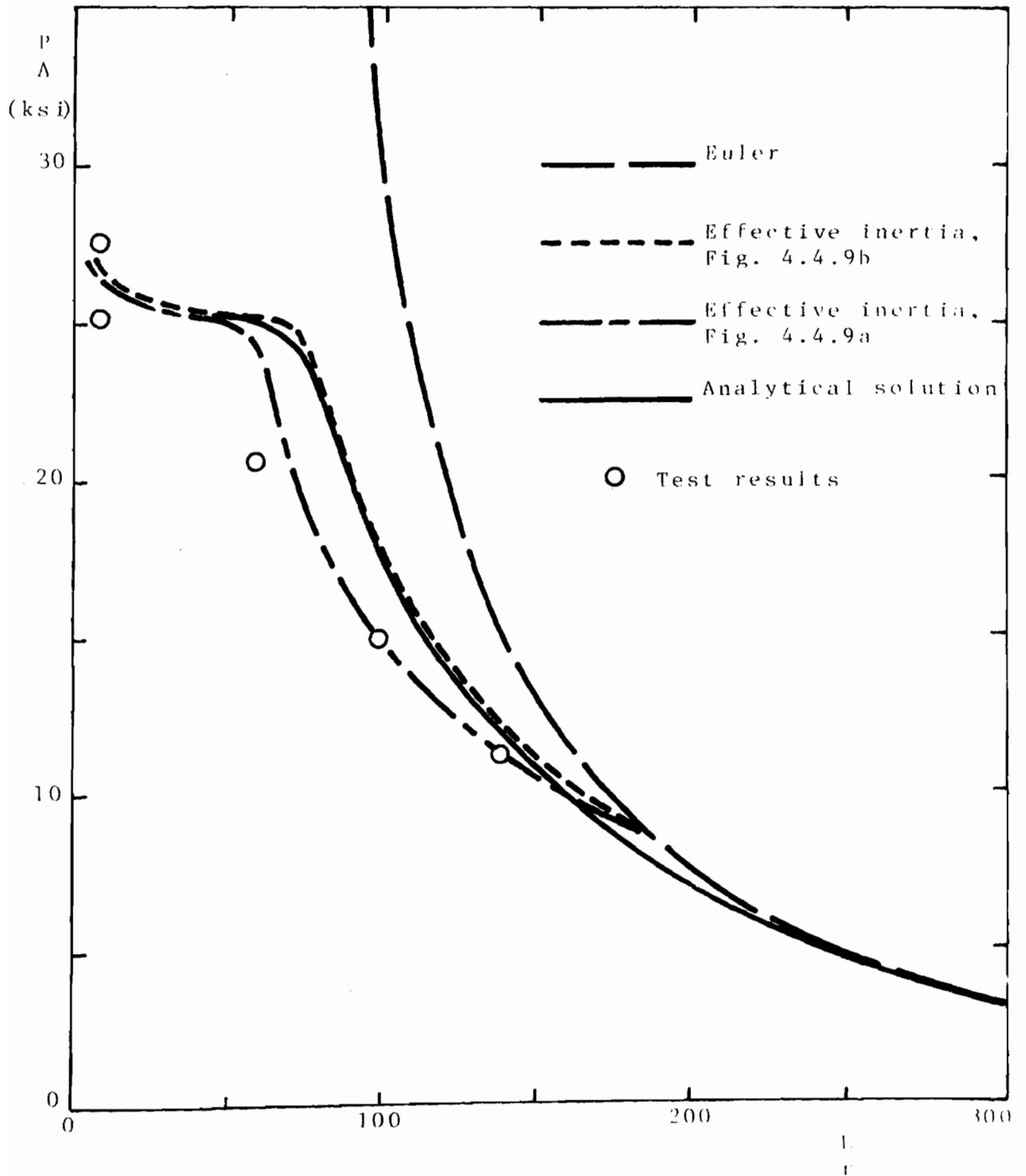


Fig. 4.4.12 COMPARISON OF TEST RESULTS, THE ANALYTICAL SOLUTION AND EFFECTIVE WIDTH EQUATION (EQN. 3.4.1) COLUMN CURVES - SPECIMENS LC-III ($w/t = 42.0$)

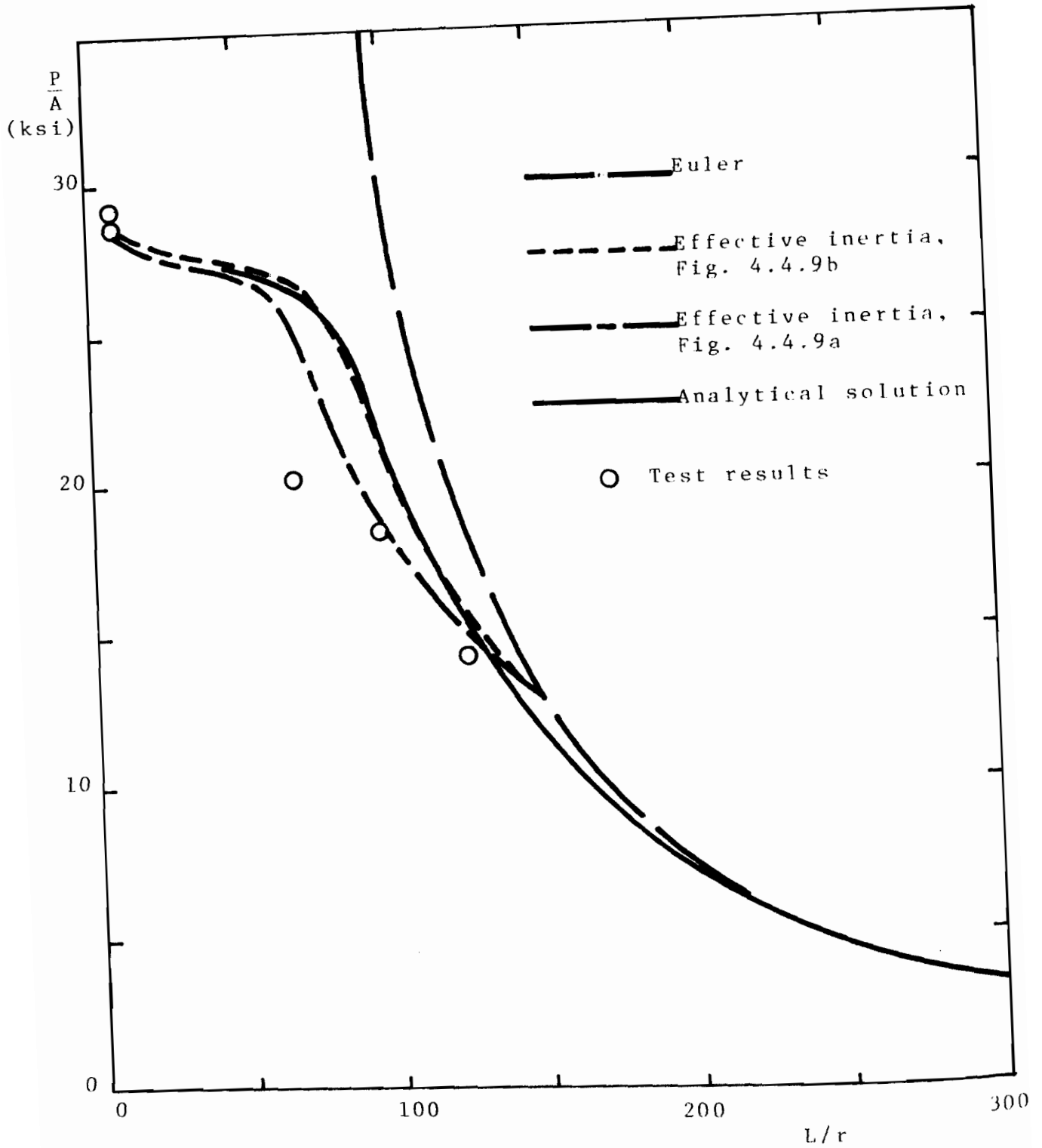


Fig. 4.4.13 COMPARISON OF TEST RESULTS, THE ANALYTICAL SOLUTION AND EFFECTIVE WIDTH EQUATION (EQN. 3.4.1) COLUMN CURVES - SPECIMENS LC-IV ($w/t = 35.0$)

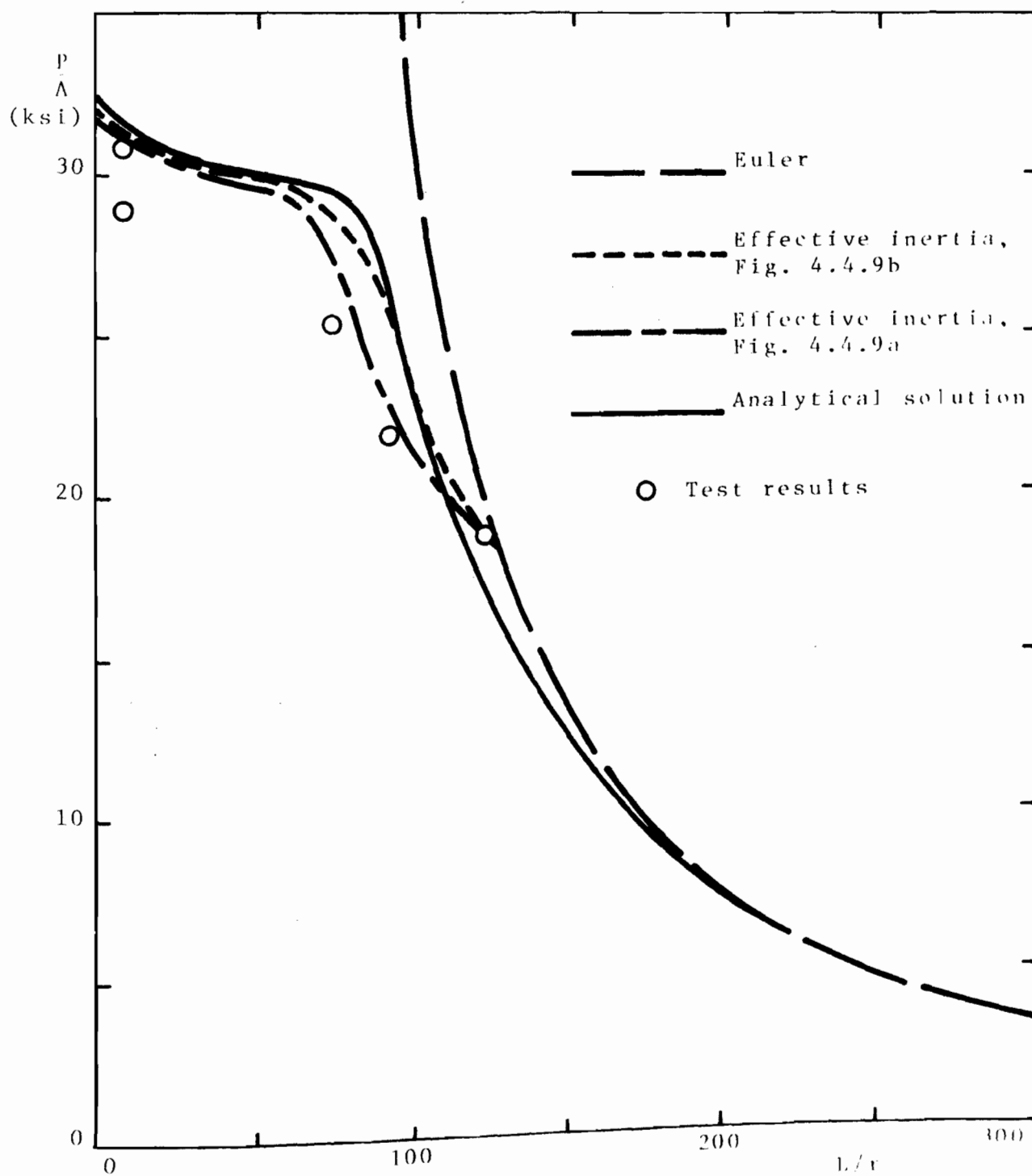


Fig. 4.4.14 COMPARISON OF TEST RESULTS, THE ANALYTICAL SOLUTION AND EFFECTIVE WIDTH EQUATION (CON. 3.4.1) COLUMN CURVES - SPECIMENS LC-V ($w/t = 29.5$)

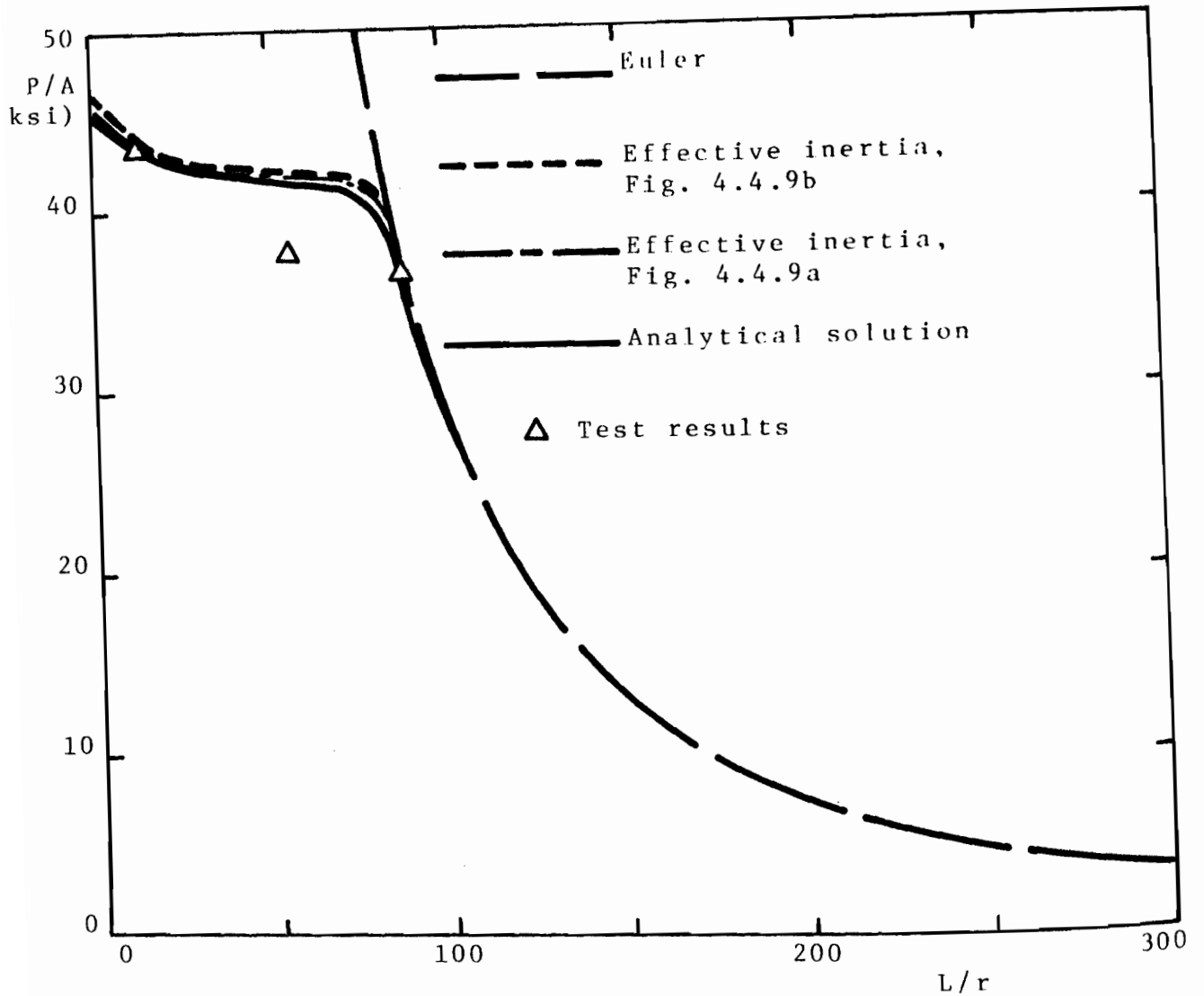


Fig. 4.4.15 COMPARISON OF TEST RESULTS, THE ANALYTICAL SOLUTION AND EFFECTIVE WIDTH EQUATION (EQN. 3.4.1) COLUMN CURVES - SPECIMENS UD-1 ($w/t = 16.2$)

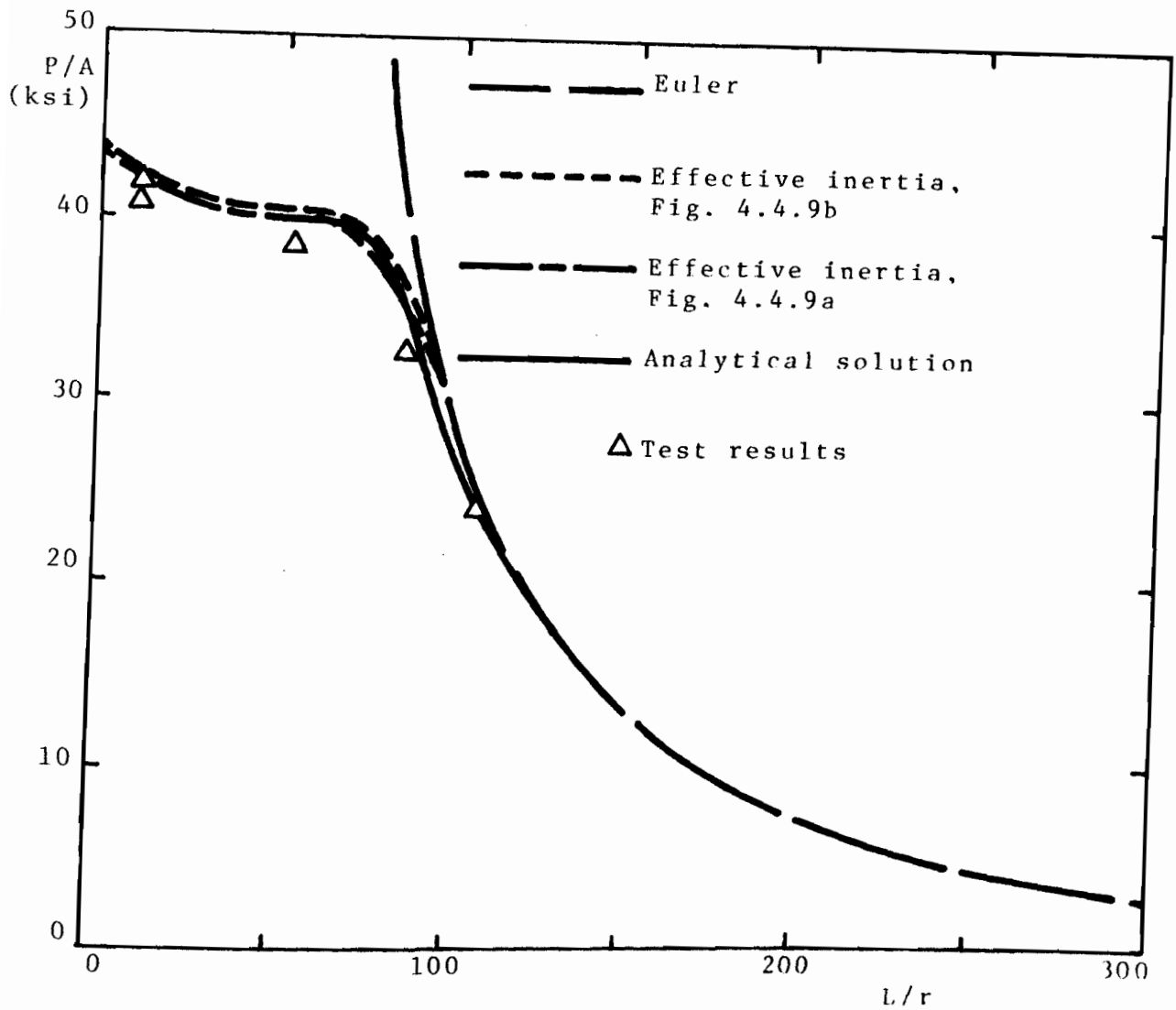


Fig. 4.4.16 COMPARISON OF TEST RESULTS, THE ANALYTICAL SOLUTION AND EFFECTIVE WIDTH EQUATION (EQN. 3.4.1) COLUMN CURVES - SPECIMENS UD-2 ($w/t = 20.5$)

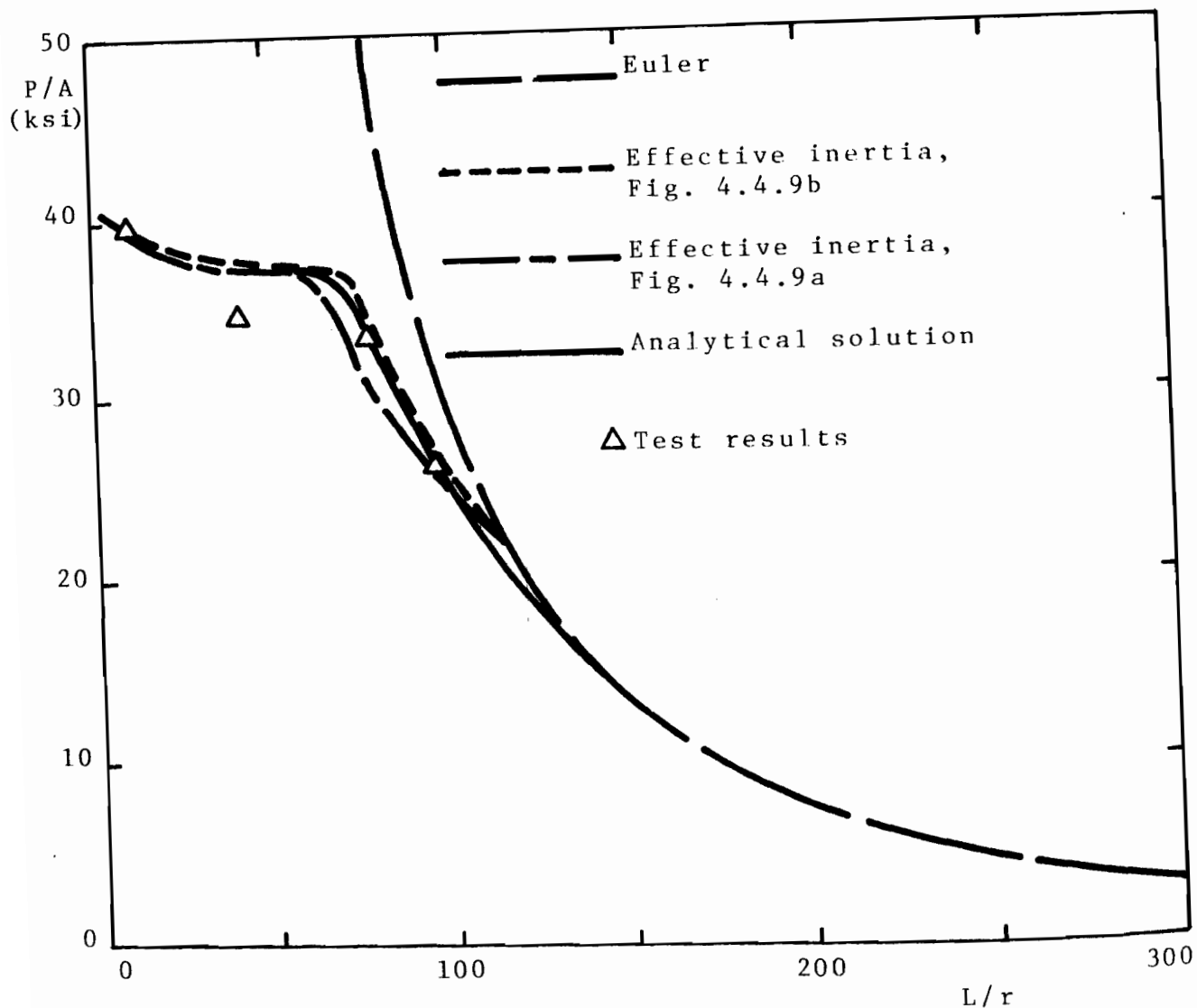


Fig. 4.4.17 COMPARISON OF TEST RESULTS, THE ANALYTICAL SOLUTION AND EFFECTIVE WIDTH EQUATION (EQN. 3.4.1) COLUMN CURVES - SPECIMENS UD-3 ($w/t = 24.8$)

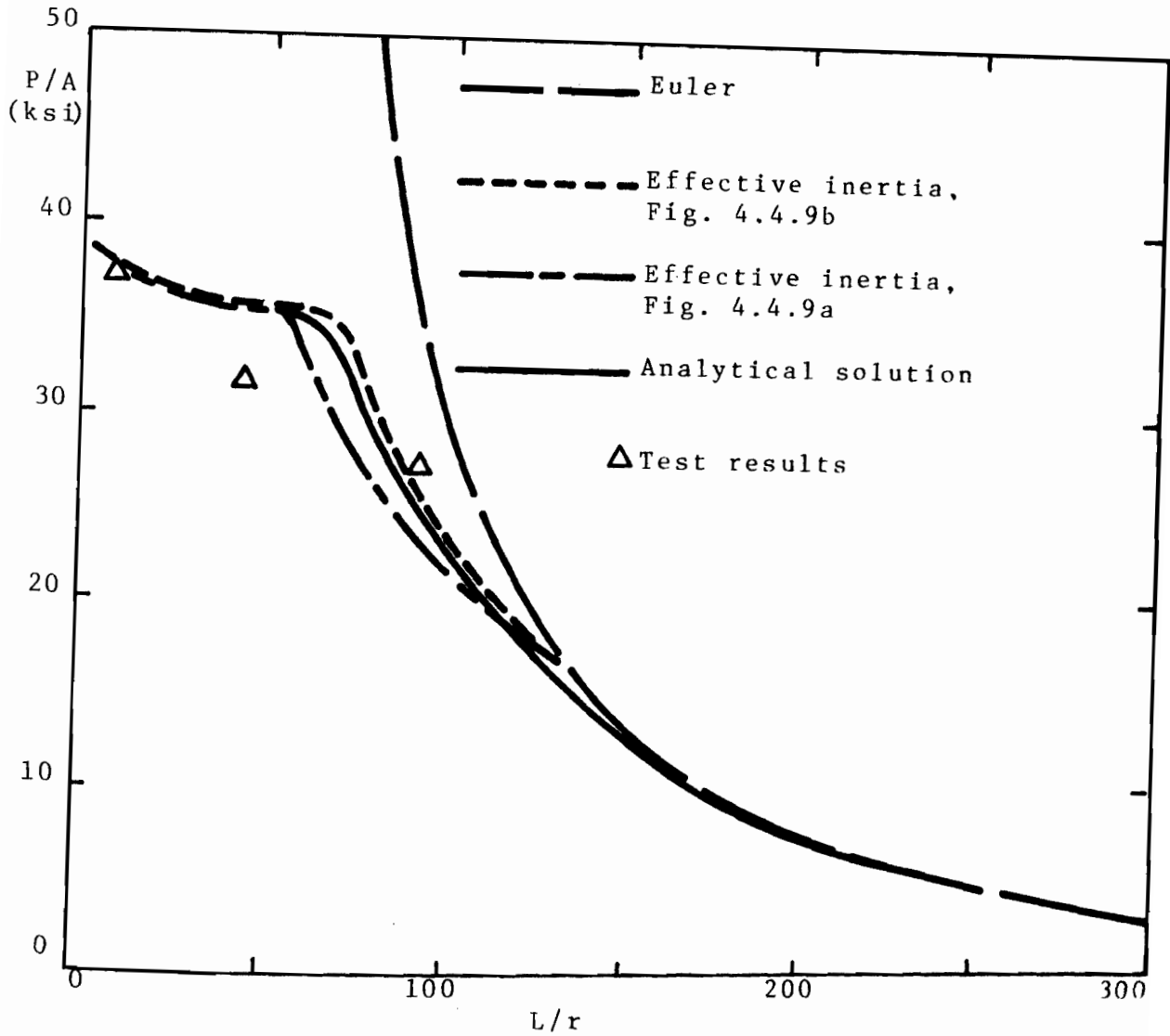


Fig. 4.4.18 COMPARISON OF TEST RESULTS, THE ANALYTICAL SOLUTION AND EFFECTIVE WIDTH EQUATION (EQN. 3.4.1) COLUMN CURVES - SPECIMENS UD-4 ($w/t = 29.1$)

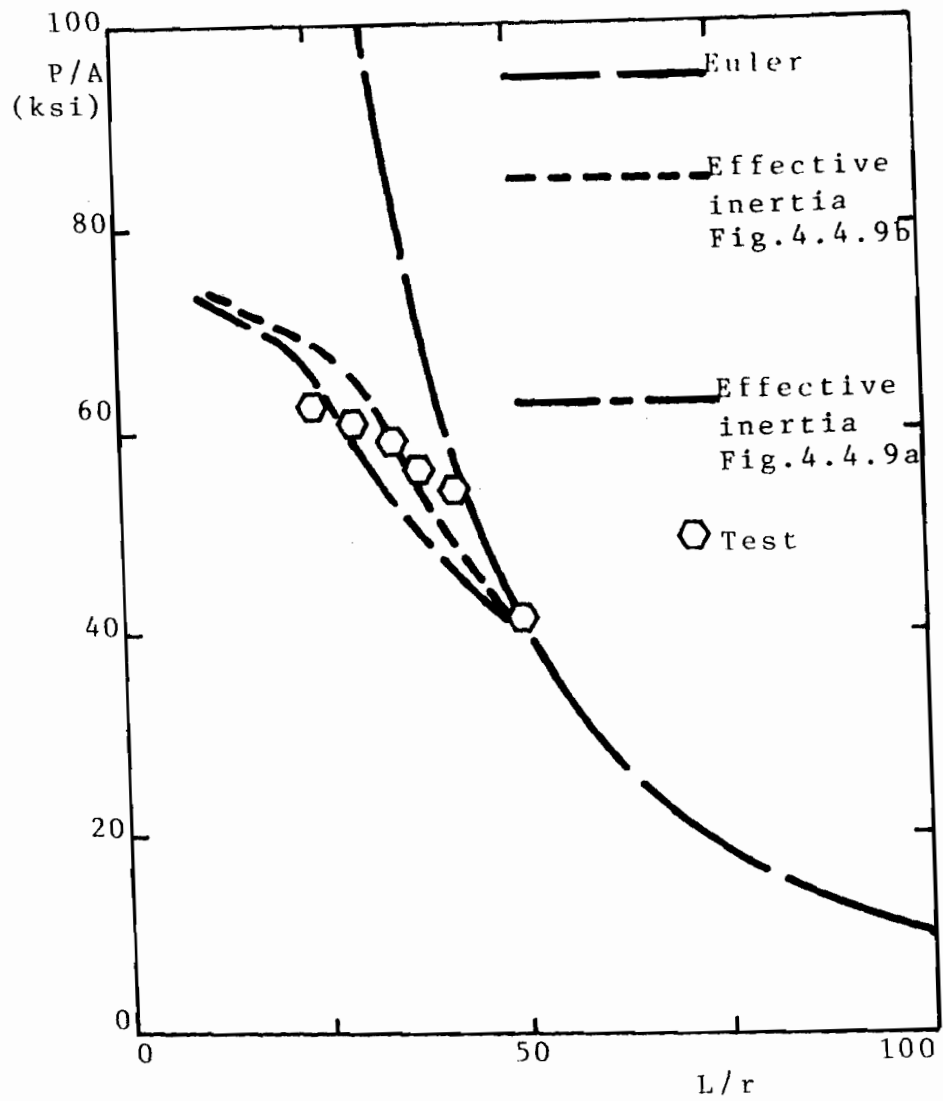


Fig. 4.4.19 COMPARISON OF TEST RESULTS AND THE EFFECTIVE WIDTH EQUATION (EQN. 3.4.1) COLUMN CURVES - ALUMINUM SPECIMENS J ($w/t = 10.5$)

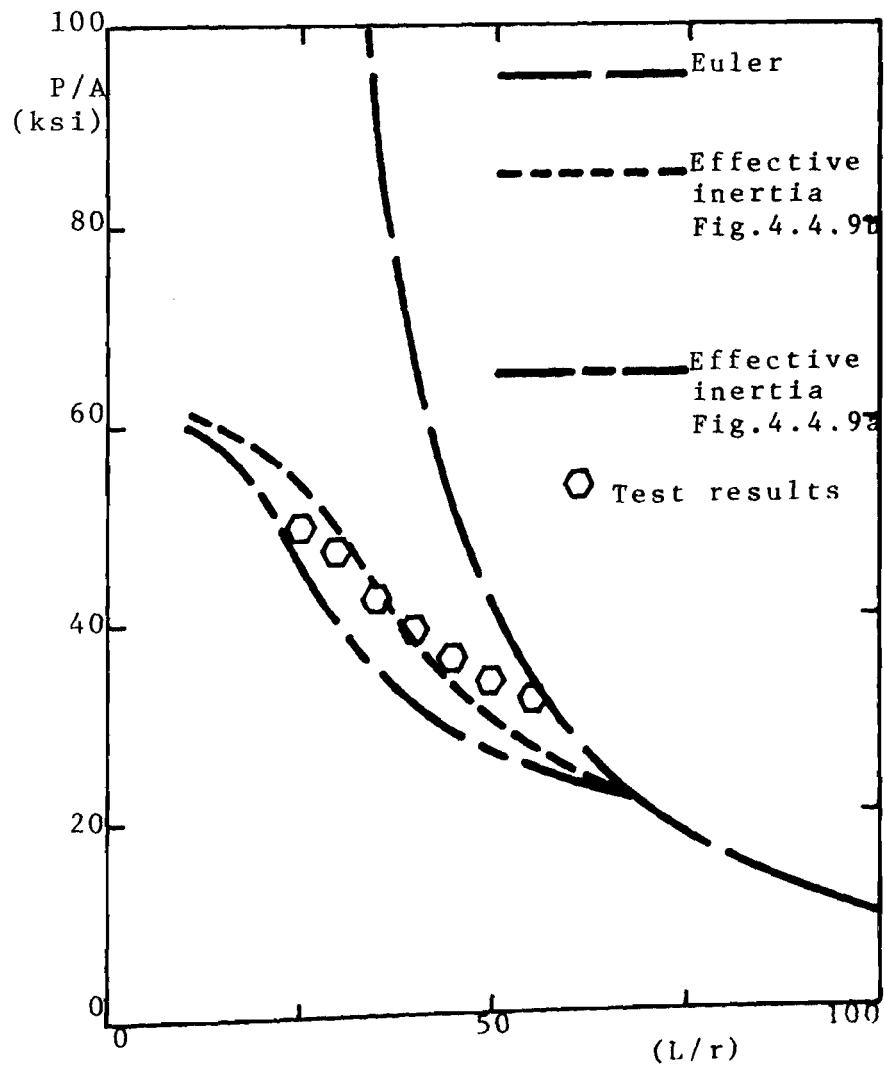


Fig. 4.4.20 COMPARISON OF TEST RESULTS AND THE EFFECTIVE WIDTH EQUATION (EQN. 3.4.1) COLUMN CURVES - ALUMINUM SPECIMENS K ($w/t = 14.3$)

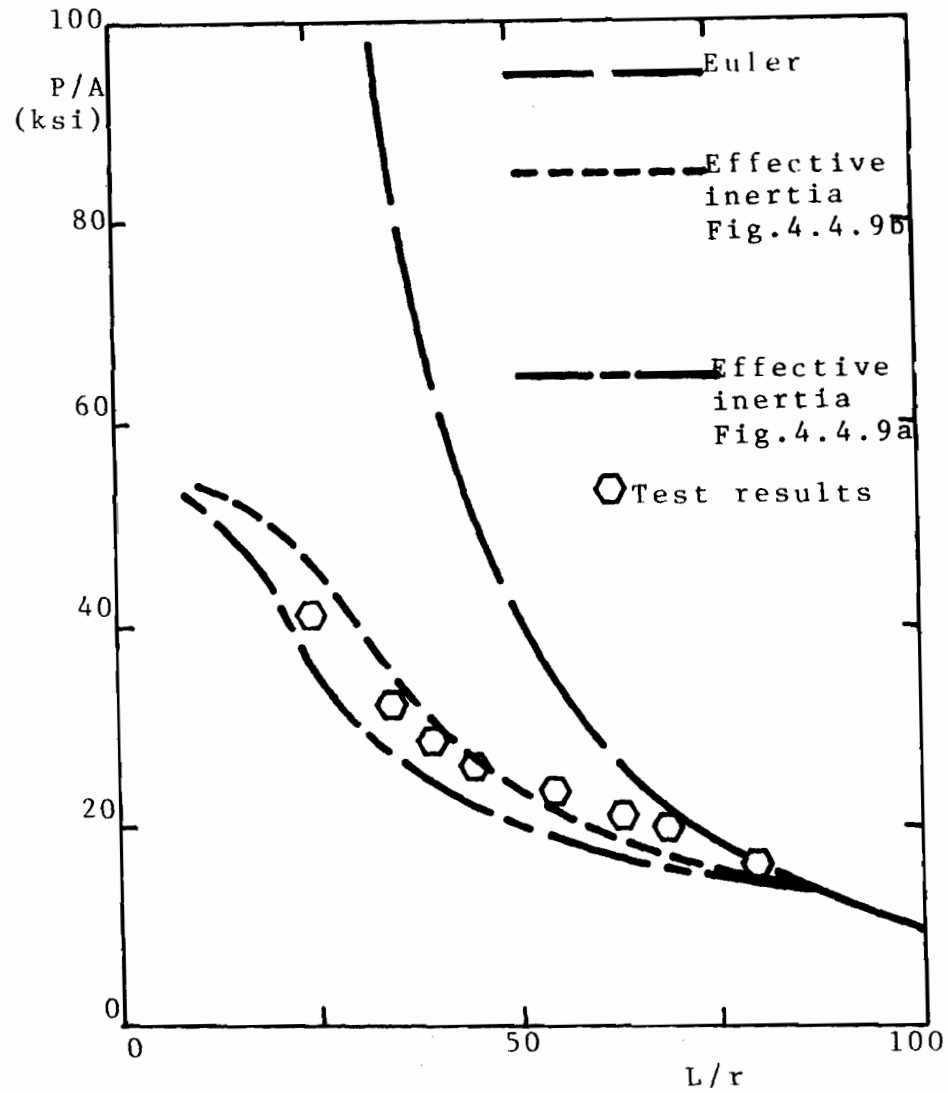


Fig. 4.4.21 COMPARISON OF TEST RESULTS AND THE EFFECTIVE WIDTH EQUATION (EQN. 3.4.1) COLUMN CURVES - ALUMINUM SPECIMENS L ($w/t = 18.1$)

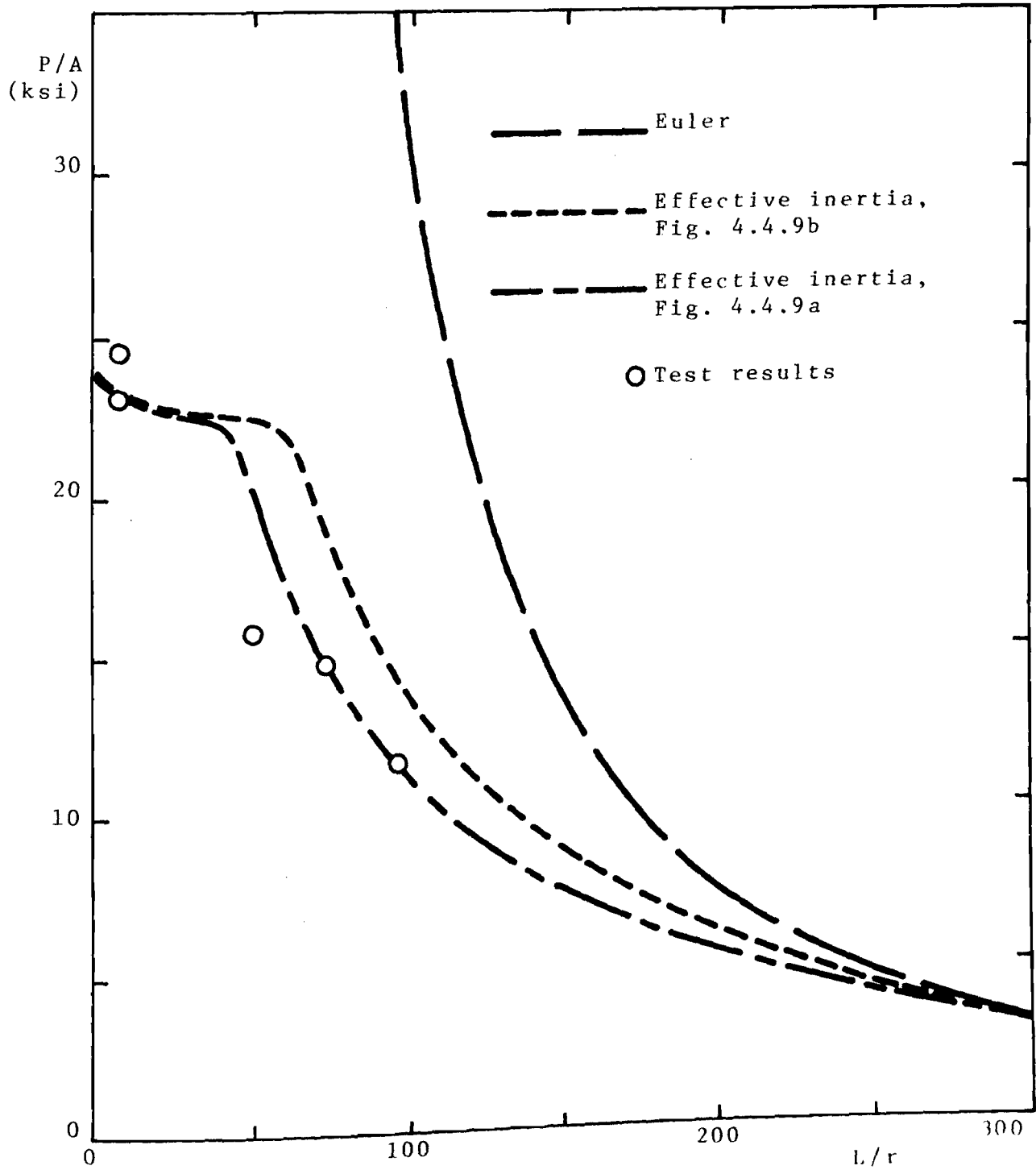


Fig. 4.4.22 COMPARISON OF TEST RESULTS AND THE EFFECTIVE WIDTH EQUATION (EQN. 3.4.5) COLUMN CURVES - SPECIMENS LC-1 ($w/t = 57.5$)

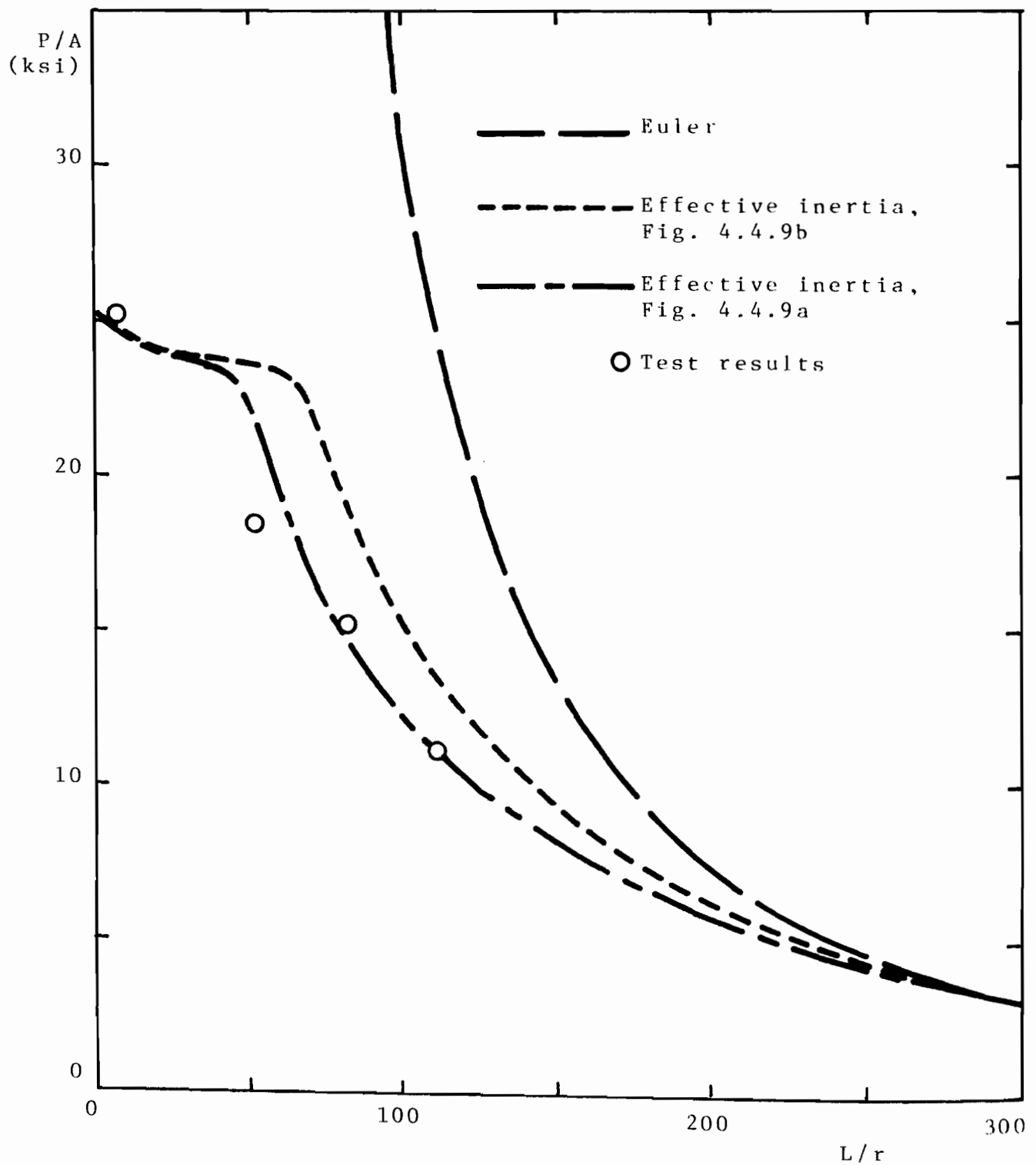


Fig. 4.4.23 COMPARISON OF TEST RESULTS AND THE EFFECTIVE WIDTH EQUATION (EQN. 3.4.5) COLUMN CURVES - SPECIMENS LC-II ($w/t = 50.5$)

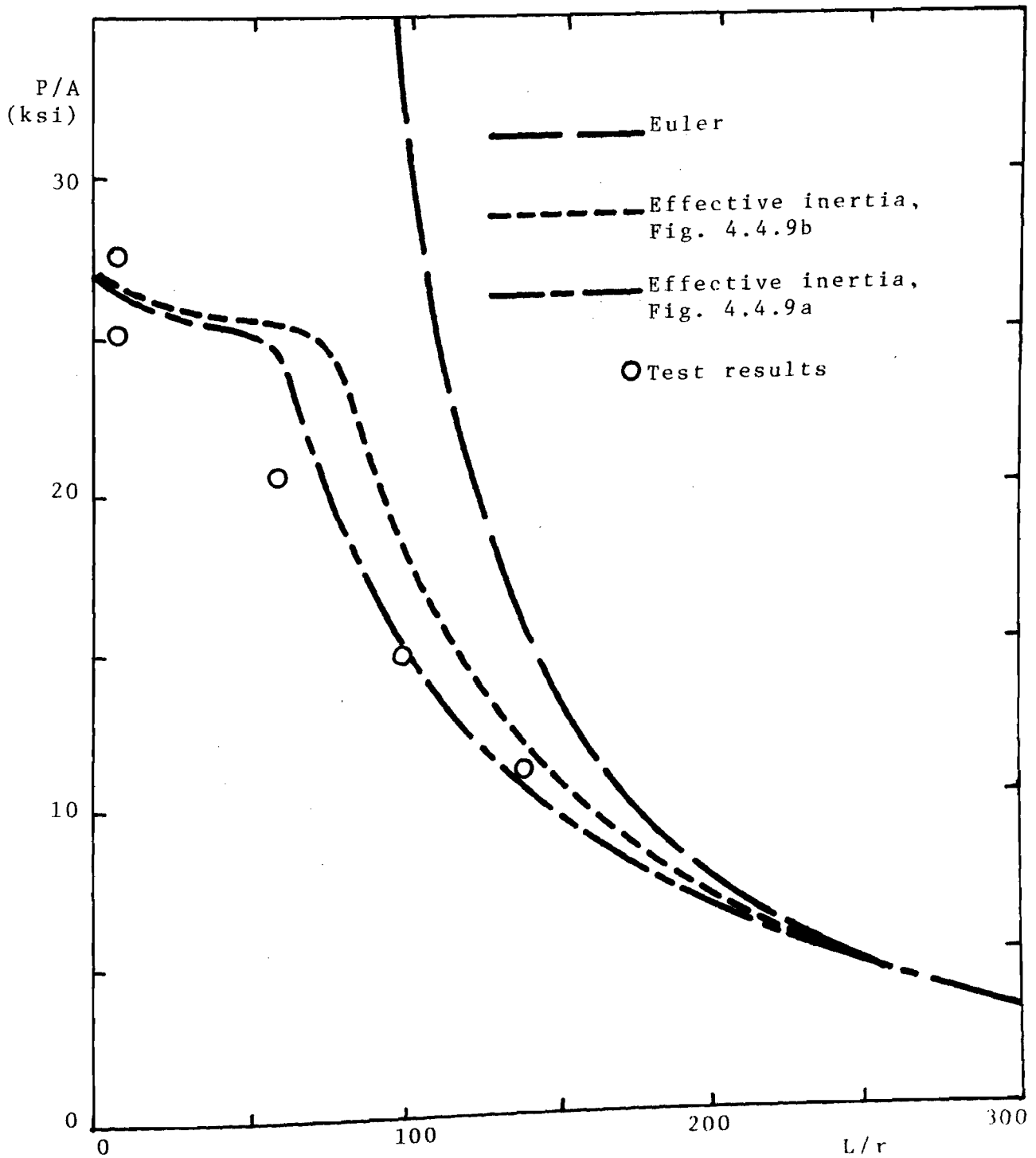


Fig. 4.4.24 COMPARISON OF TEST RESULTS AND THE EFFECTIVE WIDTH EQUATION (EQN. 3.4.5) COLUMN CURVES - SPECIMENS LC-III ($w/t = 42.0$)

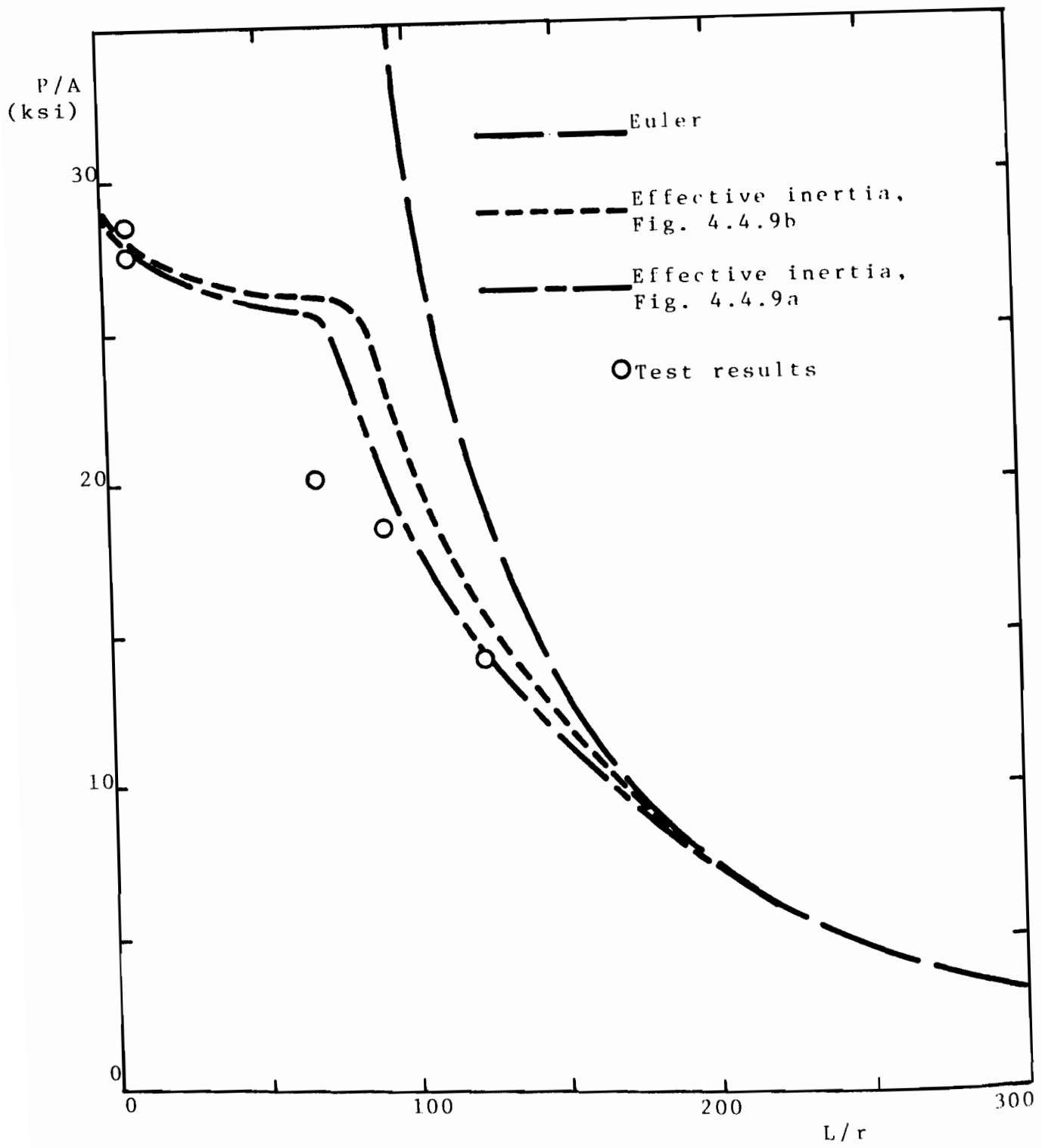


Fig. 4.4.25 COMPARISON OF TEST RESULTS AND THE EFFECTIVE WIDTH EQUATION (EQN. 3.4.5) COLUMN CURVES - SPECIMENS LC-IV ($w/t = 35.0$)

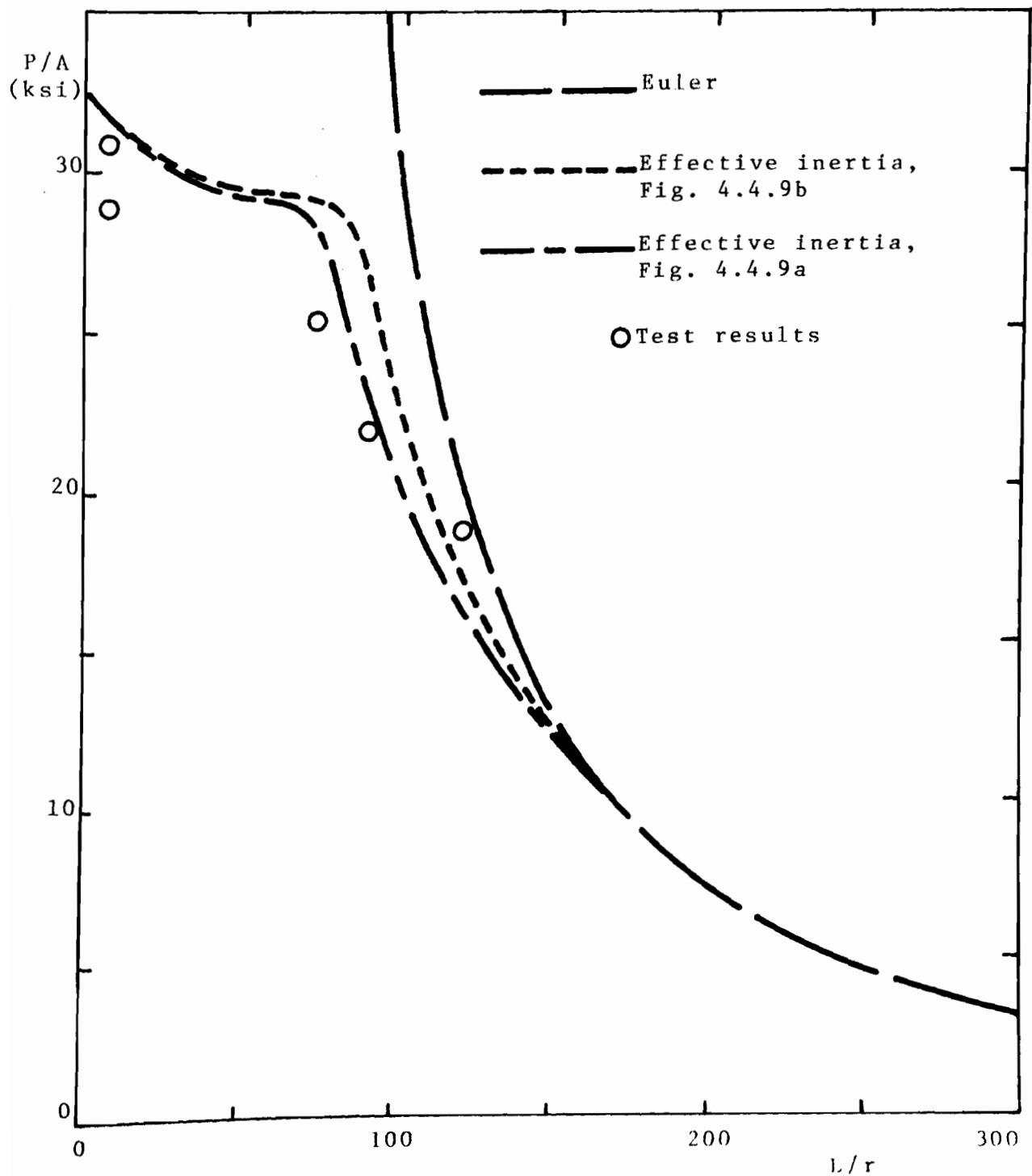


Fig. 4.4.26 COMPARISON OF TEST RESULTS AND THE EFFECTIVE WIDTH EQUATION (EQN. 3.4.5) COLUMN CURVES - SPECIMENS LC-V ($w/t = 29.5$)

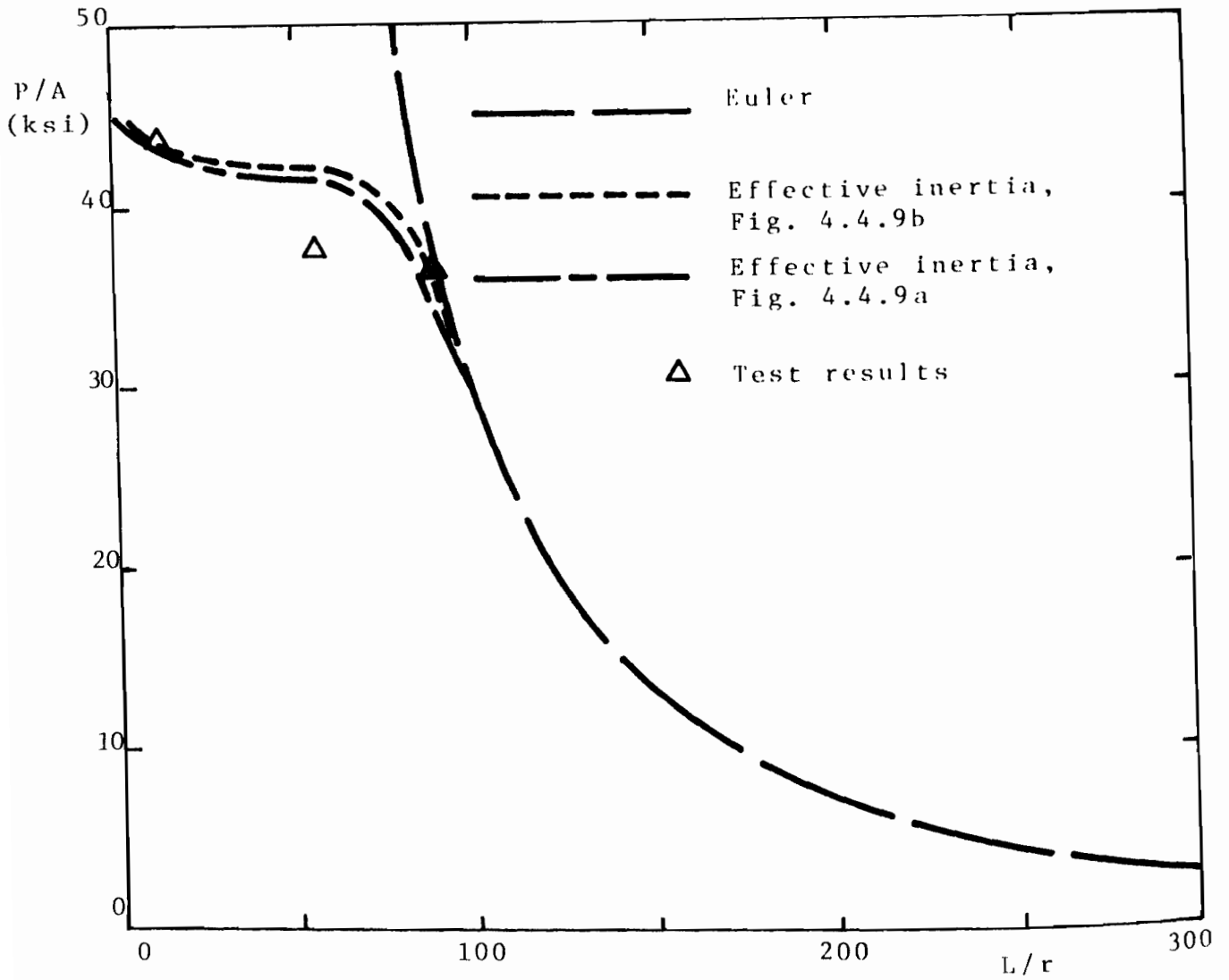


Fig. 4.4.27 COMPARISON OF TEST RESULTS AND THE EFFECTIVE WIDTH EQUATION (EQN. 3.4.5) COLUMN CURVES - SPECIMENS UD-1 ($w/t = 16.2$)

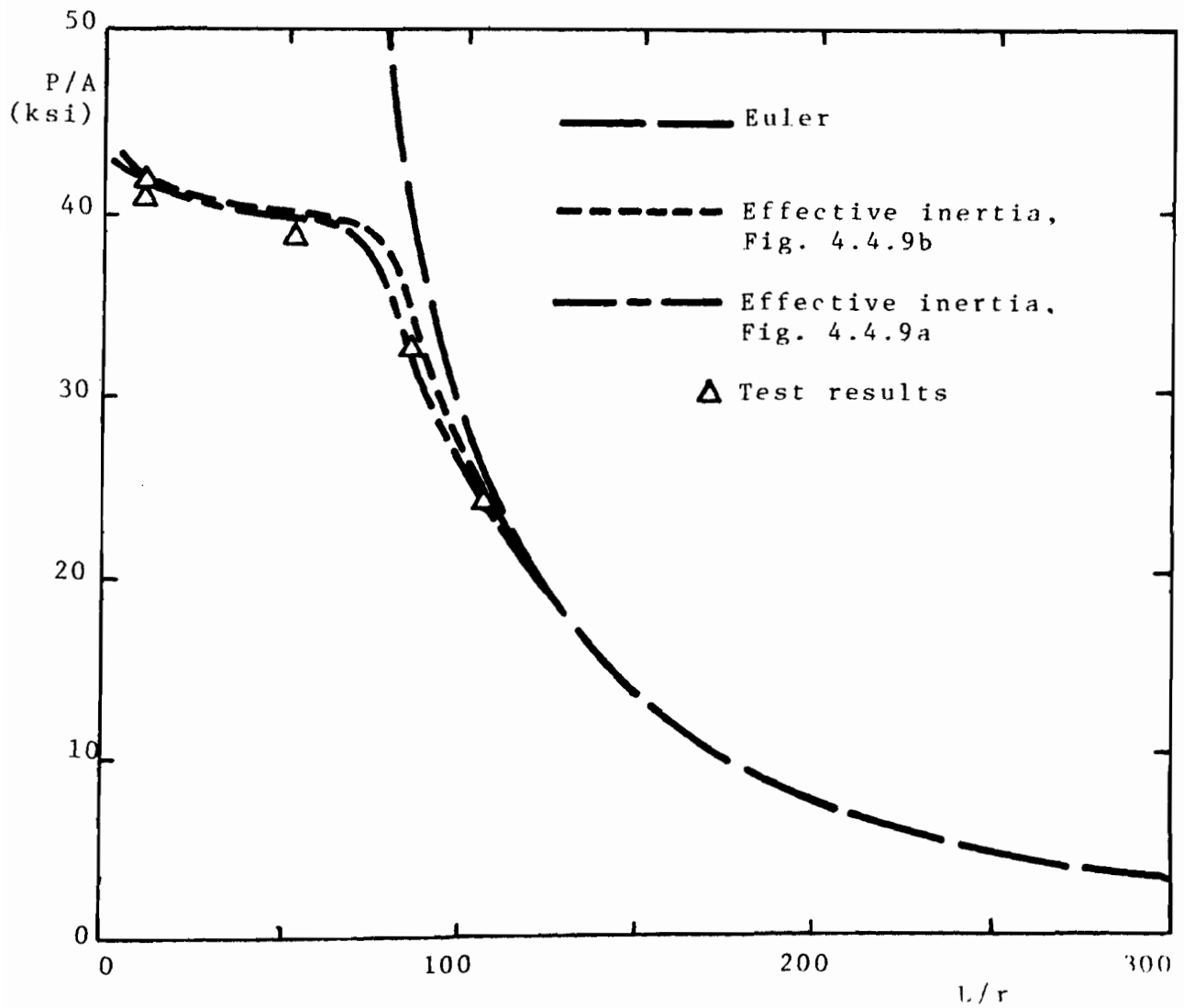


Fig. 4.4.28 COMPARISON OF TEST RESULTS AND THE EFFECTIVE WIDTH EQUATION (EQN. 3.4.5) COLUMN CURVES - SPECIMENS UD-2 ($w/t = 20.5$)

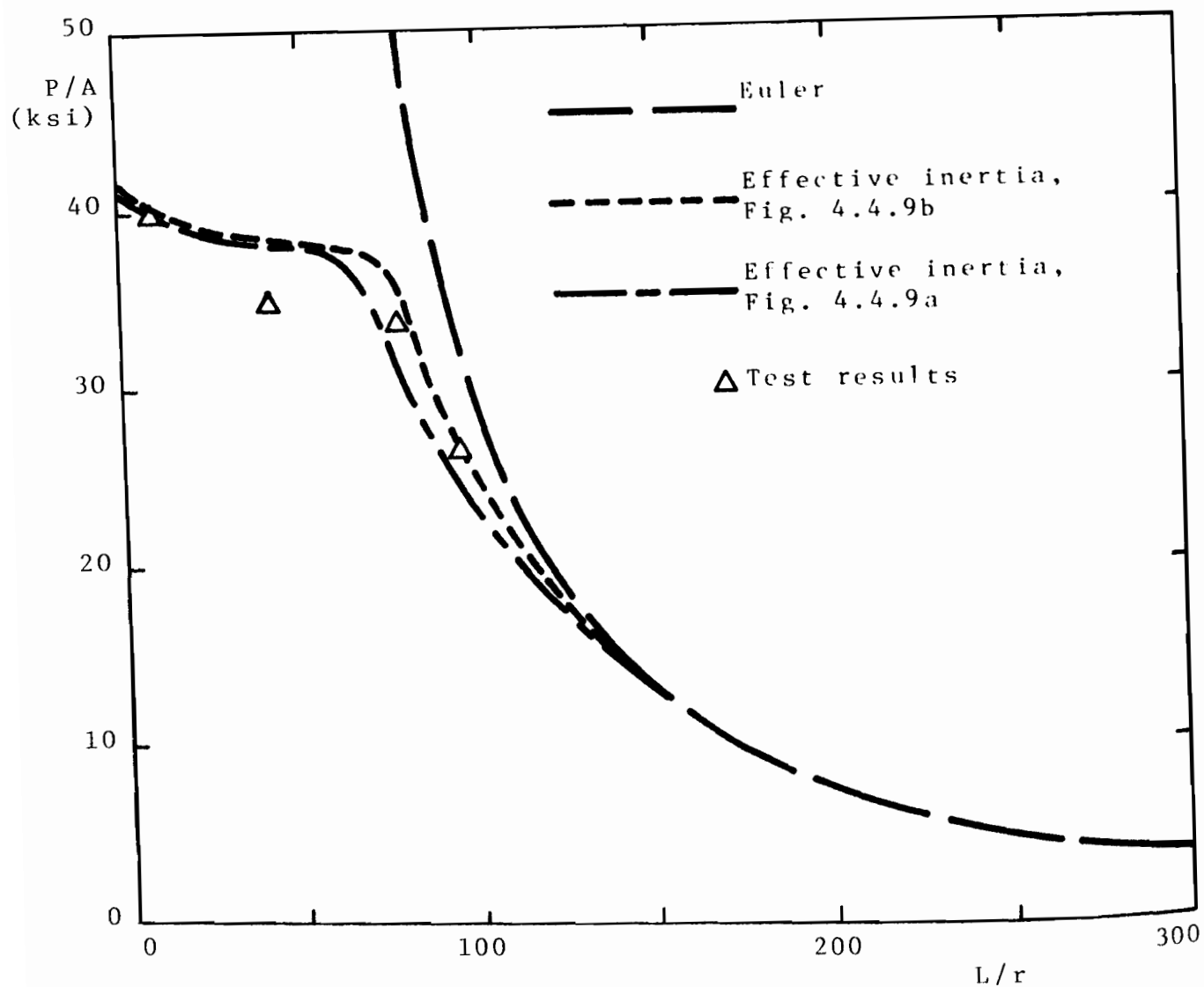


Fig. 4.4.29 COMPARISON OF TEST RESULTS AND THE EFFECTIVE WIDTH EQUATION (EQN. 3.4.5) COLUMN CURVES - SPECIMENS UD-3 ($w/t = 24.8$)

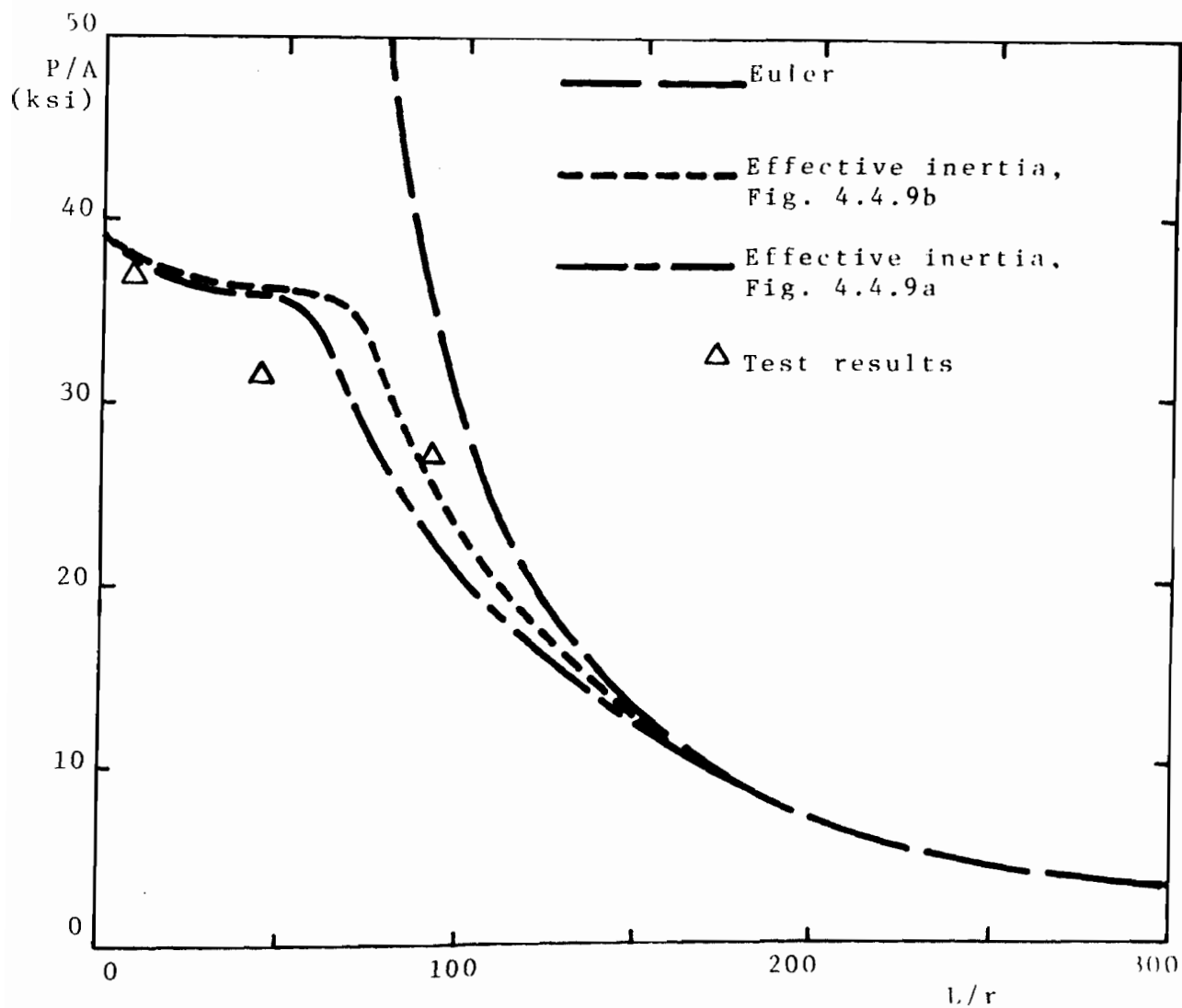


Fig. 4.4.30 COMPARISON OF TEST RESULTS AND THE EFFECTIVE WIDTH EQUATION (EQN. 3.4.5) COLUMN CURVES - SPECIMENS UD-4 ($w/t = 29.1$)

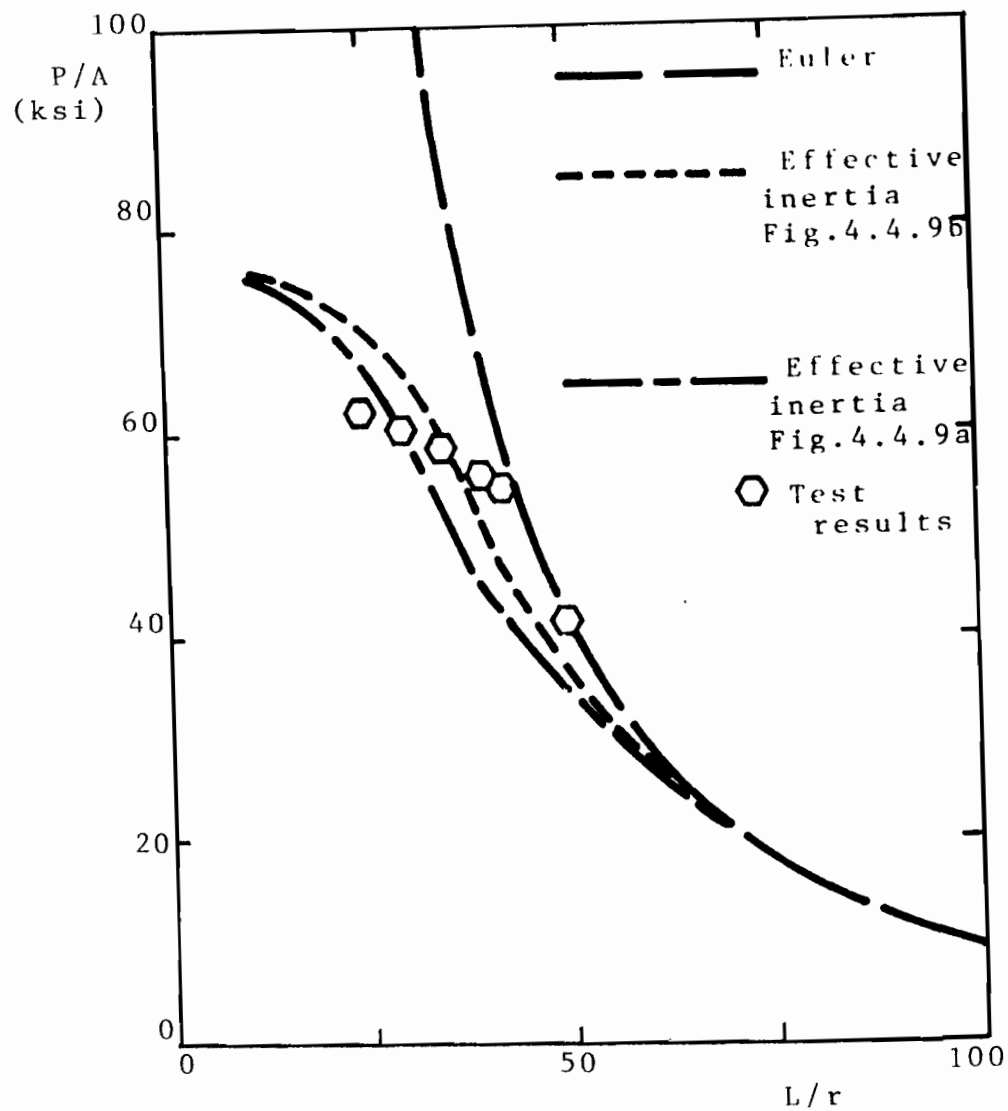


Fig. 4.4.31 COMPARISON OF TEST RESULTS AND THE EFFECTIVE WIDTH EQUATION (EQN. 3.4.5) COLUMN CURVES - ALUMINUM SPECIMENS J ($w/t = 10.5$)

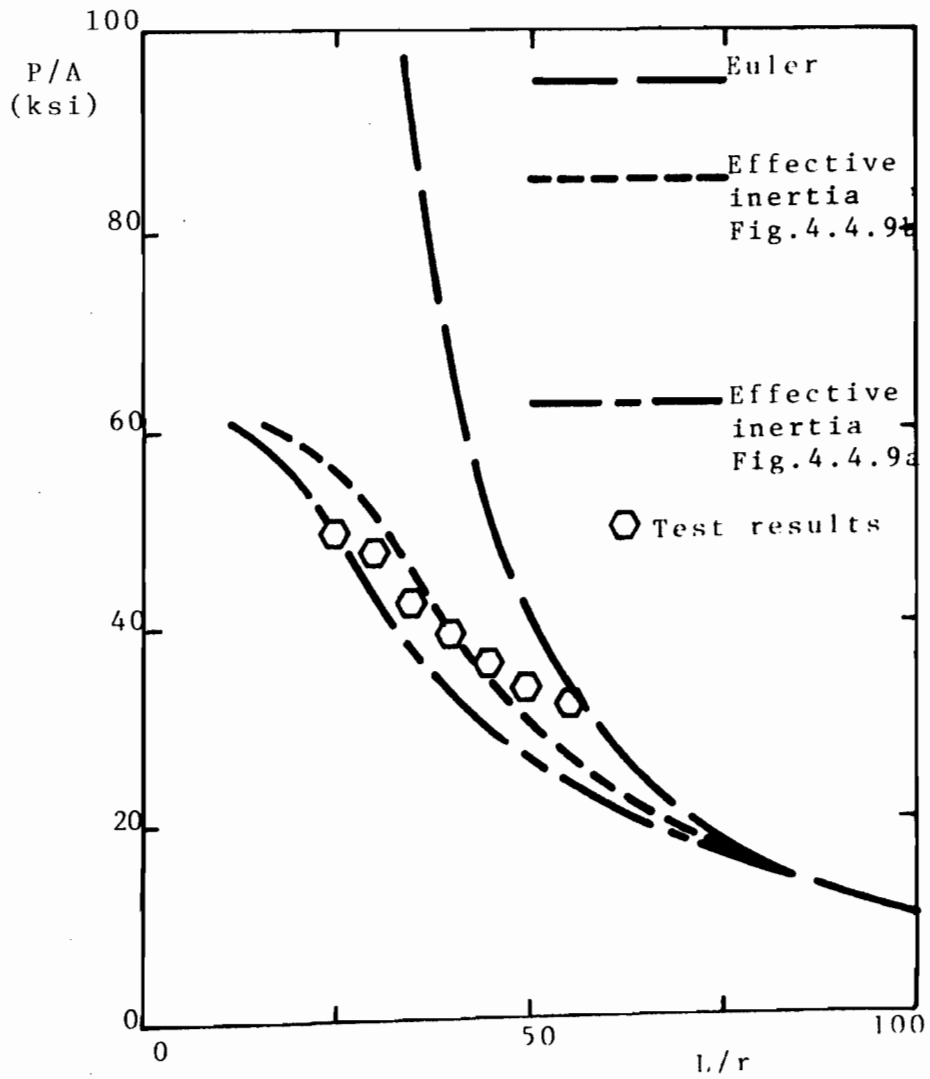


Fig. 4.4.32 COMPARISON OF TEST RESULTS AND THE EFFECTIVE WIDTH EQUATION (EQN. 3.4.5) COLUMN CURVES - ALUMINUM SPECIMENS K ($w/t = 14.3$)

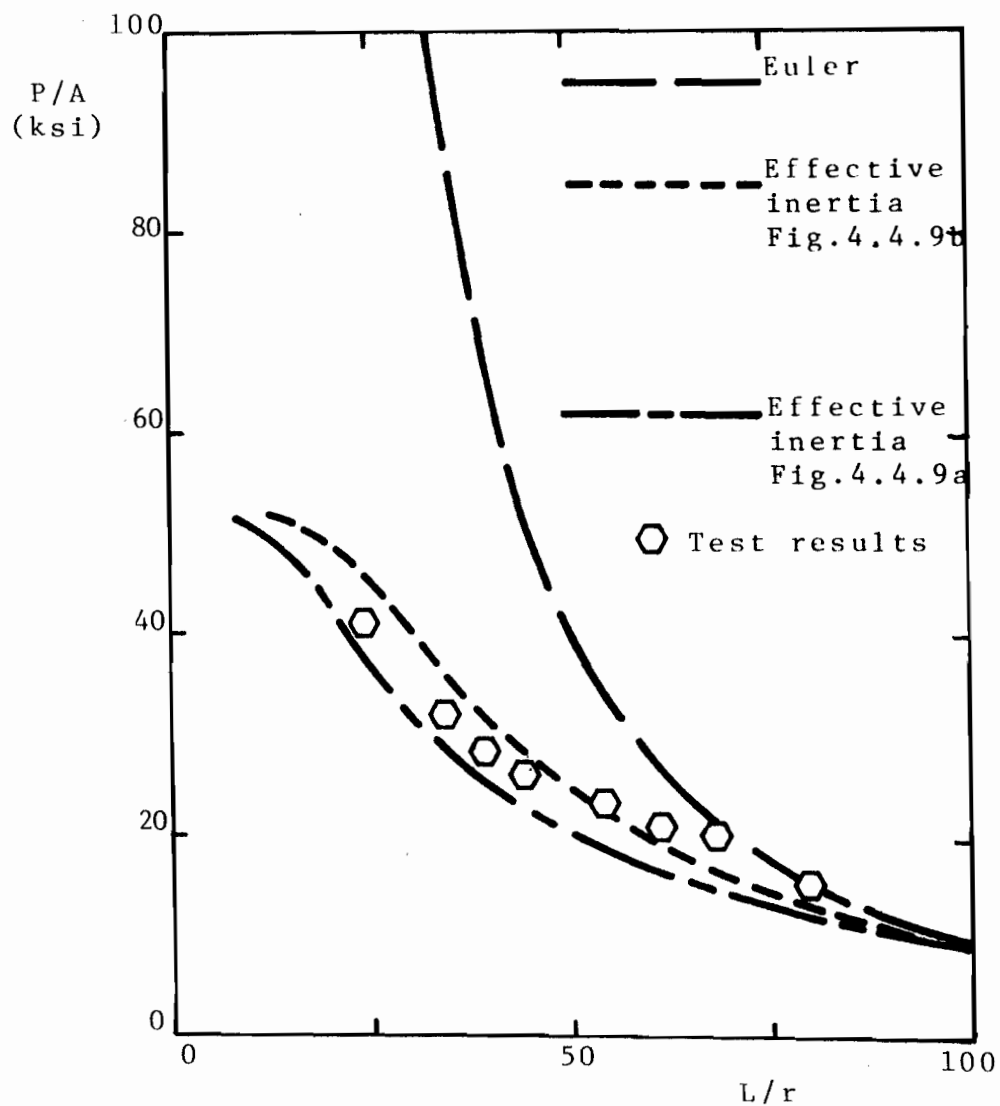
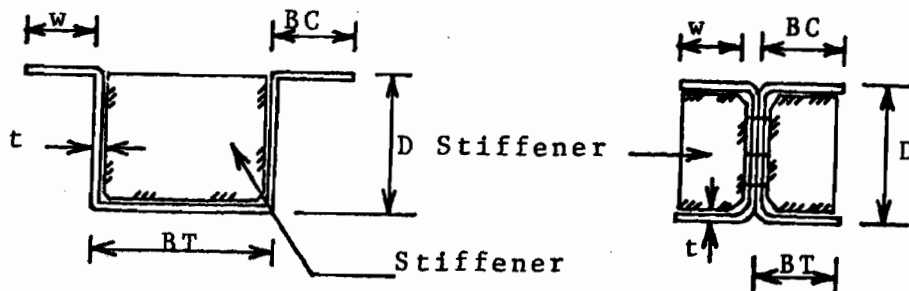
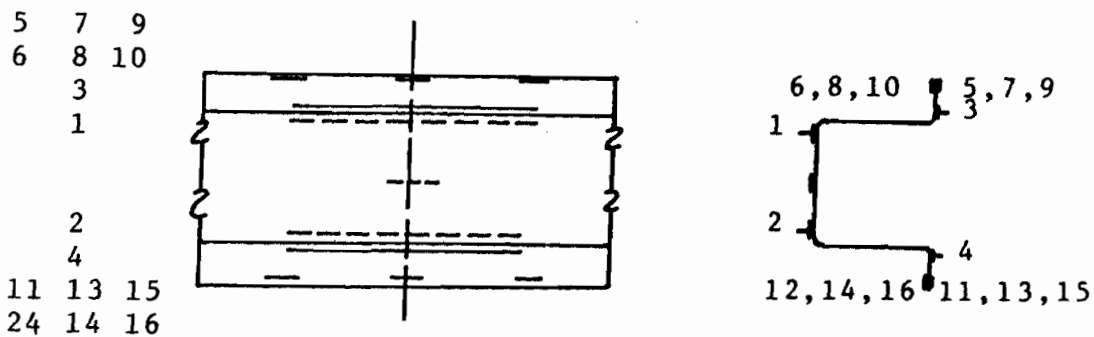


Fig. 4.4.33 COMPARISON OF TEST RESULTS AND THE EFFECTIVE WIDTH EQUATION (EQN. 3.4.5) COLUMN CURVES - ALUMINUM SPECIMENS L ($w/t = 18.1$)

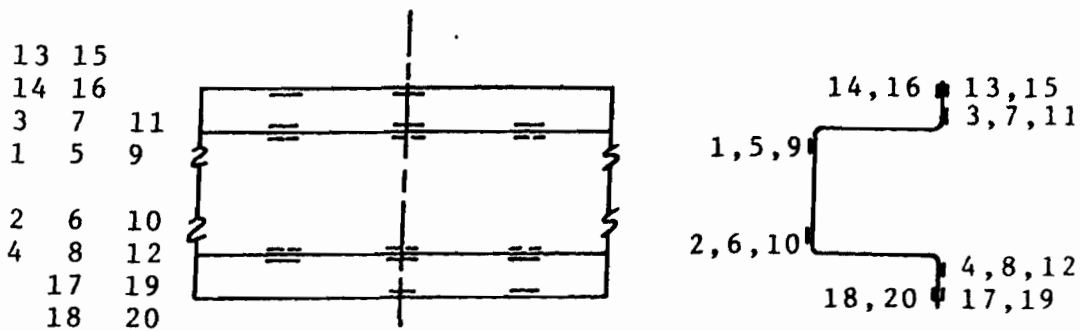


a) Inverted Hat Section

b) I-Section



c) Strain Gage Locations-Specimens Buckling in the Elastic Range



⊥ SR-4 A9 Gage

- SR-4 A12 Gage

d) Strain Gage Locations - Specimens Buckling in the Plastic Range

FIG. 5.2.1 FLEXURAL SPECIMENS-SECTION AND STRAIN GAGE LOCATIONS

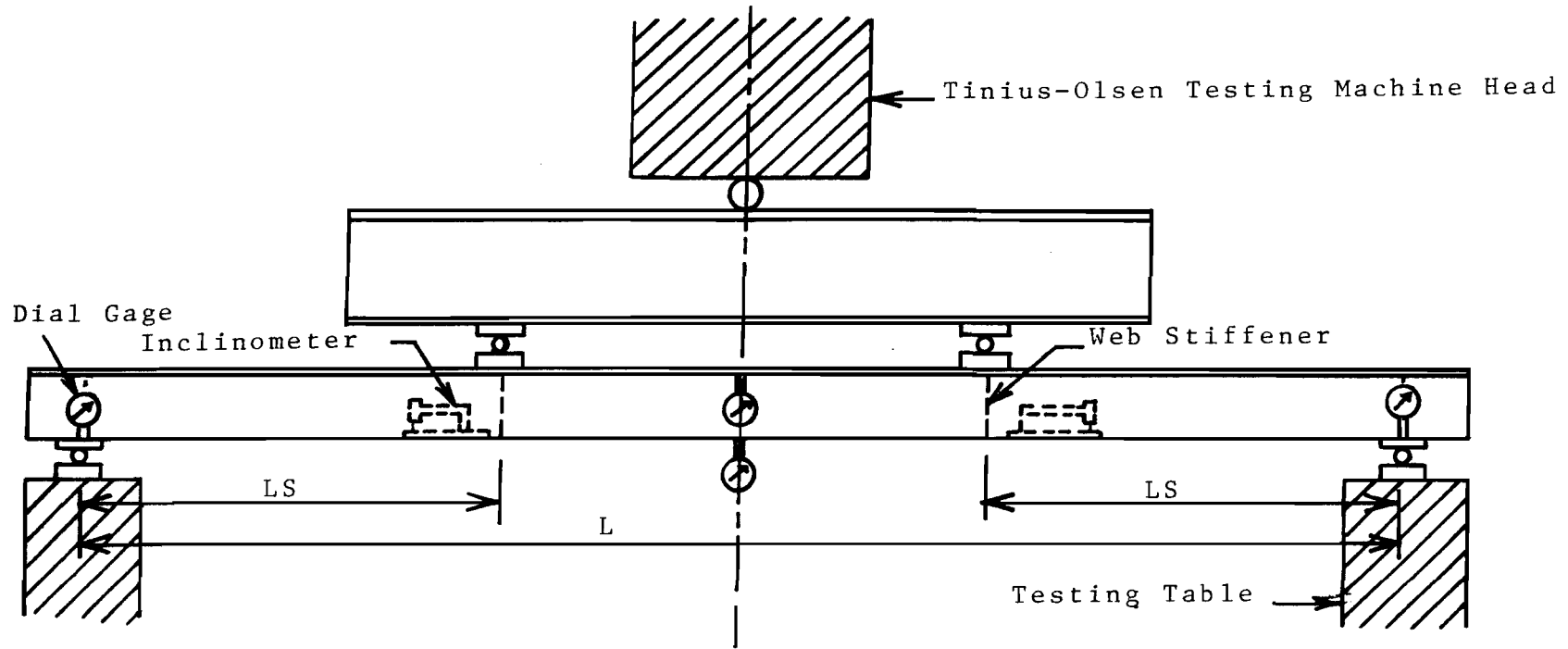


Fig. 5.2.2 BEAM TEST SET-UP AND INSTRUMENTATION

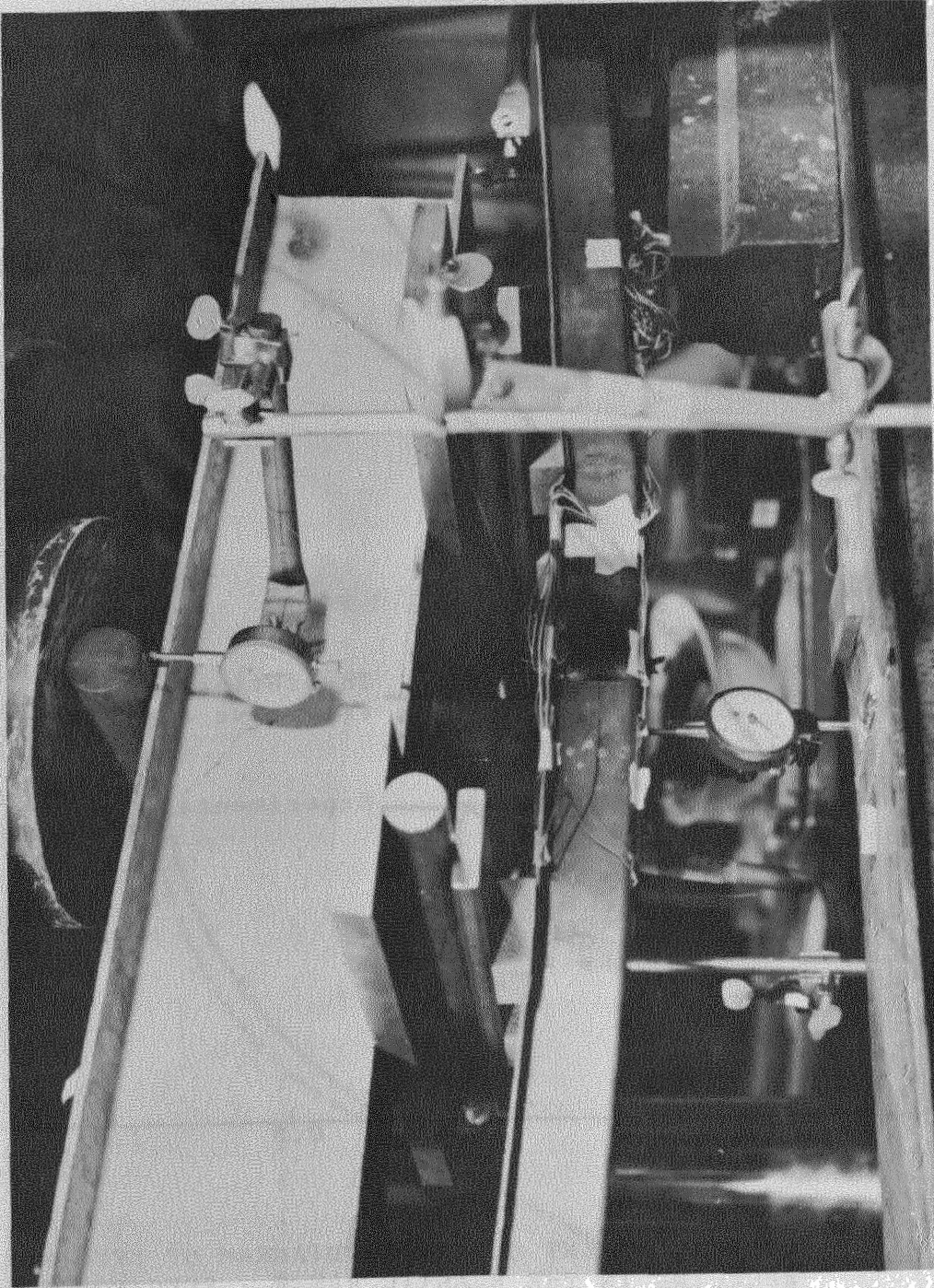


Fig. 5.2.3 BEAM SPECIMENS - LOAD SET-UP

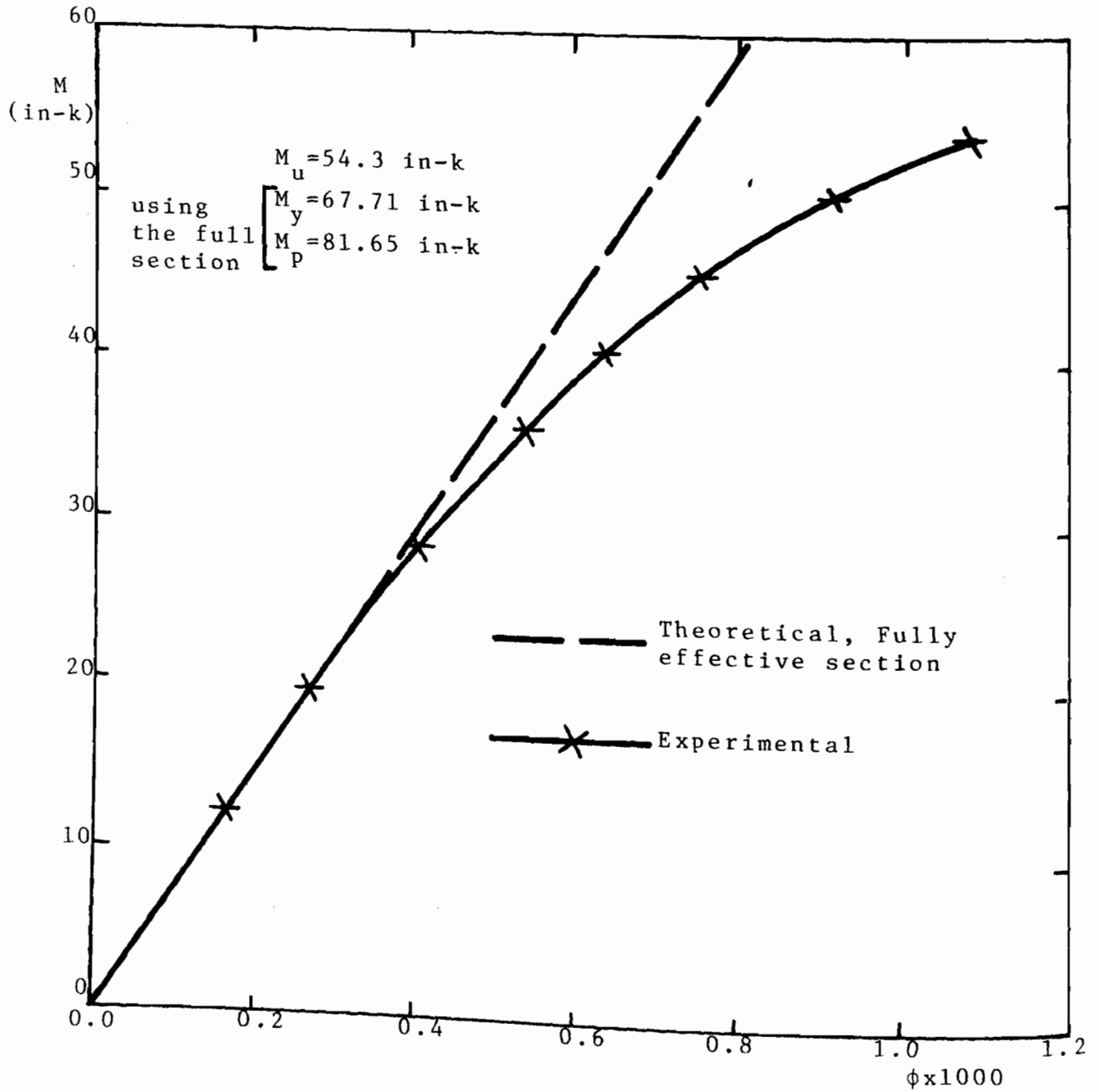


Fig. 5.4.1 TYPICAL MOMENT CURVATURE DIAGRAM OF SPECIMENS BUCKLING IN THE ELASTIC RANGE - SPECIMEN B 4 ($w/t = 36.9$)

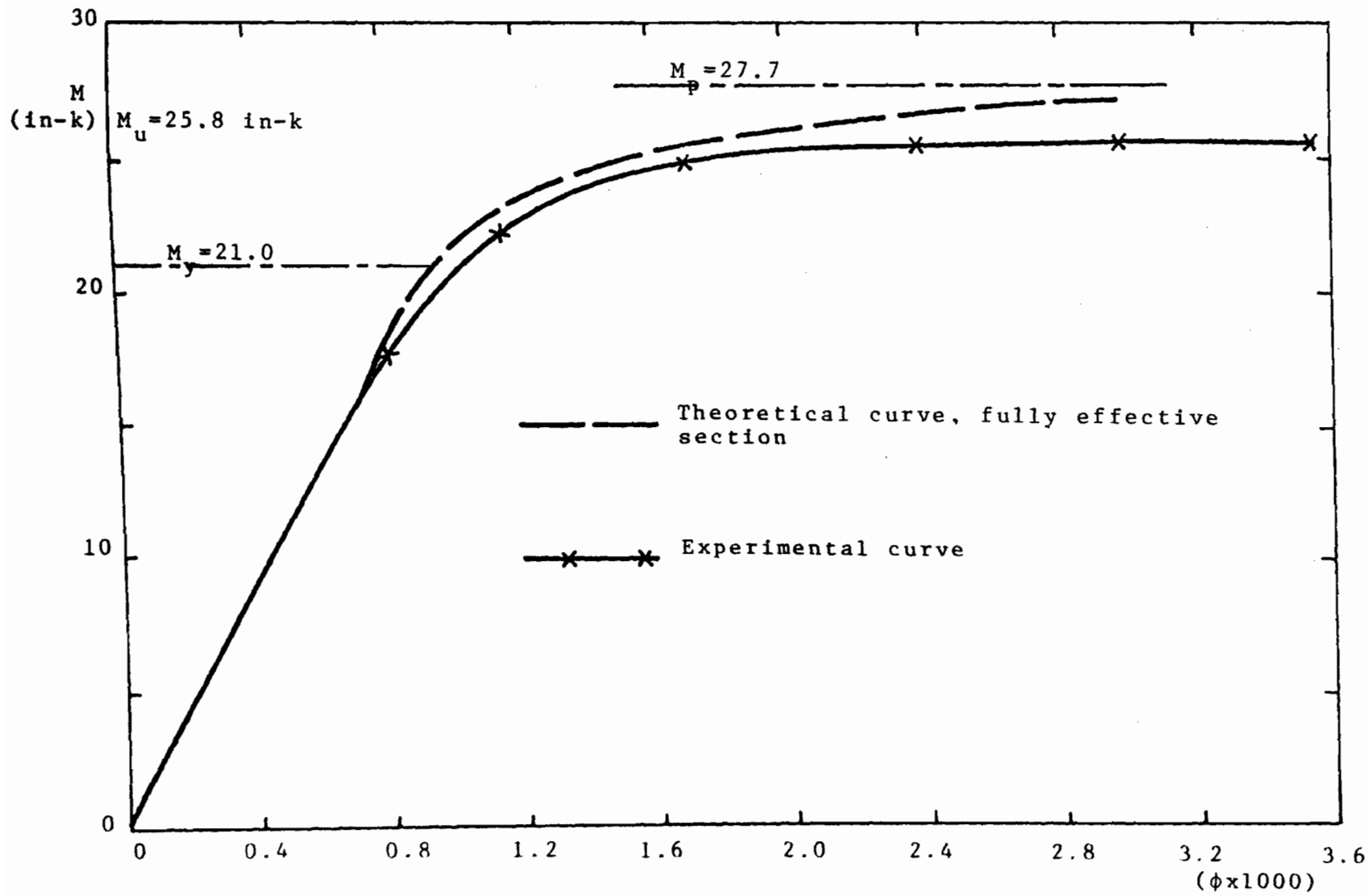


FIG. 5.4.2 TYPICAL MOMENT CURVATURE DIAGRAM OF SPECIMENS BUCKLING IN THE INELASTIC RANGE. Specimen B16 ($w/t=12.7$)

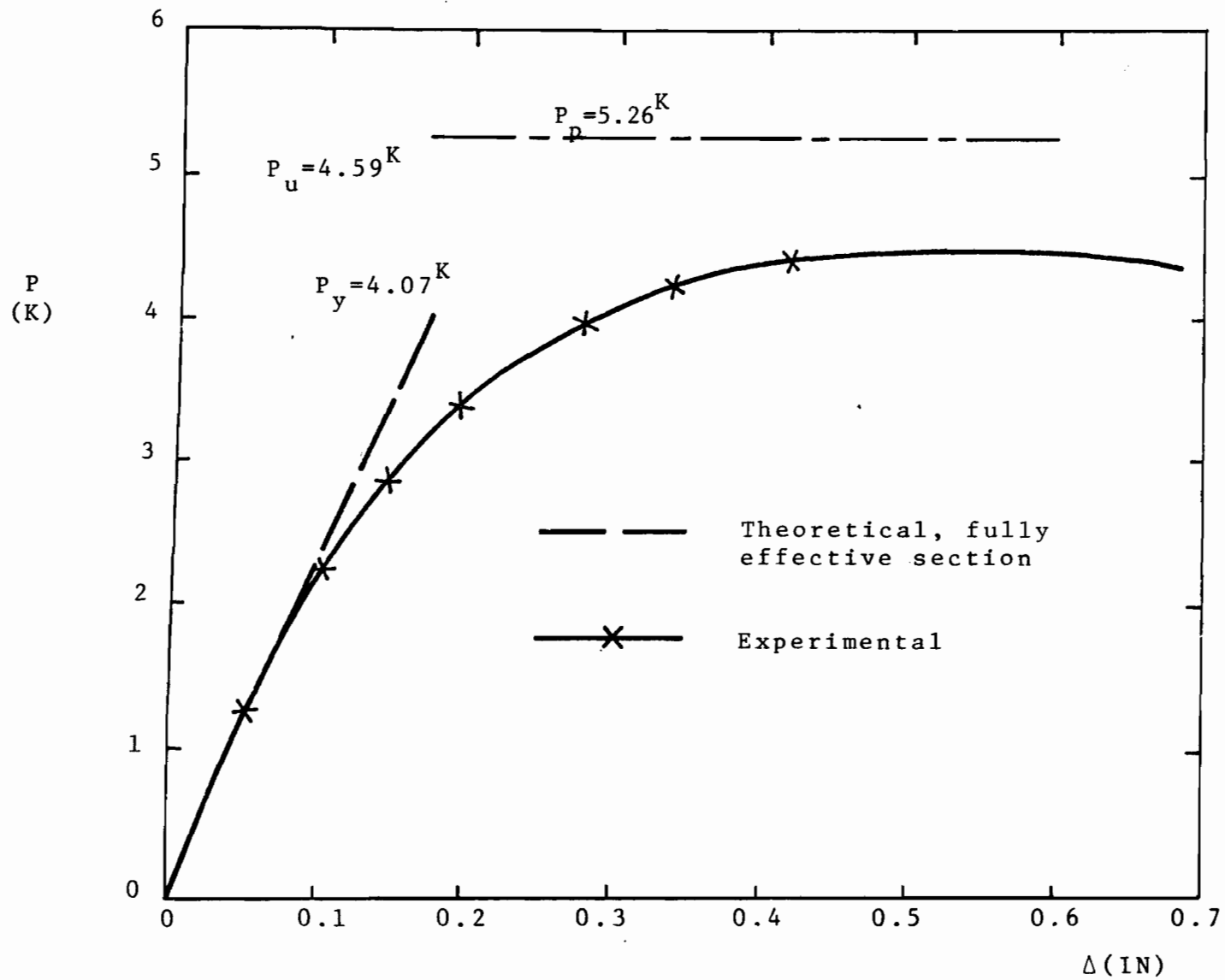


FIG. 5.4.3 TYPICAL LOAD VS. CENTRAL DEFLECTION DIAGRAM. Specimen B_{15} ($w/t=14.1$)

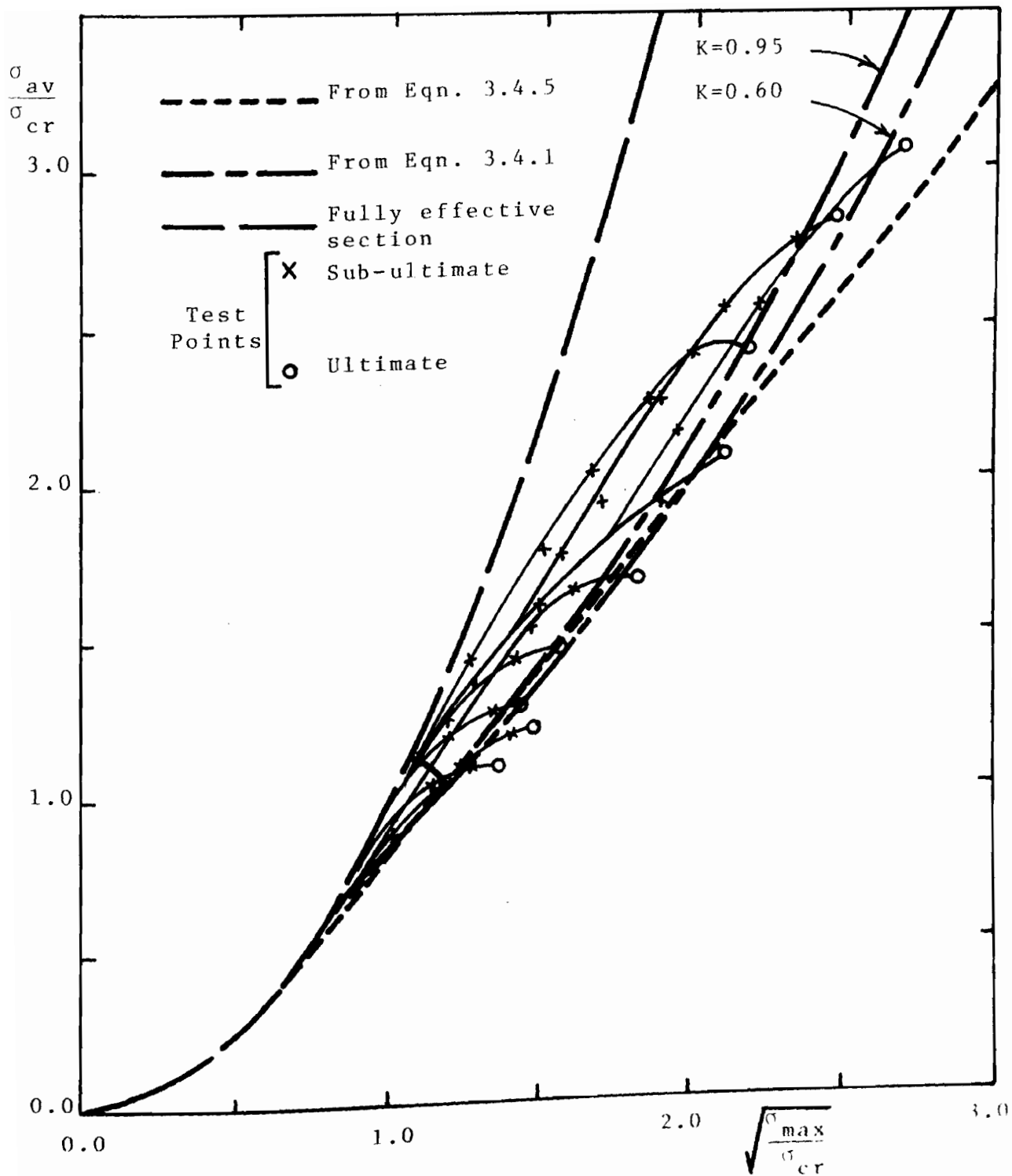


Fig. 5.4.4 COMPARISON OF SUB-ULTIMATE AND ULTIMATE BEAM TEST RESULTS AND MODIFIED FORM OF EFFECTIVE WIDTH EQUATIONS

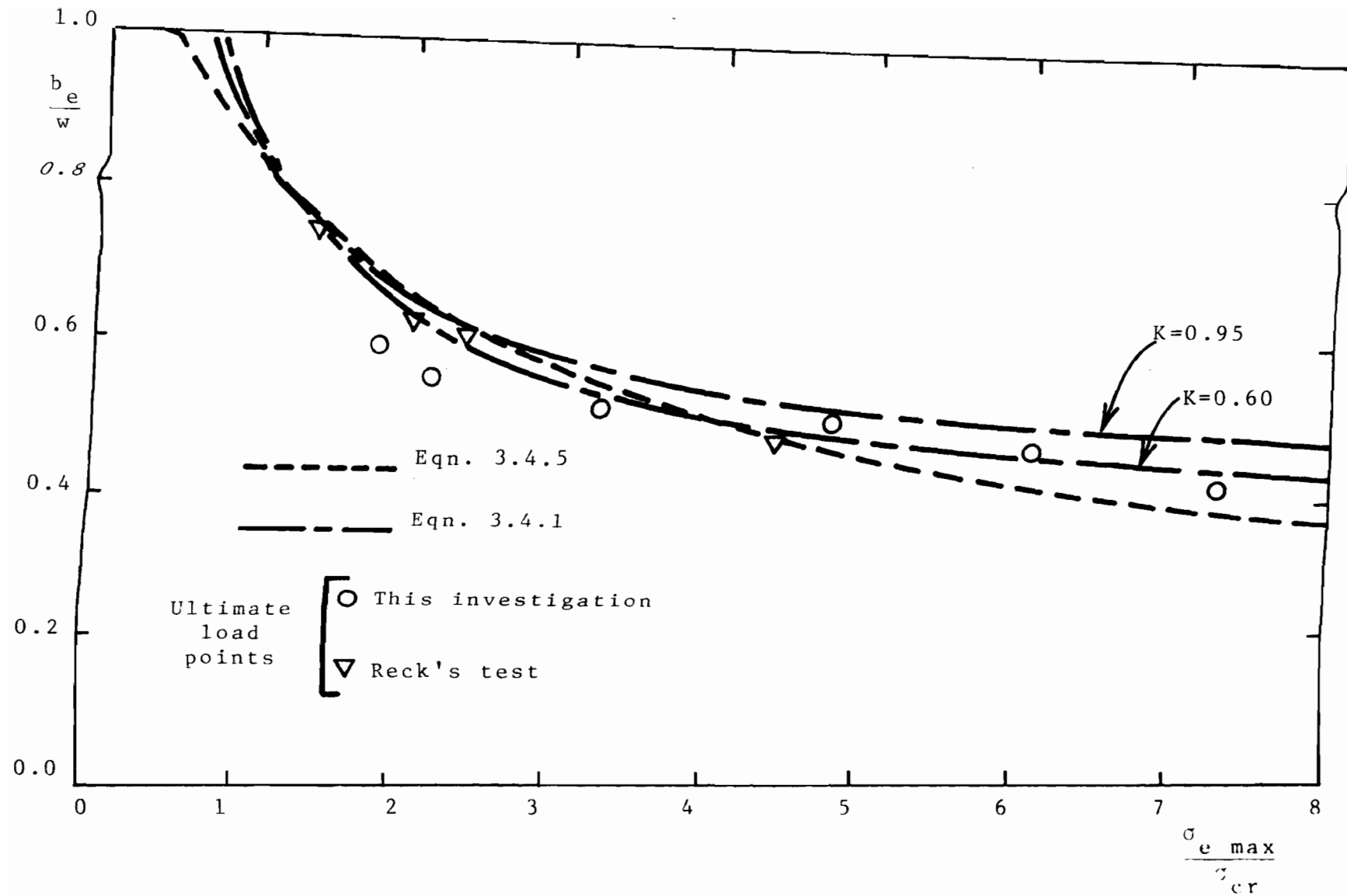


Fig. 5.4.5 COMPARISON OF EFFECTIVE WIDTH EQUATIONS AND BEAM TEST RESULTS

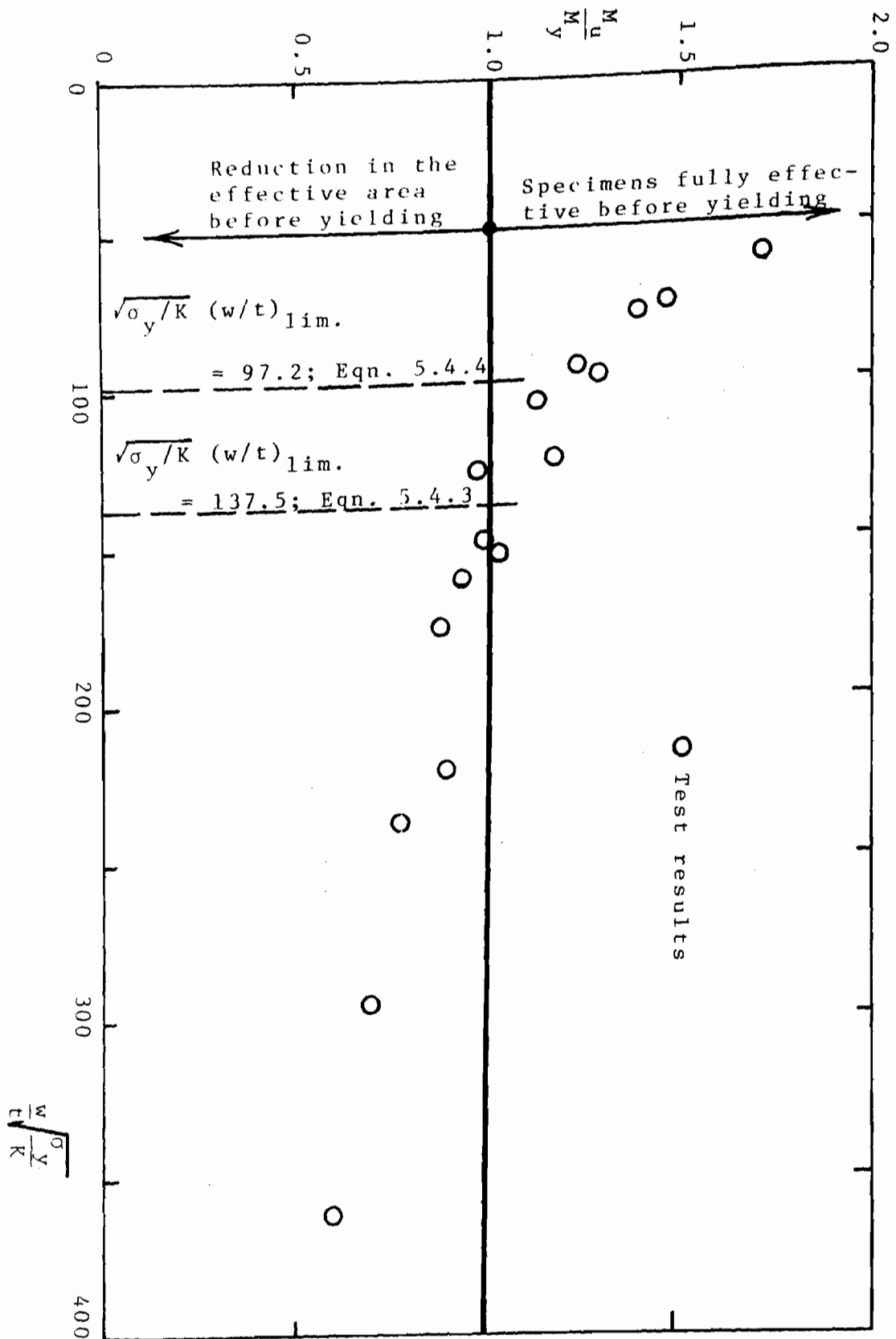


FIG. 5.4.6 LIMITING w/t RATIO OF UNSTIFFENED ELEMENTS

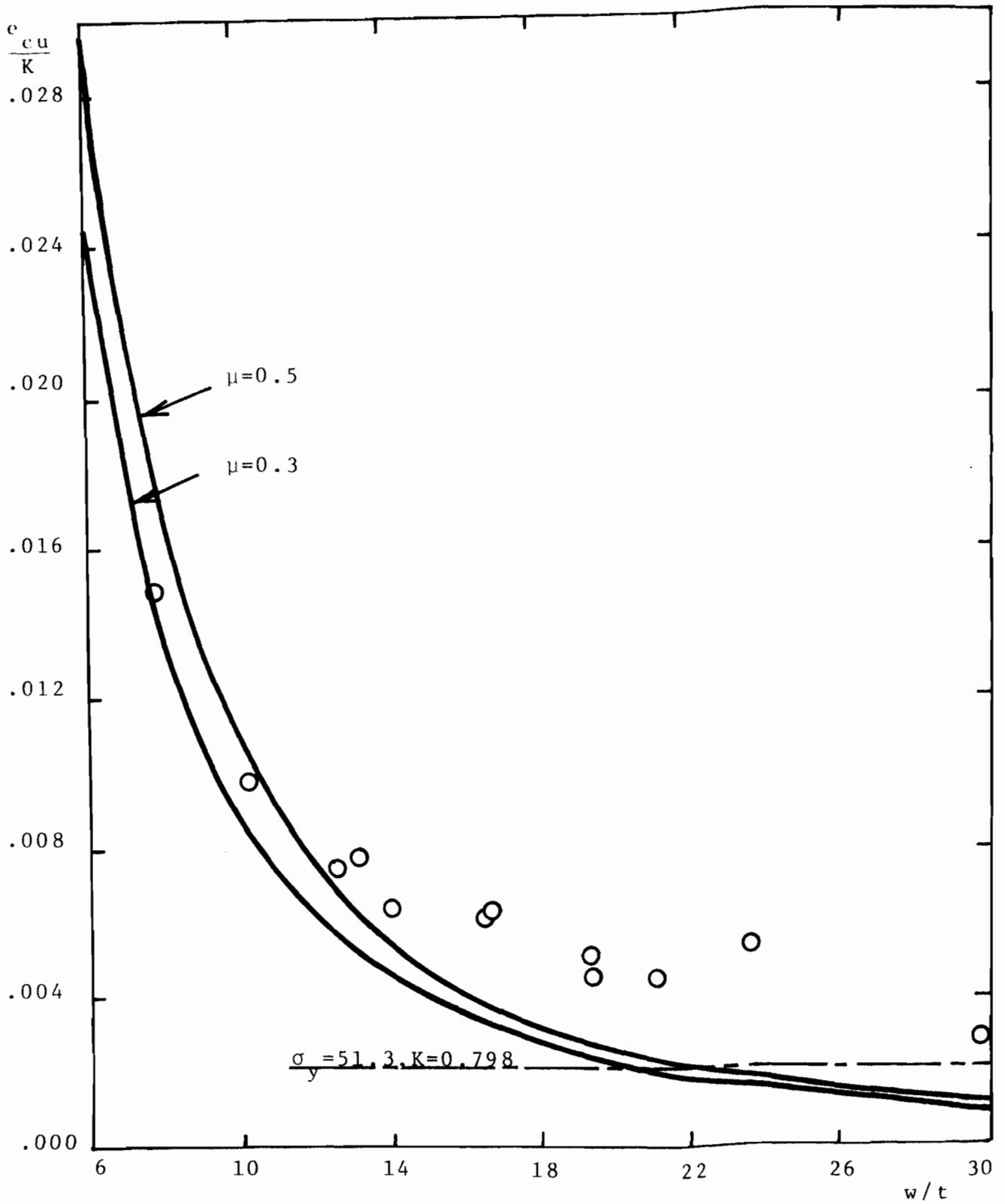


Fig. 5.4.7 PLASTIC COMPRESSIVE STRAIN CAPACITY OF UNSTIFFENED ELEMENTS

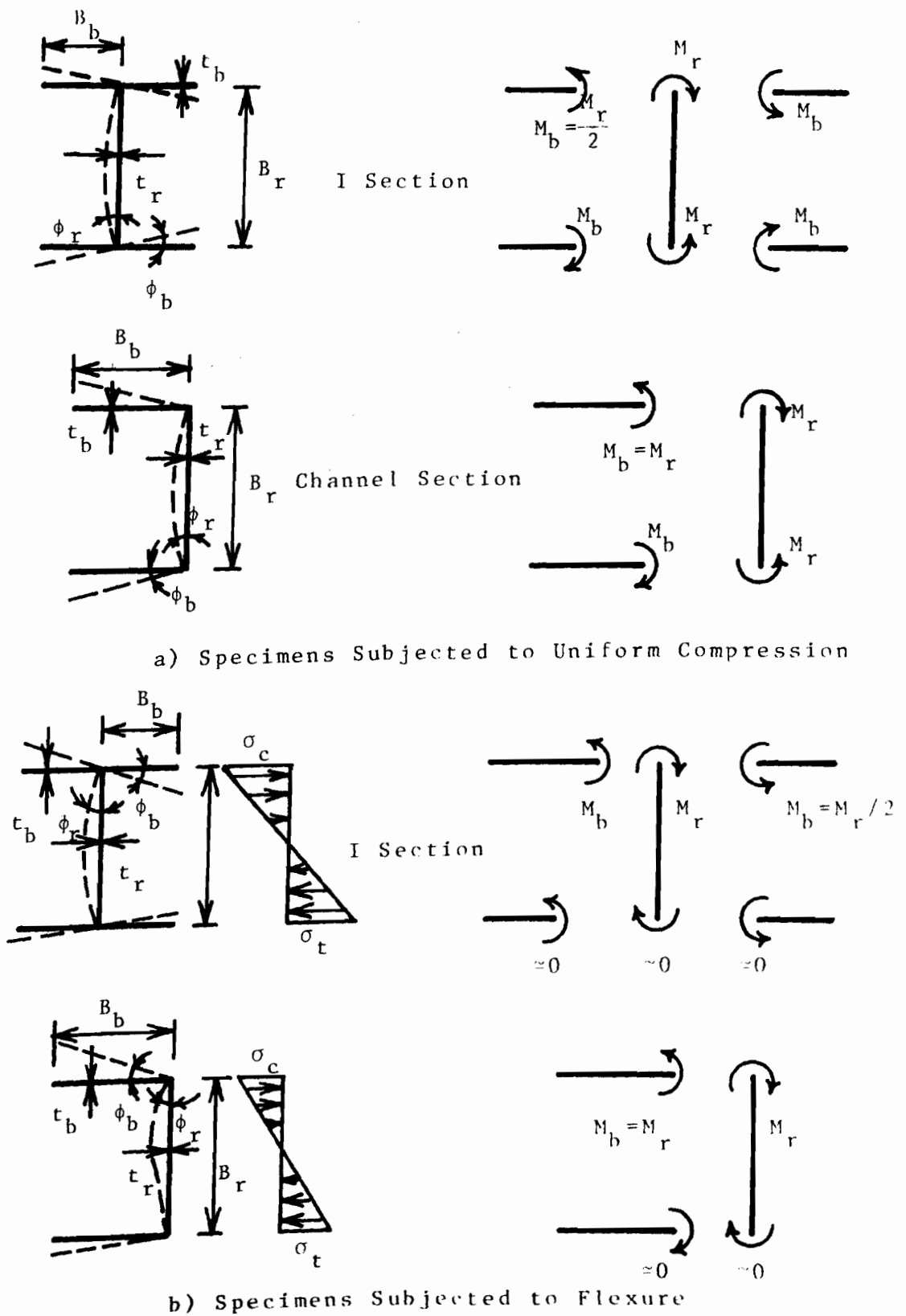
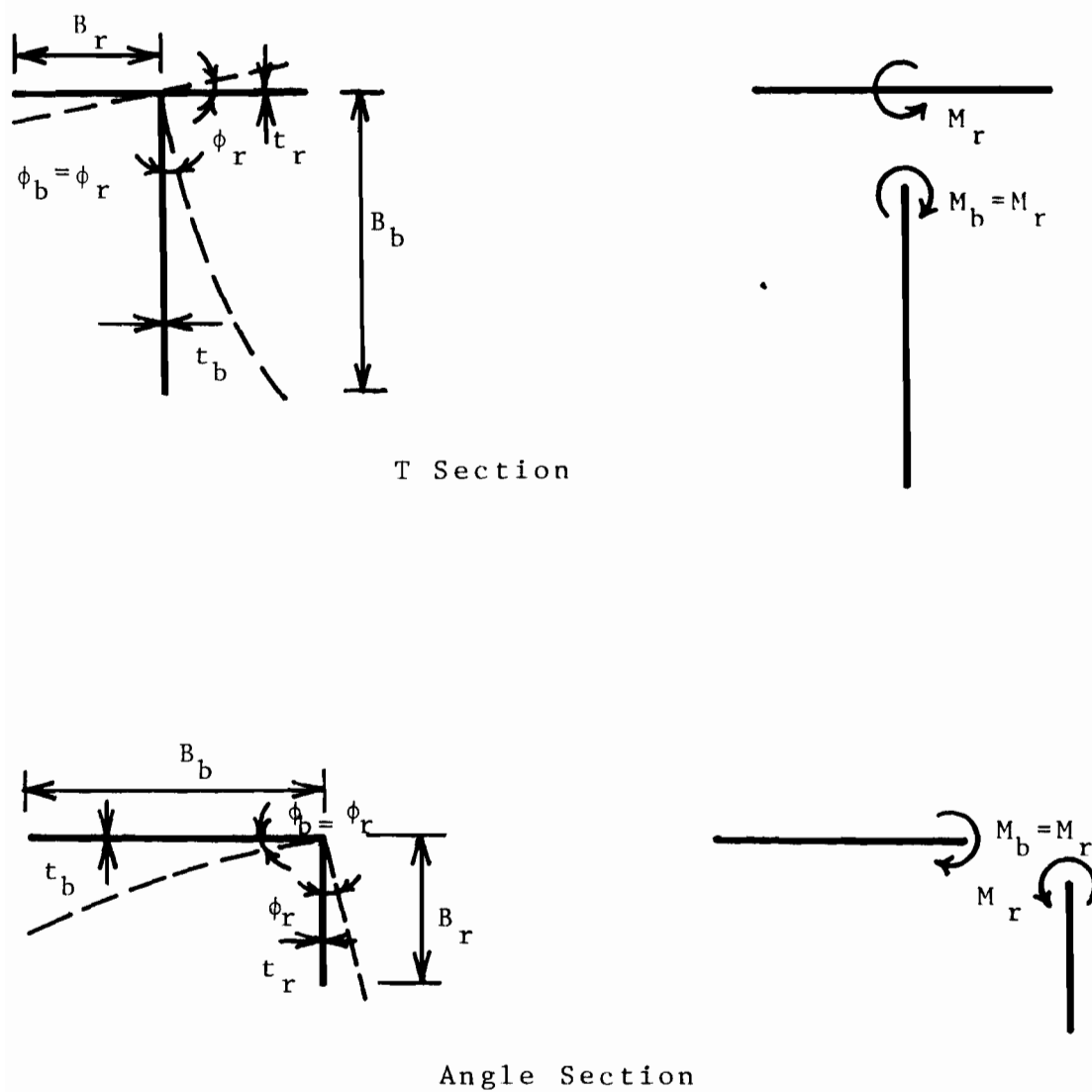


Fig. 6.2.1 DISTORTED SHAPE AND EDGE MOMENTS DUE TO LOCAL BUCKLING OF UNSTIFFENED ELEMENTS



Specimens Subjected to Uniform Compression

Fig. 6.2.2 DISTORTED SHAPE AND EDGE MOMENTS DUE TO LOCAL BUCKLING OF UNSTIFFENED ELEMENTS

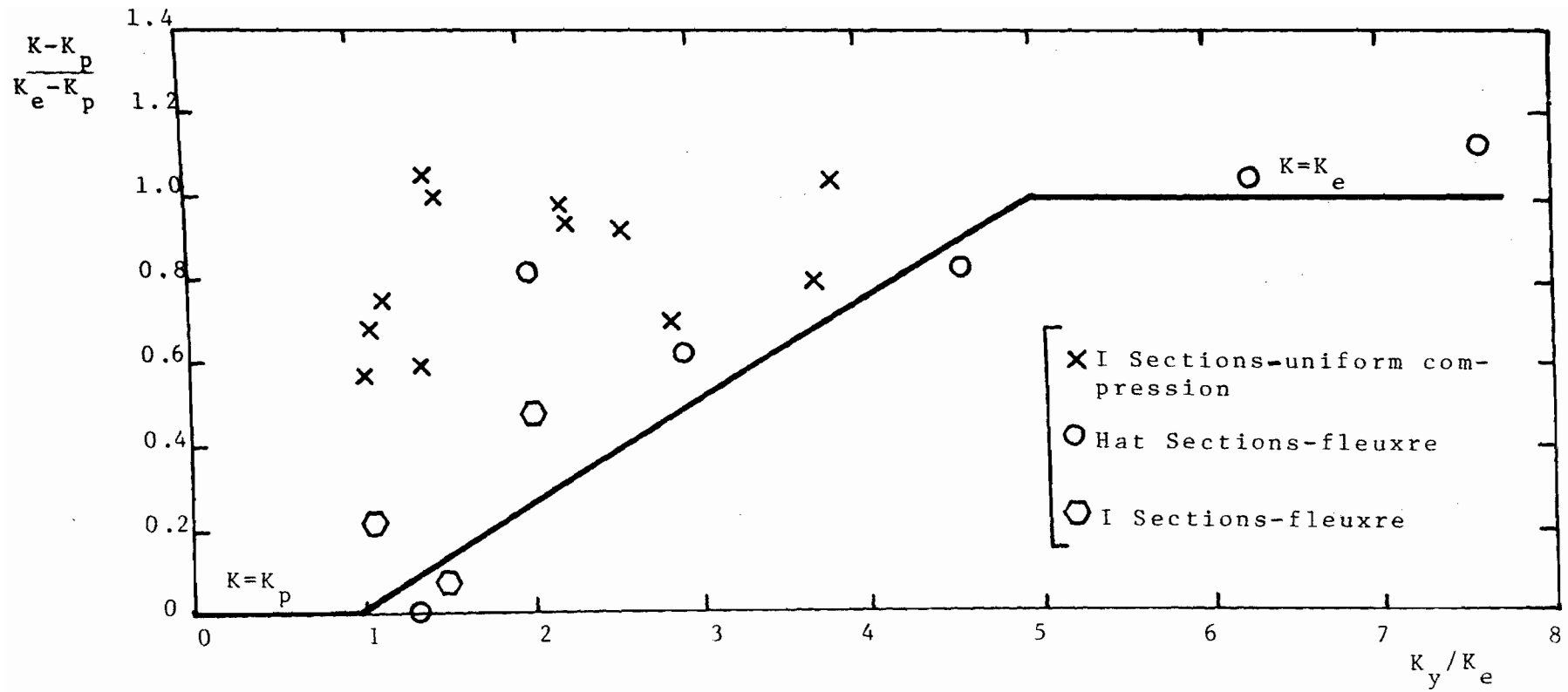


Fig. 6.2.3 VARIATION OF BUCKLING COEFFICIENT WITH THE K_y / K_e RATIO

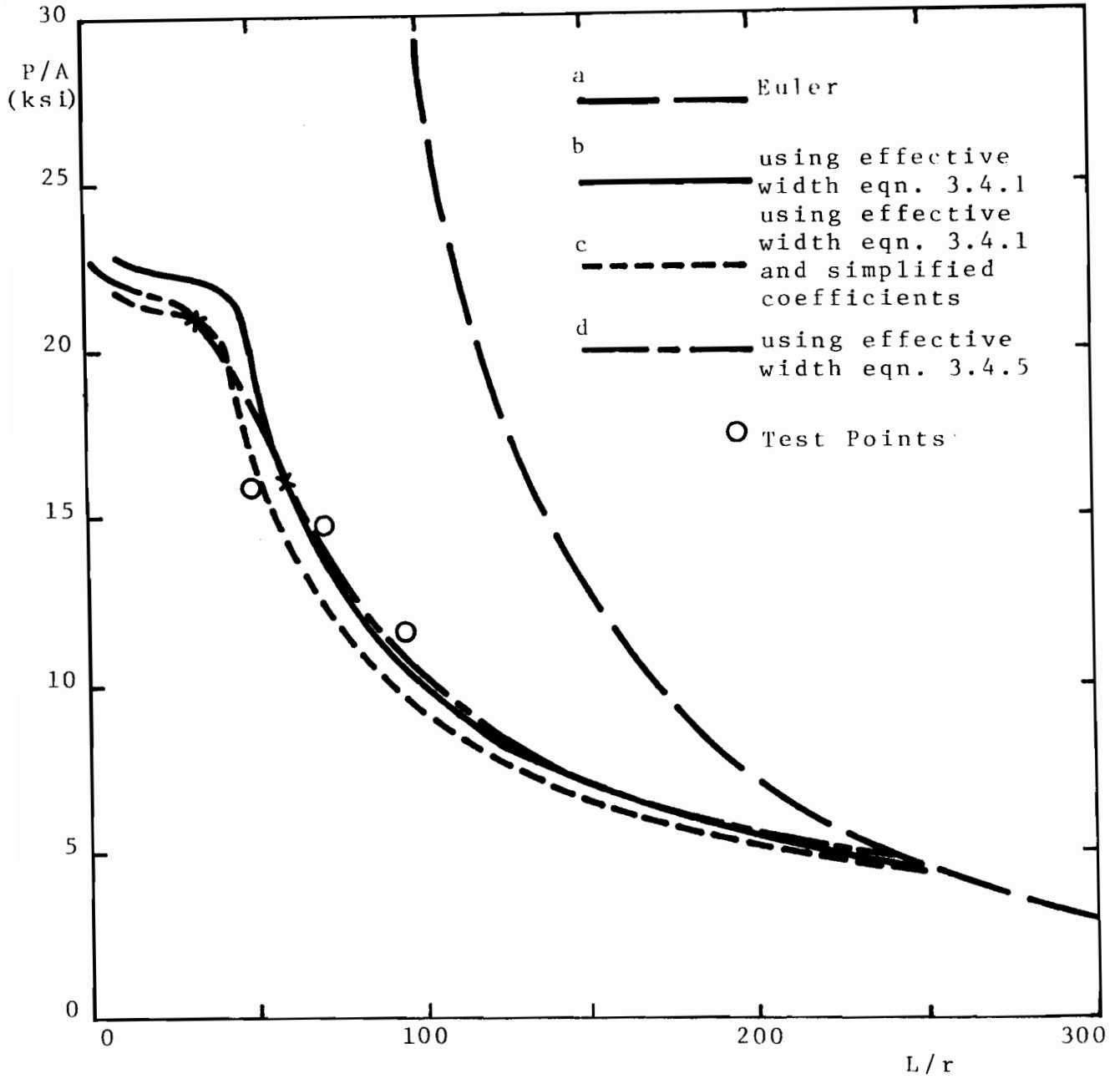


Fig. 6.4.1 COLUMN FLEXURAL BUCKLING STRENGTH CURVES AND TEST RESULTS. SPECIMENS LC-I ($w/t = 57.5$)

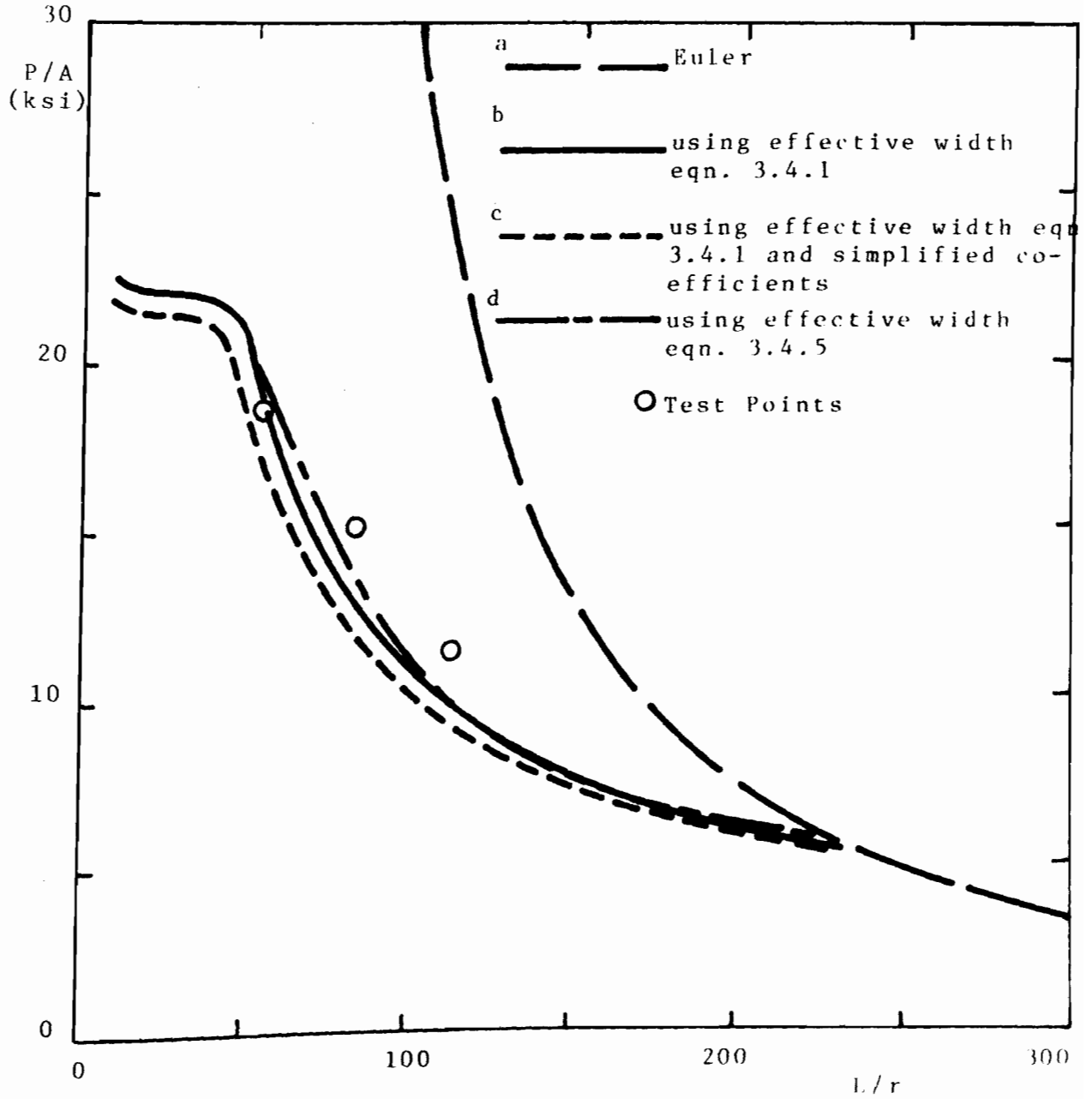


Fig. 6.4.2 COLUMN FLEXURAL BUCKLING STRENGTH CURVES AND TEST RESULTS. SPECIMENS LC-11 ($w/c = 50.5$)

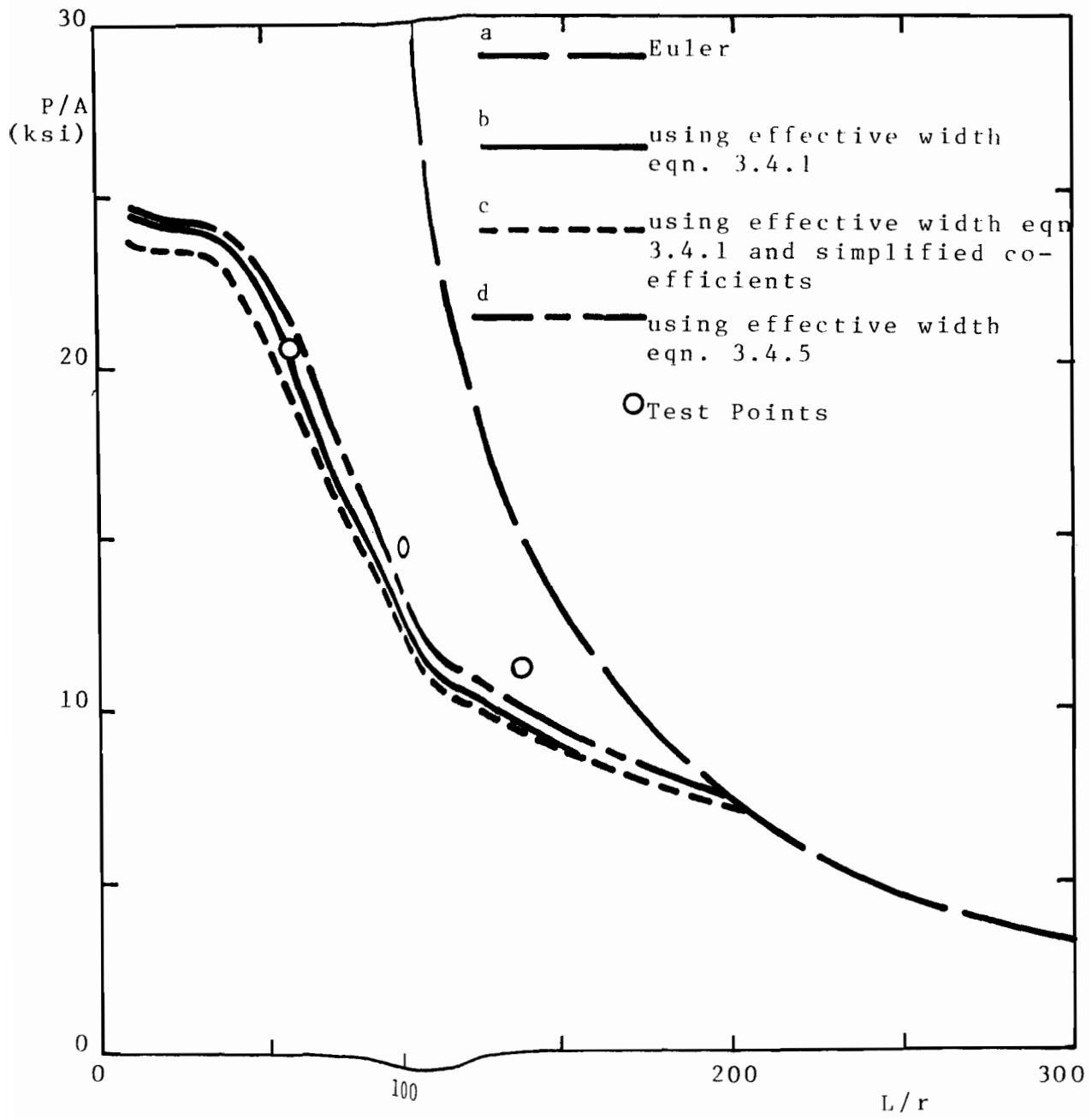


Fig. 6.4.3 COLUMN FLEXURAL BUCKLING STRENGTH CURVES AND TEST RESULTS. SPECIMENS LC-III ($w/t = 42.0$)

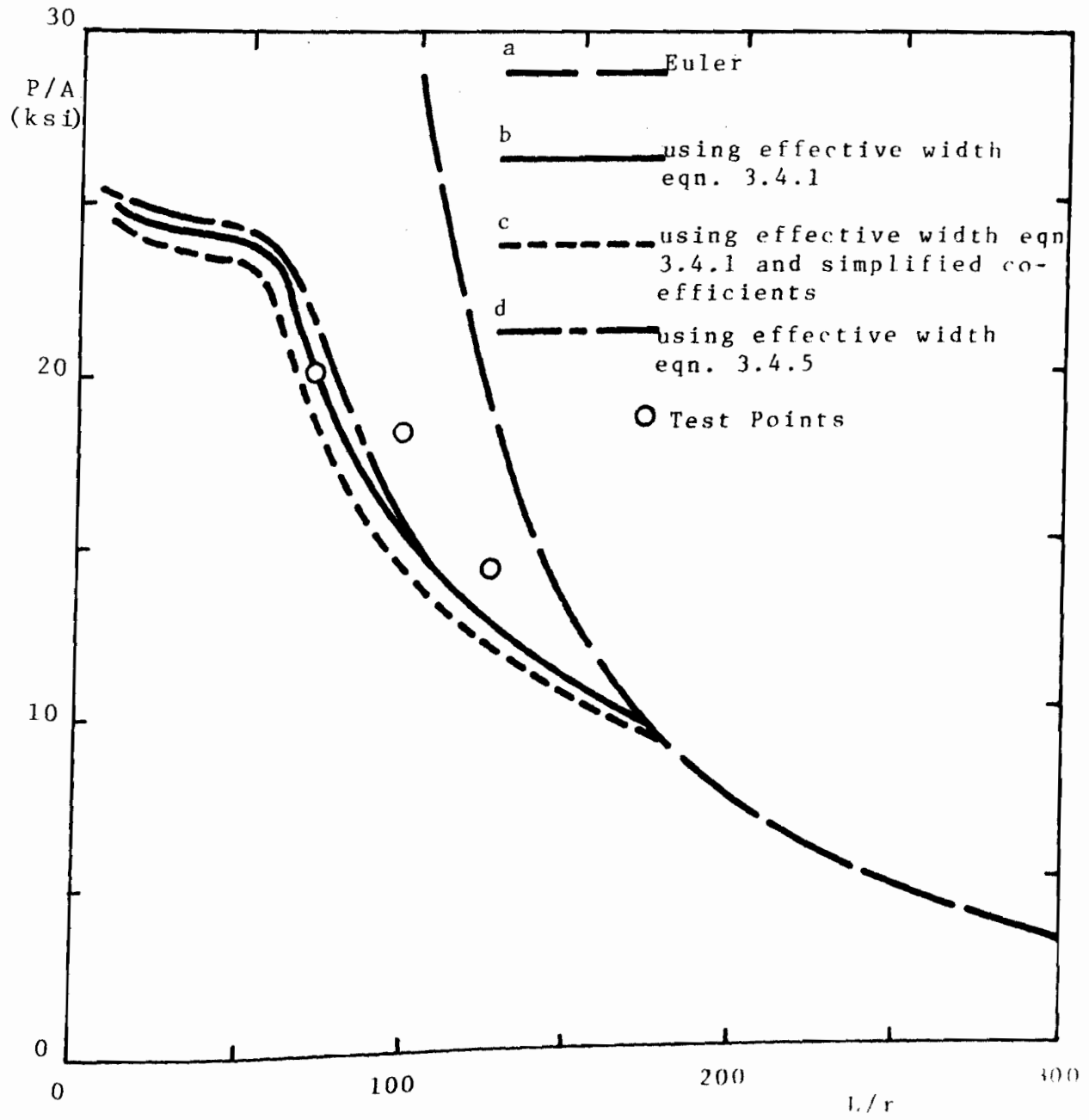


Fig. 6.4.4 COLUMN FLEXURAL BUCKLING STRENGTH CURVES AND TEST RESULTS. SPECIMENS LC-IV ($w/t = 35.0$)

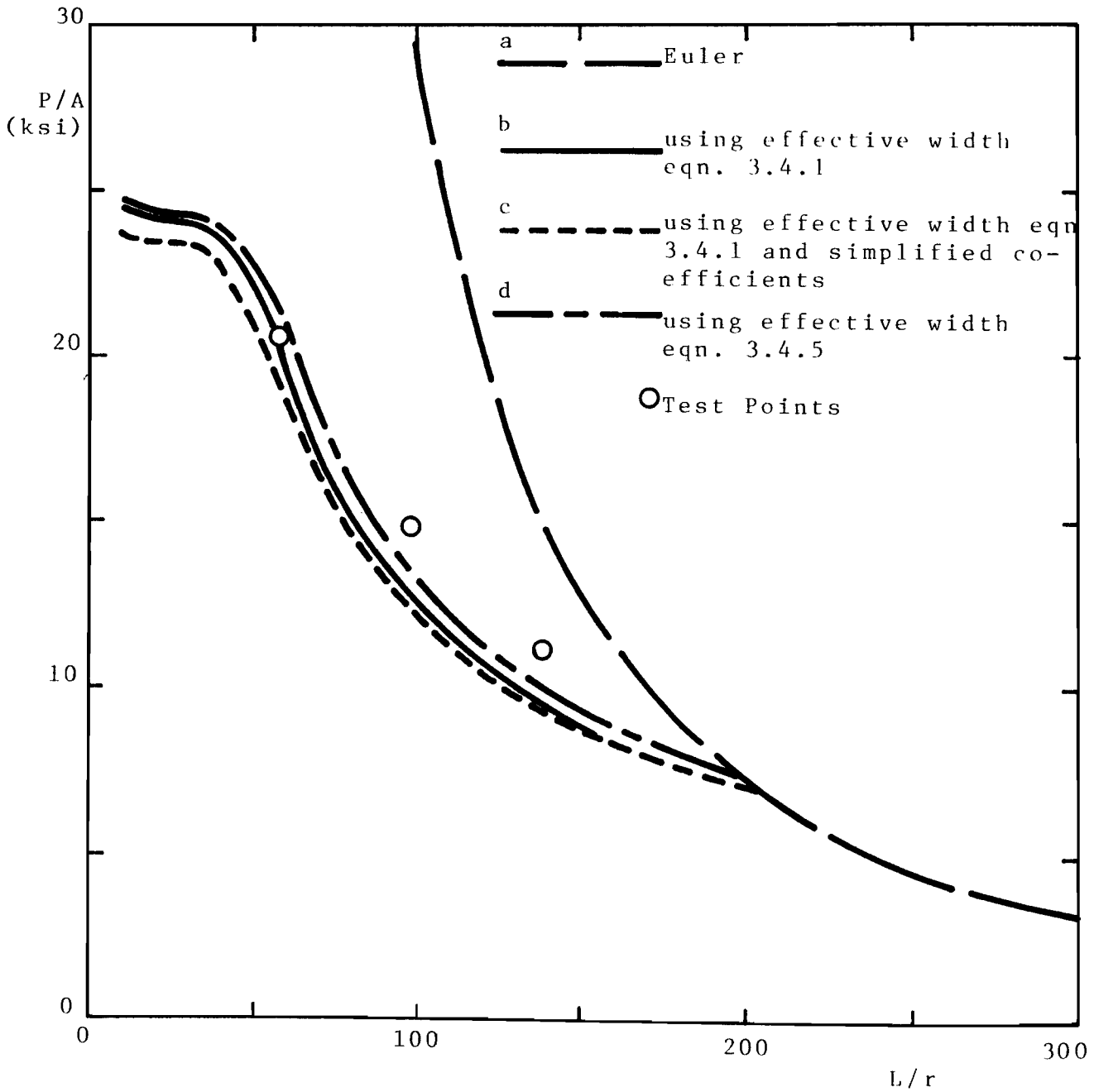


Fig. 6.4.3 COLUMN FLEXURAL BUCKLING STRENGTH CURVES AND TEST RESULTS. SPECIMENS LC-III ($w/t = 42.0$)

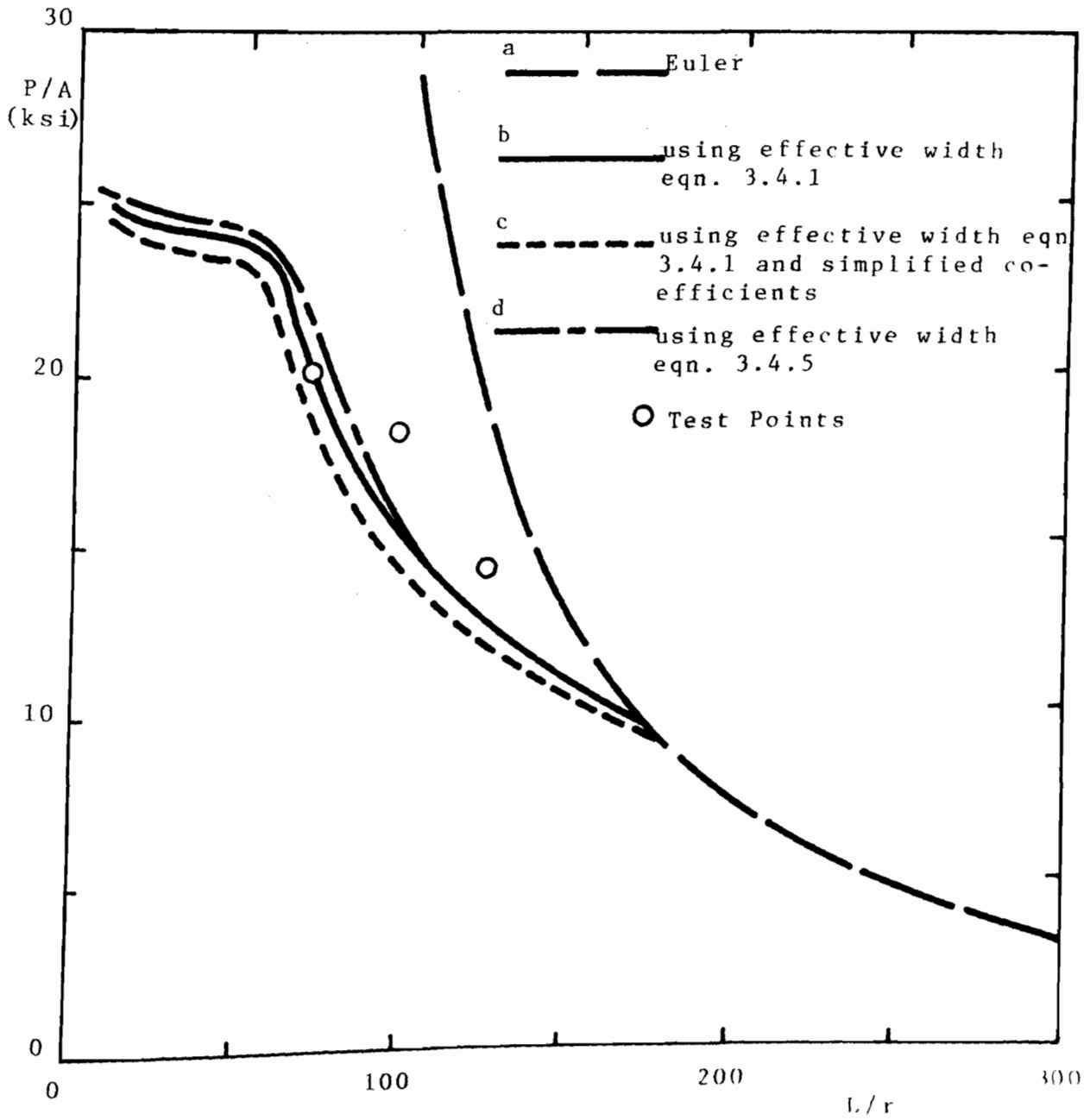


Fig. 6.4.4 COLUMN FLEXURAL BUCKLING STRENGTH CURVES AND TEST RESULTS. SPECIMENS LC-IV ($w/t = 35.0$)

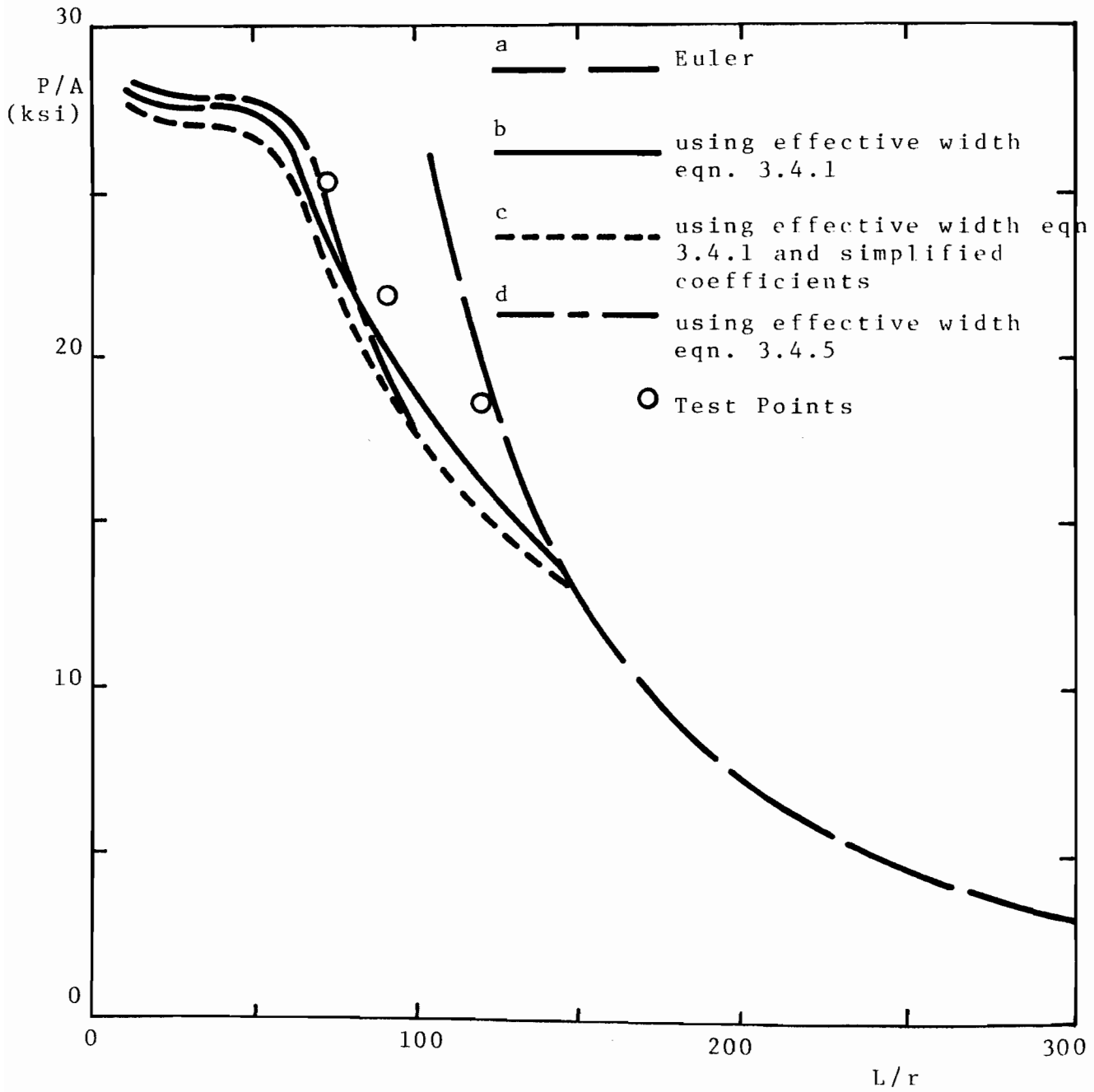


Fig. 6.4.5 COLUMN FLEXURAL BUCKLING STRENGTH CURVES AND TEST RESULTS. SPECIMENS LC-V ($w/t = 29.5$)

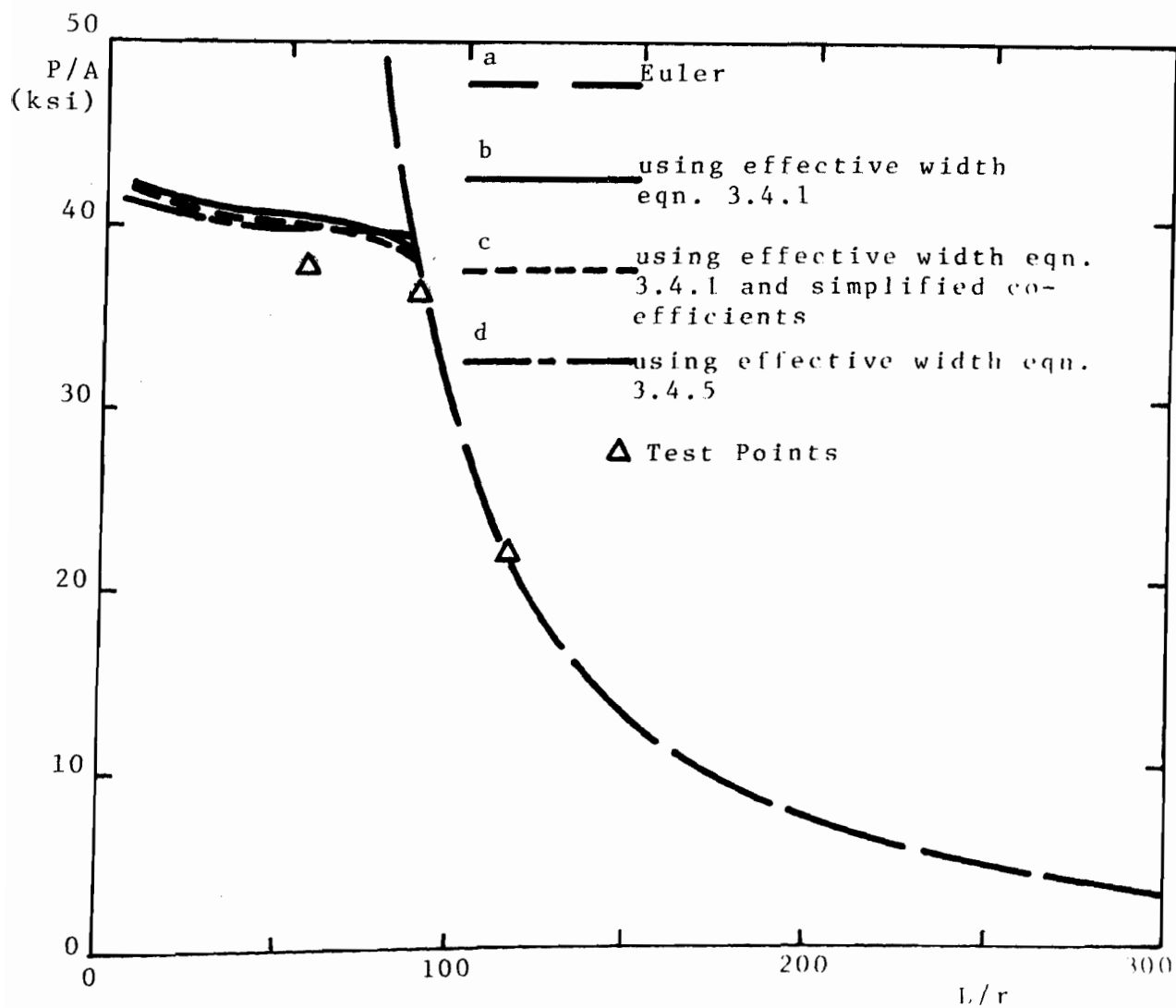


Fig. 6.4.6 COLUMN FLEXURAL BUCKLING STRENGTH CURVES AND TEST RESULTS. SPECIMENS UD-1 ($w/t = 16.2$)

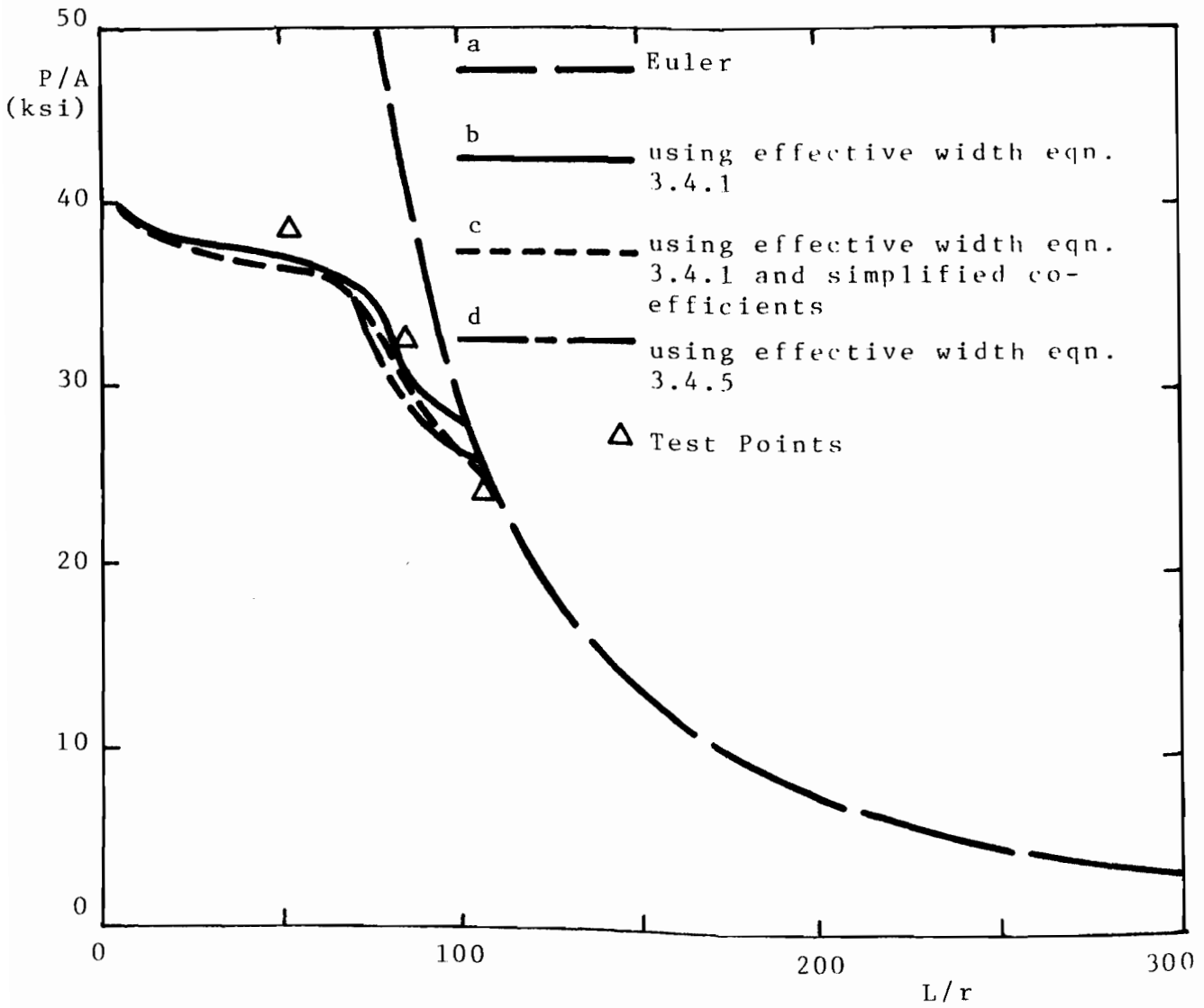


Fig. 6.4.7 COLUMN FLEXURAL BUCKLING STRENGTH CURVES AND TEST RESULTS. SPECIMENS UD-2 ($w/t = 20.5$)

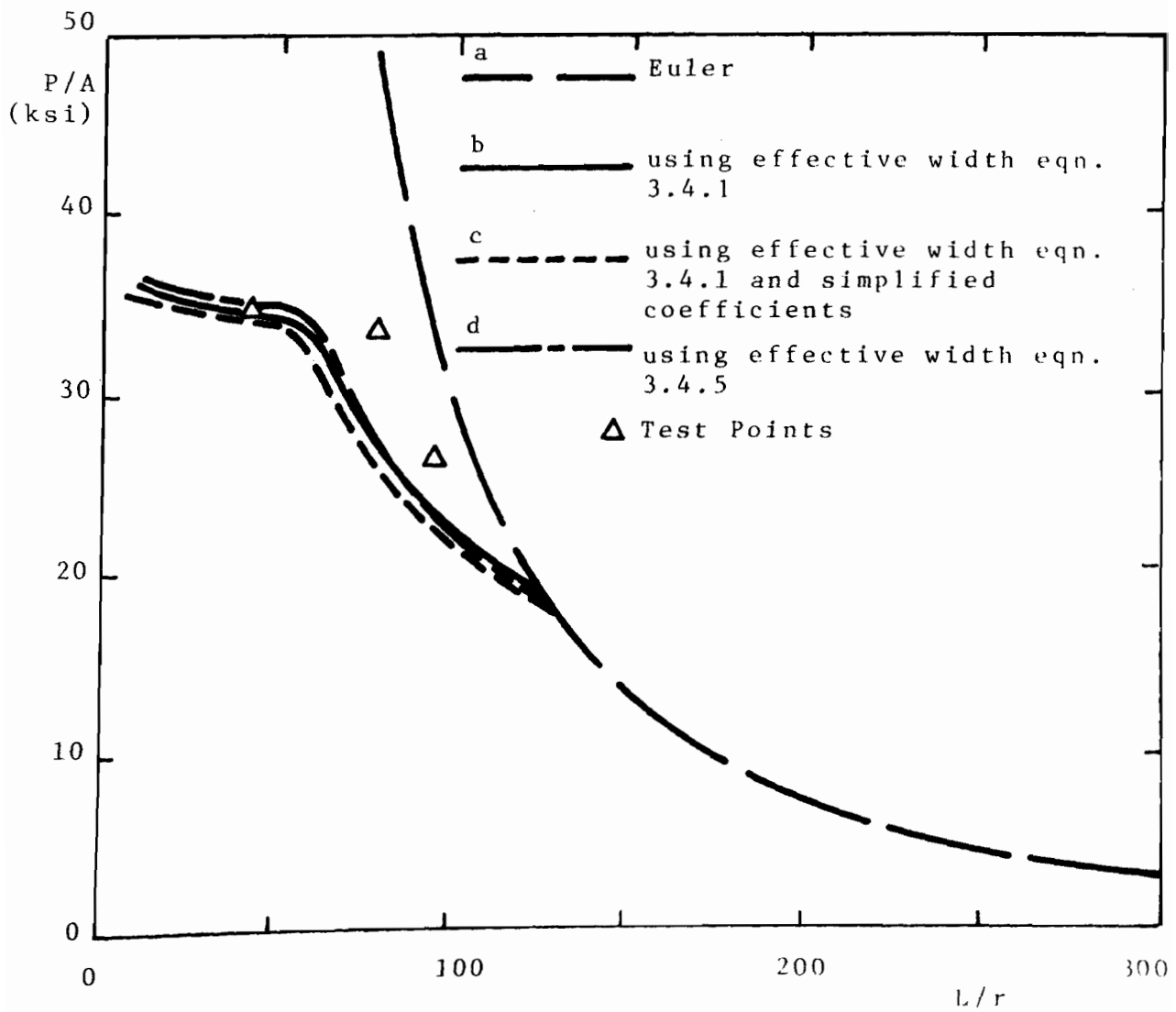


Fig. 6.4.8 COLUMN FLEXURAL BUCKLING STRENGTH CURVES AND TEST RESULTS. SPECIMENS UD-3 ($w/t = 24.8$)

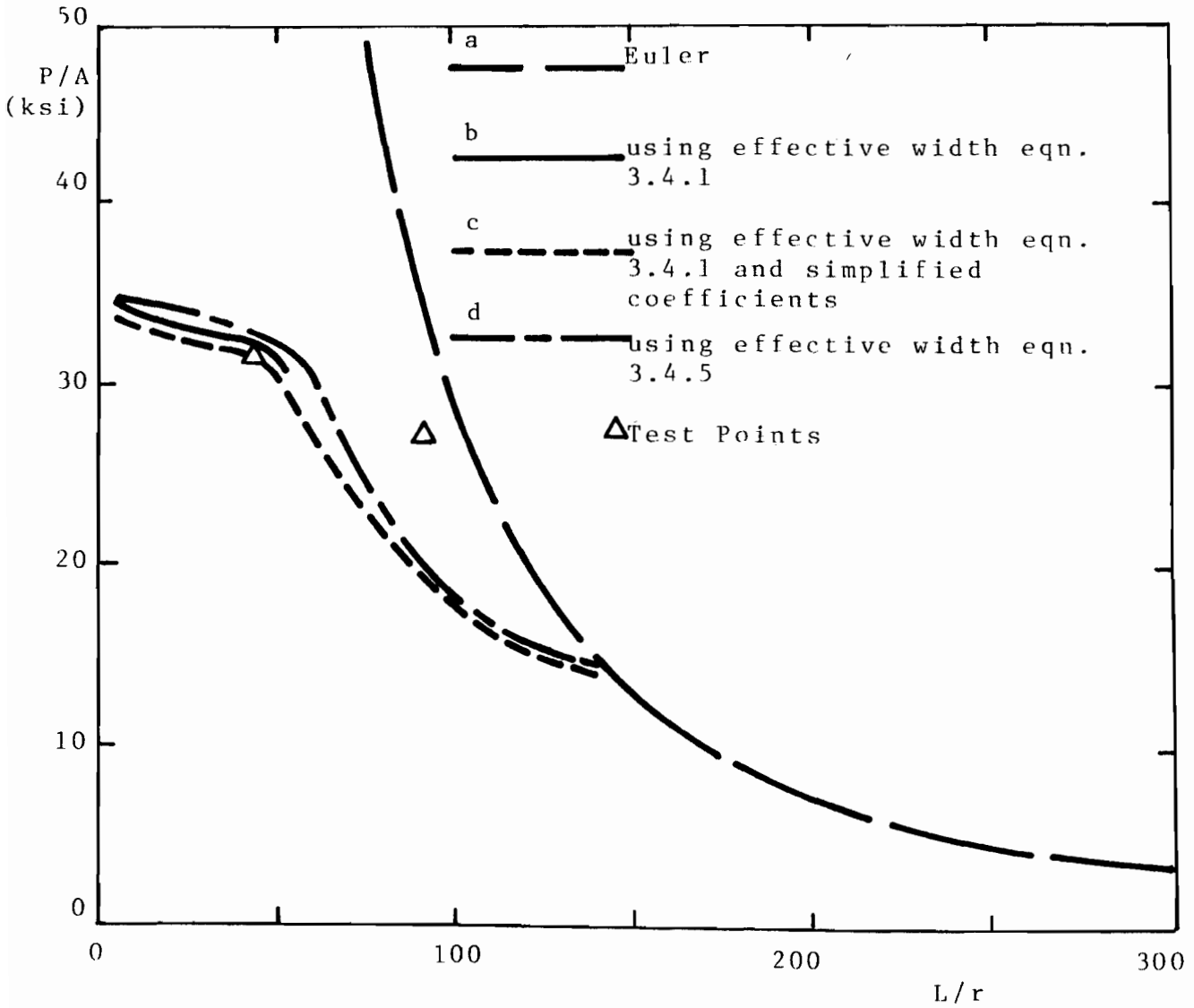


Fig. 6.4.9 COLUMN FLEXURAL BUCKLING STRENGTH CURVES AND TEST RESULTS. SPECIMENS UD-4 ($w/t = 29.1$)

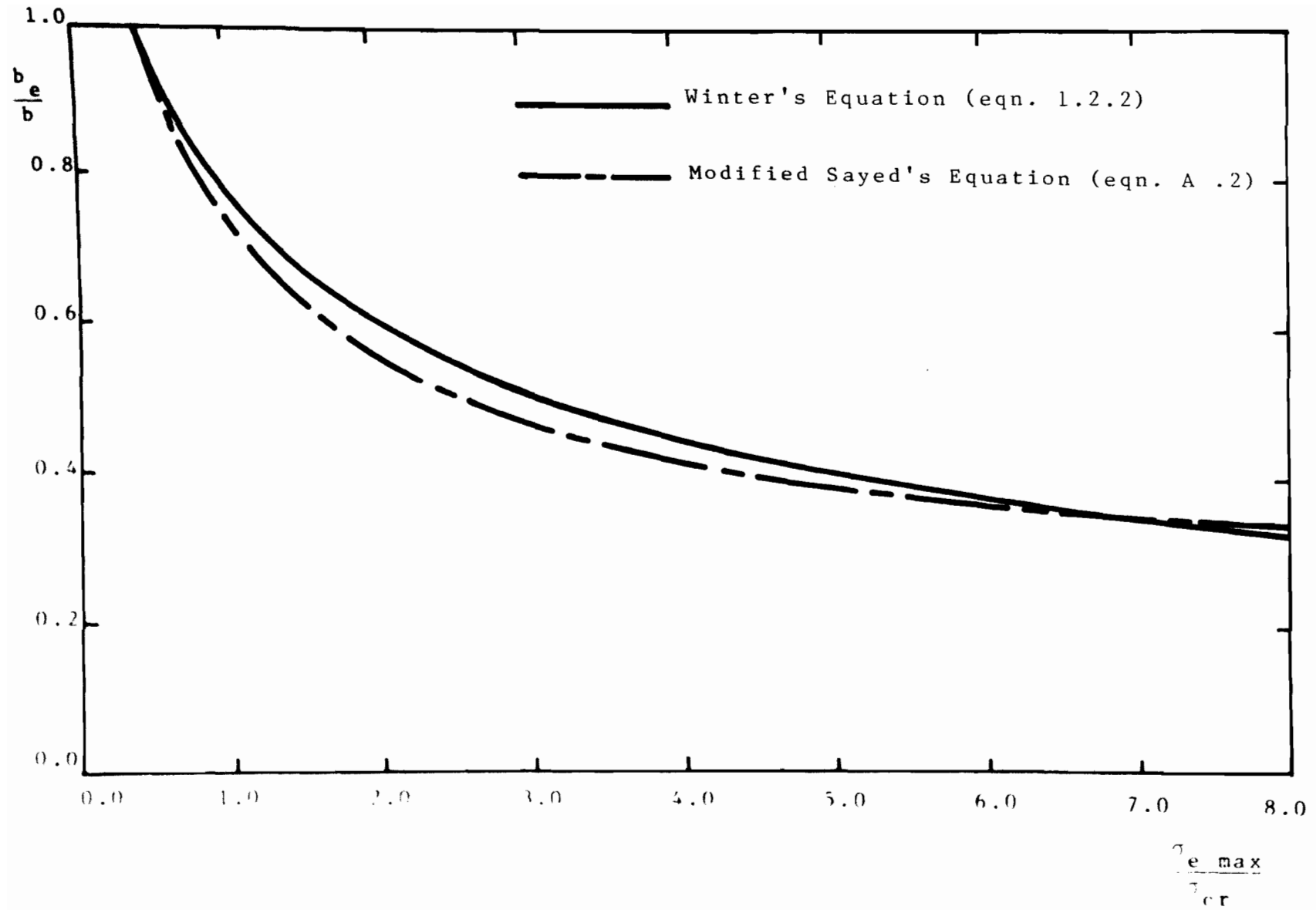


FIG. A.1 COMPARISON OF EFFECTIVE WIDTH EQUATIONS FOR STIFFENED ELEMENTS

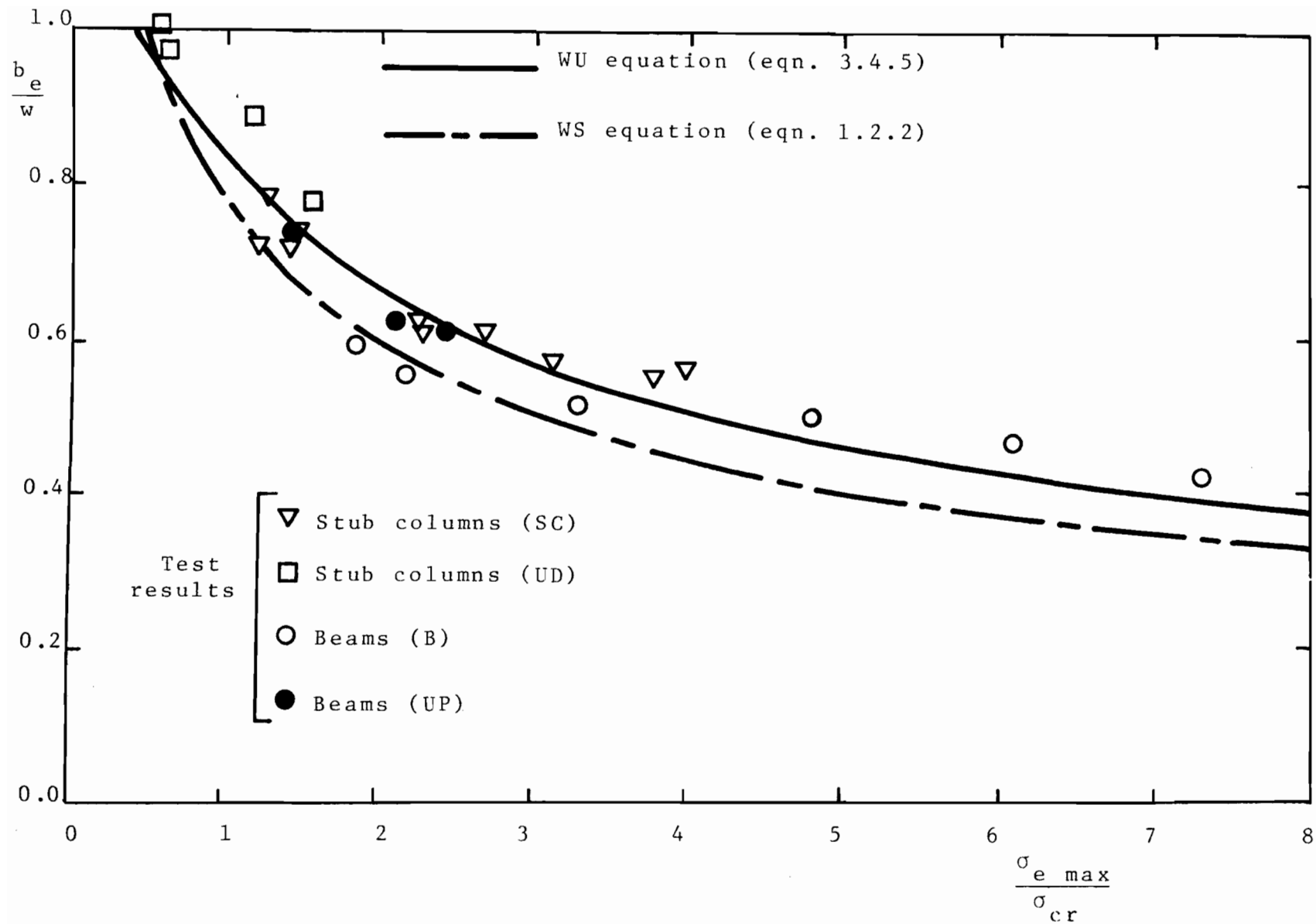


Fig. B.2.1 COMPARISON OF EFFECTIVE WIDTH EQUATIONS AND TEST RESULTS (BEAMS AND STUB-COLUMNS)

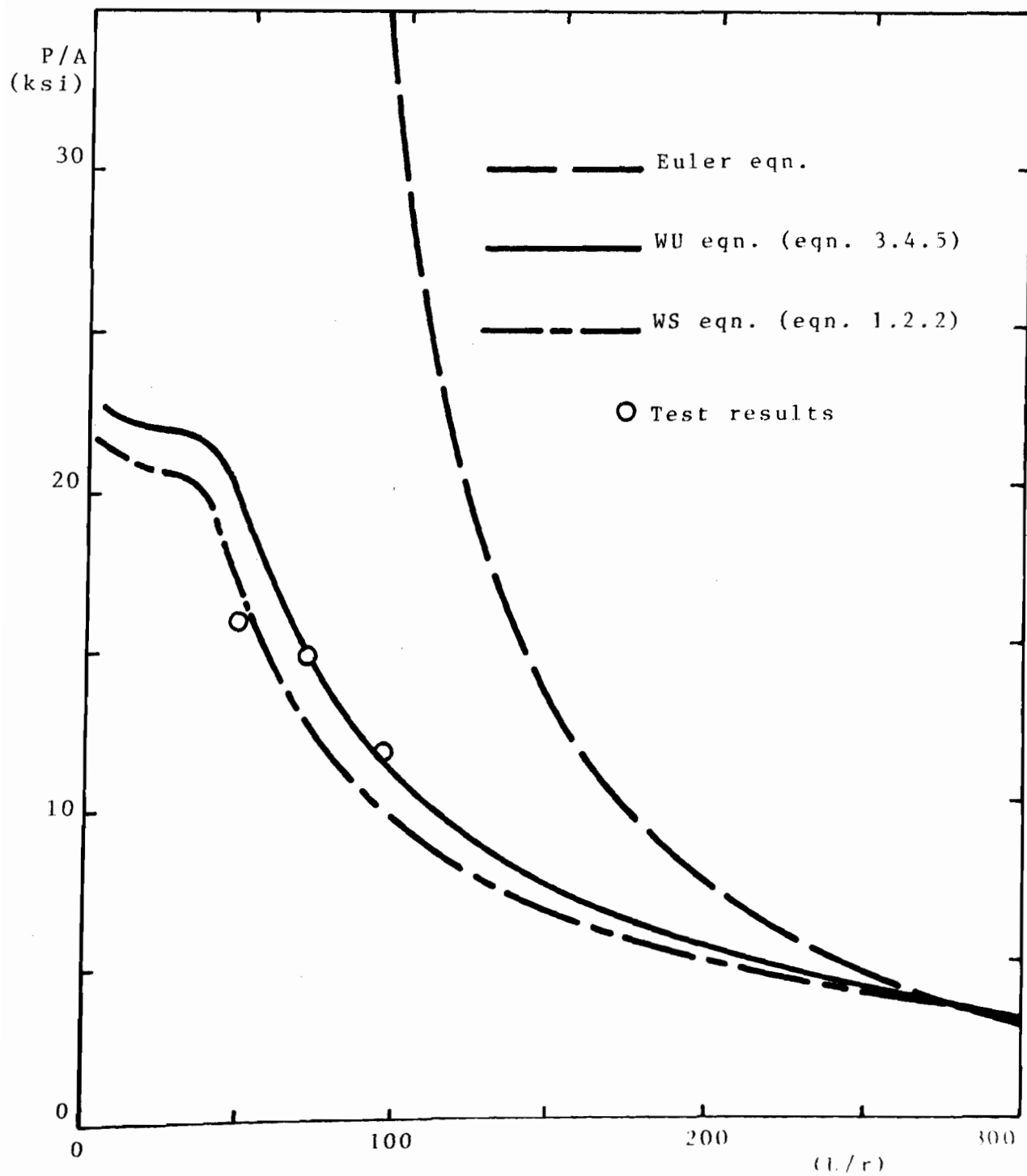


Fig. B.3.1 TANGENT MODULUS COLUMN CURVES AND TEST RESULTS. SPECIMENS LC-1 ($w/t = 57.5$)

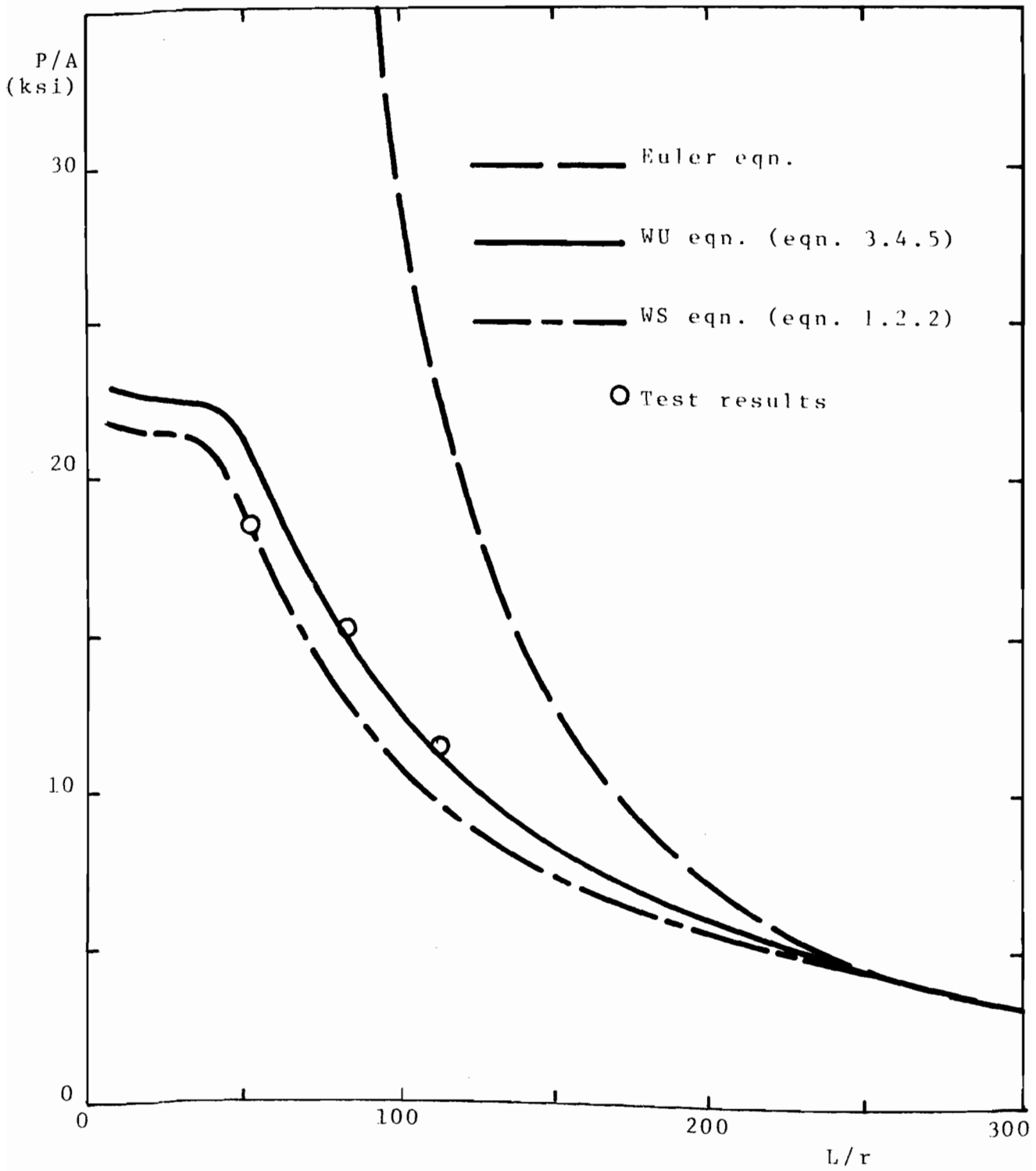


Fig. B.3.2 TANGENT MODULUS COLUMN CURVES AND TEST RESULTS. SPECIMENS LC-II ($w/t=50.5$)

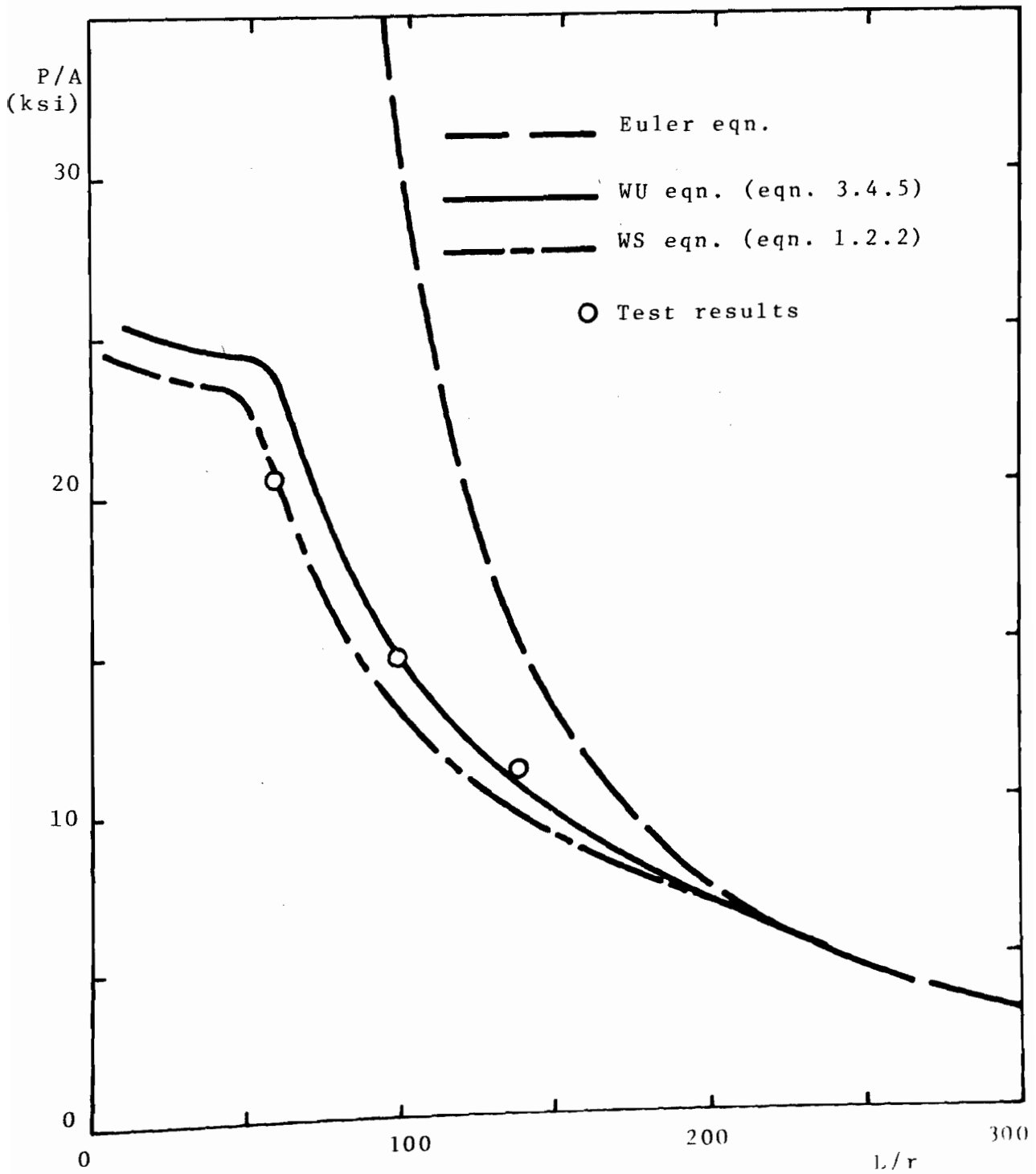


Fig. B.3.3 TANGENT MODULUS COLUMN CURVES AND TEST RESULTS. SPECIMENS LC-III ($w/t = 42.0$)

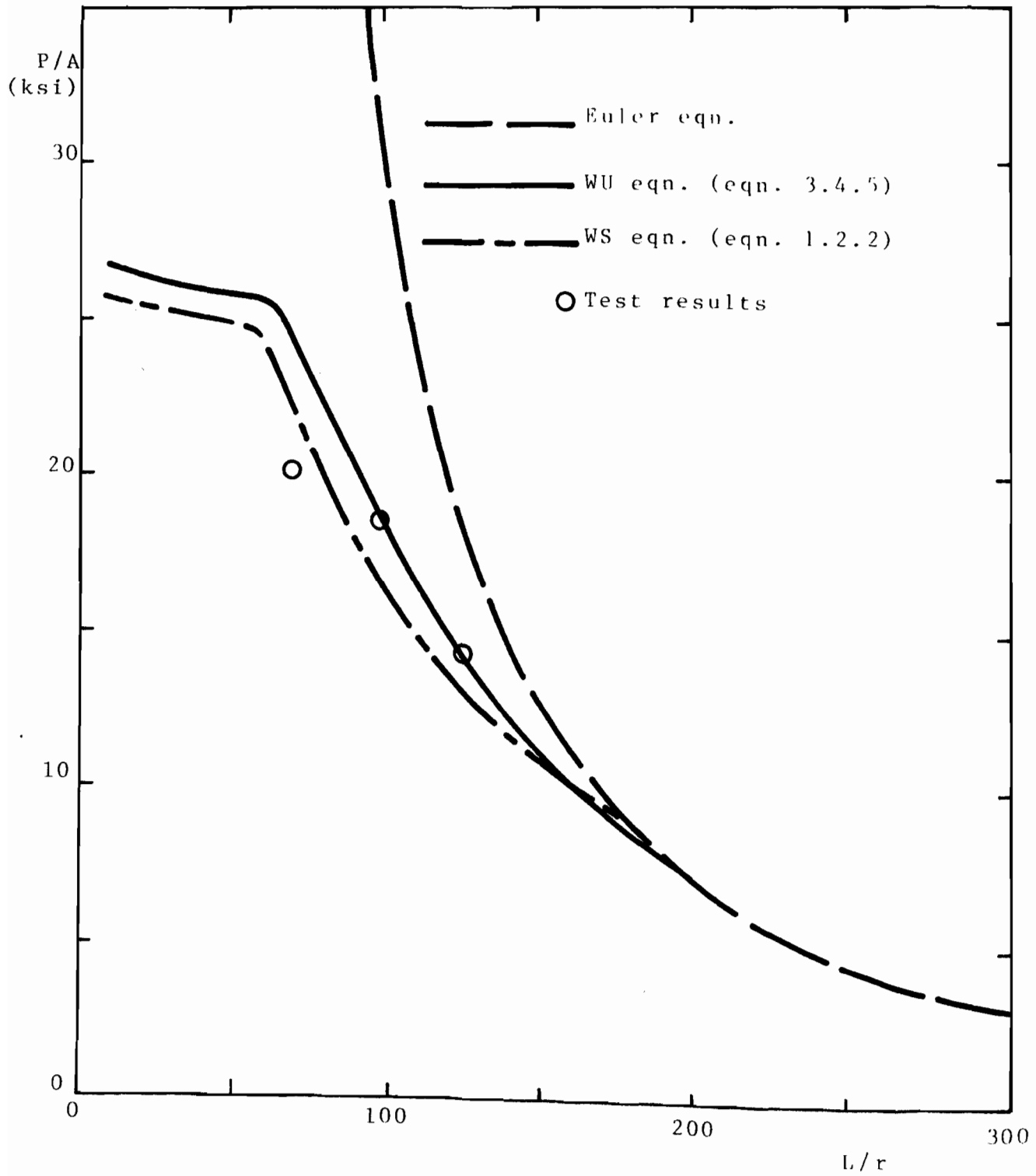


Fig. B.3.4 TANGENT MODULUS COLUMN CURVES AND TEST RESULTS. SPECIMENS LC-IV ($w/t = 35.0$)

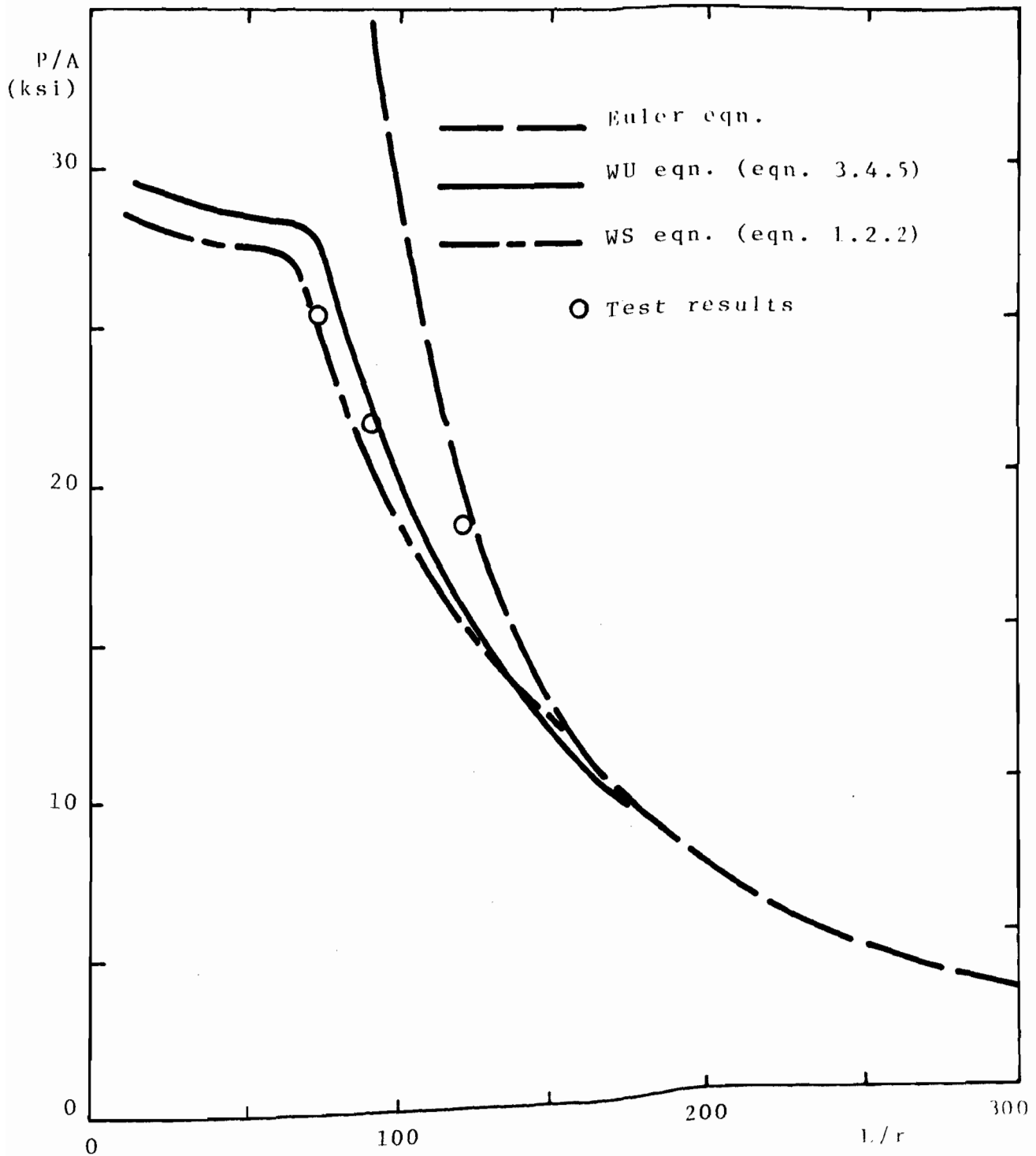


Fig. B.3.5 TANGENT MODULUS COLUMN CURVES AND TEST RESULTS. SPECIMENS LC-V ($w/t = 29.5$)

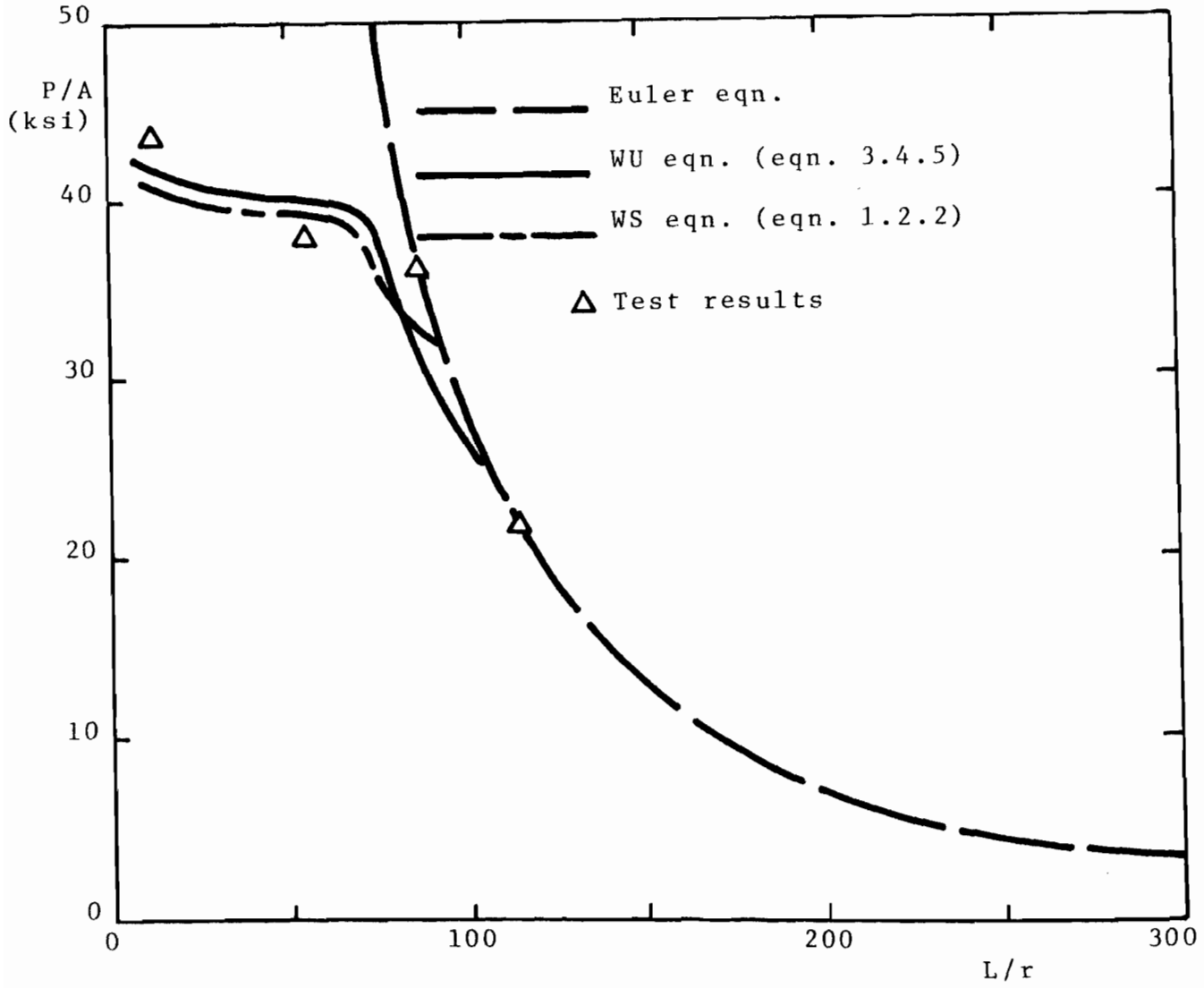


Fig. B.3.6 TANGENT MODULUS COLUMN CURVES AND TEST RESULTS. SPECIMENS UD-1 ($w/t = 16.2$)

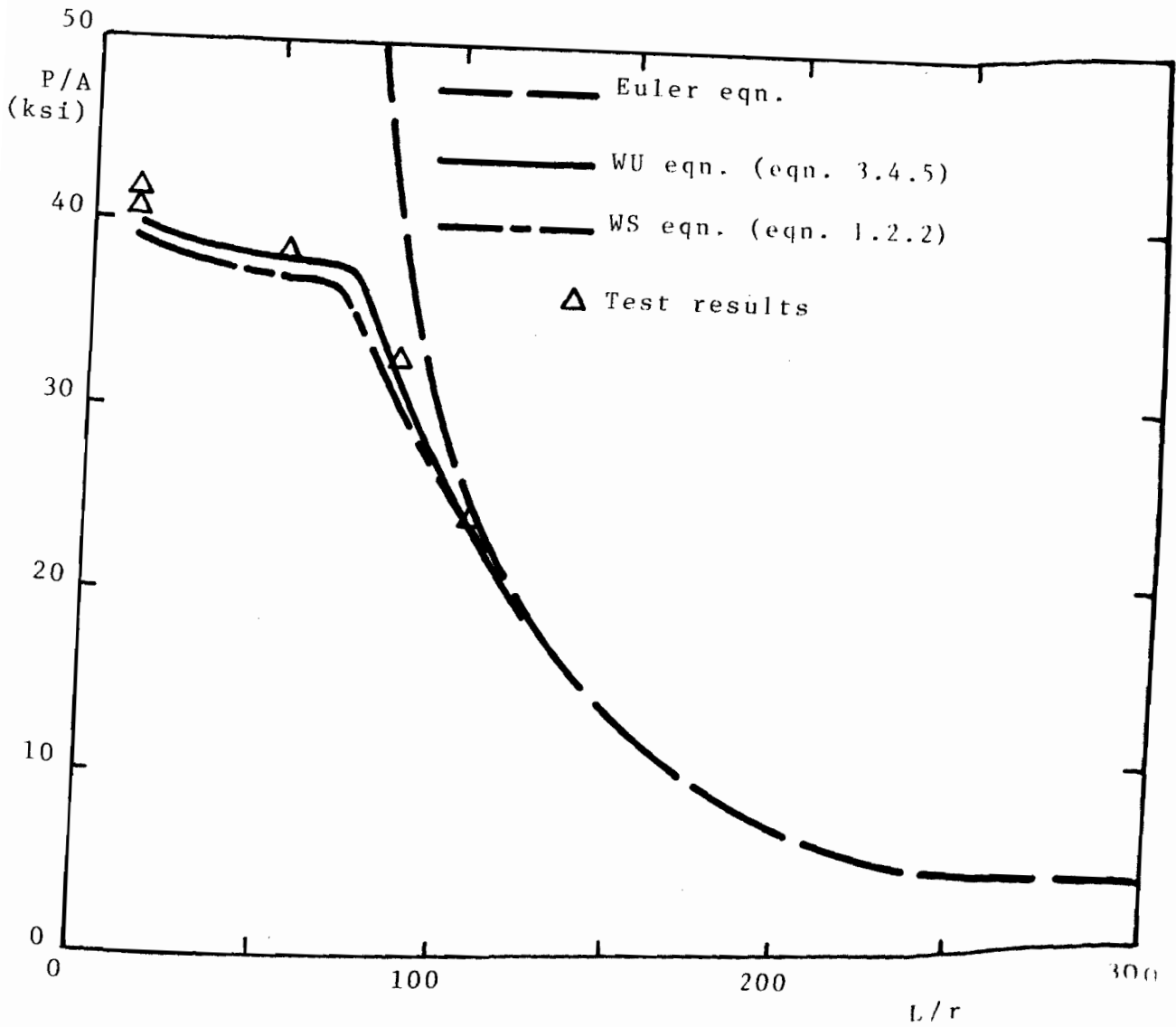
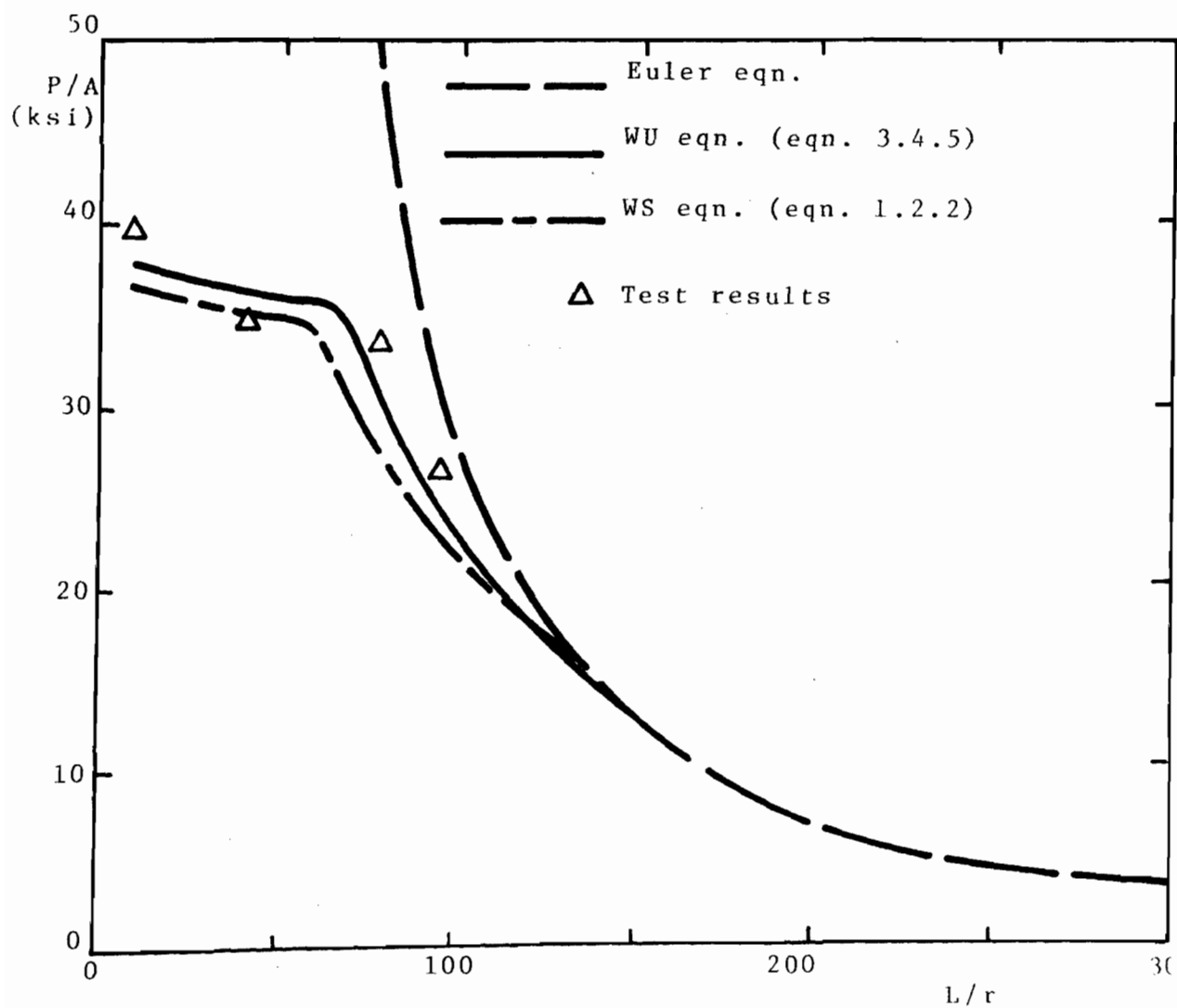


Fig. B.3.7 TANGENT MODULUS COLUMN CURVES AND TEST RESULTS. SPECIMENS UD-2 ($w/t=20.5$)



ig. B.3.8 TANGENT MODULUS COLUMN CURVES AND TEST RESULTS. SPECIMENS UD-3 ($w/t=24.8$)

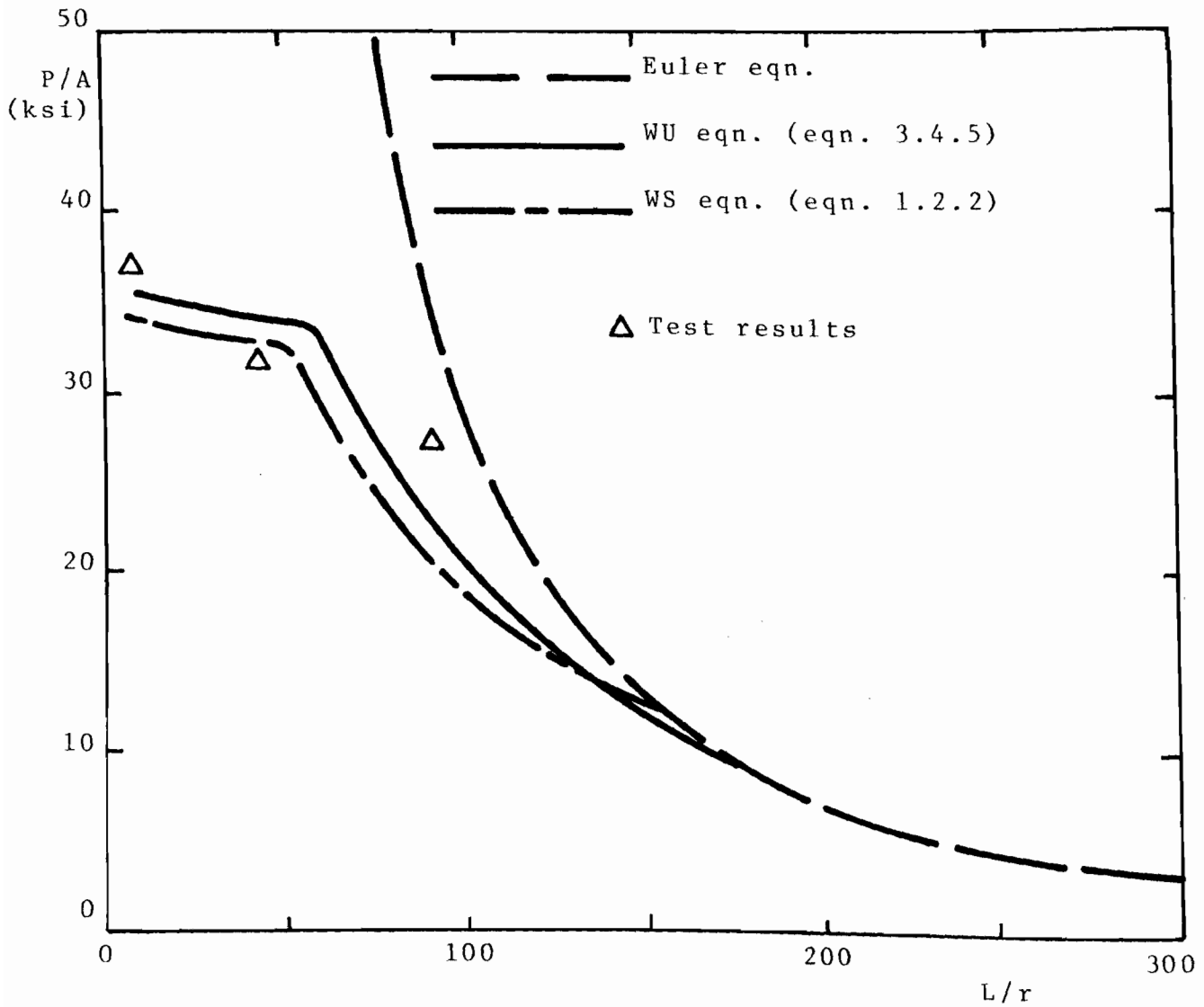


Fig. B.3.9 TANGENT MODULUS COLUMN CURVES AND TEST RESULTS. SPECIMENS UD-4 ($w/t=29.1$)

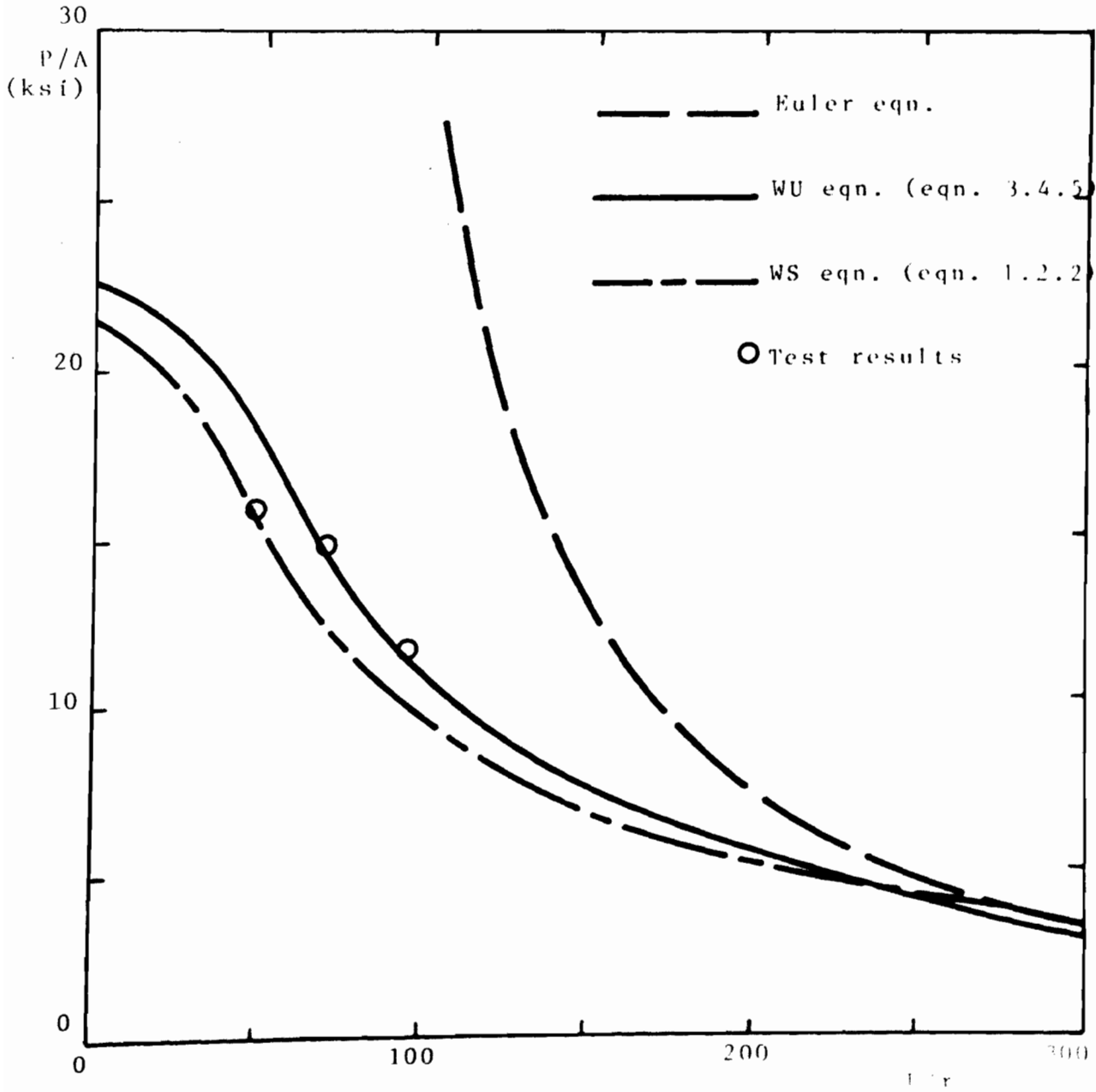


Fig. B.3.10 MODIFIED CRC CURVES AND TEST RESULTS.
SPECIMENS LC-1 ($w/t=57.5$)

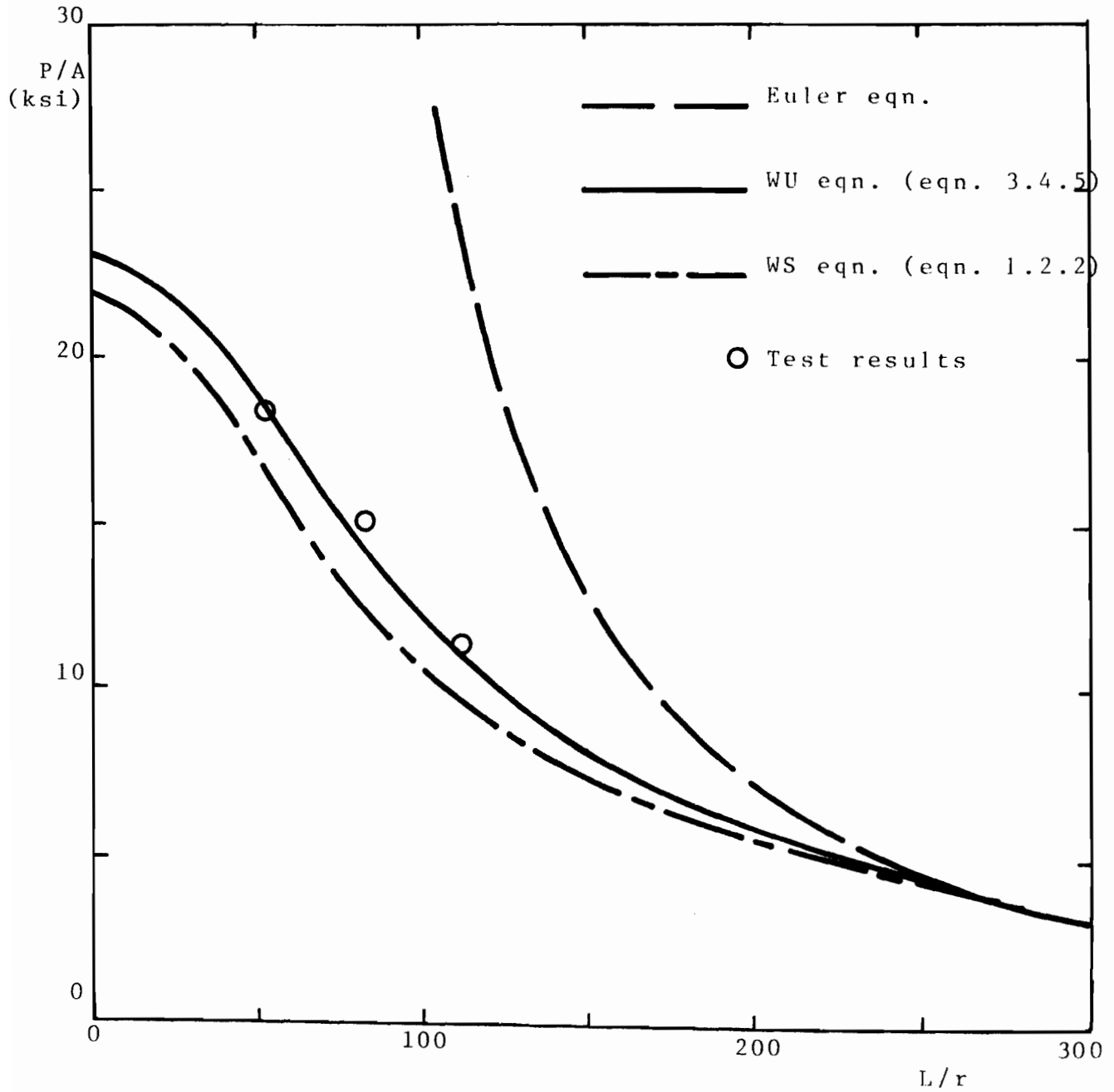


Fig. B.3.11 MODIFIED CRC COLUMN CURVES AND TEST RESULTS.
SPECIMENS LC-II ($w/t=50.5$)

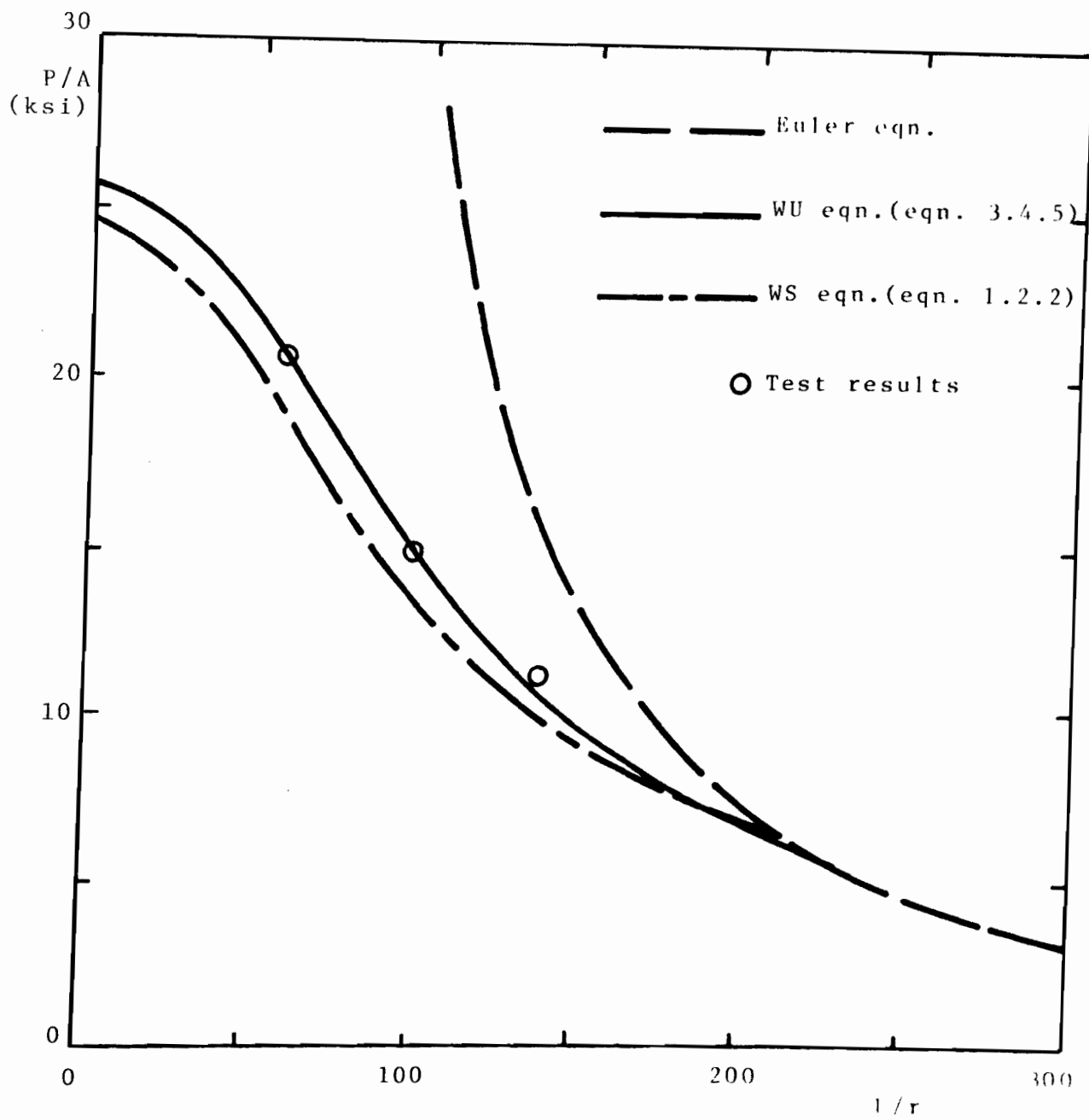


Fig. B.3.12 MODIFIED CRC CURVES AND TEST RESULTS,
SPECIMENS LC-111 ($w/t=42.0$)

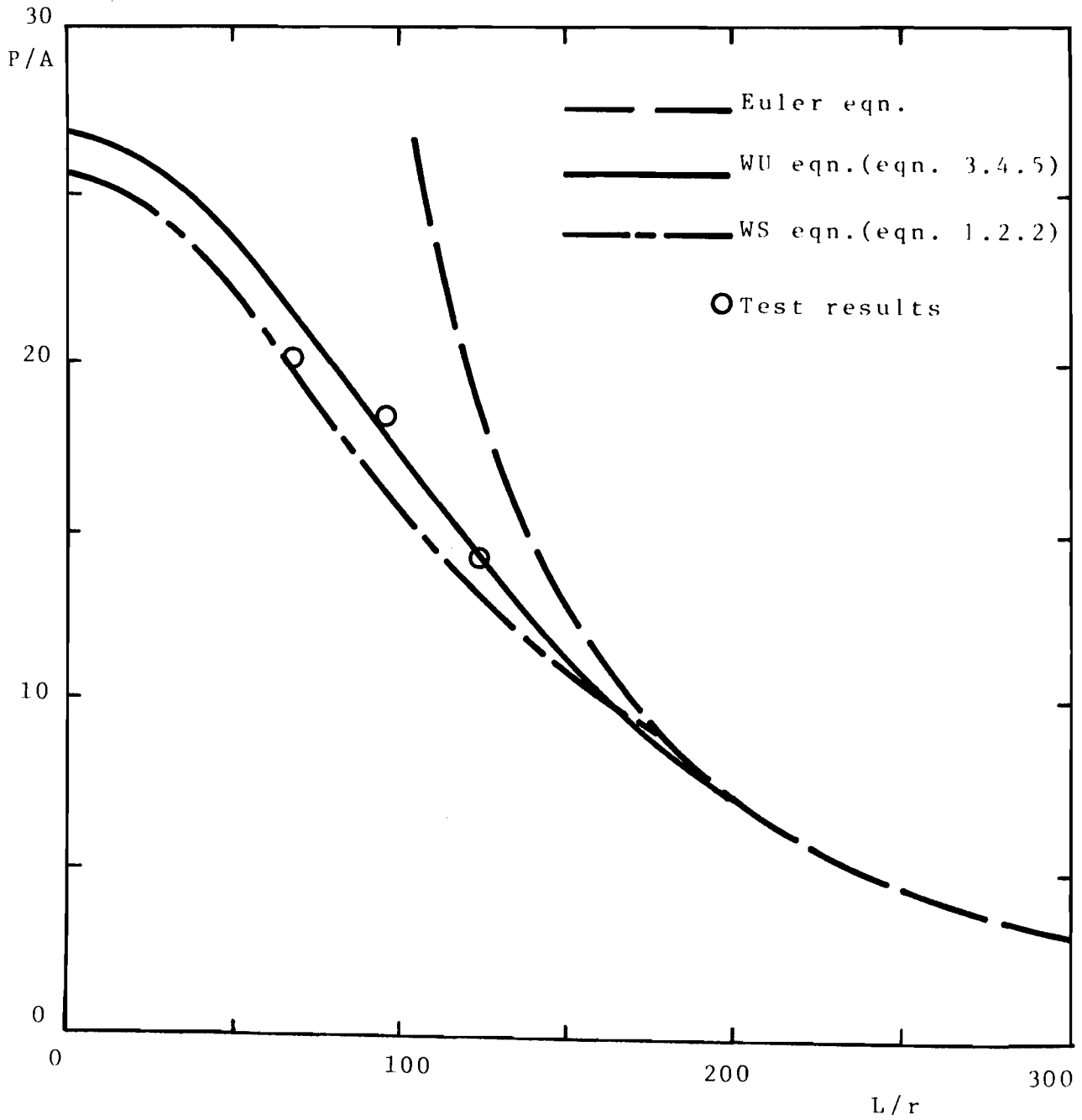


Fig. B.3.13 MODIFIED CRC CURVES AND TEST RESULTS.
SPECIMENS LC-IV ($w/t=35.0$)

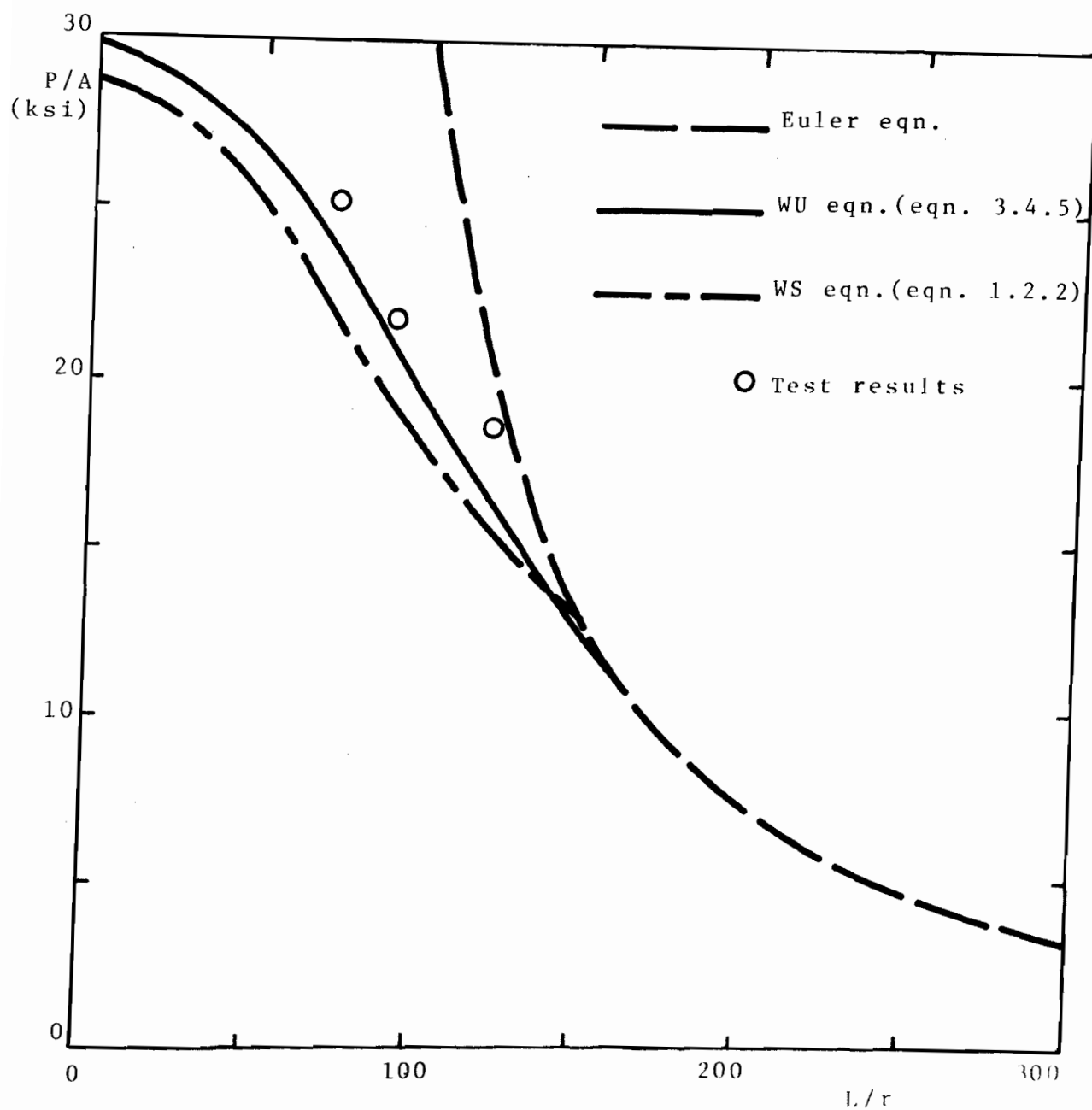


Fig. B.3.14 MODIFIED CRC CURVES AND TEST RESULTS.
SPECIMENS LC-V ($w/t=29.5$)

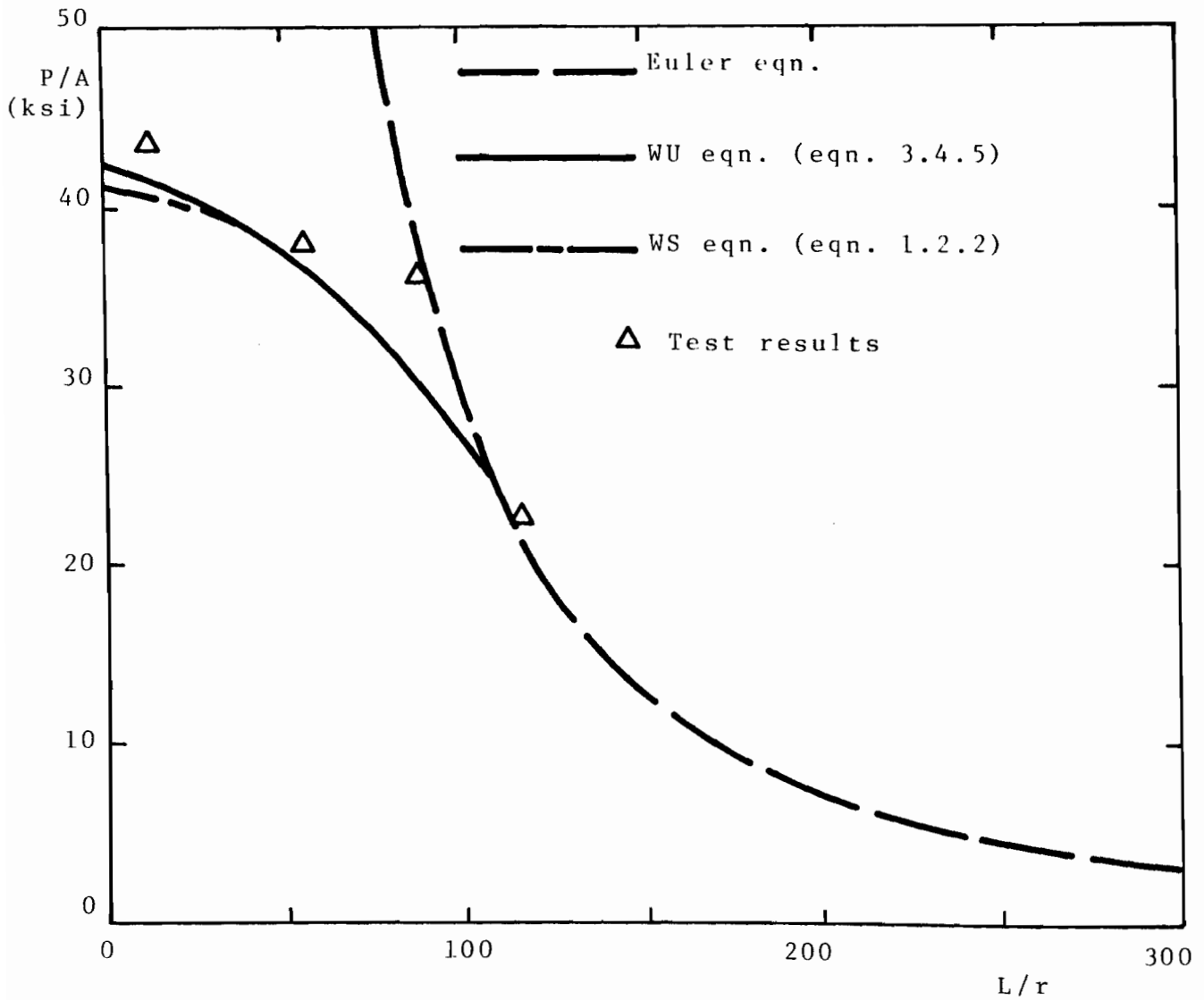


Fig. B.3.15 MODIFIED CRC CURVES AND TEST RESULTS.
SPECIMENS UD-1 ($w/t=16.2$)

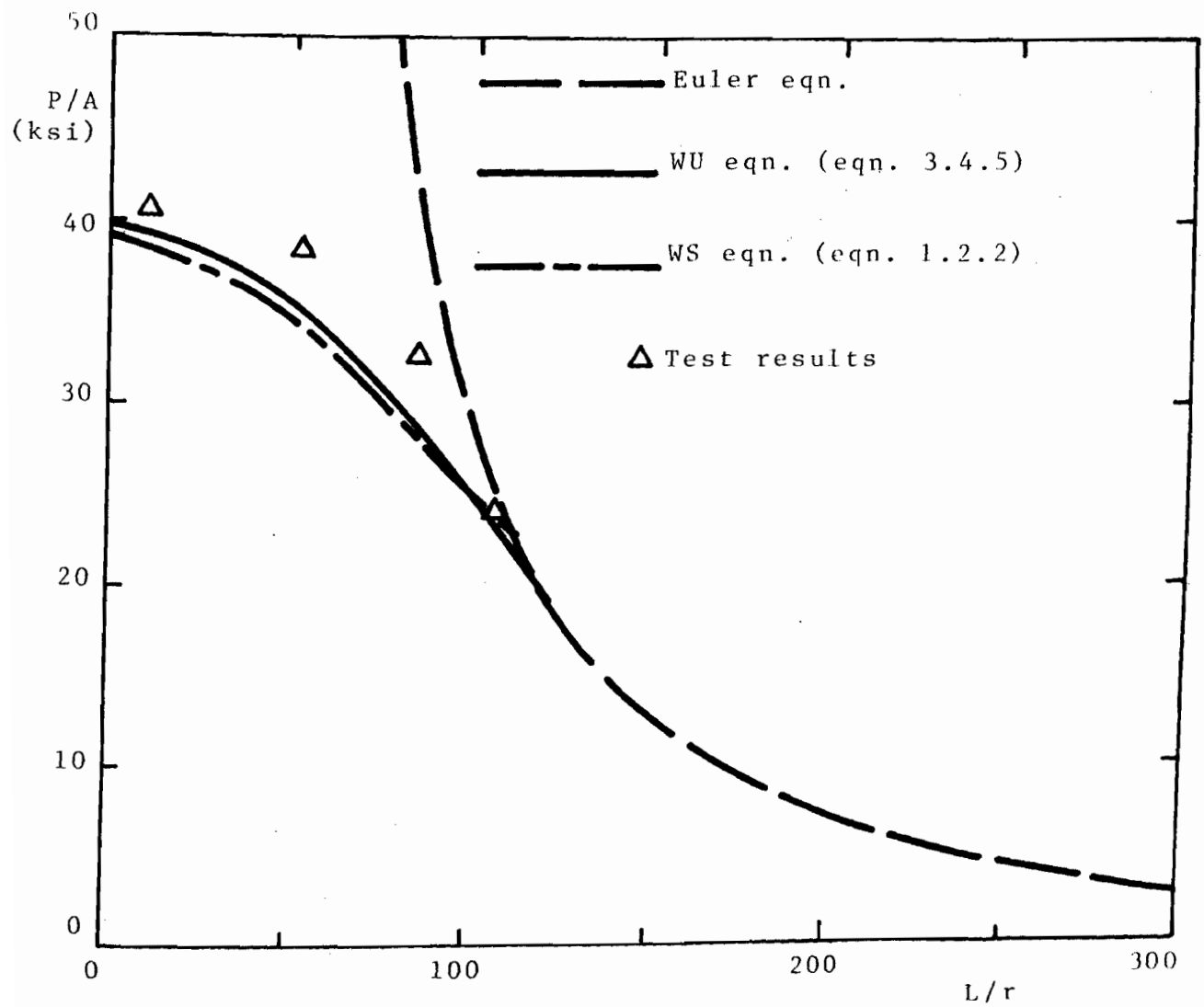


Fig. B.3.16 MODIFIED CRC CURVES AND TEST RESULTS.
SPECIMENS UD-2 ($w/t=20.5$)

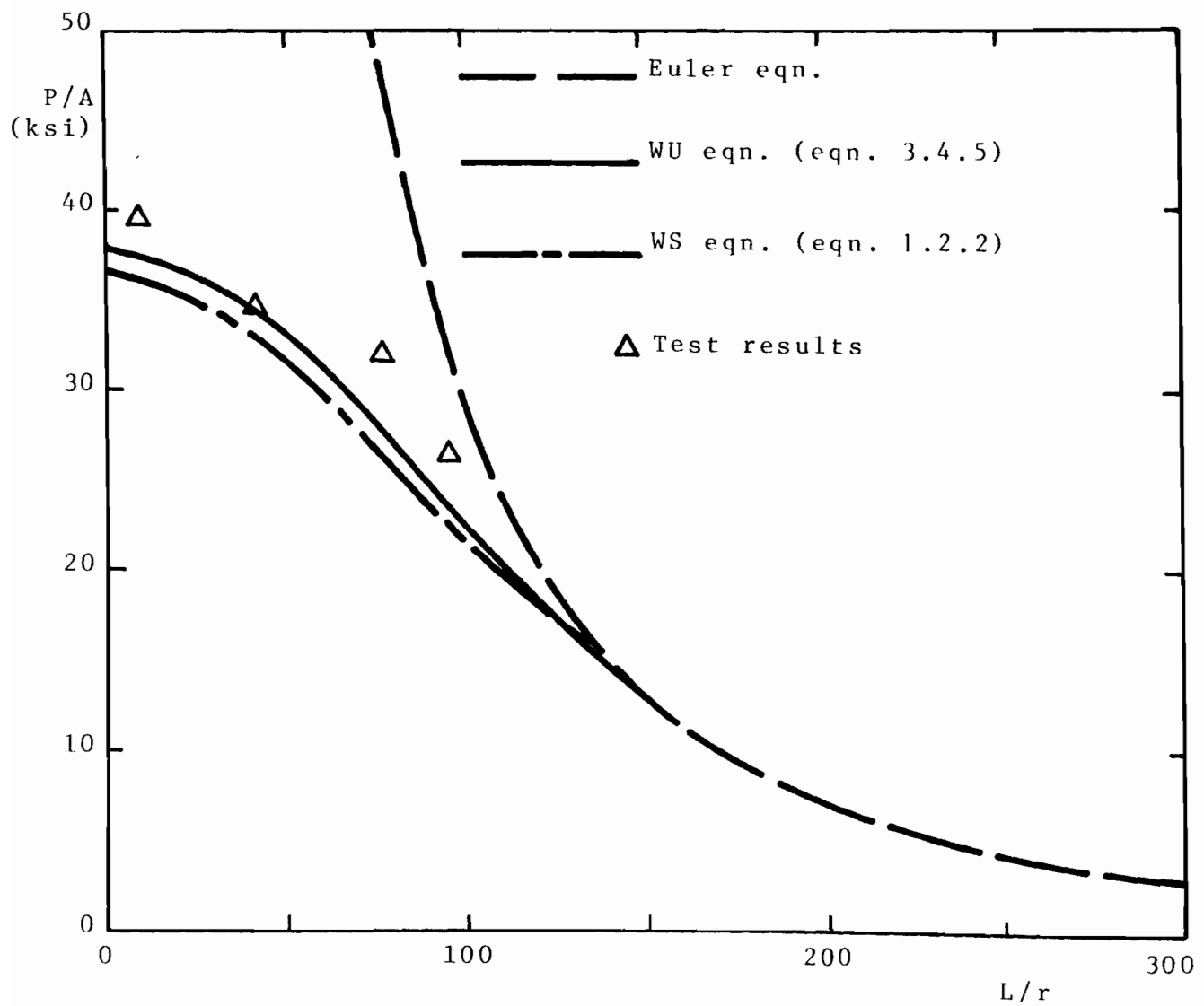


Fig. B.3.17 MODIFIED CRC CURVES AND TEST RESULTS.
SPECIMENS UD-3 ($w/t=24.8$)

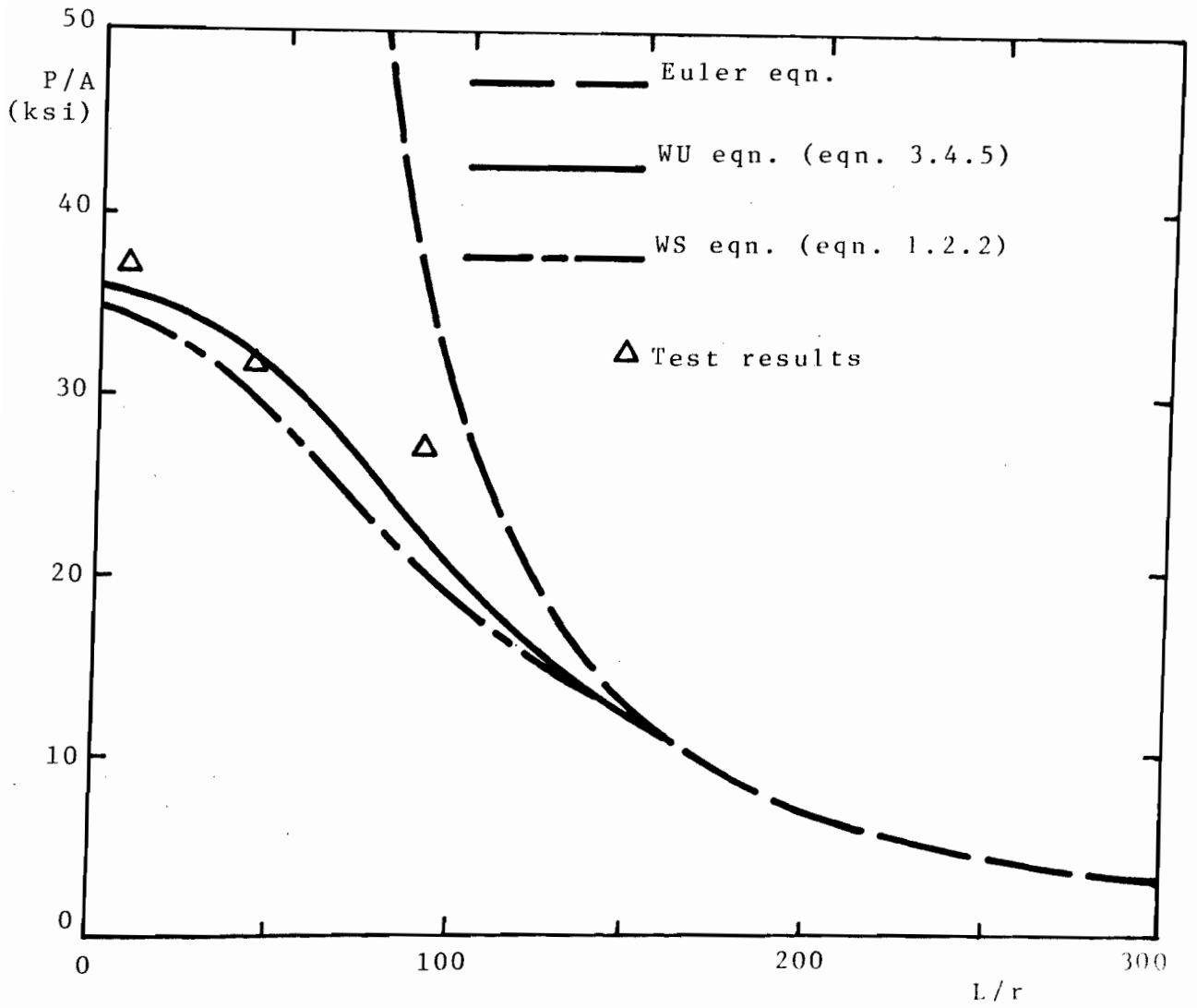
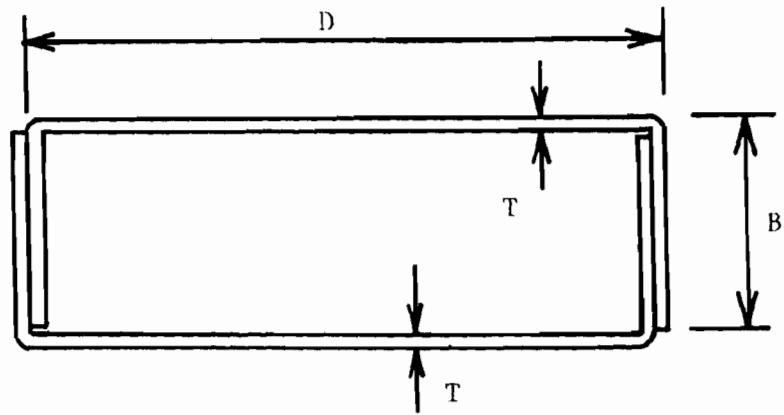
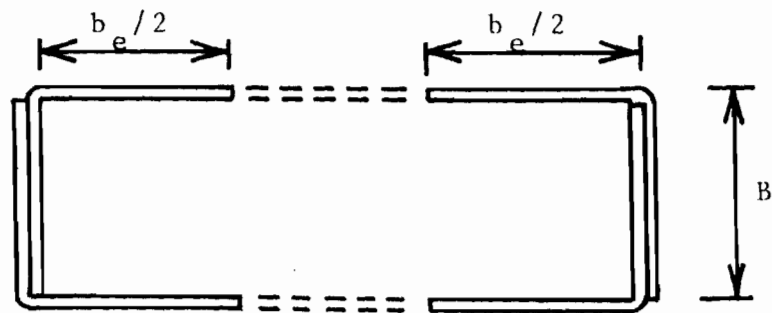


Fig. B.3.18 MODIFIED CRC CURVES AND TEST RESULTS SPECIMENS UD-4 ($w/t=29.1$)



(a) Cross-section



(b) Effective section

Fig. B.3.19 DeWOLF'S COLUMN SPECIMEN WITH STIFFENED ELEMENTS

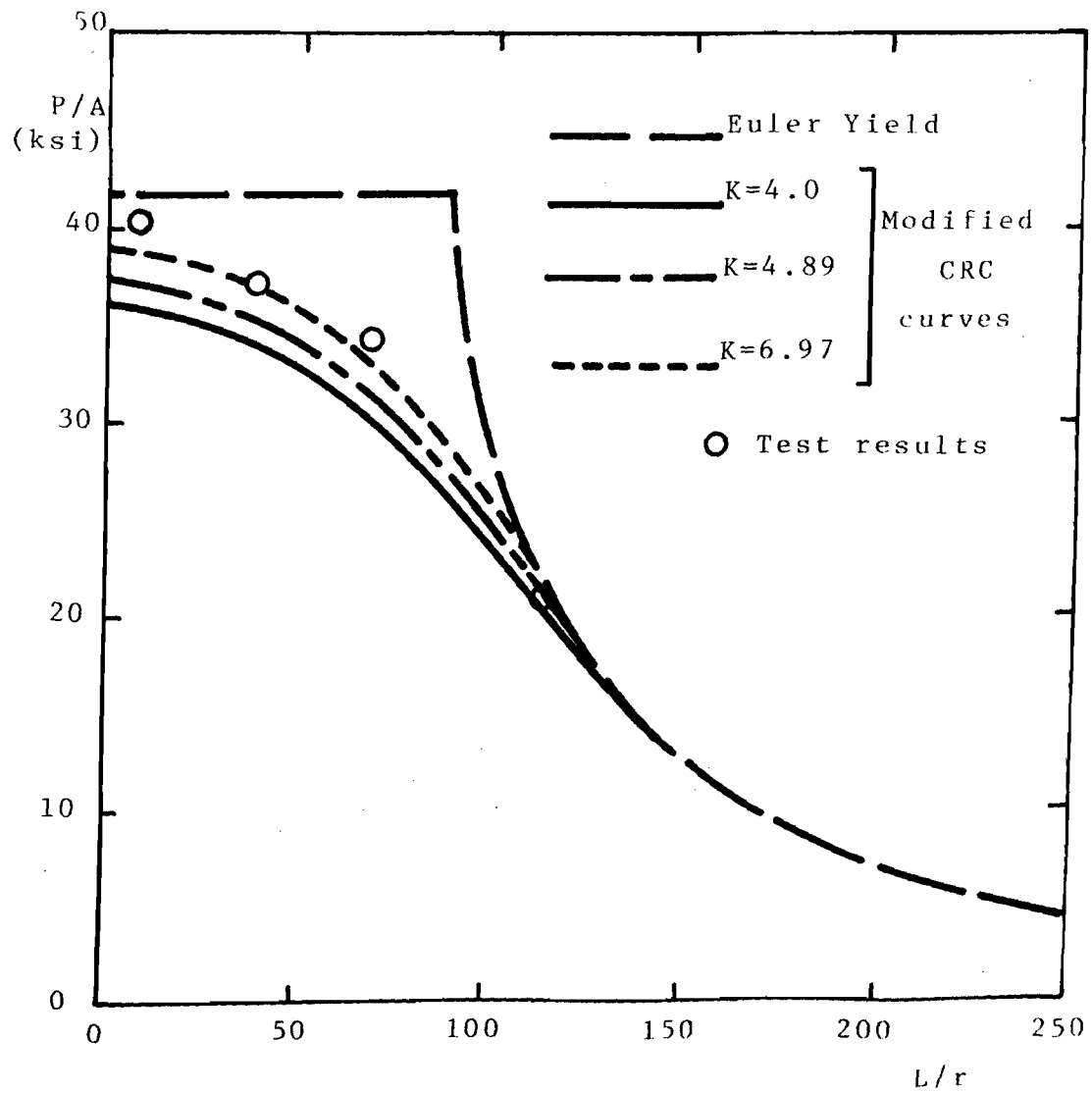


Fig. B.3.20 MODIFIED CRC CURVES AND TEST RESULTS.
SPECIMENS S-1 ($w/t=57.2$)

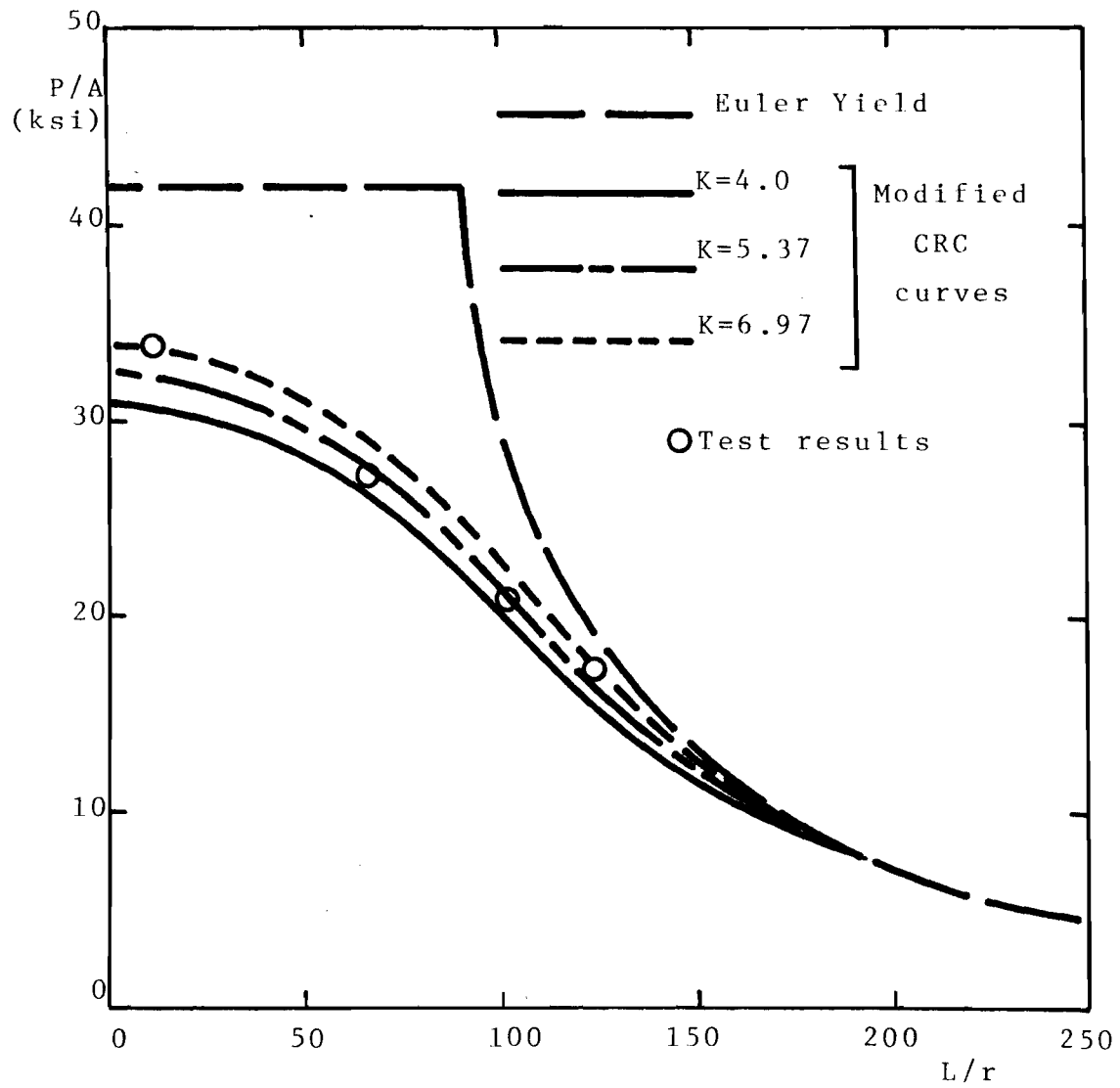


Fig. B.3.21 MODIFIED CRC CURVES AND TEST RESULTS.
SPECIMENS S-2 ($w/t=83.0$)

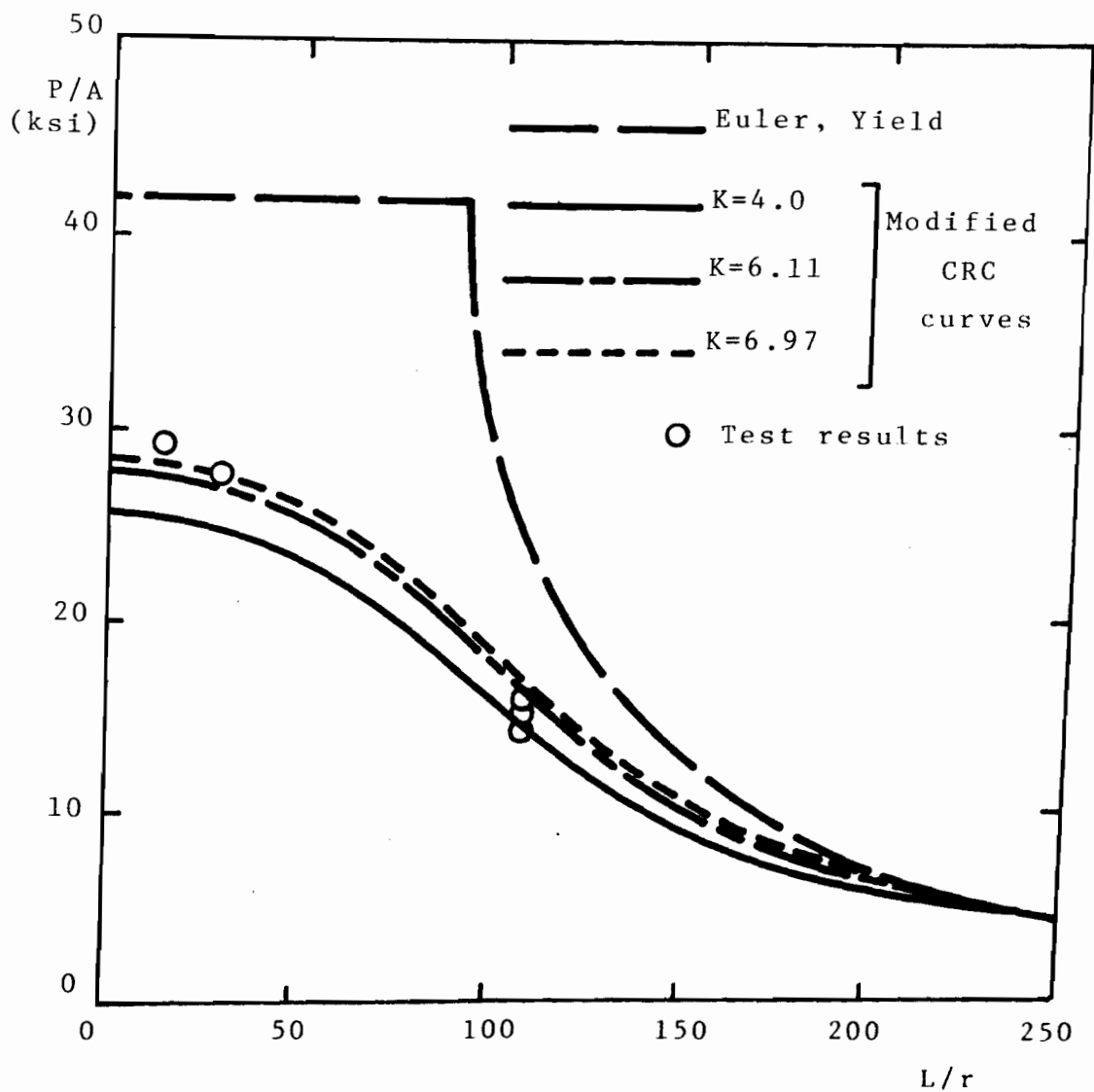


Fig. B.3.22 MODIFIED CRC CURVES AND TEST RESULTS.
SPECIMENS S-3 ($w/t=117.4$)

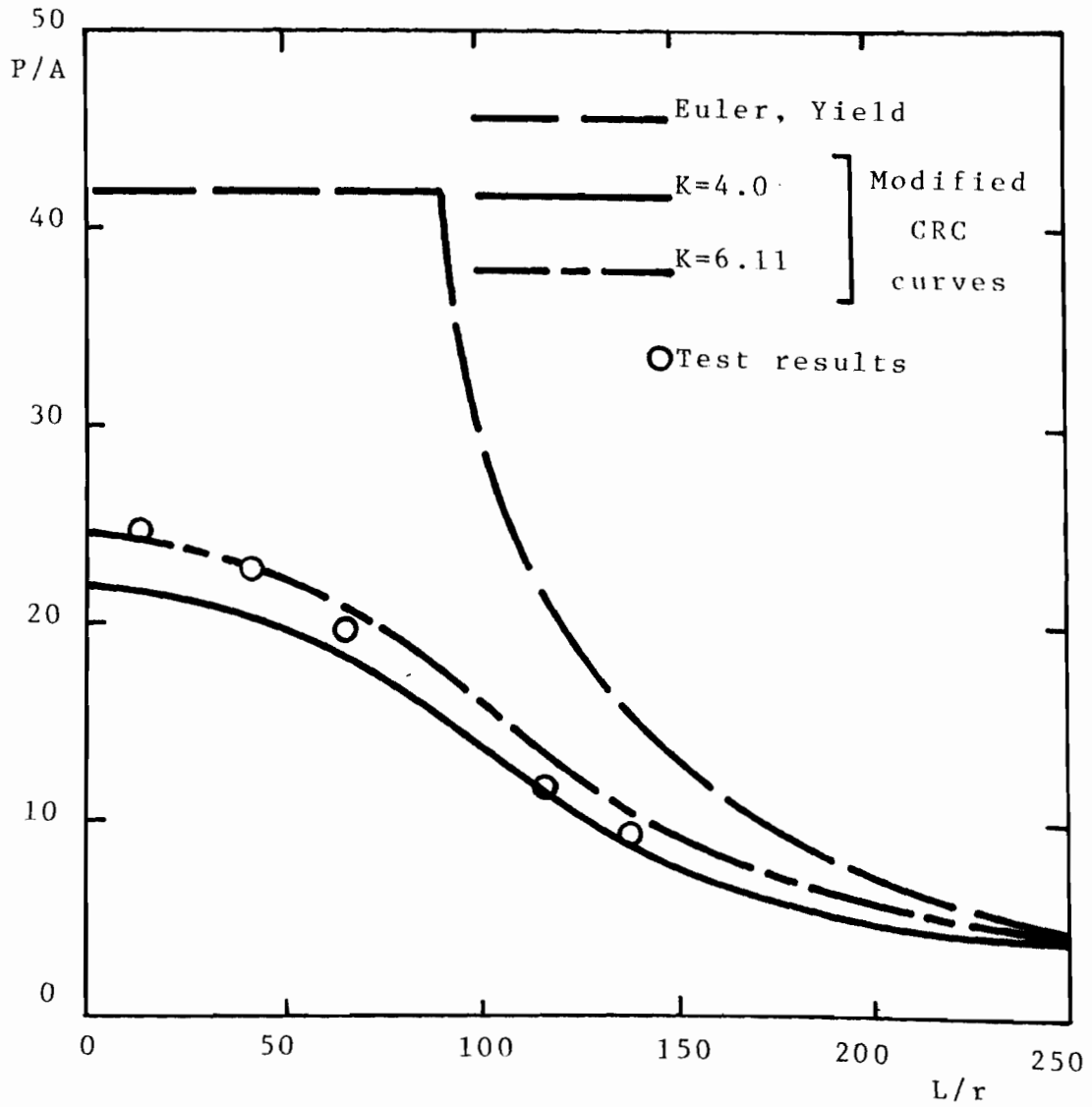


Fig. B.3.23 MODIFIED CRC CURVES AND TEST RESULTS.
SPECIMENS S-4 ($w/t=151.8$)

got 12